UC Berkeley
UC Berkeley Electronic Theses and Dissertations

Title
Enhancing Seismic Performance of Tall Buildings by Optimal Design of Supplemental Energy-Dissipation Devices

Permalink
https://escholarship.org/uc/item/8sv179sq

Author
Wang, Shanshan

Publication Date
2017

Peer reviewed|Thesis/dissertation

Enhancing Seismic Performance of Tall Buildings by Optimal Design of Supplemental Energy-Dissipation Devices

By

Shanshan Wang

A dissertation submitted in partial satisfaction of the

requirements for the degree of

Doctor of Philosophy

in

Engineering – Civil and Environmental Engineering

in the

Graduate Division

of the

University of California, Berkeley

Committee in charge:

Professor Stephen A. Mahin, Chair

Professor Jack P. Moehle

Professor David R. Brillinger

Summer 2017

COPYRIGHT

Enhancing Seismic Performance of Tall Buildings by

Optimal Design of Supplemental Energy-Dissipation Devices

ABSTRACT

Enhancing Seismic Performance of Tall Buildings by
Optimal Design of Supplemental Energy-Dissipation Devices

by

Shanshan Wang

Doctor of Philosophy in Engineering– Civil and Environmental Engineering

University of California, Berkeley

Professor Stephen A. Mahin, Chair

This dissertation focuses on the use of supplemental energy-dissipation devices to improve the seismic performance of tall steel buildings. It is divided into two parts. Part 1 focuses on exploring cost-effective retrofit strategies to improve the seismic performance of an existing tall building. The selected building is a 35-story steel moment-resisting frame, with representative details from the early 1970s. Detailed seismic evaluations were conducted in the framework of Performance Based Earthquake Engineering (PBEE), using the scenario-based performance assessment methods. A three-dimensional numerical model capturing the mechanical properties of the most critical structural elements was generated using the program: Open System for Earthquake Engineering Simulation (OpenSees). Seismic evaluation of the selected building was done following ASCE 41-13, FEMA 351 and FEMA P-58, and two hazard levels: basic safety earthquake levels 1 and 2 (BSE-1E and BSE-2E) prescribed by ASCE 41 were used for the assessment. Results predicted that this building failed to meet the recommended performance objectives and had a variety of seismic vulnerabilities, and possible retrofits were needed.

Therefore, a two-level retrofit approach was examined that focused on achieving the collapse prevention limit state under the BSE-2E hazard level. In Level-1, the brittle column splices were fixed everywhere in the building, and the massive concrete cladding was replaced with lightweight substitute in the exterior of the building. Level-2 strategies augmented the Level-1 methods by adding different supplemental energy-dissipation devices. Devices investigated include: fluid viscous dampers (FVDs), viscous wall dampers (VWDs) and buckling restrained braces (BRBs). Among these, the scheme that used FVDs was expected to be the most promising to upgrade the seismic performance of the case-study steel moment frame, and thus was examined first. In this approach, feasible damper locations and overall effective damping ratios were evaluated through a series of preliminary studies, and then a two-phase manual design method was used to refine the distribution and mechanical properties of the dampers. Thorough assessments of the refined design were carried out and the results indicated that the proposed retrofit method of using FVDs could achieve the retrofit goal and provide a cost-

effective means of improving the structural behavior and reducing economic losses in a major seismic event for this case-study building.

The study was extended to examine alternative measures to upgrade the case-study building by using either VWDs or BRBs, and compared their relative effectiveness and economy with the scheme using FVDs. The locations and effective damping ratios were kept the same for all three schemes to insure a valid comparison. Results indicated that the proposed schemes of VWDs and BRBs both failed to achieve the targeted performance goal for this structure under a BSE-2E event, and special design considerations were required.

Part 2 of the dissertation focuses on developing an automated tool to streamline the design of FVDs in tall buildings. Aided by the high-performance computers and parallel processors, a large amount of complicated nonlinear response history analysis was conducted to facilitate the automate design procedure. The optimization problem was devised in a simplified PBEE framework under one hazard level each time. Basic optimization ingredients were selected to reflect the target performance goal, and several cases using different objective functions were evaluated.

Two tall buildings: the existing steel moment frame examined before and a newly-designed mega-brace steel frame were selected to rely on the automated procedure to optimally design FVDs. In both cases, the automated procedure turned to be very efficient, help identify design parameters of dampers in selected locations and reduce a great amount of engineering efforts. With only limited number of iterations, optimal design patterns of FVDs in a tall building could be found, which were able to improve the structural performance under different hazard events. The suggested optimal design could meet retrofit goal for the existing tall building, as well as achieve enhanced performance goal for both existing and new tall buildings.

To these who bring passion and smiles to my life

ACKNOWLEDGEMENT

I would like to take this special moment to express my sincere gratitudes to these who have helped me greatly and made my Ph.D. journey quite enjoyable at UC Berkeley.

First and foremost, I want to thank my research advisor, Professor Stephen Mahin for his support, encouragement and patience over these years. Prof. Mahin not only provides me with mentorship and encouragement on my study and life, but also grants me with great academic freedom to explore my potentials, let alone continuous financial support for study and attending conference. All these work is not possible without his support and smile. I feel more than blessed to have the chance to take the journey with him, and grow to be a confident and tolerant person. No matter how far I will go in the future, his mentorship and friendship will always be a most valued thing that accompanies me in every aspect of my life.

Besides, I greatly appreciate other professors at Berkeley. In particular, Prof. Jack Moehle and Prof. Davis Brillinger who serve as members of my dissertation committee and provide advice on this work. Great support and suggestions from Prof. James Kelly on related research topics are also deeply acknowledged. In addition, special thanks are given to Prof. Xilin Lu from Tongji University, China and Prof. Kasai Kazuhito from Tokyo Institute of Technology, Japan, who constantly force me ahead and provide help and suggestions.

Studying and living at Berkeley makes me feel so lucky: the acedamic atmostphere, lovely and respected professors, and more importantly, so many brilliant and nice people around. My co-workers: Jiun-Wei Lai, Frank McKenna, Andreas Schellenberg and Matthew Schoettler are always there to help, making my endeavors much less painful. Selim Gunay and Vesna Terzic, who are like a big brother/sister to me, show their caring and patience in every possible way. Other researchers or engineers, to name a few, Amarnath Kasalanati, Dimitrious Lignos, Byounggeon Kim, John Hooper, Joe Maffei, Lawrence Burkett, Kit Miyamoto, Amir Gilani, Jim Malley and Rob Smith granted me with so much help and information; their advice and insights are muchly appreciated. Moreover, I would like to thank Tim Cockerill and Stephen Mock from Texas Advanced Computing Center to generously provide the high-performance computing resources and tremendous technical support. Additionally, I owe Claire Johnson, a professional editor at Pacific Earthquake Engineering Research center a big thanks to proofread my work with great dedication and patience.

Another treasure I gained during these years of study in the U.S. is the friendship with a group of my peers, who are sharing a similar goal and taking a similar life path as myself. Prof. Mahin always tells the students how important these peers will be in our future journey, and I firmly believe so. Looking at these familiar names: Cindy Qian, Barb Simpson, Thanh Do, Benshun Shao, Sifat Muin, Yingjie Wu to name a few, I could not be more thankful to get to know them well and develop strong relationship through classes we took together, examines we suffered together and places we explored together.

As the only child to my parents, I understand how much they would desire me to be around them as close as possible. However, they seldom let their desires to influence my decision. Ever since I was born, they have shown tremendous care and support for every aspect of my life. Thanks my mom and dad (theoretically my step father), you two have defined the place of happiness and sweetness for me.

Last but not least, I still owe a thanks to my significant other. People meet for a reason, and I think my boyfriend, Ruoying is my reason to be a happy "Miss sunshine". Thanks Ruoying for being a great company, bringing me so much joy and happiness over the past few years. Thanks for serving as a great history teacher as well. Keep the positive attitudes towards life, and enjoy the rest of your Ph.D. journey.

Shanshan Wang

Aug. 1st, 2017

TABLE OF CONTENTS

LIST OF FIGURES

LIST OF TABLES

1   Introduction

1.1   MOTIVATIONS

The seismic performance of tall buildings raises unique problems in terms of the complexity of their dynamic characteristics, typically inelastic, three-dimensional responses they experience during strong earthquakes, and the large direct and indirect impacts that their loss of function would have on occupants and the surrounding community. The seismic performance of new tall buildings located in high seismicity areas of California has been the focus of investigations by the Pacific Earthquake Engineering Research Center (PEER) for more than a decade ago as part of its Tall Buildings Initiative (TBI) program. The first phase of the TBI program has culminated in a set of engineering guidelines that allow new tall buildings to be designed with high confidence to achieve desired performance objectives.

However, there are many older tall buildings worldwide that were designed and constructed when the understanding of earthquake hazards and structural behavior were not as advanced as now. This is especially true in California, where significant numbers of buildings greater than 20 stories in height were built between 1960 to1990. Given the number and importance of these tall buildings in California, it is important to assess their likely seismic performance during future earthquakes. An equally or possibly even more important issue is whether economical and practical methods can be found to upgrade their performance, if seismic deficiencies are identified. While providing adequate safety under hazards posed by future seismic events is the immediate goal of such efforts, identification of retrofit measures that not only enhance an existing building's resilience but also reduce losses due to post-earthquake repair and business interruption is an important next step. Such strategies for enhancing safety and performance might also be applied to newly-designed tall buildings to upgrade their seismic performance to levels where damage is limited and post-event functionality is maintained. Improving the safety of existing and new tall buildings and minimizing post-event disruption and losses associated with damage repair and loss of post-event functionality are important steps to move towards the goal of building seismically resilient communities.

An impediment to realizing this long-term goal has been the difficult and time-consuming nature of the sophisticated nonlinear, three-dimensional dynamic analyses needed to evaluate the seismic performance of tall buildings, and the challenges of interpreting the massive amount of data produced by such analyses to identify the most economical and effective retrofit measures. Today, the iterative design-analysis process needed to identify and optimize a retrofit/upgrade

strategy can easily overwhelm the resources of many engineering firms. To remedy this situation, it is beneficial to investigate more formal and automated approaches that rely on recent advances in software applications for nonlinear dynamic analysis, performance-based evaluation, and workflow management and the computational power of high-performance, parallel processing computers.

1.2 BACKGROUND OF TALL BUILDING INITIATIVE PROGRAM

1.2.1 Phase 1—Designing New Tall Buildings

With the resurgence of tall building construction at the beginning of the 21st century, PEER has embarked on a multidisciplinary, multi-institutional program to assess the seismic performance of newly constructed tall buildings of different architectural styles, height and configuration, structural and foundation systems, seismic hazards, and acceptance criteria since the previous generation of tall structures were constructed. Phase 1 of the TBI program has culminated in a series of background documents and design guidelines intended to provide designers, public officials, and occupants with high confidence that these structures would achieve the targeted seismic performance. The first edition of this guideline was published in 2010: *Guidelines for Performance-Based Seismic Design of Tall Buildings* (Version 1.0) [PEER 2010a]. The second edition of this guideline (Version 2.01) [PEER 2017] was recently released, which accounts for lessons and experiences gleaned from applications of the first edition on a variety of projects, and the conditions and state-of-practice worldwide. The TBI program also developed additional technical reports to augment the recommendations provided in the guideline, including:

- *Seismic Performance Objectives for Tall Buildings* [Holmes *et al.* 2008];

- *Modeling and Acceptance Criteria for Seismic Design and Analysis of Tall Buildings* [PEER 2010b];

- *Input Ground Motions for Tall Buildings with Subterranean Levels* [Stewart and Tileylioglu 2010]; and

- *Case Studies of the Seismic Performance of Tall Buildings Designed by Alternative Means* [PEER 2011].

Those guidelines and supporting documents are widely used in designing tall buildings that have seismic performance capabilities at least equal to, and in some respects, superior to that intended for similar buildings designed in full conformance with the prescriptive building code provisions [PEER 2017]. As such, the TBI Guidelines are used as an alternative means to demonstrate that a structure satisfies the basic safety and other requirements of building codes.

Two other guidelines are often used specifically for the design of tall buildings. These are:

- *An Alternative Procedure for Seismic Analysis and Design of Tall Buildings Located in the Los Angeles Region* [LATBSDC 2017]; and

- *Requirements and Guidelines for the Seismic Design of New Tall Buildings using Non-Prescriptive Seismic-Design Procedures* [SFDBI 2014].

1.2.2 Phase 2—Assessing Existing Tall Buildings

The inventory of existing tall buildings (taller than 20 stories) in California, with emphasis on buildings located in Los Angeles, Oakland, and San Francisco, were covered in Lai *et al.* [2015]. A great number of tall buildings were constructed following the post-World War II in California between the late 1960s and 1990s. During this period, the understanding of earthquake hazards and structural behavior was not as advanced as now. Many changes have been made since then to improve modern building codes, which consequentially identified several known vulnerabilities associated with existing tall buildings [Lai *et al*. 2015].

Given the number and importance of these existing tall buildings in California, it is prudent to assess their seismic performance and the feasibility of retrofitting these buildings to address seismic vulnerabilities. Phase 2 of the TBI focuses on the seismic performance of existing tall buildings. These existing buildings and their seismic performance provide the focus of the first part of this dissertation.

1.2.3 Continuing Scope of Work

A logical extension of the TBI program would be to explore methods focused on enhancing the seismic performance of tall buildings, both existing and new structures. This is especially a rewarding area for continued research considering the ever-increasing interest in community/city resilience. Tall buildings play a special role in an urban community given their own characteristics and their interaction with surrounding structures and spaces. The seismic performance and resilience of individual tall buildings can have a critical impact on the overall community resilience. Thus, a potential third phase for the TBI program could explore methods for enhancing the seismic performance and resilience of tall buildings. This dissertation presents pilot investigations that might provide the initial blueprint and/or stimulus for Phase 3 of TBI.

1.3   OBJECTIVES AND SCOPE

The overall objectives of this dissertation are to assess the ability of various Performance-Based Earthquake Engineering (PBEE) methodologies to identify seismic deficiencies in existing tall buildings, and to explore the use of supplemental energy-dissipation devices and modern computer-aided engineering tools to improve the safety and performance of existing and new tall buildings. As such, this research: (a) investigates the capabilities of supplemental energy-dissipating devices, in particular, fluid viscous dampers, to improve the seismic performance of an existing tall building; (b) identifies cost-effective methods to reduce the post-event repair cost, business interruption loss, and achieve enhanced seismic resilience for an existing as well as for a new tall building; and (c) develops an automated computational tool to optimize the design of supplemental energy-dissipation devices in a tall building in a simplified PBEE framework.

The scope of the studies presented herein is as follows:

- Provide a preliminary overview of past work on seismic retrofit methods for existing tall buildings;

- Select a representative existing tall building for a case study, conduct comprehensive structural analyses, and assess its seismic performance using available standards for seismic evaluation, such as ASCE 41-13 [ASCE 2013], as well as advanced PBEE methods, such as FEMA 351 and FEMA P-58 [FEMA 2000b, FEMA 2012a-2012c];

- Examine the feasibility and cost-effectiveness of upgrading the case-study building to achieve a targeted retrofit goal using different supplemental energy-dissipation devices and other methods, and identify the most effective means of improving the seismic performance of the case-study or similar existing tall buildings;

- Develop an automated tool to streamline the design efforts and identify optimal design patterns of fluid viscous dampers to achieve a targeted performance goal for an existing tall building;

- Select a new tall building for a case study, and assess the effectiveness and efficiency of the automated damper design procedure to achieve enhanced resilience in newly-constructed tall buildings; and

- Propose procedures to design fluid viscous dampers in tall buildings for practical applications; and

- Recommendation of topics suitable for future research.

1.4   ORGANIZATION OF DISSERTATION

In order to achieve the research objectives and scope described in Section 1.3, a series of analytical studies were conducted on two case-study buildings: one representing an existing tall building, and the other representing a new tall building. In both cases, the state-of-the-art simulation tools were used.

Chapters 2 through 5 focus on improving seismic safety and performance of an existing tall building by different retrofit strategies. Chapter 2 presents a brief literature review with regard to the various retrofit strategies used in engineering practice.

One representative case-study building is identified in Chapter 3. The building information and several seismic vulnerabilities of the building in its as-built conditions were reported in Lai *et al.* [2015] and are summarized in this dissertation for the convenience of the readers. A preliminary Level-1 retrofit method is presented and discussed.

In Chapter 4 and Chapter 5, a Level-2 retrofit is investigated to augment the measures taken in level-1 retrofit. As a performance goal, the complete two-level retrofit strategy targets collapse prevention under a basic safety level 2 earthquake event per ASCE 41 [2013]. Level-2

retrofit plan considers three types of passive energy-dissipation devices in addition to the strategies adopted for the Level-1 retrofits, including: fluid viscous dampers (FVDs), viscous wall dampers (VWDs) and buckling restrained braces (BRBs). Among these three, the strategy incorporating FVDs is considered as a most promising retrofit solution, and is thus investigated first and presented in Chapter 4. A comprehensive literature review is provided to understand the development and mechanical properties of each type of device. Design considerations, such as proper locations for installation, the overall effective damping ratio and mechanical parameters of dampers, are selected. A simplified manual optimization procedure is proposed to refine the size and location of the dampers. Several design issues of FVDs are raised and investigated. In Chapter 5, the two-level retrofit strategy is expanded to consider the relative effectiveness and economy of two other energy-dissipation devices: VWDs or BRBs. The design considerations for each of these two devices are provided.

In Chapter 6, seismic damage and losses are estimated within the framework of PBEE. Based on the predicted repair costs and duration, a downtime model is used to quantify the business interruption and the total financial losses. Additionally, the benefit of the various retrofits is assessed in combination with the cost of each retrofit strategy, and the cost-effectiveness of different retrofit strategies are compared.

Chapters 7 to 9 focus on developing automated tools to facilitate the optimal design of economical and efficient structures employing energy-dissipation FVDs. A comprehensive literature review on optimization methods, algorithm and optimization ingredients is presented in Chapter 7. The computational efforts between optimization algorithms and their applicability are also discussed. The algorithm, objective function, constraints and design variables used in this study are identified.

Chapter 8 introduces the flowchart used to develop the automated optimization procedure. A simplified PBEE optimization problem for the case-study building is formulated to limit complexity. The automated design procedure is applied to the existing case-study building, and compared with the results of the manual design scheme. A general step-by-step procedure for designing FVDs in an existing tall building is illustrated, with recommended design patterns to arrange and size FVDs in a high-rise steel moment frame.

To further extend the applicability of the proposed automated design procedure, Chapter 9 focuses on a newly-designed tall building that utilizes a mega-brace lateral load-resisting system. The mega-braces incorporate BRBs. The building information and initial structural responses are evaluated. Then, a design supplementing the BRBs with FVDs that arranged in parallel with the BRB elements is investigated. Finally, the automated procedure is implemented in this new building to identify optimal damper arrangement patterns. Design patterns of FVDs in a mega-brace tall steel building is recommended.

Chapter 10 summaries the results of this study and lists topics suitable for further research.

2 Review of Past Seismic Retrofits

2.1 INTRODUCTION

This chapter summarizes the background information related to the assessment of the potential seismic risks posed by older tall buildings in California, and focuses on possible retrofit methods. A detailed review of background work was conducted in a previous report [Lai *et al.* 2015], with participation by the author. Part of the reviewed work is summarized below for the convenience of readers to identify the particular vulnerabilities that might be associated with various vintages of construction.

As part of the previous work, an inventory was compiled of buildings 20 or more stories tall whose construction was completed before 2012. The inventory includes buildings with any type of lateral force-resisting system, revealing that there are 271 existing buildings taller than 20 stories in three major cities of California (San Francisco, Los Angeles and Oakland), with more than 50% of these buildings constructed between 1969 and 1989; steel moment-resisting frame systems are the most prevalent type of building design used during this time period.

Only a few relatively modern buildings have collapsed or partially collapsed in past earthquakes, but considerable damage to structural and nonstructural elements and contents was noted in modern high-rise buildings in response to recent earthquakes (e.g., 2010 Chile earthquake [EERI 2010a], 2010 Canterbury Earthquake [EERI 2010b], 1999 Chi-Chi, Taiwan earthquake [Uzarski and Arnold 2001], and 2011 Great East Japan earthquake [EERI 2012]). Moreover, substantial transient motion and consequent distress to occupants were reported in high-rise buildings located at large distances from the causative fault ruptures during the 2008 Wenchuan earthquake [Liang *et al.* 2009], the 2010 Chile earthquake [EERI 2010a], and 2011 Great East Japan earthquake [EERI 2012]. In addition, the review in Lai *et al.* [2015] noted numerous instances of serious problems related to steel moment-resisting frame buildings from observations following the 1994 Northridge, California, earthquake and 1995 Kobe, Japan, earthquake, including premature brittle fractures of beam-to-column connections and column splices. The occasional poor behavior in these and other buildings, and improvements in science and engineering knowledge underpinning seismic-resistant design have resulted in rapid changes in building codes over the past three decades. Paralleling these activities has been the development of various guidelines for assessing the adequacy of older buildings (e.g., ASCE 41-13 [2013], FEMA 351 [2000], and FEMA P-58 [2012a-2012c]).

The next section reviews seismic retrofit strategies that have been carried out on tall buildings in practice. These provide a starting point to explore the feasibility of retrofitting tall buildings in this dissertation.

2.2   PREVIOUS SEISMIC RETROFIT OF EXISTING TALL BUILDINGS

As noted above, the performance of tall structures to recent earthquakes has revealed a number of design deficiencies that prevent these structures from meeting designated seismic performance objectives by current code. Retrofit techniques that can effectively address these deficiencies in buildings located in highly seismic regions are critical. Several known vulnerabilities of existing tall buildings were reported in Lai *et al*. [2015].

This chapter revisits several major vulnerabilities common in existing tall steel moment frame buildings, with an emphasis on retrofit strategies to address these vulnerabilities. The review will be centered on steel moment-resisting frames, which according to the building inventory mentioned above, represent a large portion of existing tall buildings located on the highly seismic west coast of U.S. Some of these strategies are also suitable to improve the seismic performance of a new structure, and will be discussed.

By the large, commonly observed seismic deficiencies of existing tall buildings can be categorized as follows:

- Global strength: insufficient frame strength;

- Global stiffness: excessive drift ratios;

- Configuration: vertical irregularity and/or plan irregularity;

- Load path: inadequate shear, flexural and uplift anchorage at soil-foundation-structure interface; and

- Component detailing: inadequate "strong-column weak-column" design, inattention to capacity design principles, brittle beam-to-column connections, column splices and panel zones.

Each deficiency could possibly belong to more than one category; however, regardless of which category it is considered, similar mitigation techniques are usually adopted for that deficiency [FEMA 2006a]. Therefore, the emphasis for this review is on seismic retrofit techniques used to address above-listed vulnerabilities. A principal reference considered herein related to seismic retrofit is FEMA 547— *Techniques for the Seismic Rehabilitation of Existing Buildings* [2006a]. Several other professional handbooks or research publications in the literature were also used [Bruneau 2005; Menon and Sengupta 2007; FEMA 2006b; Kabeyasawa 2005; Sarno and Elnashai 2002]. A few engineering applications will be presented for illustration.

2.2.1 Add New Elements

The steel moment-resisting frame is one of the most commonly used lateral force resisting systems for existing tall buildings in the U.S. What characterizes this system is its flexibility,

which tends to result in large story drift ratios. Braced frame or shear walls, in comparison, are relatively stiff and strong. Thus, converting a few moment frames into brace frames, and/or adding concrete shear walls or steel plate shear walls might be a viable solution to increase the global strength and stiffness of an existing tall building. Another strategy is to add new columns in the middle of a bay, resulting in a moment frame with more bays having shorter spans; although easier, it is generally less effective in adding stiffness and strength than the other methods.

There are several design considerations that should be taken into account for all retrofit measures in this category, including selecting proper locations to add new elements, minimizing the interference with structural and nonstructural components, and so on. Coordination with architects and multiple construction trades on site should not be overlooked or underestimated regardless of the methods used.

Add braced frames

The addition of new brace frames or new braces in existing moment frames would increase stiffness and strength without significantly increasing structural mass. This method is believed by many to be the most cost-effective alternative and has been applied widely. Figure 2.1 shows the percentages of three major types of seismic devices used in high-rise steel buildings in Japan, where buckling restrained braces (BRBs) constitute 46% of the total [Xie 2005]. A more detailed examination of using BRBs is discussed in Chapter 4.
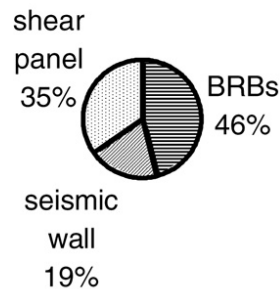
Figure 2.1   Percentage of three types of devices used in high-rise steel building in Japan (adapted from Xie [2005])

Figure 2.2 shows a few examples where exterior braces were added to stabilize some buildings at UC Berkeley campus against lateral movement during earthquakes [Comerio *et al.* 2006]. Nevertheless, while this approach is attractive from the perspective of minimizing disruption to the interior of a structure, seismic demands on existing beams, columns, and connections might increase due to the shortened structural periods, and connection of the exterior braced frames to the structure may involve large force transfers. Thus, further checks of the adequacy of existing members and load paths are necessary.

Adding new braces to existing moment frames to convert them to braced frames may be effective and economical. This approach utilizes the existing strength and stiffness of the frame members, connections, and foundations, but the forces in these members in a braced bay may be significantly increased due to the forces developed in the braces. In terms of disruption, adding

braces to interior frames may make continued occupancy difficult due to the noise or logistical issues arising from construction workers accessing occupied spaces, temporary removal of the nonstructural elements, etc.

(a) Retrofit of Hildebrand Hall at UC Berkeley (b) Retrofit of University Hall of UC Berkeley

Figure 2.2   Applications of adding brace members in existing buildings at UC Berkeley campus (adapted from Comerio et al. [2006])

Add reinforced concrete or steel plate shear walls

An alternative of adding braced frames is to incorporate concrete shear walls or steel plate shear walls to increase the strength and stiffness of an existing structure. Adding concrete shear walls to an existing building may be expensive and disruptive and introduces additional mass, thereby increasing the force demands. Steel plate shear walls are lighter and take up less space. Moreover, steel plate shear walls avoid the need for formwork and pumping concrete, which may make installing them in the interior of tall steel buildings particularly feasible. The major drawback to using either of these shear wall systems is that it is necessary to provide new foundations or other systems (backstays) to resist the overturning moments developed by the new walls (these may significantly increase the difficulty and cost of this type of retrofit). If new walls are added in the interior frames, this might cause a significant impact on the occupants.

Figure 2.3 shows the retrofit scheme of Burrows Hall at UC Berkeley campus by jacking both ends of the building using concrete shear walls [Comerio *et al*. 2006]. Steel plate shear walls have been used in retrofit low- to median-rise hospitals and other buildings [Astanel-A. 2000]. Figure 2.4 shows the retrofit of a critical care facility in Los Angeles using steel plate shear walls to meet higher standards of California Building Code after it was damaged after the 1994 Northridge earthquake [Love *et al.* 2008].

(a) New jacketing scheme on east and west side of Barrows Hall
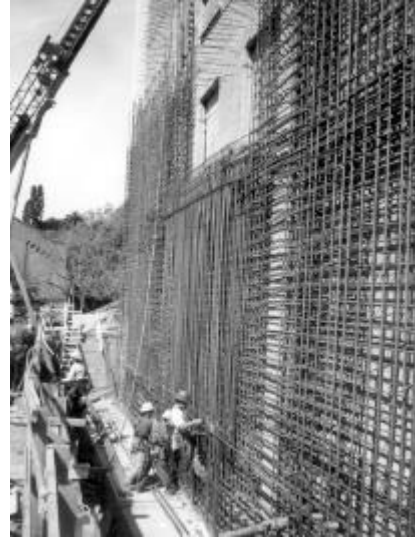
(b) Installation of rebars for new shear walls

Figure 2.3   **Retrofit of Barrows Hall at UC Berkeley campus (adapted from Comerio et al. [2006])**

(a) Exterior view
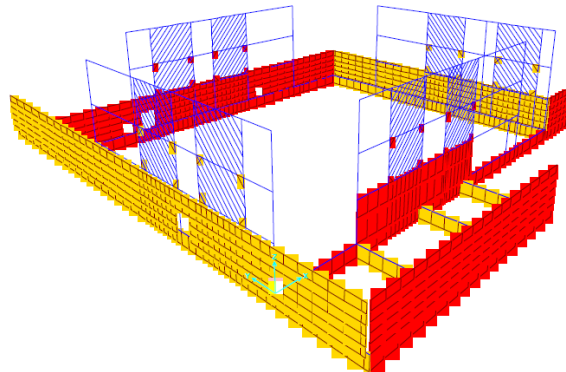
(b) Numerical model of the building in SAP 2000

Figure 2.4   **Retrofit of a critical care facility in Los Angeles with steel plate shear walls (photo source: Google Map (left); Love et al. [2008] (right))**

2.2.2 Enhance Existing Elements and Improve Connections between Elements

Deficiencies at the local level can be mitigated to reduce their impact on the integrity of the whole structure. In a tall moment-resisting steel frame building, fragile columns and beams, and brittle column splices or beam-to-column connections are the most common examples of seismic vulnerability that can be addressed at local level. Several common strategies to mitigate these vulnerabilities are addressed below. Design considerations and cost factors are discussed, and example projects where these methods have been applied are presented.

Utilize strength and stiffness of existing steel gravity load framing

The "gravity-load only" framing in a structure where moment resisting frames are used for lateral load resistance provide only a small fraction of the lateral stiffness and strength of the structure. However, this gravity framing can have a large impact on the ultimate capacity of the system once yielding commences, especially in structures where soft-story mechanisms develop. Thus, evaluation methods [FEMA 2000a-2000b] recommend incorporation of "leaning columns" to account for the stiffness and strength of the columns that are part of the gravity load resisting system. More refined models of the gravity load resisting system, where the partial rigidity of pinned beam to column connections can be modelled considering the partial composite action of the floor slab and shear tab connections, have been found to be beneficial in improving the seismic response of older steel moment frame buildings (Liu and Astanel-A. 2000; Flores *et al*. 2012]. These gravity framing elements are shown to enhance the safety of many types of existing moment resisting frame structures.

Miranda *et al*. [2014] and Judd *et al*. [2015] proposed using enhanced gravity load framing connection details to improve overall seismic performance. These techniques enable the gravity load system to contribute to the lateral load resistance of the structure, and can be used for existing and new construction. A side bonus of this strategy is that it does not significantly alter the architectural character of the building. If a large number of gravity connections are changed, the increase of stiffness and strength could be large. The costs associated with this strategy will largely rely on the total number of connections that require fixing, the complexity of the detailing, and for existing buildings, the architectural furnishings that need to be removed and replaced.

Enhance beam-to-column connections

In response to the poor performance during the 1994 Northridge, California, earthquake, several techniques have been proposed to enhance the ductility of welded beam-to-column connections in welded steel moment-resisting frames. Techniques used include: (a) removing vulnerable brittle welds and replacing them with notch tough weld consumables and improved details; (b) introducing a weakened region away from the face of the column (reduced beam section); or (c) strengthening the beam near the face of the column by adding cover plates, welded haunches or rib plates; see Figure 2.5 for commonly used strengthening methods. These retrofit strategies were mostly able to achieve ductile behavior for existing connections, with a minimum plastic rotation of the 2% under cyclic loading [FEMA 2000b; Chi *et al.,* 2006; Gross *et al.,* 1999; Blaney *et al*., 2010; and Newell and Uang 2006].

One existing steel moment frame in Okaland: Caltran District 4 office building, was retrofitted by Degenkolb Engineers, Inc., by using a connection-strengthening-plus-damper scheme [Malley *et al.,* 2009]; see Figure 2.6. This scheme was selected as the most cost-effective among four candidate solutions. In this project, 746 beam-to-column connections (61% of the total connections) were modified using several strengthening methods such as single-welded haunch, double-welded haunch, gusset plate and haunch, and bolded bracket etc. The selected locations to upgrade connections were kept consistent with the locations for damper installation to minimize work disruptions to occupants. Additionally, project specific tests were conducted to validate the proposed connection behaviors given the limited test results for deep column sections and large beam sizes.

(a) Reduced beam section   **(b) Haunches**

(c) Cover plates   **(d) Rib plates**
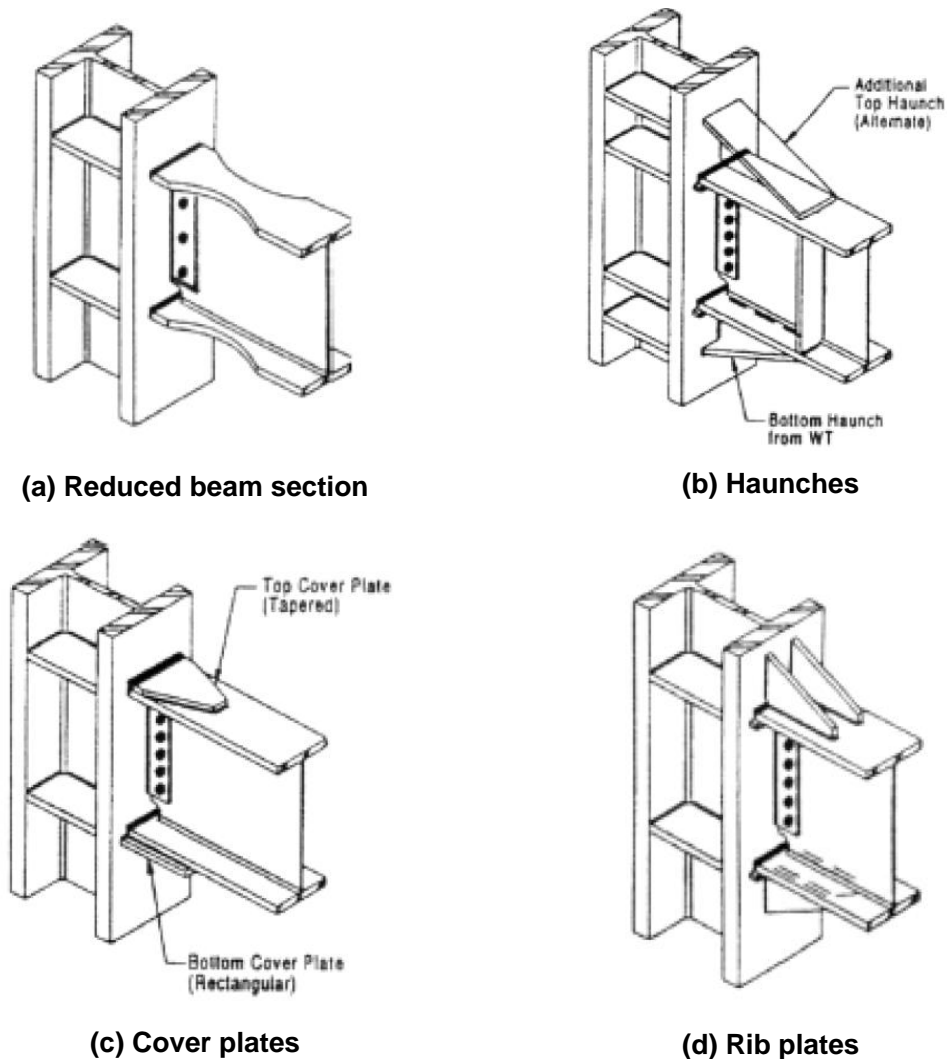
Figure 2.5   Different types of beam-to-column connection strengthening (adapted from Sarno and Elnashai [2002])

Such connection modifications may disrupt occupants near the locations where each connection is fixed. In addition, each connection retrofit is costly and the accumulated costs of repairs over many connections could be significant. This strategy was investigated in Lai *et al*. [2015], where every brittle pre-Northridge beam-to-column connection was fixed for a case-study building; whereas this strategy was not as cost-effective as other alternative approaches. Moreover, Krishnan and Muto [2011] demonstrated that once a certain fraction of beam-to-column connections were retrofitted, additional beam-to-column connections achieved little further improvement of performance.

Figure 2.6   Caltrans District 4 office building after retrofit (photo courtesy of Degenkolb Engineers, Inc.)

Add steel side plates to connections or to columns

A proprietary detail suggested to improve beam-to-column connection deformability is the SidePlate Connection. In this case, cover plates are added to the top and bottom of the beam flanges and matching side plates are added to the columns. These are generally joined using fillet welds. In existing buildings, these details reinforced the region around the connection, moving the plastic hinge location away from the critical weld at the face of the column and improved the flow of stresses from the beam to the column. Figure 2.7 shows an example of improving brittle pre-Northridge beam-to-column connections using side plates and cover plates.

In some tall steel buildings, typical rolled or built-up wide flange sections might not have adequate axial or flexural strength. In such cases, steel cover or side plates can be added to increase flexural, shear and axial strength. In addition, the cells created by side plates can be filled by concrete to further increase axial strength and stiffness. Note: this approach introduces construction difficulties where beams and columns intersect.

Issues related to such vulnerable columns are discussed in more detail in Section 4.4.1 for a situation occurring in the case-study building. A possible upgrade method is examined, where side plates are added to existing wide-flange section columns, and filled with concrete.
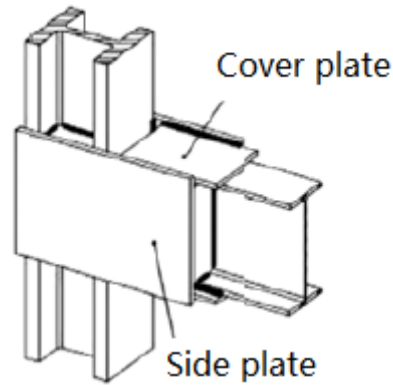
Figure 2.7   Upgrade of Pre-Northridge beam-to-column connections using side plates (photo courtesy of SidePlate System, Inc.)

Enhance column splices

Seismic retrofits of pre-Northridge steel moment-resisting frames have been largely focused on beam-to-column connections. The lack of observed column splice failures after the Northridge earthquake might be due to (1) the premature failure of the beam-to-column connections, which limited the axial and bending forces that could be developed at the splices, and (2) the relative moderate level of shaking felt by the damaged steel buildings in Los Angeles. However, a study by Nudel *et al.*, [2015] demonstrated the potential for column splices failures, highlighting what could be a significant problem that needs to be addressed.

The options to upgrade column splices depend on the splice types. In older tall steel moment-resisting frames, column splices were usually welded either in the form of complete joint penetration (CJP) or partial joint penetration (PJP). PJP welds are vulnerable to brittle fracture due to the unpenetrated region of the section acting like a crack defect when the section is loaded in tension. This can be alleviated by welding plates or stiffeners across the splice areas, or more commonly by removing the existing PJP weld and replacing it with a CJP weld made from a notch tough consumable. Special considerations should be accounted to avoid undesired concentration of stresses in the welded areas. The cost and disruption of this method are similar to upgrading or repairing other type of connections.

Figure 2.8 [Panian *et al.,* 2015] shows one example where all potentially brittle column splices were fixed in a 17-story steel moment-resisting frame located in San Francisco. Here access was limited so it was difficult to replace the PJP welds, and plates were added parallel to the column webs to help tie the upper and lower portions of the column together in the event of a brittle bending failure. Fixing fragile column splices often means incorporating other methods in tandem. Because the integrity of columns is essential to maintaining structural stability under

seismic excitation, fixing fragile column splices is used as a preliminary retrofit strategy for the case-study building presented in Chapter 3.

(a) Building after retrofit

(b) Fix column splices with added plates: before retrofit (left) and after retrofit (right)

Figure 2.8   Upgrade column splices of a 17-story steel moment frame in San Francisco (adapted from Panian et al. [2015])

Enhance the connections of steel column to the foundation and/or strengthen foundation

Insufficient connections between column base plates and foundations is another common vulnerability. Examination of structural drawings from a few existing buildings constructed in San Francisco in the 1970s revealed that it was not common practice to weld columns to the base plate. Moreover, anchor rods were consequently not used to connect the base plate and foundation [Lai *et al*. 2015]. Several studies have been done that suggest limited uplift or rocking of foundations, or uplift of column bases from the foundation may be acceptable [Espinoza and Mahin 2012; Antonellis and Panagiotou 2014].

15

However, it may be necessary to enhance the tensile, compression or shear capacity of the connections of steel columns to the foundation; methods for modifying the base of the column need to be explored. Adding anchor rods, welding shear lugs to base plate, enlarging the base plate, or encasing columns in a concrete pedestal above the footing are feasible techniques to ensure adequate transferring of tensions, shears, and moments from columns to foundation. Figure 2.9 shows an example to weld the stub to a base plate and erected it using anchor bolts embedded into a concrete foundation. Correspondingly, a foundation upgrade would be needed to ensure the adequate load transfer. Enhancing the foundation is usually included when other retrofit strategies are implemented, because additional forces are generated by the newly added braces, walls etc. Figure 2.10 is a retrofit project of a school in Monthey, Switzerland [FOEN 2008], where the foundation was expanded. To resist the overturning moments, the foundation of the elevator shafts was secured to the soil with twelve micro-piles. The cost of implementing this strategy was smaller than upgrading an overall lateral force-resisting system or an entire foundation, and the disruption was much less since only the basement level would be involved.

Figure 2.9   **Retrofit of column to foundation connection by welding plates (source: https://www.sefindia.org/forum/files/baseplate_364.jpg)**

| (a) Rear façade after retrofit | (b) Construction of foundation with micro-piles |

Figure 2.10   Extending foundation of a school building (adapted from FOEN [2008])

2.2.3 Reduce Seismic Demand

In addition to improving the strength, stiffness, or ductility globally or locally, it may be possible to reduce demand. There are several ways of doing this, including reducing the weight of a building, or adding protective systems such as seismic isolators or supplemental energy-dissipation devices.

Reduce seismic weight

For those tall buildings that are both flexible and heavy, reducing the seismic weight by removing several top floors or replacing heavy concrete cladding with light curtain walls may be an economical and practical strategy. Due to a shortened structural period, the displacement response could be reduced, but it is worth noting that the peak ground acceleration could be increased. Figure 2.11 shows a 12-story steel frame that underwent a voluntary seismic upgrade, where the exterior precast concrete façade was replaced by a new high-performance glazed curtain wall system. In cases where a medium- to high-rise building experienced a mid-level collapse in an earthquake event, a rapid and efficient retrofit scheme involved removing the upper stories. Figure 2.12 shows the No.2 Kobe City Hall, an 8-story building that collapsed at the 6th floor during 1995 Kobe, Japan, earthquake. The 6th, 7th and 8th floors of the building were removed, and it was back in use by March 1996. Another example building: Library of Central Bank of Nicaragua (Figure 2.13) was retrofitted by removing 15 damaged floors after the 1972 Nicaragua earthquake, and retained the government offices at the basement level.

The disruption and cost of these approaches may be considerable, but might be mitigated in cases where occupancy or use of a building changes and the building will be unoccupied during the construction activity, or other cases that require extensive internal and/or external architectural modifications. In addition, if the exterior concrete cladding is removed, seismic upgrades to connections and the addition of shear walls, bracing schemes and supplemental

energy-dissipation devices would be more convenient. This method was investigated in Lai *et al.* [2015] for the case-study building reported herein and adopted as an effective preliminary retrofit strategy; refer to Chapter 3.

| (a) Original concrete façade | (b) New high-performance glazed curtain wall system after retrofitting |

Figure 2.11   Retrofit of 680 Folsom building in San Francisco (photo courtesy of SOM, Inc.(left) and Cesar Rubio (right))

| (a) Mid-story collapse in the 6th floor | (a) Removal top 3 floors after earthquake |

Figure 2.12   Retrofit of Kobe City Hall after Kobe, Japan, earthquake (source: Kobe University Library, retrieved from http://japanpropertycentral.com/2016/02/kobe-to-redevelop-no-2-city-hall/)

(a) Central Bank of Nicaragua before the earthquake	**(a) Remaining government offices after removing damaged upper floors**

Figure 2.13   Retrofit of Central Bank of Nicaragua after 1972 Nicaragua, earthquake (source: Skycrapercity.com, retrieved from: http://www.skyscrapercity.com/showthread.php?t=489808)

Incorporate seismic isolation

A more widely used method to reduce seismic demands in an existing building is to use a seismic isolation system. This technology is widely applied to low- and medium-rise buildings. For a relatively tall and flexible building, this system is generally considered less effective. Moreover, it would be difficult to introduce a seismic gap within a large building in order to install isolation at base. Given the relative high costs and complicated design procedure, the application of base-isolation has been mainly limited in the U.S. to important historical buildings. One project of note is the national landmark Beaux Arts City Hall in San Francisco, California (Figure 2.14). The 83-year-old historical building was preserved with a total of 530 lead-rubber bearings. Other federal or historical buildings upgraded with base isolations include the Los Angeles City Hall, San Francisco Asian Art Museum, Oakland City Hall, and the Martin Luther King Jr. Civil Center, to name a few. Among these, the 23-story Los Angeles City Hall (Figure 2.15) is the tallest building being base-isolated so far in the United States [Youssef and Hata 2010].

In designing isolation systems, special considerations should be given to minimize the tension in bearing. While the cost to implement isolations, and remove structural/non-structural components at selected levels and reworking of the base would be large, the modifications needed for upper stories may be relatively minor. That said, this option has limitations for implementation in existing buildings since it might introduce substantial changes to the architectural components, elevators, stairs, and utilities. In addition, if one or more stories above the isolation plane were ungraded, then all columns below the isolation plane would be expected to experience large bearing lateral displacements and high axial loads would be likely, as well as extra moments induced by P-Δ effects. Special consideration should be given when implementing isolation systems in an existing building.

19

(a) Implementing base isolation

(b) Isometric view of San Francisco City Hall after retrofit

Figure 2.14   **Retrofit of San Francisco City Hall (photo courtesy of Sheedy Drayage Co. (left) and Forrel/Elsesser Engineers, Inc. (right))**

(a) Flat sliding bearings

(b) 23-story Los Angeles City Hall

Figure 2.15   **Retrofit of Los Angeles City Hall (photo courtesy of Nabih Youssef Associates, Inc.)**

2.3   CONCLUDING REMARKS

Steel moment-resisting frame systems comprise of a majority of tall buildings constructed in California prior to 1990. These older buildings have a variety of vulnerabilities as demonstrated

by their response in past earthquakes. In particular, steel moment-resisting frame systems are vulnerable to brittle fracture of beam-to-column connections and column splices. The rapid advancement of evaluation methods and more modern and complex analysis methods has made assessing the adequacy of older tall buildings, especially tall steel moment-resisting frame buildings, possible. A detailed examination of possible upgrade solutions to steel moment resisting frames was presented in this chapter, with a focus on traditional upgrade methods used in practice. The pros and cons of each strategy were evaluated and examples of retrofit applications presented. Some of these applications will be selected as preliminary retrofit plans for a case-study existing building. Other retrofit strategies that utilize supplemental energy-dissipation devices will be reviewed and examined in Chapters 4 and 5.

3 Evaluation and Preliminary Retrofit of a Case-Study Building

3.1 INTRODUCTION

It is theoretically impossible to select a case-study building that represents the entire inventory of existing tall buildings so that all potential seismic deficiency issues can be investigated comprehensively. Consequently, an inventory of tall buildings gathered in a previous study [Lai *et al.* 2015] was examined, and several representative buildings were identified as a starting point. Because buildings in the database range from 20 to more than 50 stories, and the majority from the time period of interest are welded steel moment-resisting frames, the first building selected for evaluation is a 35-story tall steel building in downtown San Francisco having welded steel moment resisting frames for both vertical and lateral load resistance, designed by a well-known and highly respected structural engineering firm. A thorough evaluation of the building's likely performance is performed when subjected it to earthquake shaking corresponding to hazard levels used in typical seismic evaluations. Seismic deficiencies are identified, and a two-level seismic retrofit is designed and evaluated.

The primary evaluation procedure used in this study is ASCE 41-13, *Seismic Evaluation and Retrofit of Existing Buildings* [ASCE 2014]. This procedure is a nationwide standard for evaluating and retrofitting as-built structures, and has been adopted by reference as part of the California Building Code [CBSC 2014]. Today, ASCE 41-13 is widely used, just as ASCE 7-10 [2010] for the design of new buildings. ASCE 41-13 integrates two previous standards (i.e., ASCE 31-03 [ASCE 2003] and ASCE 41-06 [ASCE 2007]), so that it is applicable to both seismic evaluation and the design of retrofit measures. Although not intended for the design of new construction, ASCE 41-13 indicates that it can be used in the design of new buildings that are not covered by ASCE 7, or are to be designed to performance criteria other than the minimum criteria of ASCE 7.

In addition, the older, but more probabilistically oriented procedures in FEMA 351 *Recommended Seismic Evaluation and Upgrade Criteria for Existing Welded Steel Moment-Frame Buildings* [FEMA 351, 2000a] is used to estimate the confidence with which standard performance objectives could be achieved. Lastly, estimates of likely damage repair costs, downtime, and business interruption losses for a generic business occupancy are obtained for the case-study building using the procedures in FEMA P-58 *Seismic Performance Assessment of Buildings* [FEMA P58, 2012a-2012c].

In each of these evaluations, two sets of ground motion records corresponding to two earthquake hazard levels are used. These are defined according to ASCE 41-13 as basic safety earthquake (BSE) hazard level 1 and level 2, and denoted as BSE-1E and BSE-2E, respectively. For existing buildings, the BSE-1E events have a mean return period of about 225 years, while the BSE-2E events have about a 975-year mean return period.

Many of the results presented in this chapter are similar to those resulting from the previous study of this building [Lai *et al*. 2015]. However, in several cases the results have been updated based on more refined modeling assumptions. The basic findings of this and the previous study are similar. The summary results presented here provide essential background materials needed to understanding subsequent refined studies of retrofit measures.

3.2   CASE-STUDY BUILDING

3.2.1 Building Description

The existing case-study building considered is a 35-story tall steel office tower located in San Francisco, California. Its construction began in 1968. The tower is about 185 ft × 135 ft in plane, and 490 ft in height. The typical beam span is 36 ft, and typical floor height is 13 ft. The building is constructed over three basement levels. A full moment-resisting framing system is provided in both principal directions of the building as the vertical and lateral load-resisting systems. Figure 3.1 shows an isometric view of the building, along with an elevation view of one frame and a plan view of a typical floor. Typical dimensions are indicated in this figure. Columns constitute built-up wide flange and built-up box sections. As noted in Figure 3.1(c) columns are not placed at the intersections of all beam-grid lines.

The steel frame members consist of both built-up and rolled sections. Typical member sizes for one exterior frame are listed in Table 3.1, with section sketches and dimension notations illustrated in Figure 3.2. It is important to note that many of the built-up structural elements used in the case-study building are unable to fully develop their flexural yield capacity because of the undersized welds used to connect the beam webs and flanges. Thus, these welds may yield or fail in shear before flexural plastic hinges can form at the ends of the members. This mode of behavior is not well understood, and is ignored in the analysis models and results presented in this dissertation.

A 6-in.-thick normal-weight concrete slab rests on top of a metal deck at each floor. Very limited reinforcement is provided to attach the metal deck and slab to the supporting girders. Thus, composite action is not considered in the analyses reported herein.

Welded beam-to-column moment connections used were those typical of buildings built prior to the Northridge earthquake. Wide-flange beam-to-column connection details are shown in Figure 3.3. While the strength of the welds is specified as E70, the welding procedure and the notch toughness rating of the electrodes used are not known. These types of connections are considered very brittle based on field observations and laboratory tests conducted after Northridge earthquake [FEMA 2000b].

Column splices were erected using partial joint penetration (PJP) welds, located 5 ft above the floor level. A representative detail for a wide flange column splice is shown in Figure 3.4. The width of such PJP welds range from a quarter to a half of the thickness of the flanges or webs for the members being joined and are not expected to be able to develop the nominal capacity of the net welded section because of fracture mechanics considerations [Bruneau *et al*. 1987].

Framing irregularities occur at the ground level due to an extra-tall story at the base of the building that includes a mezzanine floor on one side of the building. This can be seen schematically in Figure 3.1(a).

The building's foundation consists of a 7-ft-thick mat located 40 ft below grade. The columns simply rest on the top side of the mat foundation. There is no weld or tension capable attachment of the column to the base plate, or of the base plate to the foundation.

The perimeter of the building is sheathed in heavy cladding made from concrete attached to slabs of natural stone. These cladding panels add considerable weight and mass to the structure, but not significant stiffness or strength.

Member sizes, structural detail drawings, foundation details and other information were collected from the building owner and the City of San Francisco's Department of Building Inspection.

| (a) Perspective view (basements not shown) | (b) Typical frame elevation (X-dir.) | (c) A typical floor plane |
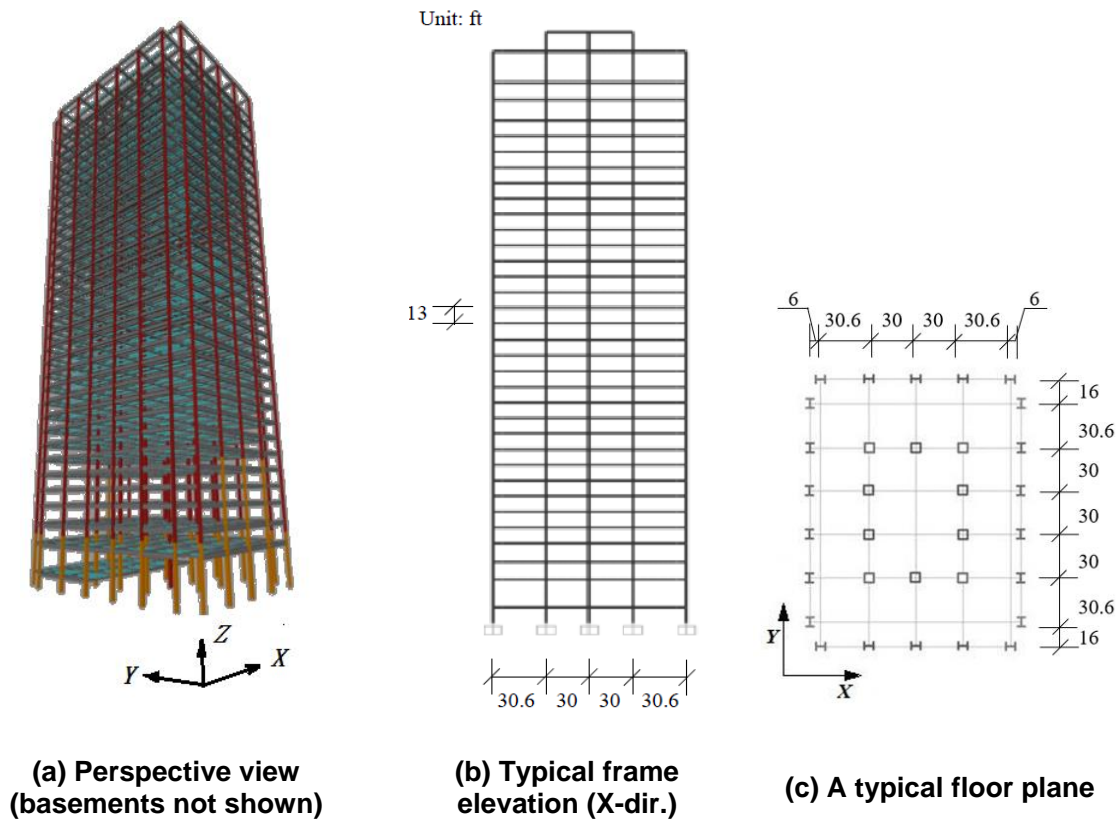
Figure 3.1   Illustration of building model (unit: ft)

Table 3.1   Typical element sections of an exterior frame (unit: in)

Floor level	Exterior bays		Interior bays	
	Columns	Girders	Columns	Girders
Sub~3	24x24 H[1] 4x4	W 18x50 W 36x135	26x36 HBox 4x2	36x22 G 2x0.5 48x22 G 3x0.75 W 36x260
3~9	24x24 H 3.5x1.5	42x22 G 2.25x0.75 36x22 G 1.5x0.5	26x24 H 4x2	42x22 G 2.25x0.75 36x22 G 1.5x0.5
9~33	24x24 H 3.0x1.5 24x24 H 2.5x1 24x24 H 2.0x1	36x22 G 1.5x0.5	26x24 H 3.5x1.5 26x24 H 3x1.5 26x24 H 2.5x1.5	36x22 G 1.5x0.5
33~roof	24x24 H 1.5x1	W 36x135	16x22 Box 0.875	W 36x135

[1] Section notations are illustrated in Figure 3.2

Notation: $W \times D$ **Box** t

(a) Box-section columns

Notation: $W \times D$ **H** $f \times t$

(b) H-section columns

Notation: $D \times W$ **HBox** $f \times t$

(c) HBox-section columns

Notation: $D \times B$ **G** $f \times w$

(d) Built-up girders
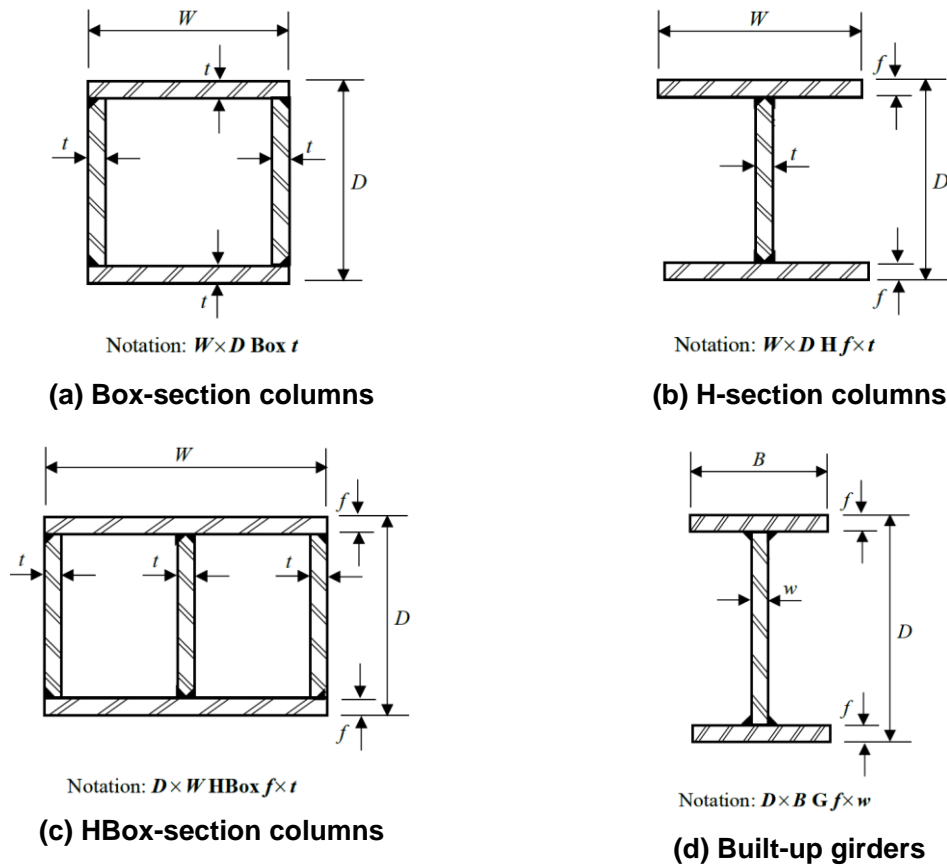
Figure 3.2   Sketch of built-up sections

25
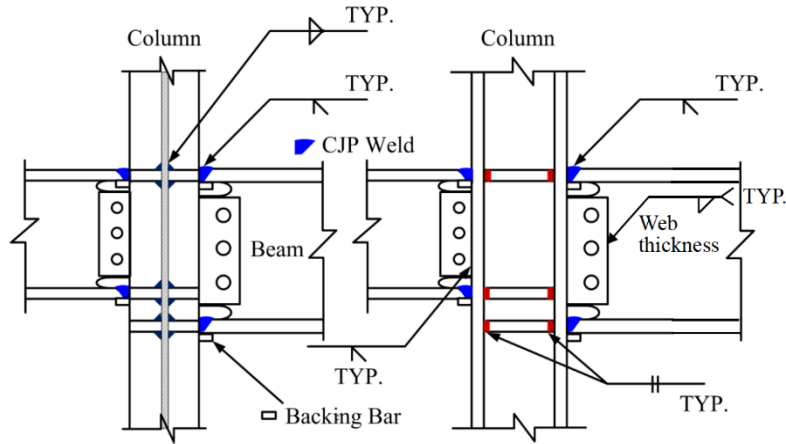
Figure 3.3   Typical beam-to-column connection details
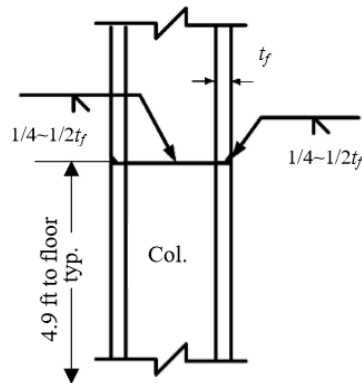
Figure 3.4   Typical wide flange column splice details

3.2.2 Performance Objectives

ASCE 41-13 provides guidance on selecting the Basic Performance Objectives of an Existing building (BPOE). These depend on the Risk Category of the building and the evaluation procedure being used. A Seismic Risk Category of III is selected for this office building, considering its functional importance and the number of occupants. According to ASCE 41, the first two tiers of its three-tier evaluation approach are not needed, and a Tier 3 evaluation based on dynamic analyses is required.

Because of the decision to assign a Seismic Risk Category III to the building, performance exceeding collapse prevention is required. As will be noted subsequently, the as-built structure could not achieve the performance objective targeted for an ordinary building (Seismic Risk Category II; collapse prevention). The BPOE criteria considered for a Seismic Risk Category III building for the ASCE 41-13 Tier 3 procedure are damage control (DC) at the BSE-1E hazard level and limited safety (LS) at the BSE-2E hazard level.

26

3.2.3 Ground Motion Selection and Scaling

Ground motion selection and scaling were completed with the assistance of Professor Jack Baker from Stanford University. Several sets of ground motions at a site very near the case-study building were developed based on various code requirements and probabilities of exceedance. Each set consisted of 20 three-component records. Ground motions were adapted from the PEER NGA West2 database, and no more than five ground motions were taken from any single event. Given the site of the building, ground motions were selected such that the distance to rupture was less than 50 km, the magnitude of the event was 6.5 or larger, and the amplitude scale factor needed was less than 9.

A selection and scaling algorithm was used that resulted in the response spectra for the set of ground motions to match a target mean and variance [Baker *et al.* 2011]. All three components of each ground motion were scaled by the same scale factor. The resulting ground motion selections and scale factors are provided in Appendix A of Lai *et al.* [2015]. Figure 3.5 shows the horizontal response spectra of the selected ground motions and target spectra for the BSE-1E and BSE-2E hazard levels.

(a) BSE-1E   (b) BSE-2E
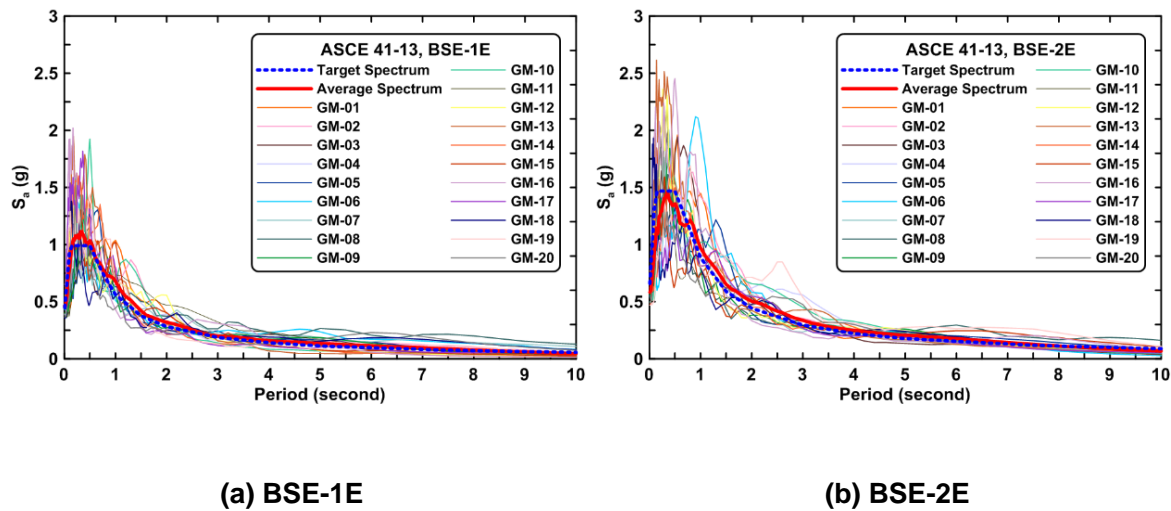
Figure 3.5   Response spectra of selected ground motion records and target spectra with 5% viscous damping

3.2.4 Numerical Modeling

A three-dimensional building model was constructed using the program: Open System for Earthquake Engineering Simulation (OpenSees) [McKenna *et al.*, 2010] to investigate the nonlinear dynamic behavior of the case-study building. All above ground main framing members contributing to the seismic lateral force-resisting systems were included (see Figure 3.1). Given the nature of this investigation, certain modeling simplifications were made: (1) the basement levels were disregarded; (2) a fixed-base boundary condition was assumed at the column bases at the ground level; (3) floor diaphragms were assumed to be rigid in-plane, but the contribution of the concrete floor slabs to the flexural behavior of the beams was not included in the numerical

model; and (4) any contribution of the non-structural elements—including the perimeter concrete façade—to the strength and stiffness of the structure was ignored. Dead loads and 25% of design live loads were included in the models in accordance with ASCE 41-13 and PEER TBI guidelines [PEER 2010a]. Masses were lumped at the joints in proportion to tributary area, considering element self-weight, concrete slab weight, superimposed dead loads, and 25% of live loads.

Columns were modeled using displacement-based nonlinear beam–column elements with fiber sections at five integration points along the length of each element. Each web or flange of a column section was discretized into four layers along its depth and four layers along its thickness. A Giuffré–Menegotto-Pinto material model with isotropic strain hardening (*Steel02*) was used to define the fiber materials. The expected steel material strength was estimated as the multiplication of the nominal strength and modification factor per ASCE 41-13. The use of fiber section models automatically accounted for *P-M-M* interaction. Shear and torsion properties were aggregated into each section using an ideally elastic component. Column splices were modeled by zero length elements. To simulate the brittle fracture of column splices, a fracture material model was used for each splice in combination with a maximum permitted tension strain derived from a simplified fracture mechanics model [Stillmaker *et al.*, 2016].

Beams were represented as single line elements following a formulation proposed by Ribeiro *et al.* [2015]. Six integration points were introduced along the length of the beam, with each plastic hinge taken 1/6 of the beam length (Figure 3.6). Interior integration points were assumed to remain elastic. With these assumptions, the moment of inertia of the beam need not be adjusted to produce the correct elastic flexural stiffness of the member [Ribeiro *et al.* 2015]. The moment-curvature behavior for a plastic hinge was modeled using the hysteresis material model in OpenSees, with the defining backbone curve (right part of Figure 3.6) based on ASCE 41-13 modeling recommendations. In many cases, ASCE 41-13 recommendations resulted in quite small or "zero" plastic rotation capacities for the connections in the case-study building.

Panel zones were not explicitly modelled in the current study. Rather, center-to-center elements models were used, as permitted by FEMA 451 [FEMA 2006c].

Rayleigh viscous damping was assumed, with coefficients derived assuming the first- and 24th-mode critical damping values both equal to 1.71 % ($\alpha/N = 60/35$), according to the Equation 2-10 in *PEER Report 2010/111* [PEER 2010b]. As a result, the mass-proportional and stiffness-proportional coefficients are 0.04731 and 0.00165, respectively. The initial stiffness is used in generating the damping matrix.

A limitation of the numerical model used is that it did not account for the inadequate web-to-flange welds of many built-up column and beam sections. Yielding or failure of these welds would result in a reduced flexural capacity for many members. In addition, soil–structure interaction effects were not considered in this dissertation. According to ATC-83 report [NIST 2012], the effects of damping and flexibility at the foundation–soil interface are expected to be small because of the building's relatively long fundamental periods.

Modal dynamic properties were computed, and the first three elastic modal periods of the structure were: 4.70 sec (*X*-translation), 4.53 sec (*Y*-translation), and 4.15 sec (rotation about the *Z*-axis).
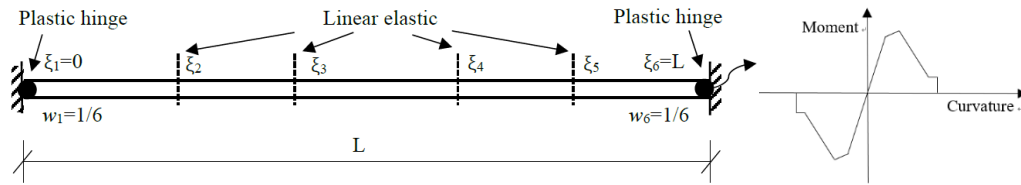
Figure 3.6   Sketch of concentrated plastic hinge model

3.3   STRUCTURAL EVALUATIONS

As mentioned, a three-tier approach is incorporated in ASCE 41-13; with increasingly complex methods used in each successive tier. However, for complex structures like the case-study building, the nonlinear response history analysis (NRHA) procedures of Tier 3 are recommended by ASCE 41, and the Tier-1 rapid screening and Tier-2 deficiency check procedures are not considered necessary. Thus, most of the results presented in this dissertation are thus based on nonlinear time history response analyses. Nonlinear static 'pushover' analysis methods, included as acceptable analysis methods in some Tier 3 evaluations, are not permitted for tall buildings with fundamental periods as long as those of the case-study building, since higher mode responses are expected to be significant and are not directly accounted for in a pushover analysis. Nevertheless, the simpler Tier-1 screening procedures were carried out anyway to help quickly identify critical vulnerabilities, and a simplified Tier-3 pushover analysis was also done to help pinpoint likely failure modes and locations.

The simplified Tier-1 screening identified a number of possible vulnerabilities. Detail checklists, shear capacity checks, and weld capacity checks carried out in accordance with Tier-1 procedures are presented in Appendices B, C, and D of Lai *et al.* [2015]. The vulnerabilities identified include:

- A potential weak story at the mezzanine level;
- Brittle "pre-Northridge" beam-to-column connections;
- High column tension and compression stress levels;
- Modern strong column−weak beam requirements not satisfied;
- Inadequate anchorage of column bases to the foundation;
- Welds used in some built-up sections insufficient to develop member flexural capacities;
- PJP welds at column splices regions inadequate to develop significant net tensile loads.

Special attention was placed in the studies reported by Lai *et al.* [2015] to either capture these and other possible deficiencies in the structural system or to bound their effects.

3.3.1 Nonlinear Pushover Analysis (Nonlinear Static Analysis)

Although not recommended by ASCE 41-13, a nonlinear pushover analysis was carried out for the building. The distribution of lateral load employed in these analyses corresponded to the first-mode shape in each direction, and pushover analysis was conducted for each direction, respectively. Plots of roof displacement versus base shear obtained in the *X*- and *Y*-directions are shown in Figure 3.7, along with the deformed shapes of the building at three different damage states. The peak base shear capacity computed in *X*-direction was about 13,500 kips and 13,700 kips in *Y*-direction, which correspond to 8.7% and 8.8%, respectively, of the total building weight. The design base shear of the building required by the building code at the time of construction [ICBO 1967] was only 2,993 kips or 1.9 % of the building weight. This allowable stress based value is only 45% of the value that would be required according to the load and resistance factor design provisions of ASCE 7-10 [2010], which was about 6650 kips (4.3% of the building weight).

The star symbol marks on the pushover curves in Figure 3.7 designate the roof displacement at the onset of structural yielding. Triangular marks represent the point when the peak base shear is reached. Cross-shaped marks indicate where the seismic response, or numerical simulation become unstable.

The maximum roof displacement attained in the pushover analyses was about only 34 in (or 0.7% of the building height). The response under the pushover loading was initially linear, with gradual softening as the peak base shear was approached. At this point, response was characterized by numerical instability or sudden loss of lateral load capacity. The limited inelastic deformability of the beam-to-column connections, the high axial compression loads in the columns, and the brittle column splices combined with geometric nonlinearities resulted in quite brittle global behavior of the structure that is quite difficult to predict numerically.

The deformed shape of the building at the three cited instances are shown on the right-hand side of the pushover curves. Once yielding occurs, lateral displacements increased rapidly. In the *Y*-direction, an obvious multistory side-sway (weak-story) type mechanism occurred between floors 5 and 10. Because of the sudden loss of strength of the building, many portions of the building unloaded and had smaller story drifts, while drifts between floors 5 and 10 rapidly increased. However, this weak-story trend was not evident in the results shown for the *X*-direction. It is assumed that the deterioration of the structure was so sudden that the simple static pushover analysis model was unable to track the collapse of the structure in this direction.
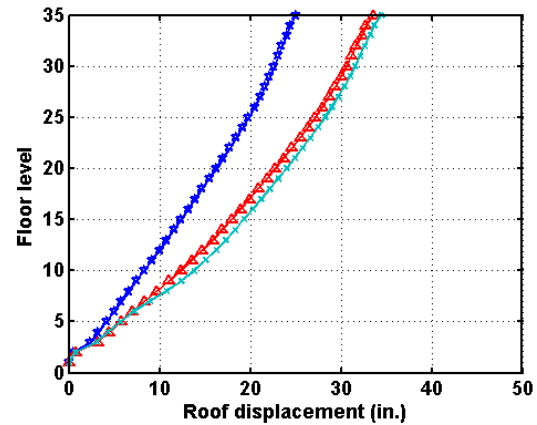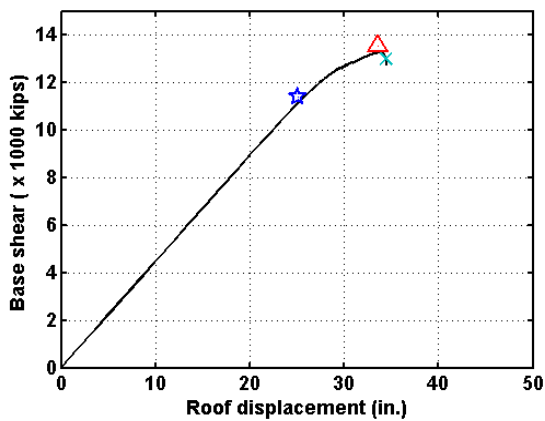
(a) X-dir.
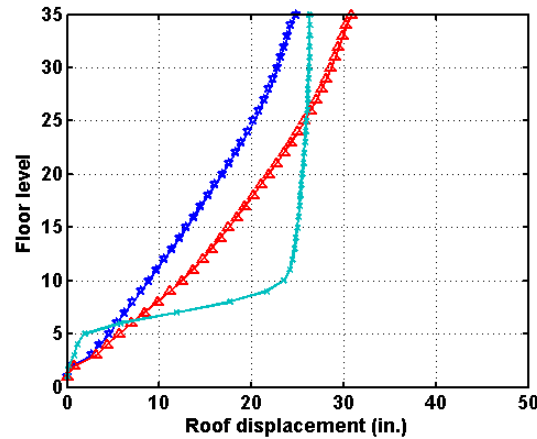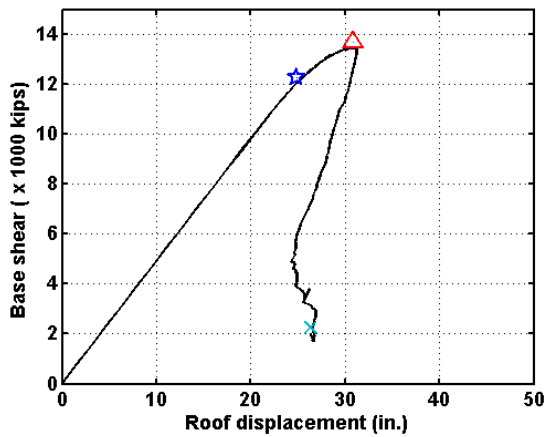
(b) Y-dir.

Figure 3.7   Static pushover curves and deformed shapes

3.3.2 Nonlinear Dynamic Analysis (Tier-3, ASCE 41-13)

Nonlinear response history analyses were performed using OpenSees for the BSE-1E and BSE-2E hazard level events according to recommendations of ASCE 41-13. Each hazard level contains 20 three-component records, with two-horizontal components and one vertical component. Note that although ASCE 41-13 does not require consideration of vertical ground shaking in dynamic analyses, it was incorporated in this dissertation to simulate earthquake input as realistically as possible. More extensive discussions on the effects of vertical components are included in Lai *et al*. [2015].

The results presented below are based on a realistic model that could simulate the brittle fractures of beam-to-column connections and columns splices, and include the exterior cladding mass. However, no attempt was made to realistically model the complex nonlinear dynamic behavior of the column splice regions in the as-built structure after fracture initiated. As such,

31

and as suggested by the previous static pushover analysis results, once column splices began to fracture, it was difficult to simulate the response of the structure numerically. Rather than improve the local numerical model of the column splices, it was decided to focus on retrofit measures, since failure of an analysis to converge, or failure of elements that are responsible for carrying gravity loads, are specifically cited in some modern building codes as constituting a global failure [ASCE 7 2017].

Results plotted and discussed in this section only include simulation runs where the numerical analysis completed successfully or where the analyses predicted a maximum story-drift ratio larger than 10% would develop. Note: in the latter case, the analysis was terminated at a time-step when the peak drift ratio exceeds 10%. As such, the results reported below anticipate a maximum drift ratio larger than 10%. Widespread rupture of column splices resulted in numerical instabilities (and convergence failures) in 9 of the 20 ground motions considered for BSE-1E level shaking and in 13 out of 20 records from the BSE-2E set. As a result, the results presented in this dissertation are for cases where numerical convergence occurred, and for the as-built structure, around half of the structures had sufficient damage that numerical convergence was not possible.

The distributions of computed story drift over the height of building for BSE-1E and BSE-2E level shaking are shown in Figure 3.8. A multistory side-sway (weak-story) mechanism in the lower third of the structure was predicted. Median peak story drifts for the converged analyses reached 9.5% at BSE-1E and 10.0% at BSE-2E for the analyses that did not manifest numerical instabilities. A significant dispersion in peak values is noted, where the maximum values reached 32% at BSE-1E and 28% at BSE-2E. The relatively small increase in median story drift may simply reflect the ability of the numerical models used to obtain numerically stable results as the damage associated with these large drifts occur (4 more records resulted in numerical instability for the BSE-2E motions than BSE-1E motions). In both hazard events, the median maximum values were much larger than 3.0%, a limit on maximum drift ratio suggested by several guidelines [PEER 2017; LATBSDC 2017] for new tall buildings.

Consistent with the distribution of drift ratios, predicted failures of beam-to-column connections concentrated at floors in the bottom one-third of the building. Here, failure is defined here when the beam end rotation exceeds values for the collapse prevention state limit provided in ASCE 41-13. The median value of the number of connection failures for the analyses that converged reached 30% out of the total number of beam-to-column connections at floor 6, at both BSE-1E and BSE-2E; see Figure 3.9.

The residual drift ratio distributions exhibited a trend similar to that for the peak drift ratio; see Figure 3.10. The median residual story drift ratio for the runs that converged for the BSE-1E and BSE-2E motions were 9.1% and 9.5%, respectively. Large dispersions of residual story drifts were observed between floor levels 5 and 10. According to FEMA P-58 [2010a], it would likely be technically or economically unfeasible to repair a building having residual drift ratios in excess of 1%, and is not permitted to exceed this value by several guidelines [PEER 2017; LATBSDC 2017] when consider a new tall building. Damaged tall buildings with large residual displacements may also pose a special danger to adjacent structures in the event of major aftershocks.

Peak story-shear distributions are shown in Figure 3.11. The median base shear at both BSE-1E and BSE-2E was about 15,000 kips, which is about five times the minimum design base shear considered when the building was designed [ICBO 1967].

Another important concern relates to the building's fragile columns. In addition to flexural demands, columns are subjected to significant fluctuations in compression and tension loads during a seismic event. To more closely examine column behavior, six groups of columns were established according to their plan location, size, cross-sectional shape, and tributary area; see Figure 3.12. Group 1 and Group 5 were selected as representative exterior corner columns and interior corner columns, respectively, for investigation here. These columns generally had larger axial force demands than other groups of columns.

The axial load demand-to-capacity (*D/C*) ratio distribution for exterior corner columns (Group 1) and interior columns (Group 5) are plotted in Figure 3.13 and Figure 3.14, respectively. Both tension (positive sign) and compression (negative sign) are included. In these figures, capacities were calculated in accordance with AISC 360-10 specification [2010] and ASCE 41-13. The tension capacity of a column at even number stories was calculated based on Equation 9-8 of ASCE 41-13. For odd-number stories where column splices were located, tension capacities were calculated using Eqn. (3.1).

$$P_{CL} = \varphi \cdot A_{net} \cdot F_{rupture} \tag{3.1}$$

where P_{CL} is the lower-bound of column splice tension capacity, ϕ is a strength reduction factor set to 1.0 here, A_{net} is the net section area of the PJP weld at the spliced zone, and $F_{rupture}$ is the estimated stress in the PJP weld based on the effective strain [Eqn. (3.2)] at rupture. This strain was established based on a simplified fracture mechanics model proposed by Stillmaker *et al*. [2016]. *D/C* ratios under gravity loads are included as well, and identified as the red line in Figure 3.13 and Figure 3.14. Note that *P-M-M* interaction was not considered in the *D/C* calculations (but the column fiber model included it in the response analysis). As such, this is only a qualitative indication of the degree of yielding in the columns.

$$\varepsilon_{rupture} = \frac{K_{IC}}{E \cdot \left[9.91\left(\dfrac{a}{t_f}\right)^2 - 1.12\left(\dfrac{a}{t_f}\right) + 1 \right] \cdot \sqrt{\pi a}} = \frac{4.72 \times 10^{-4}}{\sqrt{t_f}} \tag{3.2}$$

Figure 3.13 shows the *D/C* ratios for Group 1 columns. The median peak *D/C* in tension was smaller than 1.0; however, the dispersion of results is large, especially around the third story where some results exceeded 1.0. Splices were located at every other floor, resulting in the zigzag shape of the median tension *D/C* curve. Recall that many of the analysis results are not presented in these plots, because the analyses became numerically unstable due to significant numbers of column splice failures. Also, as defined above, a tensile *D/C* ratio less than unity does not mean that that a splice has not ruptured partially or completely. As a result, column splice rupture is an important consideration in assessing the overall safety of the building.

Considering column compression loads, the median *D/C* values for Group 1 and 5 columns exceeded 0.5 from levels 1 to 20 for both BSE-1E and BSE-2E excitations. At these

levels, ASCE 41 indicates that the members should be treated as being force-controlled and therefore they should remain elastic. Gravity loads in this portion of the structure consume about 30–40% of the compression load capacity of the columns. With seismic loads added, *D/C* values commonly exceeded 0.75 for levels 3-12, where a side-sway mechanism was observed. In fact, for Group 1 columns, median compression *D/C* ratios approached unity in this region. Such high *D/C* indicates a significant reduction of column bending capacities when *P-M-M* interaction is considered. This *P-M-M* interaction would likely contribute to the weak column–strong beam behavior observed in the analysis results. As shown in Figure 3.13 and Figure 3.14, peak compressive *D/C* values increased just slightly as the hazard increased from BSE-1E to BSE-2E. This is because most beams had already yielded or fractured at the BSE-1E level.

The interior columns had higher axial load contributions from gravity loads, but smaller ones from overturning moments. Figure 3.14 shows the *D/C* for Group 5 columns. The compressive *D/C* ratios of interior columns were generally smaller than for the exterior columns, and the distribution was more uniform over height. The tension was significantly less of a concern for the interior columns, but large tension occurred for some records, presumably due to rupture of exterior splices transferring tensile load demands to interior columns.

As noted, columns were assumed to be fixed at the ground level for the results presented above. Column uplift at the base of the building could limit the tension forces in the columns, and the number of column splice ruptures. Like column splice ruptures, uplift might serve to limit the axial compression demands as well. However, the weight and structural system in the enlarged basement tower of the building suggests that uplift would be unlikely, and significant numbers of column splice failures are likely.
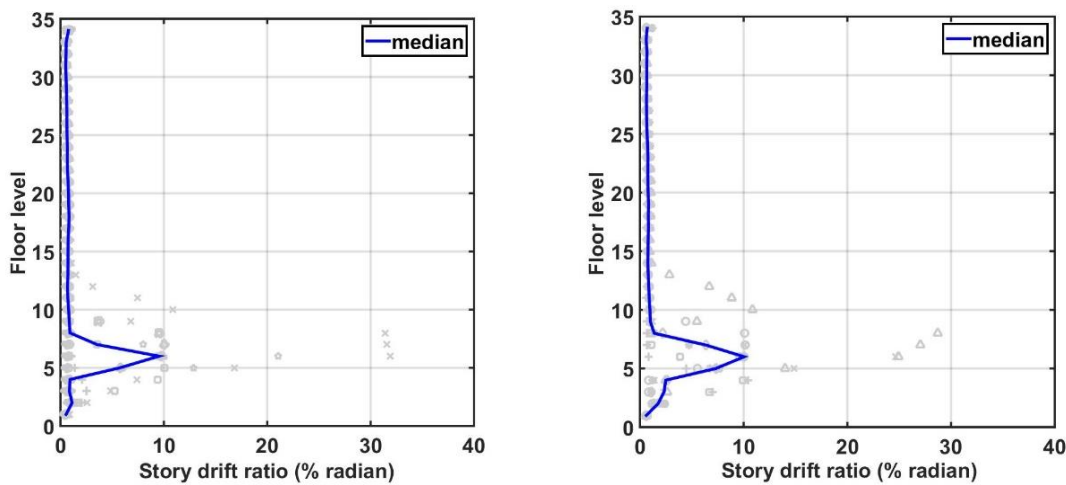
(a) BSE-1E   (b) BSE-2E

Figure 3.8   Distribution of peak story drift ratios

34
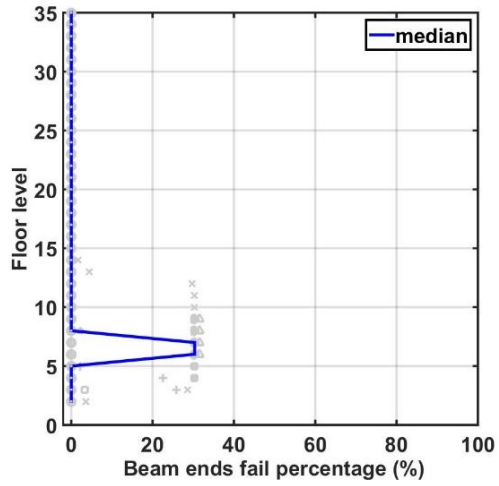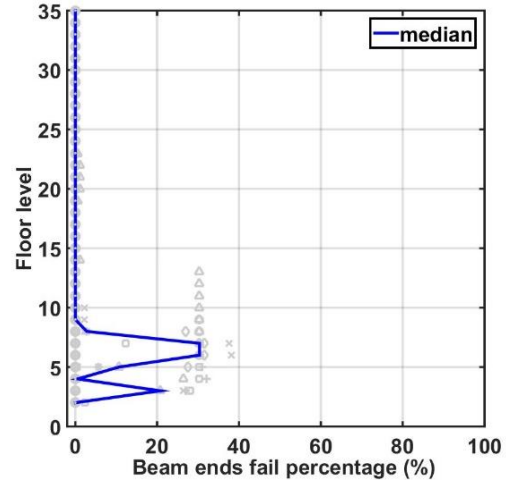
(a) BSE-1E　　　　　　　　　　　　　**(b) BSE-2E**

Figure 3.9　　**Distribution of beam connection failures (as percentage of total number of connections per floor)**
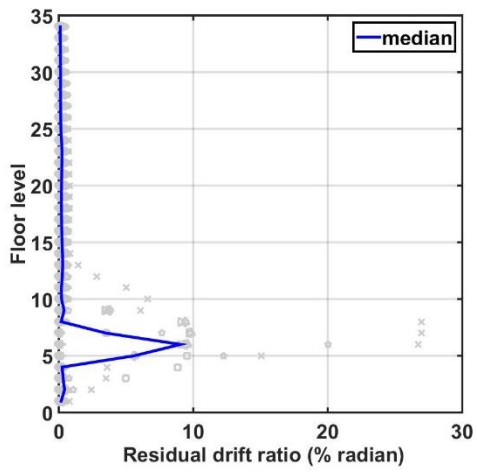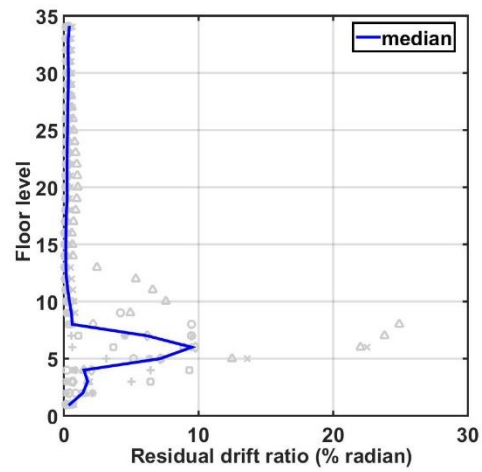
(a) BSE-1E　　　　　　　　　　　　　**(b) BSE-2E**

Figure 3.10　　**Distribution of residual story drift ratios**
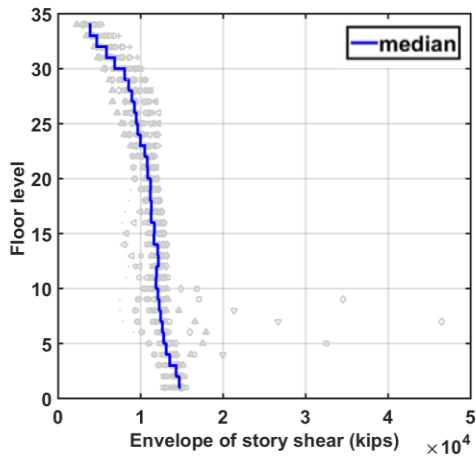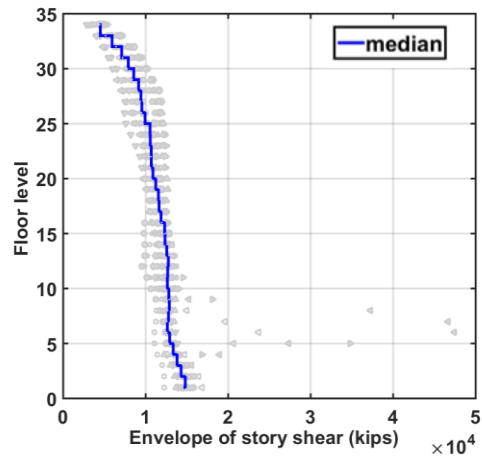
(a) BSE-1E   (b) BSE-2E

Figure 3.11   Distribution of peak story shears
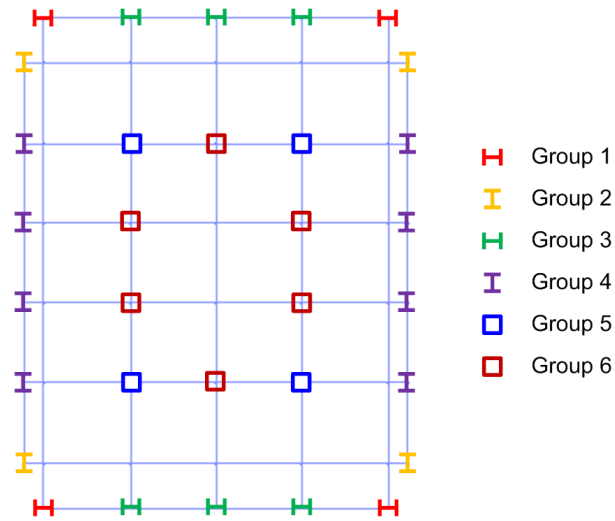
Figure 3.12   Column group designations
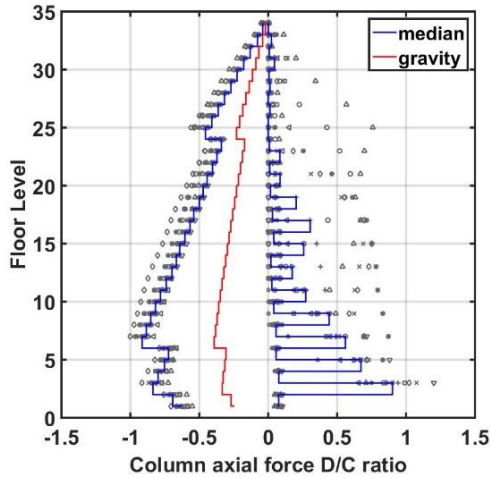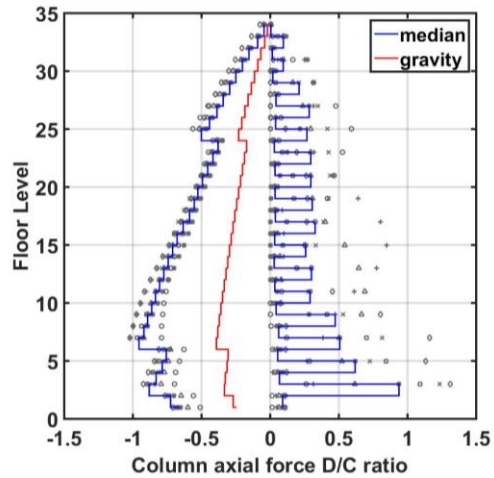
(a) BSE-1E   (b) BSE-2E

Figure 3.13   **Distribution of peak axial force D/C ratios of Group 1 columns: (+) tension, (-) compression**
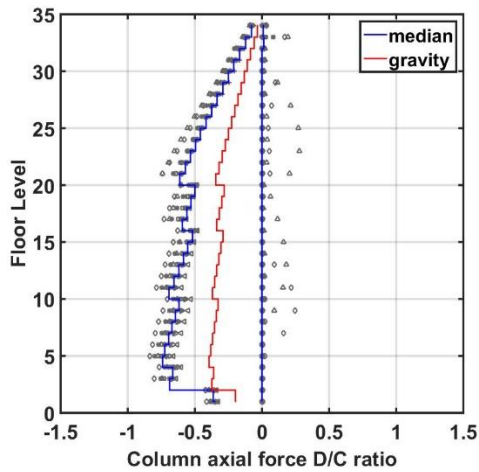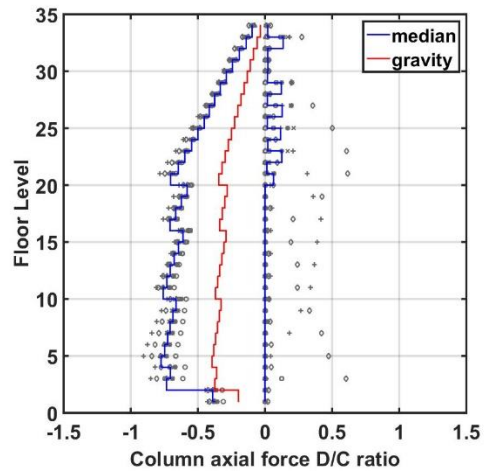
(a) BSE-1E   (b) BSE-2E

Figure 3.14   **Distribution of peak axial force D/C ratios of Group 5 columns: (+) tension, (-) compression**

3.3.3 FEMA 351 Global Collapse Evaluation

FEMA 351 provides a probabilistic approach to evaluate the seismic performance of existing welded steel moment-resisting frame buildings. It provides a means of estimating the confidence with which an immediate occupancy (IO) and global collapse prevention (CP) limit state can be achieved for a give set of ground motions. In this section, IO and CP evaluations were performed using FEMA 351 based on the maximum of the median peak story drift ratios reported in the previous section for BSE-1E and BSE-2E hazard level excitations.

The various parameters needed to perform the evaluation were determined based on FEMA 351 and the results of the dynamic analyses previously reported. The values used for the uncertainty factors, β_{UT}, demand variability factor, γ, analytical variability factor, γ_a, resistance factor, ϕ, story drift demand, D, and global story drift capacity, C are listed in Table 3.2. Type 2, pre-Northridge connections were assumed, based on the as-built conditions of the case-study building. The confidence levels were estimated by the factored demand-to-capacity ratio (λ in [Eqn. (3.3)] used by the by FEMA 351 procedure:

$$\lambda = \frac{\gamma \gamma_a D}{\phi C} \tag{3.3}$$

Here, the demand is characterized only by the computer results that were numerically stable. The confidence levels for achieving IO or CP performance goals based on global drift demands (for numerically stable runs) are summarized in Table 3.3. Based on FEMA 351, the case-study building had less than 2% confidence of achieving IO or CP at either the BSE-1E or BSE-2E hazard levels. These confidence expectations are far below the minimum confidence levels targeted by FEMA 351 for different performance levels, i.e., a confidence level of 50% to achieve IO, and a confidence level of 90% to achieve CP. For the case-study building categorized as being in Risk Category III, even higher confidence levels should be expected.

Table 3.2 Global drift limits satisfying minimum confidence level for IO and CP performance levels per FEMA 351

Factors in Eqn. (3.3)	Performance level	
	IO	CP
β_{UT}	0.2	0.55
γ_a	1.04	1.1
γ	1.6	1.8
C	0.01	0.06
ϕ	0.85	0.6

Table 3.3 Confidence levels to achieve target performance goals from global responses (obtained from numerically stable analysis runs)

Hazard level	Performance level	
	IO	CP
BSE-1E	0.0%	1.48%
BSE-2E	0.0%	0.73%

3.4   RECOMMENDED RETROFIT SCHEMES

Comprehensive seismic evaluation of the case-study building has been conducted following ASCE 41 and FEMA 351. Several significant seismic vulnerabilities have been identified. At this stage, more refined analyses could be done to remove some of the uncertainties associated with the accuracy and stability of the numerical runs. However, a possibly more important and relevant question at this point is whether there are cost-effective techniques to improve the building's structural performance and mitigate its vulnerabilities.

A number of different approaches for seismic retrofitting of tall steel moment-resisting frame building were reviewed in Chapter 2. A preliminary feasibility study has been previously conducted [Lai *et al*. 2015] to explore potential solutions to upgrade the seismic performance of the case-study building. In the following section, the two-level retrofit procedure is discussed. The Level-1 retrofit addresses the most critical vulnerabilities in the building by upgrading all of its column splices and replacing the existing heavy cladding on the building with a lightweight substitute. The Level-2 retrofit adds supplemental energy-dissipation devices to the Level-1 retrofit measures. The effectiveness of Level-1 retrofit will be discussed in the section. The Level-2 retrofit strategy will be discussed, and methods used to extend its previous scope are described in Chapters 4 and 5. The ability of these enhanced retrofits to upgrade the seismic performance of the case-study and other buildings is a major topic in this dissertation.

3.4.1 Level-1 Retrofit

The Level-1 retrofit strategies were applied to the case-study building included: (a) removing the exterior concrete cladding and (b) repairing vulnerable column splices.

Replacement of heavy cladding is a retrofit strategy that has been done as an alternative to or in tandem with an upgrade to the structural system (see Chapter 2). Since the cladding on the case-study building amounts to more than 15% of the total weight of the structure, this method was thought to be a useful first step.

In addition, the numerical simulations indicated widespread failure or rupture of the splices which jeopardized the overall stability of the structure. Therefore, the Level-1 retrofit strategy also incorporated replacing the PJP welds at column splices with notch tough CJP welds, with an intent of eliminating this failure mode.

The numerical model of the building was then adjusted to reflect the two changes associated with the Level-1 retrofits. The first three elastic mode periods of this model changed to: 4.33 sec (*X*-translation), 4.18 sec (*Y*-translation), and 3.58 sec (rotation about the *Z*-axis). The analyses reported above for the case-study building were repeated for the Level-1 retrofit model, and global structural responses are discussed below.

The distributions of peak story drift ratios at BSE-1E and BSE-2E hazard level events are shown in Figure 3.15. The maximum value of median story drift ratio for the Level-1 case under the BSE-1E events was reduced from about 10% for the as-built case to only 1.1%. But with all twenty ground motions considered, a significant dispersion of results can be observed in the lower stories. This weak-story trend in the lower stories was significant for BSE-2E events, where a median peak drift ratio reached 7% with even larger dispersions. Note: after eliminating

vulnerable column splices with Level-1 retrofits, all twenty simulation runs converged, whereas in the as-buit condition, about half or more than half simulation runs failed to converge at these considered intensity levels. Similar to the trend of the peak drifts, the residual drift ratios (Figure 3.16) were essentially zero under BSE-1E event, but reached 6.3% under BSE-2E hazard level earthquakes.

A probabilistic check on the collapse prevention limit state was again made based on global drift ratio following the FEMA 351 procedure. The distributions of peak story-drift ratios (maximum of both *X*- and *Y*-directions) for the as-built and Level-1 retrofit case are presented in Figure 3.8 and Figure 3.15, with median values identified in solid lines. The resulting confidence levels are shown in Table 3.4. For the BSE-1E level ground motions, the confidence level to achieve collapse prevention after Level-1 retrofit was significantly increased, to more than 90%. However, this retrofit did not achieve a high confidence of collapse prevention under a BSE-2E hazard event due to the weak story behavior in levels 5 to 10.

Another remaining issue is the fragility of the columns under compression. The two groups of columns that were investigated before—exterior corner columns (Group 1) and interior corner columns (Group 5)—were again selected for a axial *D/C* ratio check; see Figure 3.17 and Figure 3.18. On the tension side, fixing PJP welds eliminated the brittle splices, and the axial *D/C* ratios were small for both groups of columns. With the Level-1 retrofit, the compression *D/C* ratios were reduced mainly due to a reduction in the weight of the structure. The demand reduction was larger for exterior columns than interior ones given that removed cladding was concentrated at the exterior frames. Nevertheless, such improvements did not fully eliminate the overloading conditions previously noted for these columns, and their peak *D/C* on compression was still as high as 0.75–0.9 under a BSE-2E event. Such high axial demands would prohibit the column sections from developing full bending capacities, and methods to strengthen these overloaded columns, and reduce the weak story tendency of the building are necessary.
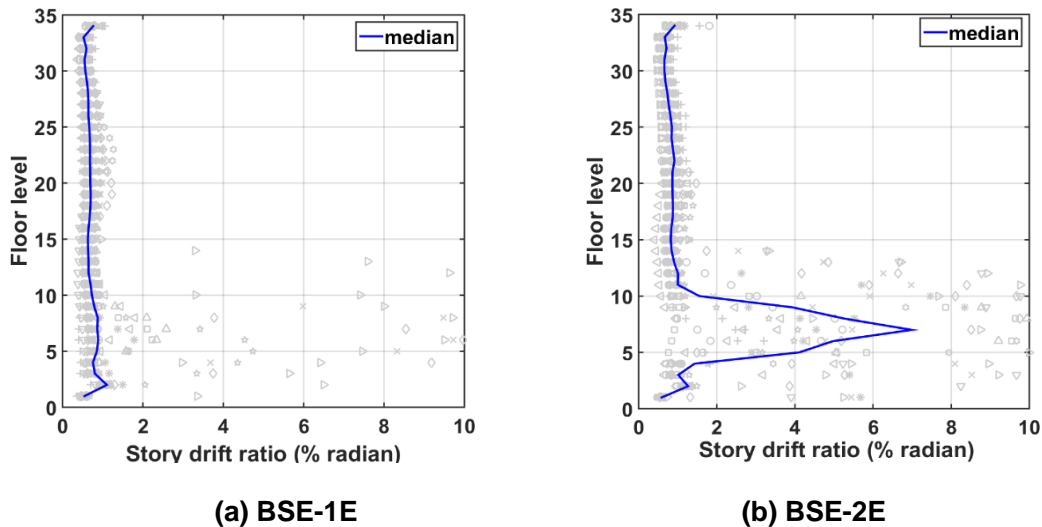
(a) BSE-1E   **(b) BSE-2E**

Figure 3.15   Distribution of peak story drift ratios after Level-1 retrofit

40
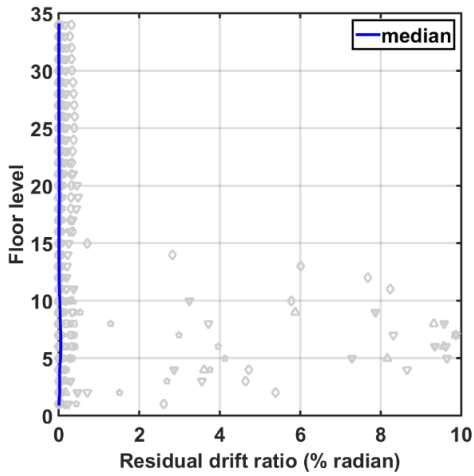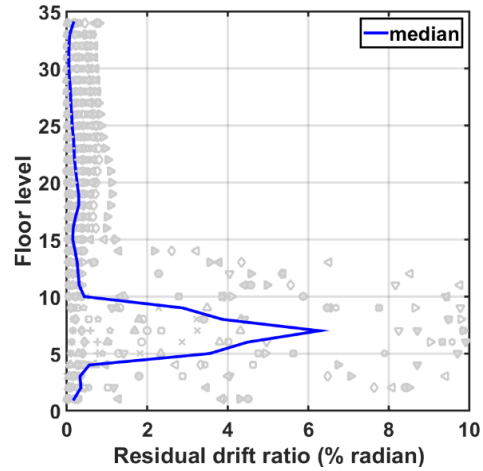
(a) BSE-1E   (b) BSE-2E

Figure 3.16   **Distribution of peak residual story drift ratios after Level-1 retrofit**
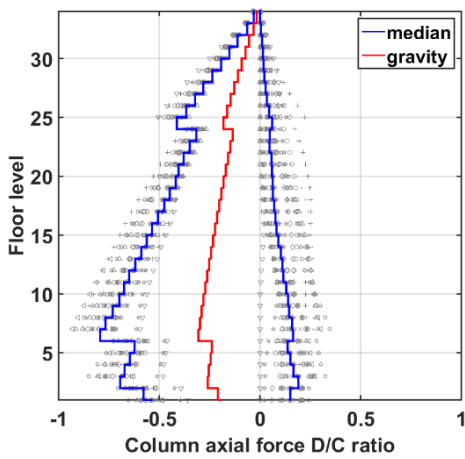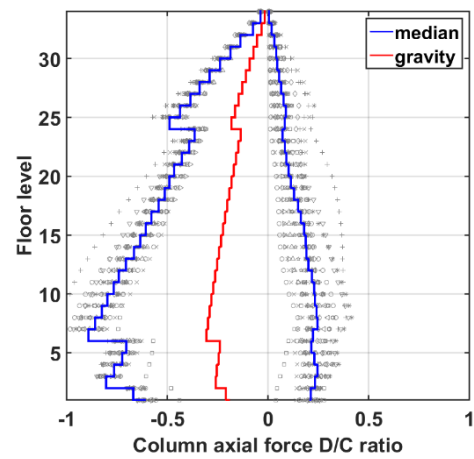
(a) BSE-1E   (b) BSE-2E

Figure 3.17   **Distribution of peak axial force D/C ratios of Group 1 columns after Level-1 retrofit: (+) tension, (-) compression**

41

(a) BSE-1E   **(b) BSE-2E**
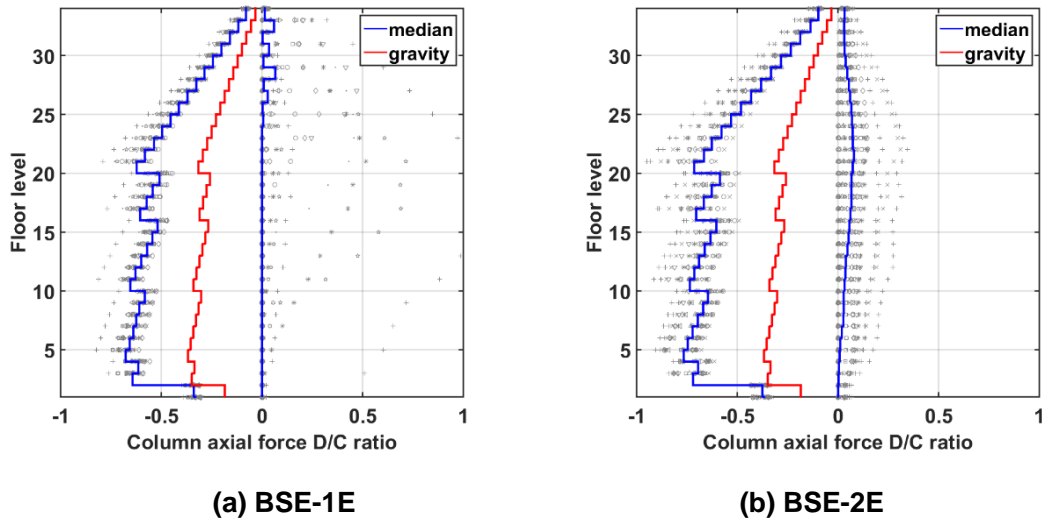
Figure 3.18   Distribution of peak axial force D/C ratios of Group 5 columns after Level-1 retrofit: (+) tension, (-) compression

Table 3.4   Confidence levels to achieve collapse prevention based on global responses

Hazard level	Performance level CP	
	As-built	**Level-1**
BSE-1E	1.48%	94.3%
BSE-2E	0.73%	5.2%

3.4.2 Level-2 Retrofit

The previous studies show that Level-1 retrofit methods could help improve the structural responses under small and moderate earthquake events, i.e., the BSE-1E hazard level. However, further actions are required to meet the performance objectives. Since the design criteria set in this research for the performance of the case-study building was collapse prevention and better under BSE-2E shaking, a Level-2 retrofit was proposed to further augment the Level-1 measures. The initial intent for the retrofit scheme suggested in the previous study focused on ensuring structural stability under a BSE-2E hazard event. In subsequent chapters, further measures to enhance performance are considered.

Some of the remaining problems for the existing building after its Level-1 retrofit is its large story drift deformation (especially in the lower third of the building), the significant number of large beam end rotational demands, and a tendency to form a multi-story side-sway mechanism in the lower stories. Therefore, an approach that reduces story drift demands, beam end rotational demands, and the tendency of the structure to form a weak-story mechanism is

warranted. That said, other deficiencies identified during the Tier-1 screening, such as the lack of column attachment to the foundation and the fragility of the columns under high axial loads, pose significant challenges that also have to be addressed.

To provide the required lateral stiffness and energy dissipation needed to reduce lateral displacements, while not increasing demands on the structure, is challenging. Common approaches in the U.S. consider the addition of buckling restrained braces, fluid viscous dampers, viscous wall dampers, or mid-level isolation (Figure 3.19). Because of the vulnerability of the columns in compression and tension, an approach using fluid viscous dampers has been explored in the past study (Lai *et al.* 2015) in some detail. In this approach, the use of fluid viscous dampers could result in a peak force resistance that is out of phase from the peak forces acting in the elastic structural elements, which may provide a way to limit drifts without significantly increasing demands on the existing structural members.

Chapters 4 and 5 examine three retrofit strategies for seismically vulnerable tall buildings using (a) fluid viscous dampers; (b) buckling restrained braces; or (c) viscous wall dampers. Several design considerations of each system will be studied. The cost-effectiveness of each retrofit method will be examined in Chapter 6.

(a) Fluid viscous dampers (photo courtesy of Taylor Device, Inc.)

(b) Buckling restrained braces (photo courtesy of CoreBrace, LLC)

(c) Viscous wall dampers (photo courtesy of Dynamic Isolation Systems, Inc.)
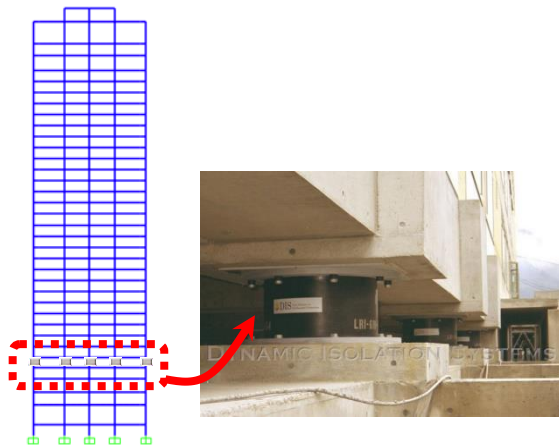
(d) Mid-story isolation (photo courtesy of Dynamic Isolation Systems, Inc.)

Figure 3.19   Applications of different energy dissipating devices

3.5   CONCLUDING REMAKRS

This chapter examined the seismic performance of a representative 35-story steel moment frame building in San Francisco that designed during late 1960s. Structural evaluations were carried out following procedures contained in two modern codes or guidelines: ASCE 41-13 and FEMA 351. The assessment results predicted similar outcomes. Results from ASCE 41 Tier-3 procedure were presented in detail and indicated:

- The strength of the building was inadequate, which led to a median peak drift ratio of about 10% at both BSE-1E and BSE-2E hazard events;

- The building had a tendency to form a side-sway mechanism over stories 4 to 8 of the building;

- Pre-Northridge beam-to-column connection details contributed to a 30% of total connection failures at the most deformed stories at BSE-1E and BES-2E events;

- The PJP column splice weld details caused widespread column ruptures at BSE-1E and BSE-2E events, endangering the seismic integrity of the building significantly;

- The columns at lower half floors were overloaded in compression and were likely to fail under combined axial and bending loads.

Probabilistic assessment of global response using FEMA 351 indicated that the case-study building failed to conform to a minimum 90%-confidence-level goal of achieving the collapse prevention limit state at either BSE-1E or BSE-2E hazard event.

While the substantial difficulties in analyzing the building associated with the rapid deterioration of strenght and stiffness due to wide spread ruptures of column splices and beam-to-column connections indicated that improvements in modeling assumptions and analysis methods were needed, all of the methods suggested that retrofit strategies to improve safety and reduce damage of the building should be explored.

A two-level retrofit plan was proposed. The Level-1 retrofit, which significantly reduced the weight of the structure by replacing the existing builidng's heavy cladding with lightweight substitute and upgrading all of its column splices, achieved a greater than 90% confidence of preventing collapse under BSE-1E seismic events, according to procedures in FEMA 351. However, analysis of the same building determined collapse prevention at the BSE-2E level could not be assured and demolition and replacement might be expected after such an earthquake due to the large residual drifts predicted.

As a result, Level-2 retrofit measures shall be built on the Level-1 retrofit. The initial performance goal is achiveing a high confidence of achieving structural stability under BSE-2E hazard events.

4 Seismic Retrofit with Supplemental Energy-Dissipation Devices: (I) Fluid Viscous Dampers

4.1 INTRODUCTION

Chapter 3 of this dissertation identified seismic vulnerabilities of the case-study building, including: (1) excessively large story drifts in the bottom one-third of the building; (2) a great percentage of beam-to-column connections failures at certain floors; (3) widespread column splice failures; and (4) high axial compression force D/C ratios in many columns. Two levels of retrofit were suggested with the intent of achieving the collapse prevention limit state under the major basic safety earthquake (BSE-2E) hazard level prescribed by ASCE 41. In the Level-1 retrofit, the brittle column splices were fixed throughout the entire building, and the heavy concrete cladding was removed and replaced with a lightweight substitute. The Level-1 retrofit was shown to significantly improve structural performance under BSE-1E hazard events. However, for ground motions corresponding to the BSE-2E hazard, the Level-1 retrofits were insufficient to meet the retrofit goal. Consequently, Level-2 retrofit methods, which add supplemental energy-dissipation components to the Level-1 retrofit measures, are examined in this and the following chapters.

One of the major challenges in the Level-2 retrofit is to provide sufficient lateral stiffness and energy dissipation to reduce the lateral deformations of the building while not increasing force or deformation demands on existing structural members. Using velocity-dependent devices such as fluid viscous dampers (FVDs) is considered a promising solution in such situations, since for an elastic system the peak damper forces occur when lateral displacements and forces in structural members are small, and damper forces become small or zero when forces and displacements are largest in the structure. Thus, if adding damping can reduce story drift demands to about the yield level, the likelihood and severity of ruptures in the beam-to-column connections will be reduced substantially, and the forces associated with the dampers should not increase significantly the forces in structural members. Other supplemental energy-dissipation devices, such as viscous wall dampers (VWDs) and buckling restrained braces (BRBs), are commonly used in seismic retrofit schemes and are also investigated as alternatives approaches to the Level-2 retrofit of the case-study building.

This chapter starts with a general introduction of the background and use of supplemental energy-dissipation systems, followed by more detailed descriptions of the three supplemental energy-dissipation devices investigated herein: FVDs, VWDs and BRBs. The development of code provisions for buildings using supplemental energy-dissipation systems is also reviewed. Following that, a more detailed review of mechanisms, manufacturing, mathematical modelling, design methods, and worldwide applications of one type of devices examined in detail in this chapter—FVDs—is presented.

To design FVDs for application in the case-study building, a preliminary design procedure is illustrated step-by-step, including selecting feasible damper locations and overall effective damping ratios, and identifying design parameters by a simplified two-phase refinement. In Phase 1, dampers are installed across all stories, and three alternate damper distribution schemes are compared. Phase-2 requires selecting the best of the three schemes considered in Phase 1. This scheme is then optimized to remove a large number of dampers and refine individual damper characteristics without compromising the collapse prevention objective of the retrofit at the BSE-2E event prescribed by ASCE 41 [2013]. The refined design that resulted from this process is then evaluated considering the two BSE hazard levels [*viz*., BSE-1E (225-year mean return period) and BSE-2E (975-year mean return period)] using provisions in several assessment procedures, including ASCE 41 [2013] and FEMA 351 [FEMA 2000]. In the end, five sensitivity studies are presented, highlighting critical design considerations when applying FVDs. Chapter 5 expands the study presented and considers the relative effectiveness and economy of other two types of passive energy-dissipation devices: VWDs and BRBs.

4.1.1 Supplemental Energy-Dissipation Systems

One of the underlying principles in earthquake-resistant design is to dissipate the seismic energy input from the ground motion while protecting the integrity of the structural system and limiting damage. The complete energy balance is expressed in Eqn. (4.1) [Uang and Bertero 1988]:

$$E_I = E_S + E_K + E_D + E_H \tag{4.1}$$

where E_I = total input energy, E_S = strain energy, E_K = kinematic energy, E_D = viscous damping energy, and E_H = hysteretic damping energy.

At the end of the earthquake-induced shaking, the kinematic energy is zero, and the strain energy is zero or small (zero for a structure that remains elastic and relatively small for an inelastic structure). Therefore, the input seismic energy is dissipated mainly through hysteresis damping and viscous damping. In a traditional design without supplemental energy-dissipation devices, hysteretic energy is mainly from yielding of structural elements, which is generally associated with structural damage. The intrinsic viscous damping present in most buildings is generally small, especially for tall buildings [Smith *et al.* 2010; Cruz and Miranda 2016]. Consequently, much of the energy introduced by very large earthquakes is associated with inelastic deformations in structural members. However, recent earthquakes in Chile, Japan, China, and New Zealand, where the large structural as well as non-structural damage caused undesirable disruption and high economic losses, have increased interest in design methods that can reduce repair cost and business interruption.

Thus, the goal of adding supplemental energy-dissipation devices is to reduce deformations and accelerations by providing additional hysteretic energy dissipation (BRB) or viscous damping (FVD and VWD). Such elements are especially attractive in the retrofit of existing buildings if they can be easily added and not generate excessive forces in the adjoining structural elements.

Seismic protective systems are categorized into three general types of systems: seismic isolation, active control, and passive energy dissipation [Soong and Spencer 2002]. In this dissertation, the focus is on passive energy-dissipation systems. However, it is useful to compare them with those systems based on seismic isolation and active control.

Seismic isolation is now considered a reasonably mature technology [ATC 1993]. While its application in the U.S. has been limited, it is widely used in Japan, China, Italy, New Zealand, Chile, and Indonesia [Kelly 1997]. In a seismically isolated structure, a horizontal plane of high-quality manufactured devices having high vertical stiffness and low horizontal stiffness and strength is introduced, generally near the base of a structure. These devices seek to uncouple the horizontal movement of the supported building from that of the ground and introduce hysteretic energy dissipation due to the relative horizontal displacement between the ground and building. However, if an isolated structure has a long fixed-base period, like a tall building, using isolation is likely only to slightly reduce the forces in the structure [Kelly 1997], but it can concentrate a lot of the lateral displacement of the building system in the isolation plane, thereby reducing the drifts in the upper portions of the structure. Special concerns for seismic isolation applications in tall buildings include complications related to elevators and utilities crossing the isolation plane, avoidance of excessive tension force or uplift in isolators, optimal location of the isolation plane, and detailing to resist high local moment effects in heavily loaded isolators. More than 300 buildings over 25 stories tall have been seismically isolated in Japan [Becker *et al.* 2015], and some tall buildings have been retrofitted in the US using seismic isolation [Youssef and Hata, 2010]. Another possible way to reduce the seismic demands is to use a mid-level isolation system, which has been applied in newly-constructed buildings [Tsuneki *et al.* 2008] as well as the case where additional stories are added to an existing building [STRUCTURE magazine 2008].

Active, hybrid, and semi-active control systems employ computer-controlled mechanical devices combined with real-time control electronics, algorithms, and sensors within the structure [Soong 2002]. The devices change their mechanical properties or applied forces to the structure during seismic excitation to achieve improved structural behavior. In some cases, the devices vary their effective viscous damping or load resisting capability. Control forces can also be generated by electrohydraulic or electromechanical actuators. Force control devices may need large power sources to achieve the force demands required for large buildings and earthquakes [Soong *et al.* 1991]. For these reasons, semi-active and hybrid systems, having smaller power requirements, are more common for civil structures than fully active systems that impose forces on the structure. All of these systems utilize computer systems that require maintenance and periodic upgrading due to rapid changes in technology.

As a result, passive energy-dissipation systems are currently the most common protective system used for enhancing the seismic response of buildings. As noted, hysteretic, viscous, and viscoelastic devices are available. Hysteretic devices develop forces that are related to relative

displacements imposed between the points where the device is attached to the structure, and energy is dissipated by yielding of metallic materials, sliding friction, and so on. Viscous devices develop forces related to the relative velocity of the points where the device is attached to the structure, and dissipate energy due to motion of piston through a fluid, flow of a fluid through an orifice, and so on. Viscoelastic devices exhibit properties of hysteretic and viscous dampers, and their properties depend on both relative displacement and relative velocity. Many types of viscoelastic dampers exist and usually incorporate viscoelastic materials (polymers, high-damping rubber, etc.) but viscous wall dampers and some types of FVDs exhibit viscoelastic properties. Velocity-dependent dampers develop small forces as displacements approach their maxima (where velocity is zero). Thus, for elastic or nearly elastic systems, energy is dissipated but peak forces are not generally increased when viscous dampers are added [Constantinou and Symans 1992].

4.1.2 Fluid Viscous Dampers

A commonly used type of a FVD is illustrated in Figure 4.1. It operates by forcing a fluid to flow through a restrictive control orifice during longitudinal movement of the device. FVDs can be designed to be either linearly and nonlinearly velocity dependent. The basic properties and efficiency of FVDs for use in seismic-resistant design have been studied by various pioneering researchers and manufacturers [i.e., Constantinou and Symans 1992; Reinhorn *et al*. 1995; and Taylor and Constantinou 1995]. Experimental and analytical studies on FVDs have demonstrated significant benefits of using FVDs to reduce seismic responses of buildings and bridges. Nowadays, such dampers are widely used in the design of structures to resist the effects of earthquakes and wind. For example, one of the largest damper manufacturers in the U.S., Taylor Devices. Inc., has had their FVDs installed in more than 610 buildings and bridges worldwide [Taylor Device Inc. 2015], including 57 buildings taller than 20 stories. A more detailed review of FVDs will be presented in Section 4.2.
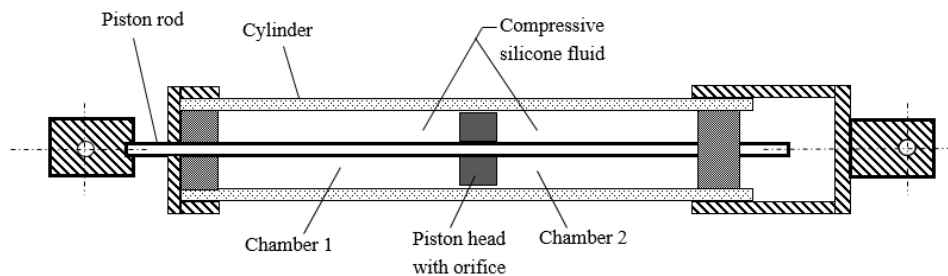
Figure 4.1   Schematic diagram of a fluid viscous damper

4.1.3 Viscous Wall Dampers

A VWD is a special kind of viscous damper that is basically configured as a wall element. A VWD consists of a steel plate moving in a highly viscous fluid that is contained in a thin steel tank (the wall). The inner plate connects to the upper floor, and the steel tank is connected to the lower floor; see Figure 4.2. During a seismic or a wind event, the relative movement between upper and lower floors generates a restoring force of the viscous fluid within the tank that

dissipates energy. With a relatively stiff steel tank and vane, a VWD can provide both additional stiffness and damping during dynamic loading [Arima *et al.* 1988].

They were first developed for building applications by Sumitomo Construction Company, Ltd., in conjunction with the Building Research Institute in Japan [Arima *et al.* 1988; Miyazaki and Mitsusaka 1992]. The first building using VWDs was the SUT-building built in 1992 and located at the center of Shizuoka city, 150 km west of Tokyo [Miyazaki and Mitsusaka 1992]. Nowadays, there are more than 200 buildings in Japan that have incorporated wall dampers as seismic resistant elements. This technology has recently been adopted in the U.S. The first application is the Cathedral Hill Hospital in San Francisco, California. The building is currently under construction. Experimental and analytical results or wall dampers in superstructures [Arima *et al.*, 1998; Reinhorn *et al.*, 1995; Lu *et al.*, 2008 and Hejazi *et al.*, 2015] have demonstrated great benefits of VWDs in reducing structural response under both seismic and wind events, and to improve performances. These studies indicated that VDWs could provide up to 44% stiffening [Arima *et al.* 1998] and 50% critical damping [Reinhorn *et al.* 1995]. During a seismic event, a large portion of story shears would be resisted by the VWDs, and the building deformation could be reduced up to 60% to 85% [Miyazaki and Mitsusak 1992; Reinhorn 1995; and Lu *et al.* 2008].
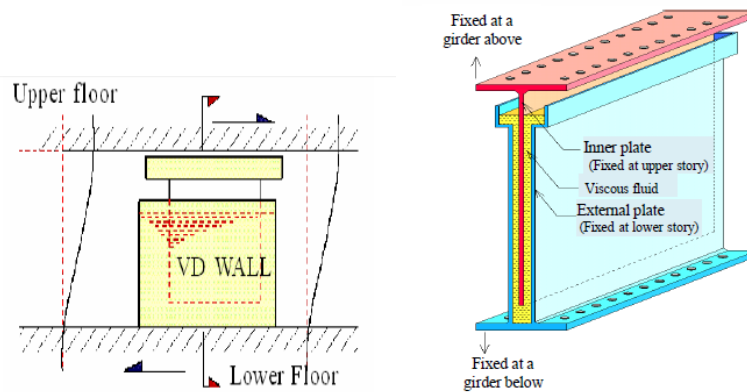
Figure 4.2   Schematic diagram of a viscous wall damper (adapted from Newell et al. [2011])

4.1.4 Buckling Restrained Braces

The brace is probably one of the most popular elements used in earthquake and wind resistant design of steel frames. However, traditional braces show unsymmetrical hysterical behavior in tension and compression due to buckling, which significantly limits their energy-dissipation capacity. Consequently, researchers have been motivated to investigate a new type of brace—BRB—to achieve yielding in compression and tension. A BRB is an example of a hysteretic damping element.

The primary part of a BRB consists of a brace (axial force-bearing component) that resists the axial forces and an encasing member (buckling restraining module) whose function is to prevent the bucking of the inner brace (Figure 4.3). These two units need to be separated properly to ensure that only the brace resists the longitudinal loading, whereas the encasing

member serves to prevent transverse displacement associated with buckling. A small separation between the yielding core and the surrounding encasement is necessary to minimize longitudinal forces being transmitted from the core to encasing material. This can be achieved by using a debonding material or a gap. A BRB element comes in various shapes and cross-sectional configurations [Lai and Tsai 2004; Tsai *et al*. 2008].

Early attempts to use BRBs for earthquake- or wind-resistant design were conducted about 40 years ago [Yoshino *et al*., 1971; Wakabayashi *et al*., 1973; and Kimura *et al*., 1976]. Since then, BRBs have gained worldwide application and have been used in both short and tall buildings, and for new and existing buildings. These devices were originally conceived as energy-dissipation devices. But later in the U.S., they came to be viewed as ordinary braces [Sabelli and Lopez 2004] so that typical rules could be retained for designing systems incorporating BRBs. Nonetheless, BRBs are still considered hysteretic energy-dissipation devices in countries such as Japan [Xie 2005].
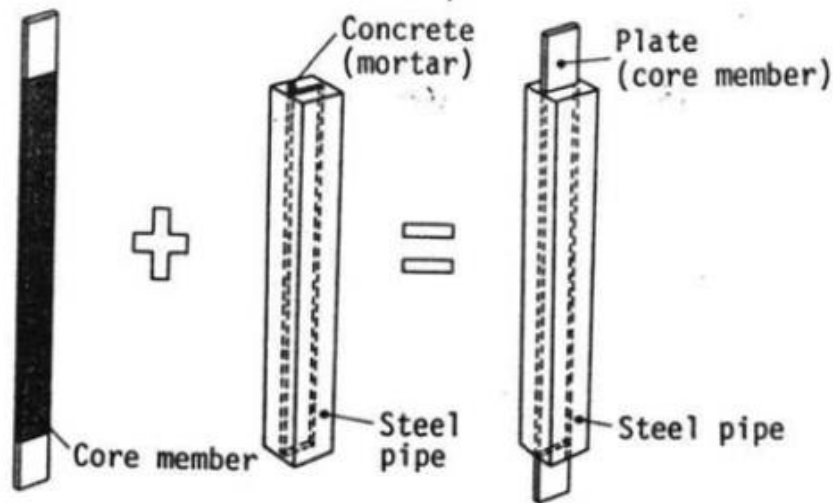
Figure 4.3   Schematic diagram of a buckling-restrained brace (adapted from Fujimoto et al. [1990])

4.1.5 Code Provisions for Design of Structures with Passive Energy-Dissipation Devices

To facilitate the widespread use of energy-dissipation devices in practice, it was critical to formulate building code requirements. The initial efforts in the U.S. to incorporate requirements for the design and implementation of passive energy-dissipation systems started in the early 1990s by the Structural Engineers Association of Northern California (SEAONC), through the Energy Dissipation Working Group of the Base Isolation Subcommittee [Whittaker *et al*. 1993]. The general guidelines in the resulting document aimed to cover a wide variety of systems. Later, these regulations became part of the National Earthquake Hazards Reduction Program (NEHRP)—*Recommended Provisions of the Development of Seismic Regulations for New Buildings* [NEHRP 1994], where a reduced base shear was permitted in designing buildings with supplemental energy-dissipation systems. In the NEHRP *Guidelines for the Seismic*

Rehabilitation of Buildings (then known as FEMA 273 and 274 [1997]), consistent procedures were presented for building retrofit implemented with energy-dissipation devices. FEMA 273 and 274 are the predecessors to the current ASCE 41-13 document. Methods presented in FEMA 273 and 274 resulted in a paradigm shift from the traditional force-based design methods to displacement-based design where more emphasis was placed on damage control. As such, engineers were allowed to select specific performance levels and objectives in seismic design.

These guidelines experienced major modifications in the 2000 version [NEHRP 2000] where more robust equivalent lateral force and response spectrum procedures were included for both displacement- and velocity-dependent energy-dissipation devices. These provisions were based on NRHA of buildings equipped with displacement- and velocity-dependent damping devices subjected to far-field earthquake excitations. Procedures to calculate effective damping and effective stiffness as well as higher mode contributions were considered for systems that incorporated linear, nonlinear viscous damping, or yielding damping devices [Ramirez *et al.* 2001]. These guidelines formed the basis for subsequent ASCE standards, such as the *Minimum Design Loads for Buildings and Other Structures* [ASCE 7-10], Chapter 18 for newly constructed buildings, and the *Seismic Evaluation and Retrofit of Existing Buildings* [ASCE 41-13], Chapter 14 for existing buildings.

Early research efforts were able to develop relatively simple equivalent linear procedures for the design of ordinary buildings. In ASCE 41-13 [2013], such linear analysis procedures are restricted to cases where the energy-dissipation devices are present in all stories of the upgraded building. Otherwise, more daunting nonlinear analysis procedures are required. Modern computers and advanced simulation software have simplified design procedures including NRHA and make consideration of nonlinear velocity-dependent damping devices feasible. This can be seen from recent guidelines [e.g., NEHRP 2015, ASCE 7 2017], where specifications for design of energy-dissipation systems have emphasized on NRHA procedures. Therefore, NRHA procedures were used throughout this dissertation.

4.2   LITERATURE REVIEW ON FLUID VISCOUS DAMPERS

4.2.1 Mechanisms and Manufacture

Fluid viscous dampers generally employ one of two different energy-dissipation mechanisms. One type of FVD involves moving a paddle-like object through a highly viscous fluid (e.g., silicone gel) in an open container [Makris and Constantinou 1990]. This type of dampers dissipates energy by converting the mechanical energy to heat, such as the VWDs described in more detail in Chapter 5. Another type relies on the flow of fluid in a closed container and dissipates energy by forcing a viscous substance through an orifice with a movable piston [Symans and Constantinou 1998]. Both types of viscous dampers are sometimes used as a component of a base isolation system [Makris and Constantinou 1990; Soong and Constantinou 1994].

In this section, FVDs are considered that rely on the flow of fluids within the closed container; see Figure 4.1. As the ends of the FVD move, the piston within the cylinder forces the

viscous fluid through a restrictive orifice from one chamber to the other. The damper force is generated from a pressure differential across the piston head, which is essentially proportional to the relative velocity of the piston head with respect to the damper housing. The orifice, known as a fluidic control orifice, provides forces that are proportional to v^{α}, where α is the damping exponent and is usually in a range of 0.3 to 1.0 when consider earthquake and wind loads for structures [Lee and Taylor 2001].

Considering the compressibility of the viscous fluids used, either a run-through rod (shown in Figure 4.1) or a rod make-up accumulator and control valve is utilized to avoid restoring forces due to reduction of fluid volumes. The run-through rod type of FVD is more commonly used for large-size dampers [Reinhorn *et al*. 1995] and was selected for the studies undertaken in this dissertation.

Such piston-type dampers perform with relatively stable mechanical properties over a wider ambient temperature range. Sinusoidal test by Symans and Constantinou [1998] found that if a 20% damping ratio was used for the design of a damper, extreme variations in ambient temperature could alter the damping ratio over a range extending from 15% to 29%. This range was very small compared to the significant temperature dependency they previously found for viscoelastic solid dampers [Constantinou and Symans 1993].

The dynamic properties of a piston-type FVD can be obtained through cyclic tests over a range of frequencies. Two parameters commonly used to characterize basic dynamic properties of viscoelastic materials or devices relate to the dynamic moduli (stiffness) relating stress and strain (or force and displacement). The storage modulus (stiffness) relates to the recoverable elastic energy stored by the material, and the loss modulus relates to the energy that is dissipated. Both parameters can be observed based on the overall configuration and manufacturing details and the viscous fluid used. The loss stiffness, which is exhibited by a force that is out-of-phase with the imposed displacement, is a desirable property of a FVD. It determines the damping effect of the FVD. However, in some devices the storage stiffness might also be present, especially for a damper with a large chamber of fluid since that would increases the damper flexibility during vibrations. The storage stiffness term would generate forces that are in-phase with the imposed displacement, providing additional stiffness to a system, but result in generally undesirable additional forces at peak displacements.

Thus, for earthquake excitations, it is desirable to have the loss stiffness dominate the behavior of a FVD (i.e., the energy-dissipation capacity of a FVD is maximized). However, the relative importance of the storage and loss stiffness is frequency dependent. For frequencies lower than a certain value, called the "cut-off" frequency, the dampers may provide little additional stiffness to the structure; but for response frequencies above the "cut-off" frequency, supplemental stiffness and damping are both provided. Thus, the effect of storage stiffness needs to be considered, especially for short-period structures or where higher modes may have an important effect on response. The "cut-off" frequency value depends on the design of the damper, especially if an accumulator is used, or if mechanical parts like valves are employed. For the types of FVD generally used in seismic design, the "cut-off" frequency is high enough that this phenomenon is typically not considered [Symans and Constantinou 1998]. In fact, in the design of many of the FVDs used for seismic resistance, the damper is specifically designed to minimize the storage stiffness.

When specifying a FVD, several controlled parameters need to be identified, including: maximum rated design and ultimate load capacity, damping constant C, damping exponent α, operating temperature range, damper mounting details, and so on [Duflot *et al.* 2008].

4.2.2 Mathematical Modeling

The steady-state force-displacement behavior of a FVD has been expressed by the general fractional derivative Maxwell model shown in Eqn. (4.2) [Makris and Constantinou 1991]:

$$P(t) + \lambda D^r[P(t)] = C_0 D^q[u(t)] \tag{4.2}$$

where $D^r[\bullet]$ and $D^q[\bullet]$ are fractional derivatives of order r and q for the contained time-dependent functions; $P(t)$ is the damper force; $D(t)$ is the relative displacement between the piston head and the damper housing; λ is the relaxation time; and C_0 is the damping constant at zero frequency. Typically, the value of the damping constant for a given viscous damper is quite stable over a wide range of frequency and temperature [Fu 1996]; thus, C_0 in Eqn. (4.2) is often considered as a constant. Such a derivative model can describe the behavior of a general FVD over a wide frequency range, which is particularly important for viscoelastic dampers. For a piston-type FVD that uses a run-through rod, the storage stiffness is insignificant; thus, a simpler model is appropriate.

Symans and Constantinou [1998] conducted tests on a FVD by subjecting it to steady-state sinusoidal cyclic motions at several frequencies to calibrate the mathematical model presented in Eqn. (4.2). The maximum damper force of the FVD being tested was 100 lb., and its stroke capacity was ± 2 in. It was concluded that the parameters of r and q were both equal to 1 for the damper tested, which reduced the model to a classical Maxwell model below:

$$P(t) + \lambda \dot{P}(t) = C_0 \dot{u}(t) \tag{4.3}$$

Additionally, it was identified that the term $\lambda \dot{P}(t)$ was insignificant as the damper exhibited a very small relaxation time based on Symans and Constantinou's test [1998]. As such, a simplified model could be used that well captures damper behavior under the "cut-off" frequency:

$$P(t) = C_0 \dot{u}(t) \tag{4.4}$$

where $\dot{u}(t)$ is the relative velocity of the piston end with respect to the damper housing. This formula could be extended to a generalized FVD to include its nonlinearity and considered as the most practical model to simulate the damper response under earthquake excitations [Symans and Constantinou 1998; Duflot and Taylor 2008]:

54

$$P(t) = C_0 \, \dot{u}(t)^\alpha \, \text{sign}(\dot{u}) \tag{4.5}$$

where α is the damping exponent designating a damper's nonlinearity, and $\text{sign}(\dot{u})$ is the sign function of the relative velocity. Based on Eqn. (4.5), the damper dissipates energy over each cycle of response, and the damper force will be out-of-phase with the displacement of the system.

Herein, the simplified model represented by Eqn. (4.5) is adopted to represent the viscous damper. Additionally, a damper is usually connected between different levels of a structure in series with a relatively long brace (or driver). To model the FVD-brace assembly in OpenSees, a *Maxwell* model is used that considers a dashpot and an elastic spring in series. The spring represents the driving brace. The dashpot, modeled by the viscous damper material, exhibits viscous behavior as described by Eqn. (4.5). Each FVD-brace assembly is simulated in OpenSees with a *two-node link* element connected to the two frame nodes to which the damper is attached; see Figure 4.4. The *Maxwell* material is assigned to align with the axial direction of the element.
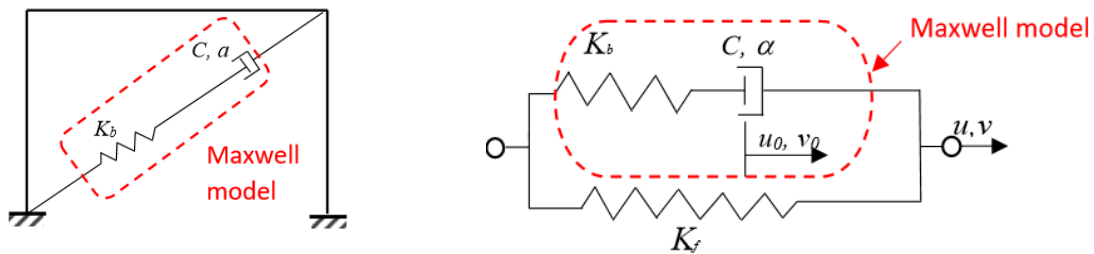
(a) Physical model of a SDOF system   **(b) Mathematical representation**

Figure 4.4   Numerical modeling of a FVD in one frame

4.2.3 Design Considerations

In designing new structural systems with supplemental energy-dissipation systems, frame elements are usually designed prior to designing the dampers. In current design specifications for a new building that uses supplemental energy-dissipation systems [ASCE 2010], a reduced base shear is allowed to size structural members in the preliminary design stage, which is at least 75% of that for a conventional building. This would result in weaker and more flexible structural members than a conventional building without a damping system. A rigorous check of the adequacy of the framing elements is then conducted after the damper locations, numbers, and mechanical properties are assigned. The design is iterated until all elements including the dampers meet the force or displacement requirements. In the case of an existing building, the size and details of the framing elements are predetermined, and the damper positions and characteristics must be selected to protect the framing elements and to provide the overall system responses desired. This study focuses on designing dampers; the efforts to check the adequacy of other structural elements are also discussed, but with limited exceptions; their properties are not changed from the as-built condition. A review of past studies on selecting damper locations, estimating effective damping ratios, and characterizing design parameters of dampers is provided

in the following paragraphs. This review is not exclusive to FVDs, but more generally applicable to all types of passive energy-dissipating dampers.

Damper locations

The first step in designing a system for a structure it to determine where the dampers are to be located. The selection is based on several factors, such as functionality requirements, architectural constraints, construction convenience, etc. Locations that have larger relative story deformation could generate large damping and thus are given priority. Other factors, such as the interaction between dampers and structural components that are connected with the dampers should also be accounted in the selection process.

Methods to find the optimum locations (story level, frames locations, etc.) to install dampers have been investigated by many researchers. Constantinou and Tadjbakhsh [1983] investigated the effectiveness of using a first-story damping system. The optimal damping ratio and its variation were derived for 1 to 5-story buildings. It was found that the first-story damping system can reduce the seismic responses of multi-story shear-type buildings. The concept of the first-story damping system was pioneering and provided an alternative strategy to a base-isolation system. However, this study is limited to short buildings and only considers shear-type buildings. Later studies by Hann and Sathiavageeswaran [1992] extended the study of damper placement to taller buildings, including a 10-story frame. Comparisons between several damper distribution schemes indicated that the first-story damping was an effective scheme for short buildings, but became less effective for taller buildings. Instead, they proposed placing dampers at lower half stories in a 10-story frame. Note: they used viscoelastic dampers, thus the added stiffness also contributed to reducing the drift ratio, though was not significantly. This study extends Constantinou's work and provides better insight into the effects of damping ratio and damper distribution in short- and median-rise buildings.

When consider a taller building, higher modes are a big concern, and thus dampers should be located in stories where shear deformations dominate [Peckan *et al.* 1999]. Correspondingly, a more rigorous method was proposed by Kasai and Jodai [2002] to select damper locations. The method studied two scenarios: state *R* and state *N*, which represented a building with "rigid damper" elements in damper locations and a bare frame, respectively. A same force pattern was laterally applied to both scenarios. State *R* captured the maximum reduction of displacement at a selected location, whereas state *N* estimated the maximum extent to which a damper could possibly deform. Locations where reduction of displacement predicted to be large were considered. Kasai and Iwasaki [2006] extended this method and used a simplified frame model to identify effective damper locations in a tall building. The effectiveness of this simplified method was investigated in later studies [Kasai *et al.* 2013]. This method was selected for application in this dissertation because it provides a plausible and efficient strategy to determine those locations with the largest potential of providing large damping effects.

Effective damping ratio

After selecting feasible damper locations, the overall effective damping ratios are estimated to provide guidance to select appropriate number and size of dampers. In practice, an effective damping value on the order of 20% is typical to represent the equivalent critical damping ratio

needed in a building [Miyamoto 2010; Occhiuzzi 2009]. Instead of relying on experience, several existing guidelines and codes provide damping modification factors to modify the design response spectrum accounting for damping values other than 5%. These coefficients help identify a value that could meet the target performance level for a specific building and thus are more widely applicable. Nevertheless, these values were typically derived based on responses of simple structural systems to a limited selection of ground motions, and in general did not include ones recorded on soft-soil sites or near earthquake fault ruptures [Ramirez *et al*., 2001]. A more refined spectrum modification method to account for variability of ground motion characteristics, site conditions etc. was proposed by Rezaeian *et al*. [2001]. This method was used in study presented herein.

If inelastic deformations of a structure become significant, the damping due to structural yielding should be accounted for. Research based on the capacity spectrum method (CSM) [Freeman *et al*. 1975] was extended to supplemental energy-dissipation systems in several guidelines [FEMA 273; NEHRP 2000] where a nonlinear static method is used to estimate the displacement demand and total effective damping ratio. This method utilizes a capacity curve of the building (adopted from a pushover curve) that intersects with an adjusted demand curve at the performance point. In the case of FVDs, these devices exhibit little storage stiffness and negligible displacement reduction due to added stiffness [Whittaker *et al.* 1997]. As such, a single demand curve could be generated, eliminating the need for iterative process. For example, Kim *et al*. [2003] used the CSM to obtain the effective damping ratio needed to achieve a target displacement using linear FVDs without iterations. However, since such a procedure relies on CSM, it shares the same shortcomings as CSM: (1) no physical principle to justify a stable relationship between the hysteretic energy dissipation and equivalent viscous damping; (2) an inability to capture higher modes using pushover analysis; and (3) inappropriate for pulse-type near-field record excitations, etc. [Kim *et al*. 2003].

A more widely acceptable method is based on Ramires *et al.* [2001], which considers nonlinear dampers (including yielding dampers and viscous dampers) used in a nonlinear frame. They proposed expressions for hysteretic damping and supplemental damping by including the ductility factor and damper nonlinear exponent. Their work laid the foundation of design guideline at that time [NERHP 2000] and was a reasonable approach to assess a nonlinear structure that incorporated a nonlinear damping system. The results have been utilized by other researchers to identify the required damping ratio [e.g., Diotallevi *et al*. 2014; Peckan *et al.* 1999]. Diotallevi *et al*. [2014] also provided graphical representation of analytical formulation using constant design acceleration curves (or constant design displacement curves and constant ductility curves) to facilitate the design. Limitations of these works include their insufficiency to consider non-proportional damping effect and brace flexibility effect, and only consider elastic-perfectly plastic behaviour.

Damper parameters

There are several design parameters that comprise the mechanical properties of a FVD, including the damping constant C and the damper exponent α; both are related to the damper force output. Current design guidelines and codes do not prescribe specific methods to identify these parameters; thus, a damper scheme is usually achieved by repetitive iterations in practice

[Miyamoto 2010]. However, damper placement strategies and these mechanical properties may have a significant impact on both structural behavior and total damper cost [Soong and Dargush 1997]. Thus, research has been conducted to help identify optimal design parameters, either separately or simultaneously.

The exponent α that designates the damping nonlinearity has been investigated by several researchers and engineers. This parameter affects the effectiveness of a FVD and its force capacity. With current technology, a FVD with α ranging between 0.15 to 2.0 could be manufactured, but 0.4 to 0.5 is most commonly-used for seismic design [Taylor 2010]. Generally, a linear damper is more capable of suppressing higher modes and has least interaction with structural forces that are in-phase with displacements [Duflot and Taylor 2008]. However, a linear damper develops larger damper forces than a nonlinear damper if the velocities are large, e.g., a long period structure subjected to intense ground shaking [Lin 2002]. Miyamoto *et al.* [2010] found that large damper forces in linear dampers under moderate or major earthquakes could exceed the damper capacity, jeopardizing the dampers and reducing their energy-dissipation capabilities.

The need to control peak damper forces has spurred research on nonlinear FVDs. Symans and Constantinou [1998] compared the energy-dissipation capacities of different FVDs by both experimental test and numerical studies, and found that a nonlinear damper with α equals to 0.5 could dissipate 11% more energy per cycle than a linear one, and 31% more than a nonlinear damper with equaling to 2.0 when subjected to a harmonic motion with a same amplitude and a same maximum damper force. Meanwhile, a nonlinear damper with α equaling 0.5 had a smaller peak damper force than the other two. Martinez-Rodrigo and Romero [2003] tried to upgrade a six-story steel structure using different nonlinear dampers. It was concluded that the peak force of a nonlinear damper would be more than 35% smaller than a linear damper assuming both dampers had an equivalent energy consumption. They found that a value of α slightly inferior than 1 was optimum based on the two quantitative parameters quantifying the overall structural performance and damper forces. In practice, nonlinear FVDs have been used in a variety of projects in buildings and bridges. [e.g., Asher *et al.*, 1996; Rodriguez *et al.*, 1996]. A sensitivity study was carried out in Section 4.4.2 of this dissertation to help identify an optimal value that could effectively control structural response without inducing excessive large damper forces.

In terms of damping constant *C*, Pekcan *et al.* [1999] proposed two methods to select damping constant *C* of linear dampers at different floor levels. A truss solution was used to resist story shear forces, with *C* sized proportional to story shears; and a load-balancing prestress tendon-fuse plus damper solution used to control the overturning moments. The second method was more applicable to a taller building where bending effects are significant. The procedure could also be applied to nonlinear damper cases but involve linearization by the equivalent power consumption method, harmonic equivalent linearization, or the energy balance method [Peckan *et al.* 1999]. The strategy to use pre-stressed tendon to suppress the building's bending behavior was novel and promising, but it is more appropriate for displacement-dependent-type damper as the pre-stressed tendon needs to act in-phase with the displacement. Note: in most practice, the selection of *C* values relies heavily on experience and trials. Miyamoto [2010] suggested *C* values were designed to be proportional to story stiffness in engineering

applications. Given the importance of this parameter and lack of guidance in selecting their values, it is selected as the major parameter in this study.

Another design parameter that impacts the behaviour of the damper is the stiffness of the driving brace that is in series with a damper. Figure 4.4 represents a damper-frame system that is modeled with a general Maxwell model. When the stiffness of the brace K_b is not large enough, its flexibility diminishes the deformation of the dashpot (damper), and generates a damper force that is more in-phase with displacement. Note: in a large device with a large chamber of fluid, the flexibility of the damper itself is not negligible and so is the connection details between a damper and a structural element. Given that the brace contributes most to the flexibility of the dashpot-spring assembly, this study assumed K_b represents the stiffness of the brace only. Further study is needed to understand the extent of flexibility introduced by a damper device and connection details.

The fact that a damper's effect is largely influenced by the brace flexibility has been acknowledged by a number of researchers [e.g., Kasai *et al.* 1998; Fu and Kasai, 1998; Kasai and Jodai, 2002; Takewaki and Yoshitomi, 1998; Dong *et al.* 2015; Park] and various design guidelines [e.g., ASCE 7-10, ASCE 41-13]. Arguably, however, it is unrealistic and probably not necessary to use a very large brace to insure the damper effect. Many studies have been conducted to determine an ideal value of K_b that maintains the damper effect while limiting the brace size. Fu and Kasai [Fu 1996; Fu and Kasai, 1998; Kasai *et al.* 1998] used the performance curves and identified an optimal brace stiffness to be 10 times that of a frame stiffness K_f in order to achieve the desired damper effect; Singh *et al.* [2003] identified a K_b to be five times of K_f; Chen *et al.* [2011] used a gradient-based algorithm and demonstrated that K_b should be sized as the first story K_f; Viola and Guidi [2008] suggested a K_b in the order of 45 times that of K_f. Other research used the damper size directly to identify K_b values: Londono [2014] used a first-order filter method to size the minimal brace stiffness based on desired damper efficiency over a predetermined frequency range, and found a K_b to be 5 times the product of damping constant C and fundamental frequency w (i.e., $K_b = Cw$). Given such a wide range of the proposed optimal values of K_b, it seems more appropriate to conduct a sensitivity study for a specific building. Section 4.4.3 contains a sensitivity study to investigate an optimal K_b for the case-study building.

Comprehensive research work has been conducted by Kasai and his colleagues in an attempt to select these parameters simultaneously. In their early work [Fu 1996; Fu and Kasai 1999; Kasai *et al.* 1998], they constructed performance curves to assess the effect a damper-frame system by using a single-degree-of-freedom (SDOF) model representation, covering viscoelastic dampers, elastoplastic dampers, and fluid viscous dampers. The SDOF model not only assesses the mechanical properties of each type of dampers, but also includes the brace in series with a damper and the frame in parallel with the damper-brace sub-assembly. As such, the effect of added damping and added stiffness could be expressed by design parameters, including C, α, K_b and K_f. To graphically aid the design and selection of these parameters, they generated the displacement reduction versus acceleration reduction curve (R_d-R_a curve), which could identify an optimum point that is closest to the origin.

This method provides a convenient way to select design parameters based on the target displacement and acceleration, and accounts for the effect of both period shifting and added damping for a damper–frame assemblage. Their work was first focused on linear dampers in

combination with a linear system and was extended to nonlinear dampers [Kasai *et al.* 2003 and 2007]. A similar procedure was done for a linear damper ($\alpha = 1$) and a friction damper ($\alpha = 0$), and system properties and peak damper forces/deformations of a nonlinear damper [$\alpha \in (0,1)$] were expressed by interpolation. Given the complexity of a nonlinear damping system, their method provides a feasible approach to understand the energy-dissipation capacities, phase angle, and peak damper capacities etc., of nonlinear system with nonlinear dampers. Furthermore, they outline a procedure to preliminarily size damper properties for a multi-degree-of-freedom (MDOF) system based on the SDOF model representation and considers the higher-mode contributions. Their work is pioneering and comprehensive, but involves very theoretical and sophisticated procedures, which might limit their wide applicability in practice.

4.2.4 Applications

Fluid viscous dampers utilizing silicon gels have been used in the military for many years for attenuation of weapons-grade shock. This technology was eventually converted for commercial applications. Extensive research by the U.S. Multi-Disciplinary Center for Earthquake Engineering Research (MCEER) and one of the largest damper manufactures in the U.S., Taylor Devices, Inc. were carried out to understand the principles of such devices and their applicability in seismic/wind design of structures. This began a new era for worldwide applications of FVDs as seismic or/and wind energy-dissipation elements in commercial buildings, bridges, and related structures [Constantinou 1994; Taylor and Constantinou 1996]. The basic properties and efficiency of viscous dampers were tested in the early 1990s [Constantinou and Symans 1992; Reinhorn *et al.* 1995; Taylor and Constantinou 1995; Seleemah and Constantinou 1997]. Since then, FVDs have gained global acceptance as a strategy to control structural response under seismic or/and wind load. In light of earthquakes such as the 1994 Northridge earthquake, 1995 Kobe earthquake etc., where a large number of structures were damaged severely, engineers discovered that using FVD provided a promising solution to accommodate the ever-increasing seismic design requirements for new buildings as well as a solution for upgrading existing buildings [Miyamoto *et al.* 1996 and 1997; Taylor *et al.* 2004].

Examples of early damper applications in buildings that have been documented include a retrofitted 1/3-sccale reinforced concrete building model [Reinhorn *et al.* 1995], a seismically-rehabilitated 4-story concrete structure that exhibited non-ductile soft story mechanism [Miyamoto *et al.* 1996], a 11-story steel pyramid-shaped office building [Miyamoto and Scholl 1997], a ¼-scale building model with both linear and nonlinear dampers [Seleemah *et al.* 1997] and a 2-story steel moment frame that was the first to use the 2000 NEHRP guideline [Miyamoto, *et al.* 2002] etc. Several other well-known projects include the 32-story Los Angeles City Hall, the 14-story San Francisco Civil Center Office building, the Pacific Northwest baseball stadium in Seattle [Taylor 2010a], and the 57-story Torre Mayor that used mega-brace configurations [Taylor and Katz 2004]. Most of these applications installed FVDs in a diagonal or chevron configurations in a building frame; some applications also involved a toggle-brace-damper system to magnify the dampers deformations for stiff structures [Constantinou *et al.* 2001; Taylor and Constantinou 1998]. Shake table tests on such a magnifying mechanism by Taylor and Constantinou [1998] revealed that it was possible to obtain a 3:1 increase in the measured story drift at the mounting points of the damper using the toggle-brace-damper system. However,

Japanese reseachers [Kasai and Jodai 2002; Kasai and Iwasaki 2006] found such a toggle-brace-damper configuration might not be able to achieve the amplifications due to flexibility of connecting elements, and that the traditional diagonal configuration could be equivalent or more effective when the construction qualify and details are considered.

A wider application of FVDs is seen in the new design or retrofit of bridges. A few well-known bridges include: the Golden Gate Bridge [Rodriguez *et al*. 1994], the San Francisco-Oakland Bay Bridge, and the London Millennium Footbridge [Taylor 2000]. In Asian and European countries, there have been a great number of applications using FVDs [Infanti *et al.* 2004 and 2006]. Besides, dampers are designed to supplement an isolation system for additional damping [Makris and Contantinou 1990; Constantinou *et al.* 1992; Constantinou *et al*. 1993; Soong and Contantinou 1994], to either control the isolator's displacement (installed in the isolation level) or control the super-structure's response. More applications of FVDs for seismic hazard mitigation can be found in lists provided by damper manufactuers, e.g., Taylor Device Inc. [2015].

Post-earthquake observations after recent major earthquakes (e.g., 2011 Tohoku Earthquake, Japan and 2003 Colima Earthquake, Mexico) have shown that incorporating dampers not only meet the life safety requirements of buildings, but could also control damage in an event of an earthquake [EERI 2012; Takewaki *et al*. 2013].

4.3   RETROFIT OF CASE-STUDY BUILDING USING FLUID VISCOUS DAMPERS

The analysis method and a two-phase design procedure to locate dampers and select their mechanical properties are discussed in this section. Note: the procedure outlined in this section is similar to those reported in Lai *et al*. [2015]; however, the results have been updated based on more refined modeling assumptions. Therefore, most contents have been retained for completeness of the dissertation.

4.3.1 Analysis Method

In ASCE 41-13 [2013], four types of analysis methods can be used depending on the complexity of the structure, the design stage, and the desired accuracy of analysis results, etc. The analysis methods are: Linear Static Procedure (LSP), Linear Dynamic Procedure (LDP), Nonlinear Static Procedure (NSP), and Nonlinear Dynamic Procedure (NDP). Linear procedures (LSP and LDP) are often used in preliminary design where linear elastic materials are assumed for the analysis; they are only allowed for structures without large irregularity or potential inelastic response. By means of checking demand-capacity ratios of primary components, one can identify if linear procedures are appropriate. Linear procedures are intended to provide a simplified strategy for design and analysis of structural response. If a structure is complex, a more robust nonlinear analysis may be mandatory.

If linear procedures are not allowed for a structure, nonlinear procedures should be performed. The NSP is usually insufficient to accurately account for changes in dynamic responses if stiffness degradation occurs, or cannot capture higher-mode effects in a MDOF system. However, the NDP can be applicable to all structures and is the only method advisable

for an inelastic structure that has incorporated supplemental energy-dissipation devices. With the advent of increasing computational capacities, the NDP procedure becomes a preferred method in most engineering practice (based on oral communication with many experienced engineers), which is also reflected in most recent design guidelines [NEHRP 2015]. When using NDP, dampers should be explicitly modeled in locations of installation to capture the interaction between the dampers and structural elements. The NDP is used in the study presented below. A damper-brace assemblage was simulated by a Maxwell material model that consisted of a spring and a dashpot in series; see Figure 4.4.

The design of FVDs in the case-study building employed two phases. To streamline the analysis effort, in the Phase-1 design only used three out of the twenty ground motions under BSE-2E hazard level (GM-01, GM-02, and GM-04 of BSE-2E). The selected three-component excitations matched the target pseudo-acceleration spectral shape near the building's fundamental period. To evaluate the refined Phase-2 design, all ground motions under BSE-1E and BSE-2E, each having twenty records, were used. See Figure 3.5 for the response spectra of ground motion records and target spectra at two BSE levels.

4.3.2 Design Procedure

To remedy several major seismic vulnerabilities identified in the existing building and achieve the collapse prevention performance level under a BSE-2E event, a two-level retrofit plan was proposed. The first level retrofit fixed all brittle column splices and removed the building's heavy exterior cladding; see Chapter 3. Analysis results indicated that the Level-1 enhancements improved structural behavior significantly at the BSE-1E hazard level, but these measures proved inadequate when the seismic intensity increased to BSE-2E hazard level. The Level-2 retrofit proposed to improve the structural performance of the case-study building to meet performance objects by installing FVDs. Using the building's numerical model incorporating the Level-1 retrofits as the baseline model, a retrofit method using FVDs was considered in Level-2 updates: Phase-1 installed dampers over the full height of the building, and the Phase-2 refined the damper design by adjusting the properties and locations of the FVDs to reduce the total number of dampers needed to achieve the same performance goal with Phase-1.

Damper locations

Figure 4.5 (a) is a sketch of a typical floor plan where the black boxes indicate column locations. Because interior frames are usually adjacent to stairs and elevator locations, putting dampers there would interfere with office space and egress. Therefore, the perimeter frames were initially selected as appropriate locations for the dampers. In preliminary trials, dampers were stacked in one or two bays on each face of the building; however, this resulted in a significant accumulation of forces in the columns adjacent to the dampers. To minimize this accumulation, the dampers considered in Phase-1 were distributed over the full height of the structure as shown in blue diagonal lines in Figure 4.5 (b); see Section 4.4.1 for a discussion about the effect of damper locations. Note that the odd number of bays in the longitudinal direction of the building resulted in a skewed distribution of dampers. Damper locations were refined in Phase-2 design, as discussed later.

WE(X-dir.)   NS(Y-dir.)

(a) Plan view   **(b) Elevations**
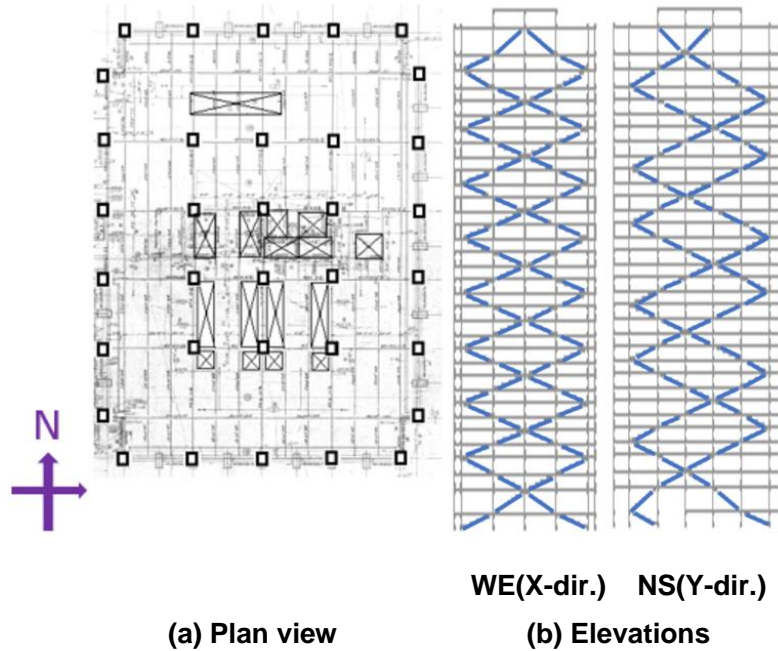
Figure 4.5   Typical floor framing plan and elevations indicating damper placement along diagonal lines crossing building perimeter

Effective damping ratio

To estimate the total effective damping needed to reduce the overall drifts and drift concentrations to acceptable levels, a method based on a damping scale factor (DSF) was utilized in this study. Based on Rezaeian *et al.* [2012], the elastic spectral ordinates were adjusted for a standard 5% damping ratio to determine the effective viscous damping ratios needed to limit roof displacements to the targeted values. The DSF represents the ratio between displacements corresponding to the target damping ratio and 5%, which was determined from a rigorous regression analysis of responses computed considering the entire NGA-West 2 database. As such, this procedure accounts for variations of magnitude, source-to-site distance, local site conditions, etc.

Based on a simplified static pushover analysis (Chapter 3) considering a first-mode lateral force pattern in the *X*-direction, beam-to-column connections began to fracture, and the building's lateral load resistance dropped precipitously at roof displacements of about 38 in. Therefore, this value was selected as the target maximum peak roof displacement for the retrofit goal.

ASCE 41 [2013] was then used to estimate the roof displacement demands under the BSE-2E excitation. This was done using Equation 7-28 in the standard:

$$\delta_{t\,5\%} = C_0 C_1 C_2 S_a T_1^2 / 4\pi^2 g$$

where C_0 is the modification factor for transforming from SDOF to MDOF, 1.3, C_1 is the modification factor for inelastic analysis, 1.0, C_2 is the modification factor for pinched hysteresis

shape, degraded stiffness and deteriorated strength, 1.0, and T_1 is the fundamental period in seconds.

For simplicity, the fundamental period T_1 of the baseline model that has incorporated Level-1 retrofits only was used to estimate displacement demand for the building with dampers. This resulted in an estimated roof displacement in the *X*-direction of 48 in at BSE-2E level. As a result, a desired DSF of (38/48=) 0.79 was derived. The value of damping required to achieve this DSF was estimated from the regression analysis equation proposed by Rezaeian *et al.* [2012]:

$$\ln(DSF) = b_0 + b_1 \ln(\beta) + b_2 \left[\ln(\beta)\right]^2 + \left\{b_3 + b_4 \ln(\beta) + b_5 \left[\ln(\beta)\right]^2\right\} M$$
$$+ \left\{b_6 + b_7 \ln(\beta) + b_8 \left[\ln(\beta)\right]^2\right\} \ln(R_{rup}) + 1$$

where the regression coefficients b_i can be found in Table 4.1 of their report.

The effective damping ratios determined in this manner were 10% in the *X*-direction at BSE-2E. The estimation of the effective damping ratio in the *Y*-direction followed the same procedure and resulted in a value of 15%. While this approach uses only the first-mode undamped dynamic properties of the building, it provides a convenient way to estimate damper sizes at the preliminary design stage without iteration. In addition, this approach is appropriate for this structure since the structure remains essentially elastic prior to the rupture of the connections. The efficacy of this method was assessed using the analysis results reported below.

Damper scheme: Phase-1

The configuration of the FVDs over the full height of the structure is shown in Figure 4.5 (b). For a preliminary estimation, only the first mode was used in conjunction with the desired effective damping ratio identified (10% for *X*-direction and 15% for *Y*-direction).

Following Eqn. (4.6), each FVD is characterized by two parameters: the damping constant *C* and damping exponent α. These could be related to the effective damping ratio using the elastic strain energy method [Soong and Constantinou, 1994], i.e.,

$$\xi_{\text{eff}} = \xi_0 + \frac{\sum_j \lambda C_j \phi_{ij}^{1+\alpha} \cos^{1+\alpha} \theta}{2\pi A^{1-\alpha} \omega^{2-\alpha} \sum_j m_i \phi_i^2} \tag{4.6}$$

where ξ_0 is the intrinsic damping ratio, λ is an expression based on gamma function, [i.e., $\lambda = 2^{2+\alpha} \times \Gamma^2(1+\alpha/2)/\Gamma(2+\alpha)$], ϕ is the mode-shape coefficients, θ is the angle between the orientation of damper and beam, *A* is the target roof displacement, and ω is the frequency of selected mode. In this dissertation, emphasis was placed on selecting the damping constants C_j. Different distributions of *C* over the height of the building were considered, as described below.

Several separate parametric studies were undertaken to help in the preliminary design. In the analyses reported herein, nonlinear FVDs with α=0.35 were used. A parametric study found that the value of 0.35 for damping exponent α provided good structural control without inducing

excessive damper forces. Details are presented in Section 4.4.2. Another parametric study identified the stiffness of the driving brace K_b to insure full damper efficiency, revealing that a summation of the stiffness of all damper braces in one story equal to twice of the lateral stiffness of that story was ideal; see details in Section 4.4.3. Moreover, the braces, arranged as a single diagonal configuration across a bay, were deemed the most appropriate configuration for an existing building; see Section 4.4.5.

In the Phase-1, three different arrangement schemes were proposed to find an ideal damper distribution pattern based on previous research results and engineering practice. Soong and Dargush [1997] suggested a uniform distribution of viscoelastic dampers design for the late World Trade Center, although as later research has proven, this strategy might not be very effective especially in the top floors. Because dampers on upper stories are less effective at reducing drift than those in the lower stories, some researchers [Hwang 2008; Pekcan *et al.* 1999] have proposed that *C* values be sized such that the damper force be proportional to the design story shear forces. Another possible approach is stiffness-proportional story-wise distribution, which results in a Rayleigh-type damping without coupling of different modes. Therefore, three distributions of damping constants *C* over the height of the building were considered:

 I. Uniform distribution;

 II. Distribution proportional to story shear demand;

 III. Distribution proportional to story stiffness.

Figure 4.6 presents a conceptual sketch of the three distribution patterns of *C* over stories. Although Scheme II and Scheme III are similar, scrutiny suggested that smaller damper sizes (*C* values) were used in stories 5-9 of Scheme II. Scheme III used small dampers at story level 2 where a mezzanine is configured.

I Uniform   **II Proportional to story**   **III Proportional to story**

Figure 4.6   Sketches of three story-wise damper distribution patterns
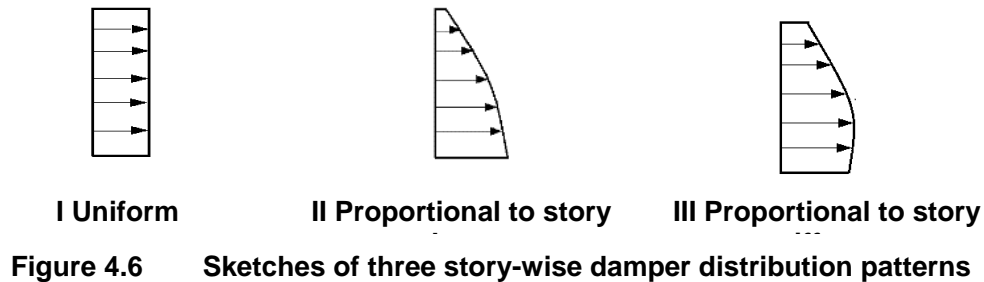
Global response, including peak displacements, peak story-drift ratios, peak floor accelerations, and peak damper responses were reported below based on the maximum values of three NRHA results at BSE-2E hazard. Each direction was evaluated separately considering different damping ratios used. Because similar trends were observed for both directions of the building, only the results for the *X*-direction are presented for global response.

Computed peak floor displacements used to determine the distribution of damper coefficients were similar for all three methods; see Figure 4.7. The predicted maximum roof displacements were about 38 in for all schemes, thus validating the adequacy of the method to estimate the effective damping ratio. All three cases helped reduce the peak floor displacements compared to the Level-1 baseline case by up to about 30%. The FVDs helped distribute the peak

story drift ratios more uniformly over the height of the building, with a larger decrease in stories 5 to 9; see Figure 4.8. However, a small difference between these schemes is noted. Scheme I, with the same damping constant *C* used for all dampers, was the least effective in stories 5 to 9 but resulted the smallest drifts in the upper stories. Scheme II, with *C* selected in proportion to story-shear demands, and Scheme III, with *C* selected in proportion to story stiffness, provided similar results; the latter scheme was slightly more effective in reducing the peak story drift ratio in the weak-story zone. Scheme III was the most successful in terms of reducing the maximum peak drift ratio, reducing it to 1.2%.

The elimination of the weak-story behavior with the FVD retrofits reduced the number of beam-to-column connection failures. Figure 4.9 shows the beam end connection failures as a percentage of the total number of beam-to-column connections per floor, considering both *X*- and *Y*-directions. Note: for figures that do not designate a specific direction, the results were based on the maximum of *X*- and *Y*-directions hereafter. The most efficient scheme identified earlier— Scheme III—reduced the percentage of beam-to-column connections failure from 58% to less than 2% in the critical levels where weak-story behavior occurred. This suggests that the retrofit goal of maintaining structural stability for BSE-2E level earthquake events was essentially achieved. The improvement would significantly reduce repair costs and business interruption losses after an earthquake.

Additionally, peak floor accelerations were reduced after installation of the dampers. The reduction ranged from 40% to 50%, with a peak roof acceleration reduced to about $0.5g$ from about $0.9g$; see Figure 4.10. Scheme I, with the relatively large damping coefficients near the roof, controlled peak accelerations at the roof level more effectively compared to other two schemes. Apart from reducing the peak floor accelerations, FVDs also led to a faster decay of vibrations. A roof acceleration time-history plot (Figure 4.11) for both the Level-1 retrofits and Scheme III of the Level-2 retrofit indicated that the latter suppressed the structural vibrations much faster during free vibration.
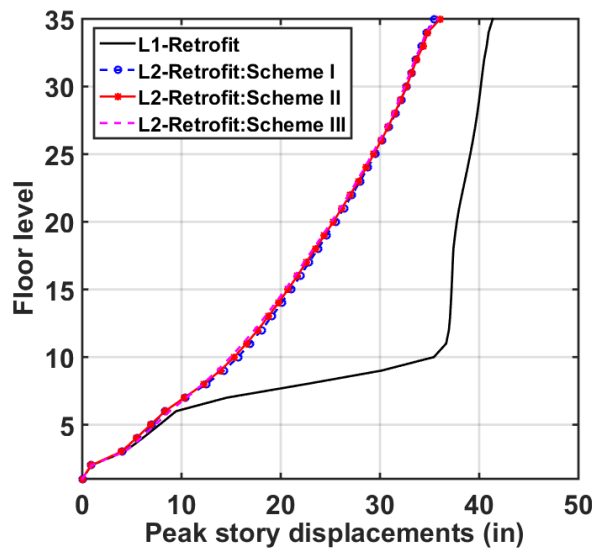
Figure 4.7   Distribution of peak story displacements for different Phase-1 designs (X-dir.) (max. of three analyses)

66
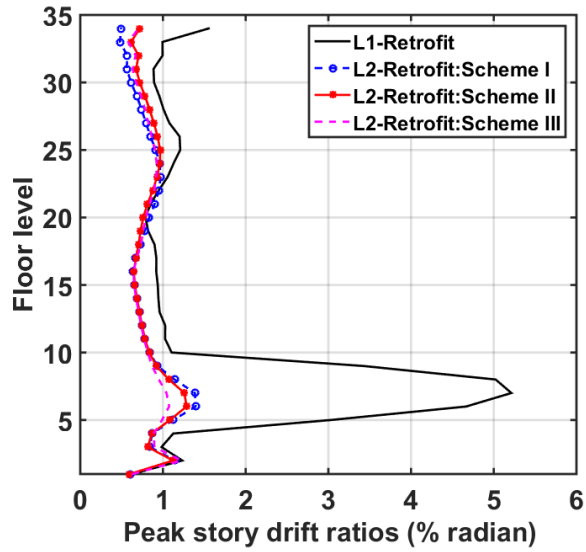
Figure 4.8   Distribution of peak story drift ratios for different Phase-1 designs (X-dir.) (max. of three analyses)
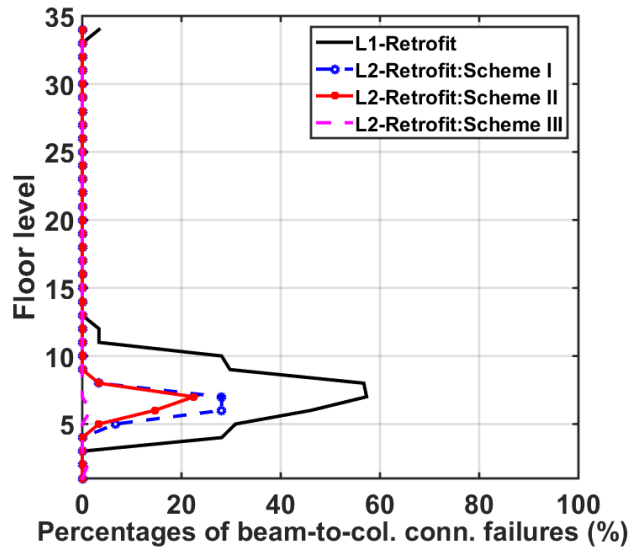
Figure 4.9   Distribution of peak beam connection failures (as percentage of total number of connections per floor) for different Phase-1 designs (max. of three analyses)
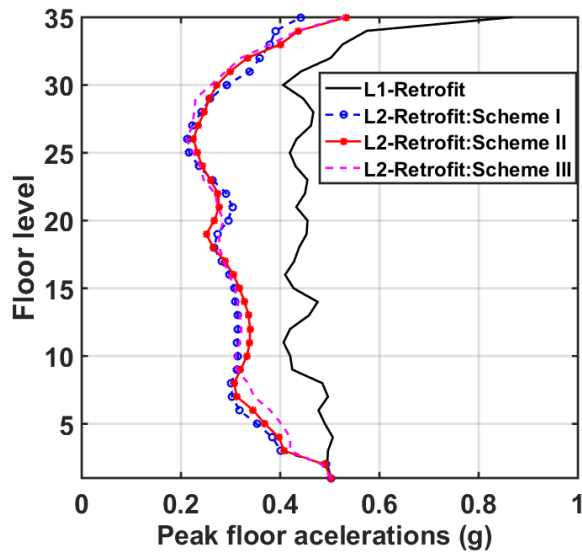
**Figure 4.10   Distribution of peak floor accelerations for different Phase-1 designs
(X-dir.) (max. of three analyses)**

Although FVDs were shown to improve structural response and maintain global stability of the building at BSE-2E events, the size of FVDs required for this goal required additional investigation of damper hysteresis behaviors and peak damper forces. The distributions of peak damper force demands were compared amongst the three schemes considered are shown in Figure 4.12. All schemes predicted fairly large damper forces, with the maximum ranging from 1200 kips to 1300 kips at the lower stories. Figure 4.13 shows typical hysteresis behavior of one FVD exhibiting large force demand under one ground motion excitation of Scheme III. Large-capacity dampers are available through several manufacturers (e.g., Taylor Devices Inc. [2010]; see Table 4.1), but large-size dampers could increase retrofit costs appreciatively due to their weight and cost, the large size of the required driving braces, complexity of connecting dampers to the existing framing elements, reinforcing collectors and diaphragms, etc. Thus, the cost-effectiveness of several alternatives is worthy of investigations, such as using two smaller dampers per driver (e.g., installed in parallel), employing more damped bays at selected stories or utilizing toggle-brace mechanisms to magnify the effective force of a damping device [Constantinou *et al.*, 2001].
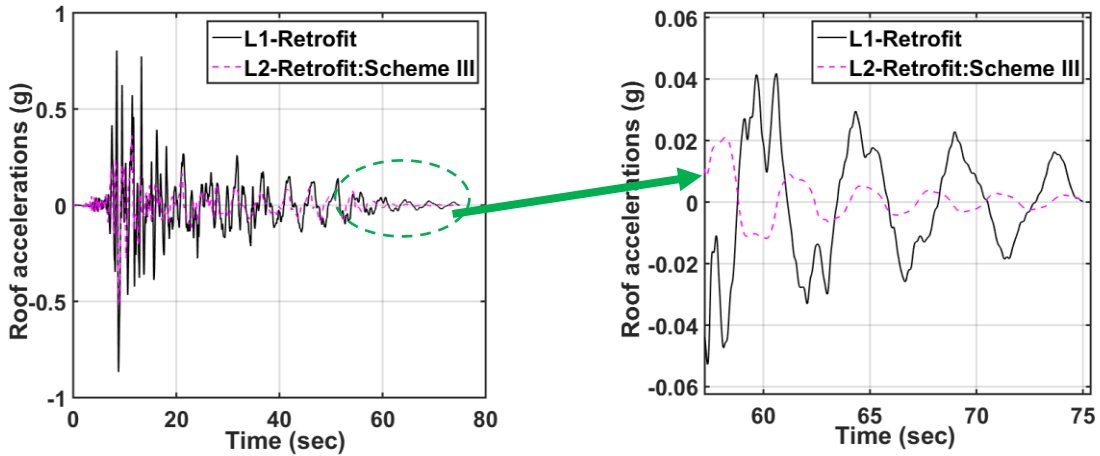
(a) Time history of roof acceleration (X-dir.)   **(b) Zoomed in view (during free vibration)**

Figure 4.11   **Time history of roof accelerations under one ground motion**

Table 4.1   **Damper size and weight (adapted from Taylor Device Inc. [2010])**

Force (kips)	Stroke (in.)	Weight (lbs)
55	±3	90
110	±4	185
165	±4	300
220	±4	425
330	±4	600
440	±5	900
675	±5	1300
900	±5	2650
1450	±5	4100
1800	±5	5500
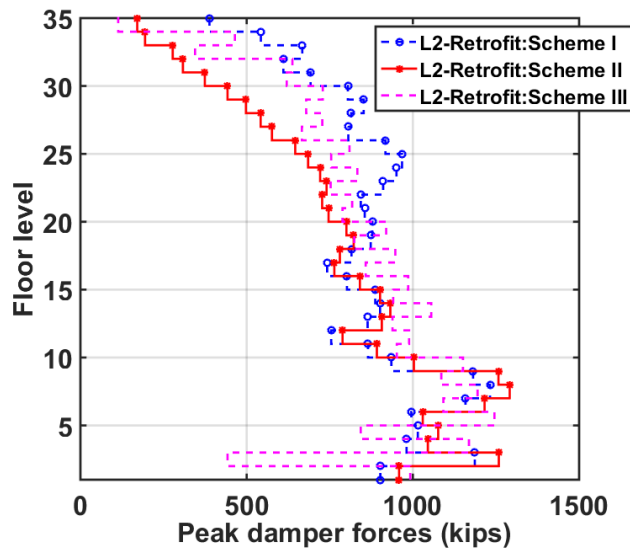
Figure 4.12   Distribution of peak damper forces for different Phase-1 designs (max. of three analyses)
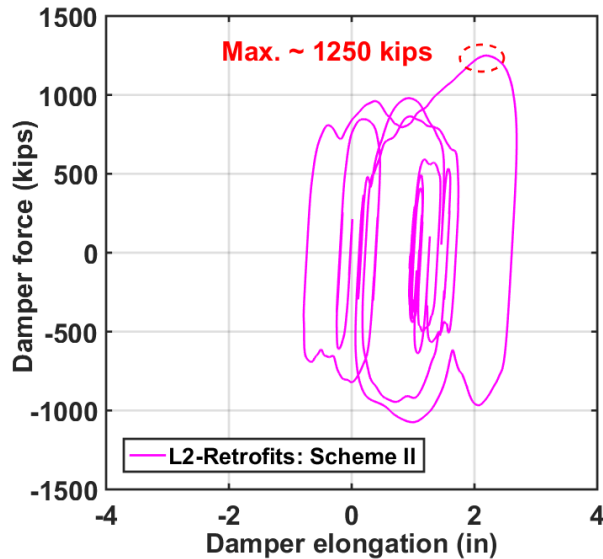
Figure 4.13   Hysteresis loop of a FVD under one ground motion (floor 7)

It is apparent from previous results that FVDs achieved the level of safety established for the retrofit goal. Among the three schemes investigated, Scheme I, with dampers distributed uniformly throughout stories, required larger dampers than necessary at the upper floors. Schemes II and III provided similar results in terms of reducing peak displacement and peak accelerations, with Scheme III being more effective in reducing the peak drift in the weak-story zone. As such, Scheme III, with damping constant C distributed proportional to story stiffness, has the benefit of generating a Rayleigh-type damping matrix and avoiding coupling between different modes; therefore, it was selected for continuing refinement.

70

Damper scheme: Phase-2

Given that Scheme III was clearly the most efficient method, it was selected in the Phase-2 refinement to minimize the total number of FVDs needed to achieve the stated performance goal. A refined scheme (denoted as Scheme III$_R$) was proposed in Phase-2 design, the goal of which was to enhance the distributions and characteristics of the dampers.

To effectively engage dampers in energy dissipation requires determining the optimal locations for installing dampers where shear deformations are large. This study used an equivalent frame model based on Kasai *et al*. [2002 and 2006]. Two states were evaluated, including state "*N*," which represents the bare frames, and state "*R*," which represents the same frame but with the addition of with rigid elements in candidate damper locations. The story stiffness at both states were evaluated, denoted as K_N^i and K_R^i (where i is the story number). A story with a large increase from K_N^i to K_R^i indicates a larger shear deformation contribution and thus ideal location for installing dampers. A consistent lateral force pattern suggested by ASCE 7 [2010] was applied for both structural status to help identify K_N^i and K_R^i. Based on estimates, the ratio K_R^i / K_N^i was then used to reflect the relative contributions due to shear deformation. The larger this value is, the larger shear deformation at that story, thus pinpointing optimum locations for installing dampers.

Kasai's study [Kasai *et al*. 2013] suggested that a K_R^i / K_N^i that is equals or larger than 2 should provide good passive control; this criterion is adopted for this study. As a result, the refined scheme had dampers located at stories below 25, reducing the number of dampers by 40%; see Figure 4.14 for the Phase-2 refined design. A detailed summary of K_N^i and K_R^i values are presented in Table 4.2. Note: a check at further decreasing the number of stories retaining dampers revealed that the weak-story zone would be shifted to stories between 10 to 20, and thus was not advisable.

In addition to identifying locations with the potential to provide large damping, the sizes of dampers were tuned based on the demand at different floor levels. As determined earlier, it was found that lower floors generally require a higher damping demand, whereas mid- and upper-stories require reduced damping demand. Therefore, a simplified method was proposed to manually tune the size of dampers (*C* values) to more effectively engage the damper effect. A performance index (PI) and a cost index (CI) were designed to quantitatively measure the damper effect. The revised layout with fewer dampers was used in this procedure (Figure 4.14).

The PI is formulated based on four engineering demand parameters (EDPs): (1) peak story drift ratio; (2) residual drift ratio; (3) peak floor acceleration; and (4) average floor accelerations 15 sec after the excitation stops. An overall PI is a weighted function of these four EDPs, with different weight coefficients arbitrarily selected to reflect the relative importance of each EDP. In terms of CI, the damper ultimate force output and the number of dampers at each floor are integrated in the weighted function to reflect the initial cost of the dampers. An examination of these parameters at different stories revealed that a larger damping demand is need in the most deformed stories. As such, the damper sizes (*C* values) at stories 4–9 were increased by 30% in the *X*-direction, and by 20% in *Y*-direction as a trial to meet the target drift requirements at these regions. The FVDs at middle and upper stories were reduced by 20% at

floors 10 to 25 in the *X*-direction and floors 15 to 25 in the *Y*-direction. More details to compute PI and CI, and the resulted values could be found in Lai *et al*. [2015]. Note: these percent values were selected based on a combination of PI and CI values at each story zone; other values are possible and might provide slightly different results, but would not affect the summary and trend reported below. Another adjustment in the refinement scheme (III$_R$) was to limit the types of different-size FVDs used to align with practical design routine; see Table 4.3. Locations where similar structural and damper responses were observed had the same damper size. Note: the number of different damper sizes could be further reduced. As a result of the refinement, the effective damping ratio for Scheme III$_R$ became 8% and 15% for *X*- and *Y*-directions, respectively.
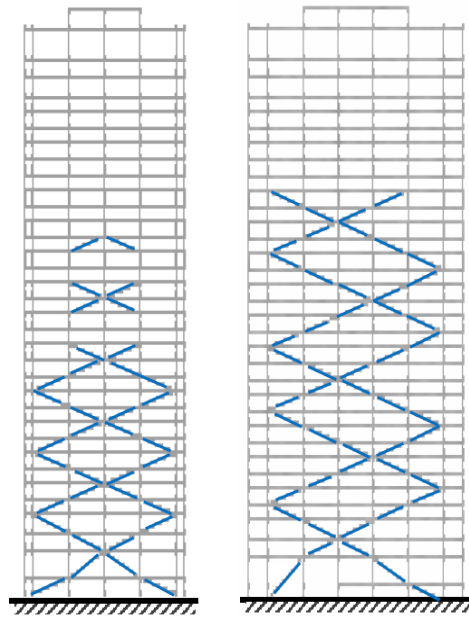
Figure 4.14   Refined damper scheme (III$_R$)

Table 4.2   Calculations of frame parameters

Story	*X*-direction			*Y*-direction		
	K_N^i (*k/in*)	K_R^i (*k/in*)	K_R^i/K_N^i	K_N^i (*k/in*)	K_R^i (*k/in*)	K_R^i/K_N^i
1	19000.0	1226694.7	64.6	20332.0	237548.2	11.7
2	5847.4	439397.8	75.1	6248.2	464943.4	74.4
3	12570.9	107043.3	8.5	13447.8	294426.0	21.9
4	11208.0	34572.6	3.1	12241.7	103710.7	8.5
5	12619.8	53602.7	4.2	14108.7	45809.4	3.2
6	12160.5	73750.8	6.1	13896.0	44654.9	3.2
7	11855.3	52716.3	4.4	13703.8	69570.8	5.1
8	11624.6	28973.0	2.5	13536.2	63099.8	4.7
9	11391.1	34034.5	3.0	13322.0	52750.4	4.0

10	11233.6	40378.2	3.6	13131.4	41550.7	3.2
11	11160.5	33184.5	3.0	12954.7	56890.5	4.4
12	11111.3	23162.1	2.1	12809.9	49931.5	3.9
13	10994.6	24778.0	2.3	12640.9	41224.9	3.3
14	10879.1	28834.7	2.7	12499.5	39237.6	3.1
15	10752.8	25953.1	2.4	12347.8	31780.1	2.6
16	10568.0	19158.8	1.8	12146.6	28447.7	2.3
17	10058.4	19765.7	1.9	11589.1	33345.0	2.9
18	9592.3	22731.7	2.4	11069.8	32771.2	3.0
19	9428.0	20893.2	2.2	10872.8	29864.4	2.7
20	9313.4	16288.9	1.7	10724.0	26920.9	2.5
21	9079.9	16173.1	1.8	10430.0	30431.4	2.9
22	8847.6	18021.8	2.0	10152.0	26342.7	2.6
23	8627.8	16629.9	1.9	9953.7	24011.6	2.4
24	8433.1	13477.5	1.6	9790.6	22762.1	2.3
25	8222.8	12840.3	1.6	9615.4	20320.0	2.1
26	8005.7	13480.5	1.7	9431.6	17376.7	1.8
27	7710.2	12210.2	1.6	9185.8	17197.7	1.9
28	7395.5	9965.1	1.3	8906.0	16584.0	1.9
29	7041.1	8825.1	1.3	8566.4	14479.2	1.7
30	6608.4	8416.5	1.3	8139.6	12373.7	1.5
31	5929.0	6982.4	1.2	7421.6	10671.7	1.4
32	3466.5	3821.9	1.1	4477.1	5909.4	1.3
33	3514.9	3279.4	0.9	4619.5	5279.4	1.1
34	985.6	1004.2	1.0	1254.3	1512.6	1.2

* Shaded boxes indicate locations where dampers are kept

Table 4.3   Allowable design C values

C $kip \cdot (sec/in)^{0.35}$	150	225	300	375	450	525	600	675	750	825

To check the effectiveness of the Phase-2 refined design, the structural response and damper forces were compared between: the baseline case with Level-1 retrofits only, the Phase-1 damper design (Scheme III), and Phase-2 damper design (Scheme III$_R$). The story drift ratios and percentage of beam-to-column connections failure were essentially the same for Schemes III and III$_R$, with a slightly larger drift ratio at mezzanine level for III$_R$; see Figure 4.15 and Figure 4.16. In addition to reducing the total number of dampers required for Scheme III$_R$, the peak damper forces were reduced at many floors (Figure 4.17). However, although peak floor accelerations (Figure 4.18) were similar at lower stories, they were noticeably larger above story 10 for Scheme III$_R$ where dampers were eliminated or smaller compared to Scheme III. For instance,

peak roof acceleration increased from 0.5g in Scheme III to 0.7g in Scheme III$_R$. The locations where these accelerations are important, damper properties can be adjusted.

Consequently, the effectiveness of the Phase-2 scheme achieved a same overall retrofit goal with the Phase-1 design while reducing the damper cost by a significant amount. While a further refinement of the damper arrangements was possible, Scheme III$_R$ was considered as the final design; more detailed assessments of its efficacy were conducted and reported in the following section.
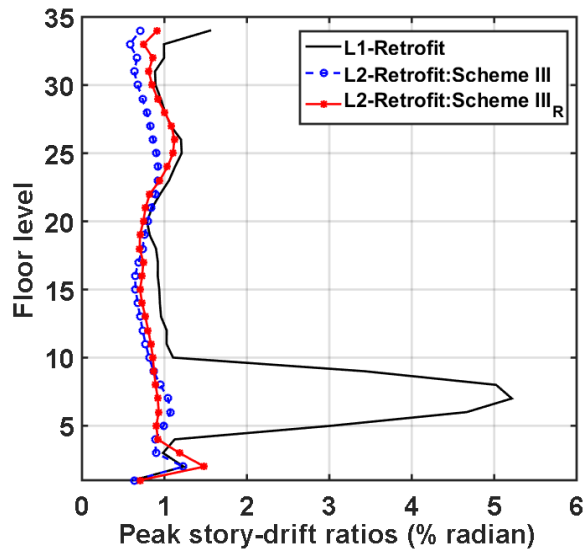
Figure 4.15   Distribution of peak story drift ratios for Phase-1 and Phase-2 designs (X-dir.)
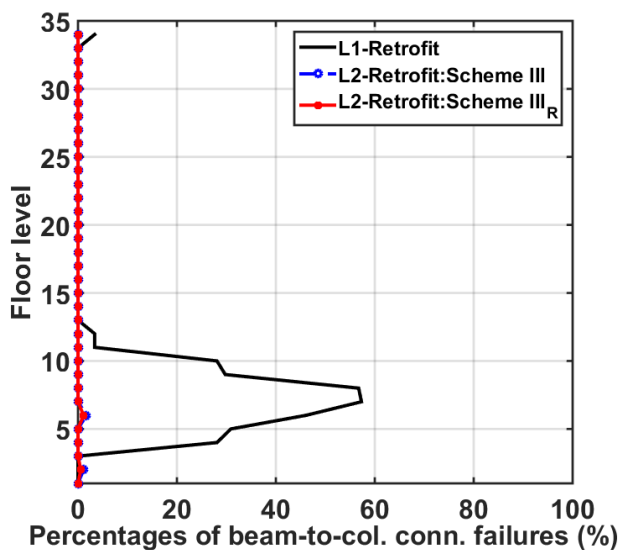
Figure 4.16   Distribution of peak beam connection failures (as percentage of total number of connections per floor) for Phase-1 and Phase-2 designs
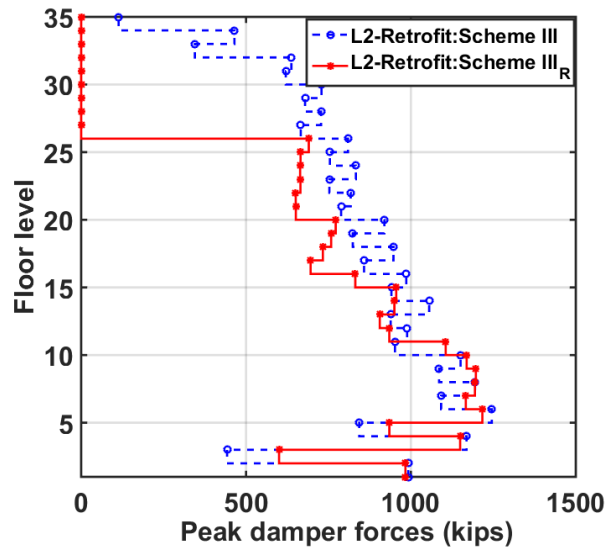
Figure 4.17   Distribution of peak damper forces for Phase-1 and Phase-2 designs
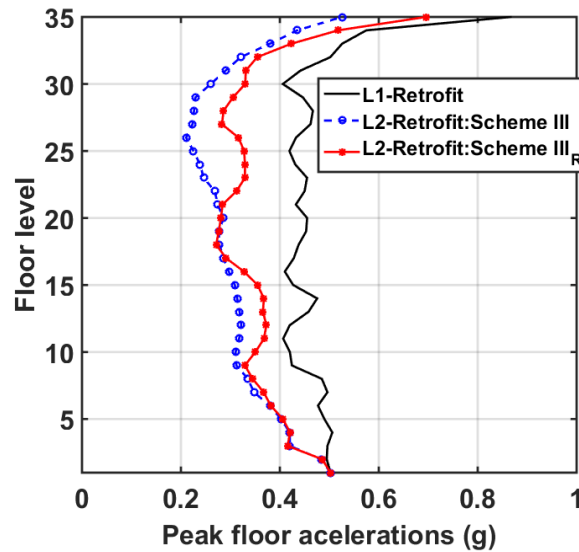
Figure 4.18   Distribution of peak floor accelerations for Phase-1 and Phase-2 designs (X-dir.)

4.3.3   FEMA 351 Probabilistic Check

A more comprehensive evaluation of the effectiveness of Scheme III$_R$ was carried out considering the full sets of 20 ground motion records for the ASCE 41 BSE-1E and BSE-2E hazard levels. The evaluation procedures described in FEMA 351 were used to compute the confidence with which the Level-1 retrofits and Scheme III$_R$ of Level-2 retrofits could achieve the collapse prevention (CP) performance goal under different earthquake scenarios.

The FEMA 351 evaluation procedure is expressed in a load-and-resistance-factor format and based on values of median computed story-drift demands and their dispersion as well as on estimated drift capacities, as discussed in Section 3.2.3. The distributions of peak story drift ratios (maximum of both *X*- and *Y*-directions) for the Level-1 retrofit case and Scheme III$_R$ designs are presented in Figure 4.19, with the median values shown as solid lines. The median drift ratios follow the same trends as noted previously (Figure 4.7 and Figure 4.15). The maximum value of median story drift ratio for the Level-1 case under the BSE-1E events was only around 1.1%, but with all twenty ground motions considered, a significant dispersion of results can be observed at lower stories. This weak-story trend in the lower stories became significant at the BSE-2E events, where a median peak drift ratio reached 7% with even larger dispersions. In Scheme III$_R$, the distributed FVDs helped suppress the peak drift ratios and dispersions at both BSE-1E and BSE-2E hazard levels. For instance, the peak median drift ratio was brought down to about 1.3% for the BSE-2E events, and the dispersion was much smaller than for the Level-1 case. Nonetheless, computed story drifts exceeded 5% in the lower stories for some of the BSE-2E records.

Table 4.4 compares the values of different variables used in the FEMA 351 evaluation process for the Level-1 case and Scheme III$_R$. The calculation was based the factored demand-to-capacity ratio expressed in Eqn. (3.3), with the values listed in Table 3.2. The Level-1 and Scheme III$_R$ cases both demonstrated high confidence of achieving CP at the BSE-1E hazard level. However, when the hazard level was increased to the BSE-2E event, Scheme III$_R$ had a significantly improved confidence level in achieving CP compared to the Level-1 case. The 85.9% confidence level achieved for Scheme III$_R$ at the BSE-2E event is high, but not as high as the 90% confidence level recommended by FEMA 351 for new buildings.
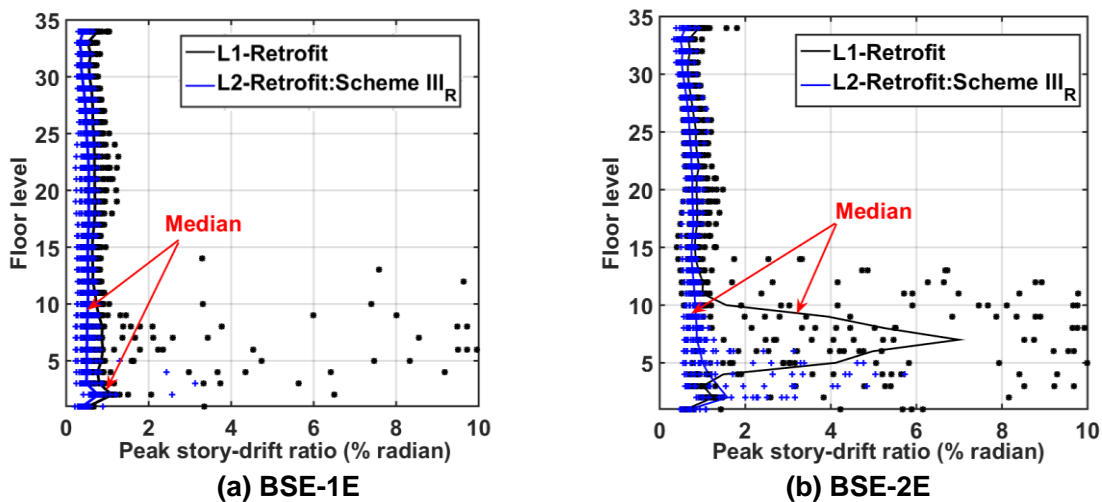
Figure 4.19   Distribution of peak story drift ratios for Phase-2 design

Table 4.4   **Confidence levels to achieve collapse prevention based on global responses**

Hazard level	Performance level CP	
	Level-1	Scheme III$_R$
BSE-1E	94.3%	99.3%
BSE-2E	5.2%	85.9%

4.4   OTHER DESIGN CONSIDERATIONS

In designing FVDs in an existing building, several issues need to be examined, such as fragile columns, damper nonlinearity, brace flexibility, effective damping ratio, and damper configurations. This section investigated each of these topics by conducting a sensitivity study. To streamline the efforts, the same three ground motions under the BSE-2E hazard event used in the Phase-1 design were selected for the structural analysis, and the maximum responses of the three analyzes were reported. Scheme III or Scheme III$_R$ was selected as the baseline model for each study.

4.4.1 Vulnerable Columns

One of the major seismic vulnerabilities in the case-study building is related to fragile columns These columns were inadequate in tension and compression under both BSE-1E and BSE-2E hazard events; see Chapter 3. After implementing the Level-1 retrofits, the vulnerable column splices were deemed adequate in tension; however, column *D/C* ratios computed for compression loads remained quite high and approached or even exceeded unity for columns located in the lower stories. As shown previously, the Level-2 retrofits reduced the story drifts by varying degrees, but additional supplemental dampers tended to increase the compression force demands on the columns connected to the devices. For example, if a structure goes well into the inelastic range, FVDs at these inelastic locations will behave in a way closer to the structural displacement, thus aggregating the damper force on top of the existing demand. Additionally, if the FVDs used are large in size, a portion of the peak damper force could impact the columns significantly. Such situation would be exacerbated if the structural elements in series with a FVD (e.g., driving braces, connecting beams, beam-to-column connections etc.) exhibit large flexibility; a FVD will act with a smaller phase angle to the structural peak displacement and elevate force demands in columns.

To help examine the column behavior, six groups of columns were studied according to their plan location, size, cross-sectional shape, and tributary area; see Figure 4.20. The groups with generally larger force demands, Group 1 and Group 5, were selected as representative exterior corner columns and interior columns, respectively.

The axial load demand-to-capacity (*D/C*) ratio distributions for Group 1 and Group 5 columns are plotted in Figure 4.21 and Figure 4.22. Both tension (positive sign) and compression (negative sign) loads are included. Axial load capacities were calculated in accordance with AISC 360-10 [2010] specification and ASCE 41-13; see discussions in Section 3.2.2. Axial *D/C* ratios under gravity loads are also shown in the figure as a green dashed line. Note that *P-M-M* interaction was not considered in the axial *D/C* calculations, but it is included in the numerical models. An axial *D/C* ratio near unity indicates that the member has very little moment capacity.

Because of the Level-1 retrofit, the tension *D/C* ratios for these columns was less of a concern: the peak axial *D/C* in tension was about 0.4 for Group 1 columns (Figure 4.21). However, a slight increase was seen (~0.5) in damper Scheme III. The refined damper scheme (Scheme III$_R$), which had a smaller number of dampers, successfully reduced the peak column tension *D/C* more effectively than the other two cases. A similar trend was observed in the interior columns (Figure 4.22), although the force demands were generally smaller.

Considering column compression loads, the peak axial *D/C* values for Group 1 or 5 columns exceeded 0.5 at most floors from levels 1 to 25. At these force levels, ASCE 41 indicates that the members should be treated as force controlled and remain elastic. Gravity loads in this portion of the structure utilize about 30%–40% of the compression load capacity of the columns. With seismic loads added, the *D/C* values commonly exceeded 0.75 for levels 3 to 15. Such high *D/C* ratios indicate a significant reduction in the column bending capacity, which would likely contribute to the weak column–strong beam behavior observed in the results for this retrofit scenario (Figure 4.8). The compressive *D/C* ratios of interior columns (Figure 4.22) were generally smaller than for the exterior columns, and the distribution was more uniform over height. Moreover, interior columns had higher axial load contributions from gravity loads but smaller ones from overturning moments. For both Group 1 and 5 columns, adding FVDs at every story (Scheme III) of the building increased the peak compression *D/C* ratios from stories 8 to 28 slightly; such an increase could be avoided if fewer dampers were used; see Scheme III$_R$.

The overloaded columns remained as an issue after Level-2 retrofit using FVDs; further investigations are suggested. Two strategies that could potentially suppress column force demands were examined: (1) strengthening existing columns or (2) distributing dampers.
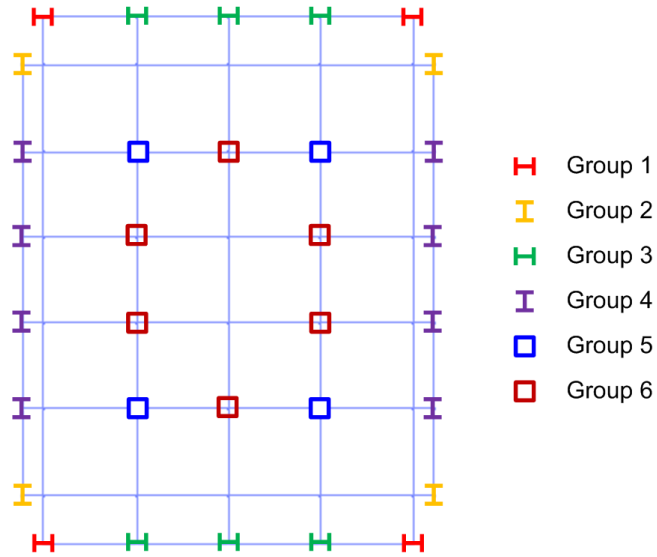
Figure 4.20   Illustration of investigated column groups
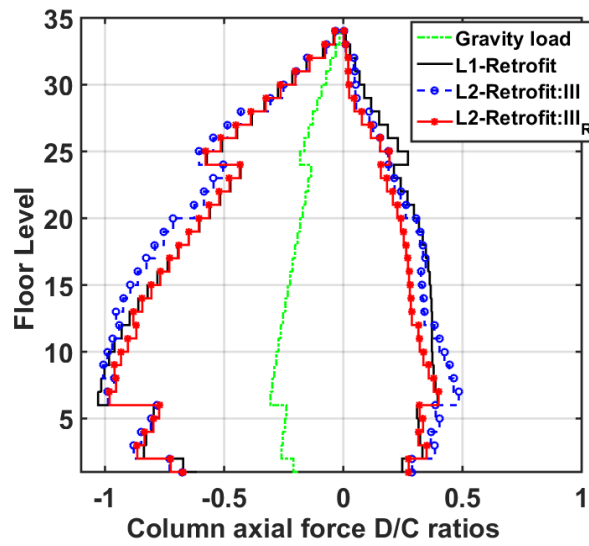
Figure 4.21   Distribution of peak axial force D/C ratios of Group 1 columns: (+) tension, (-) compression
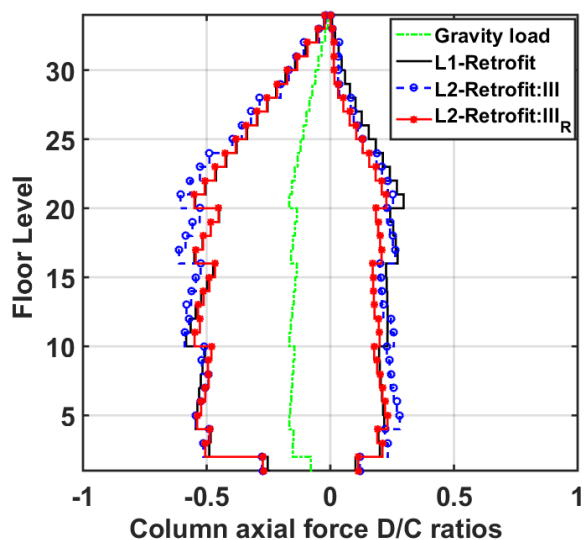
Figure 4.22 Distribution of peak axial force D/C ratios of Group 5 columns: (+) tension, (-) compression

Increase column capacity by strengthening

To reduce the axial *D/C* of columns in compression, a straightforward strategy to increase their capacity is to add steel plates to form an enclosed section and filling the inside with concrete. To demonstrate the feasibility of this strategy, the most critical columns—Group 1—were selected and augmented from floor 1 to 15. The selected columns utilized built-up H-sections [Figure 4.23 (a)], with a width *B* equal to 24 in and a height *H* equal 24 in. The strengthening method added two steel plates parallel to the web, with a width equal to the web (t_w), and formed two enclosed sections [Figure 4.23 (b)]. Concrete was poured inside as a further enhancement. The axial capacities were compared before and after strengthening; see Table 4.5. These columns increased their capacity by 53% to 63% in compression, and the fundamental period was shifted slightly from 4.33 sec to 4.29 sec due to the stiffened columns.

The selected columns after strengthening reduced the axial *D/C* in both tension and compression; see Figure 4.24. Consequently, they were less likely to yield, reducing the probability of a weak-story mechanism forming. The columns without strengthening (above floors 15 and above) showed a slight increase in compression. It was unlikely that this strategy changed the structural global responses due to limited modifications on a few existing columns, as demonstrated in Figure 4.25 and Figure 4.26, where the peak drift ratios and peak floor accelerations remained essentially the same. There were no significant changes of the damper responses either (Figure 4.27).

(a) Original H-section   **(b) Strengthened section**
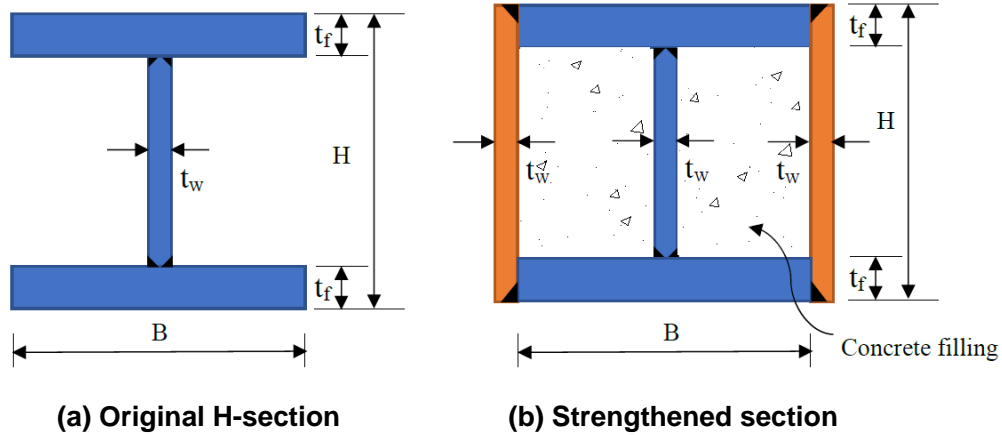
Figure 4.23   Illustration of a column strengthening method

Table 4.5   Comparison of column capacities before and after strengthening

Floor level	Compression capacity (*kips*)			Tension capacity (*kips*)		
	Original	Strengthened	Improvement	Original	Strengthened	Improvement
1	11727	17950	53%	12320	17600	43%
2	10696	16478	54%	12320	17600	43%
3-4	8450	13267	57%	8870	12672	43%
5-6	8572	13443	57%	8870	12672	43%
7-15	6540	10670	63%	6772	9623	42%

As such, improving column strength by the suggested method might be a feasible way to avoid widespread column failure and contribute to enhancing building performance under an earthquake event. Note: more rigorous studies are needed as this study only examined one critical column; the effect of strengthening columns on the global structural response and other existing members must be closely investigated if more columns are upgraded.
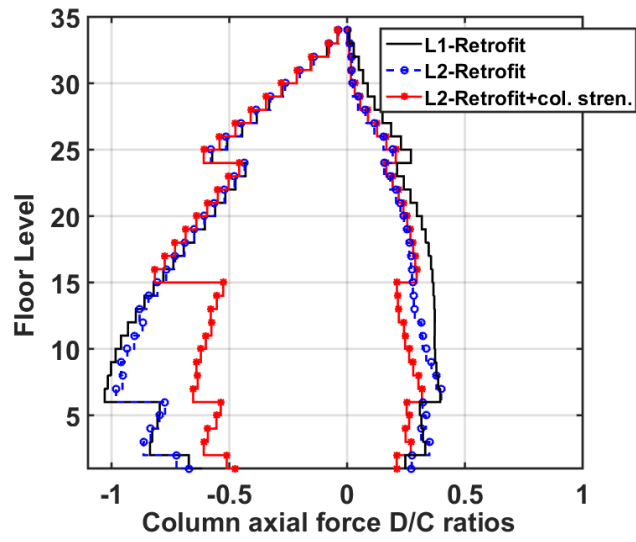
Figure 4.24 **Distribution of peak axial force D/C ratios of Group 1 columns:**
(+) tension, (-) compression
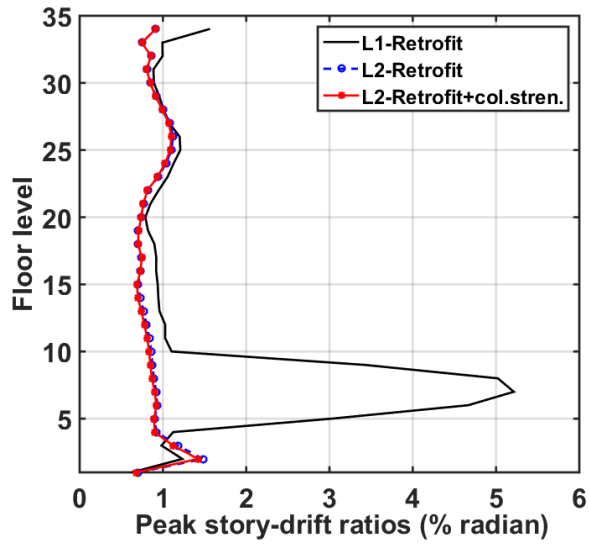
Figure 4.25 **Distribution of peak story drift ratios (X-dir.)**
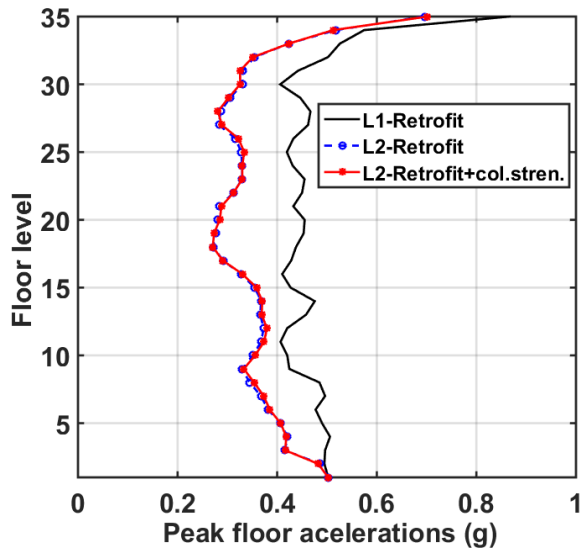
Figure 4.26   Distribution of peak floor accelerations (X-dir.)
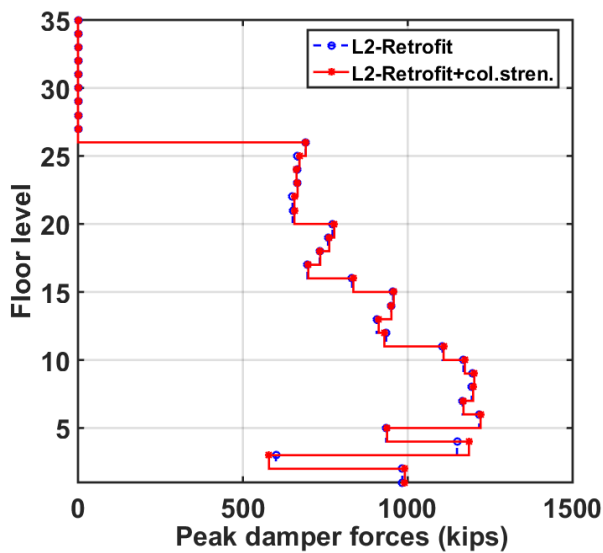
Figure 4.27   Distribution of peak damper forces

Effect of damper distribution configurations

In each face of a frame, the distribution patterns of FVDs impacts existing columns. Generally, the more distributed these dampers are, the smaller accumulated damper forces will be transferred to connected columns. Accordingly, three damper distribution patterns were selected for investigation: (a) exterior frames only, and stack dampers in corner bays; (b) exterior frames only, but place damper across multiple bays; and (c) place dampers on both exterior and interior frames, and across multiple bays. Note: Pattern (c) utilize four interior frames in the *X*-direction, but only two in the *Y*-direction; dampers are located at different floors, but distributed in multiple frames to allow for a sparser distribution; see Figure 4.28.

Installing FVDs at multiple locations improved the story drift ratios and floor accelerations more effectively than stacking dampers at limited bays (Figure 4.29 and Figure 4.30): smaller responses in most stories were observed for Patterns (b) and (c) compared to Pattern (a). Considering the column responses (Figure 4.31), Pattern (a) showed a 5% increase of peak column axial *D/C* values compared with the Level-1 retrofit scenario. Though the increase was not significant, it exacerbated the overloading condition on the columns at lower levels. In contrast, both Patterns (b) and (c) limited the damper forces transferred to the corner columns, a result that was similar to the Level-1 retrofit. Interestingly, the distribution of a few dampers to the interior frames [Pattern (c)] did not cause any significant change to the global response or column responses compared to Pattern (b). Therefore, an approach that used Pattern (b) was used in study presented herein.
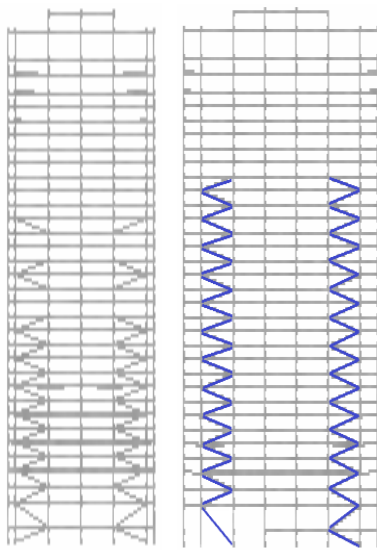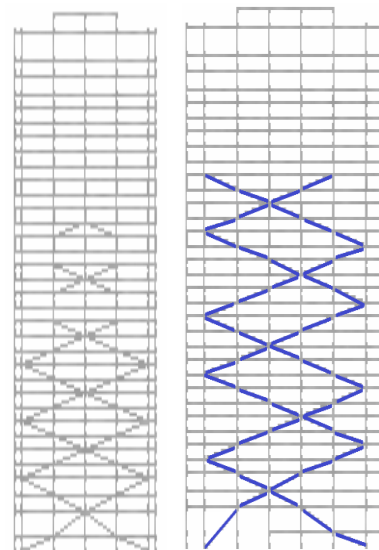
(a) Exterior frames only   **(b) Exterior frames only, distributed in multiple bays**
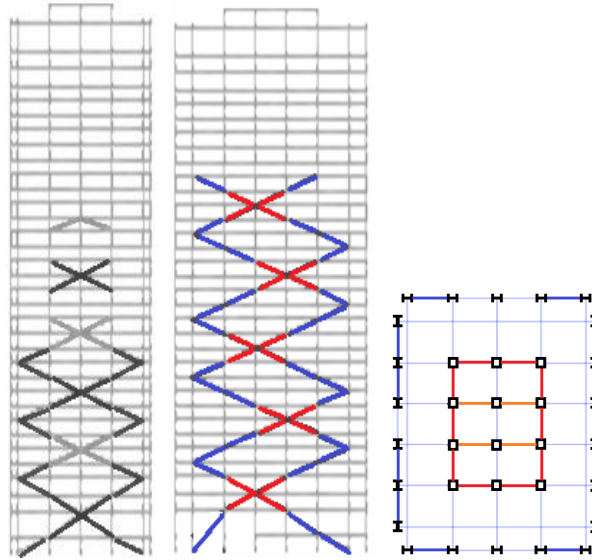
(c) Interior and exterior frames, distributed in multiple bays

Figure 4.28   Illustration of different damper distribution patterns
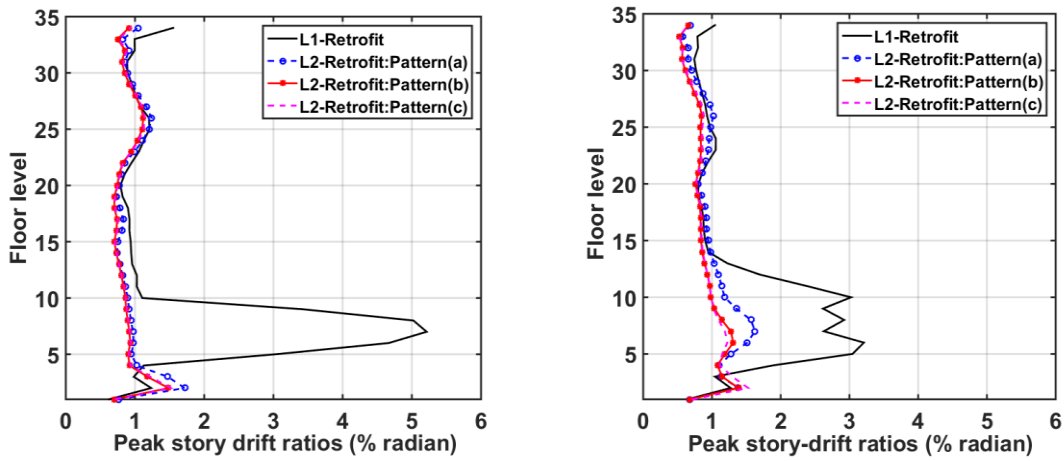
(a) X-dir.   **(b) Y-Dir.**

Figure 4.29   Distribution of peak story drift ratios

(a) X-dir.　　　　　　　　　　　　　　(b) Y-Dir.
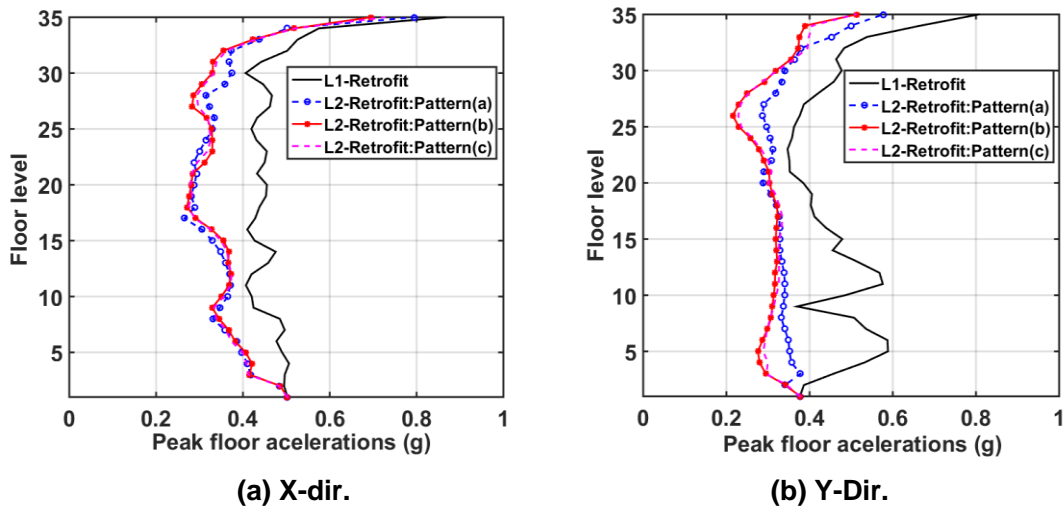
Figure 4.30　Distribution of peak floor accelerations
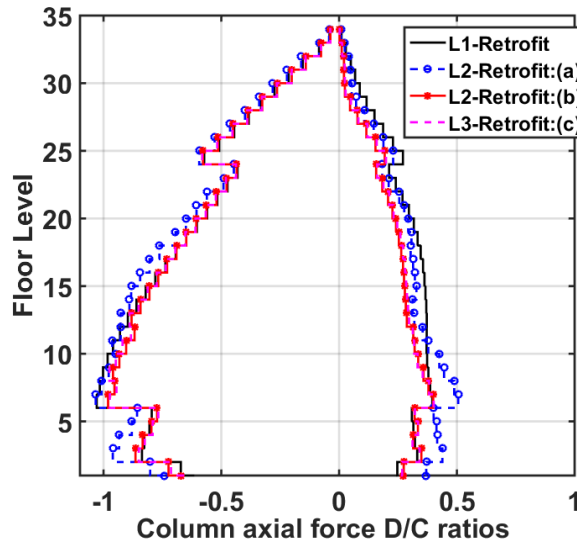
Figure 4.31　Distribution of peak axial force D/C ratios of Group 1 columns:
(+) tension, (-) compression

4.4.2 Nonlinearity of Fluid Viscous Dampers

One major mechanical property of a FVD is damping exponent α, which designates the damper nonlinearity. Assuming the same amount of energy dissipation, the same damping constant C, and displacement amplitude, the hysteresis loops of a FVD with varying damping exponent α, when subjected to a sinusoidal excitation are plotted in Figure 4.32. A nonlinear damper with damping exponent α smaller than 1.0 produced larger damper forces at smaller velocities and limited the peak force. If α equals to 0, it became a Coulomb friction damper. To characterize

the effect of damping nonlinearity on the case-study building, four values of α–0.2, 0.5, 0.8 and 1.0–were selected for this sensitivity study. The initial damper design (Scheme III) was used as the baseline case.
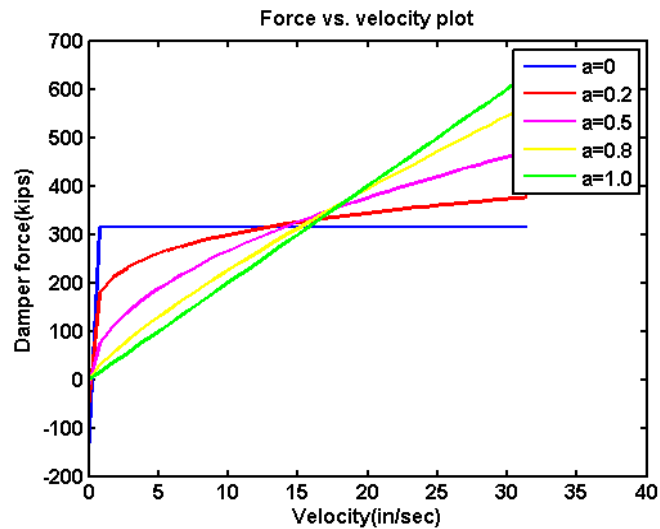
(a) Force vs. velocity
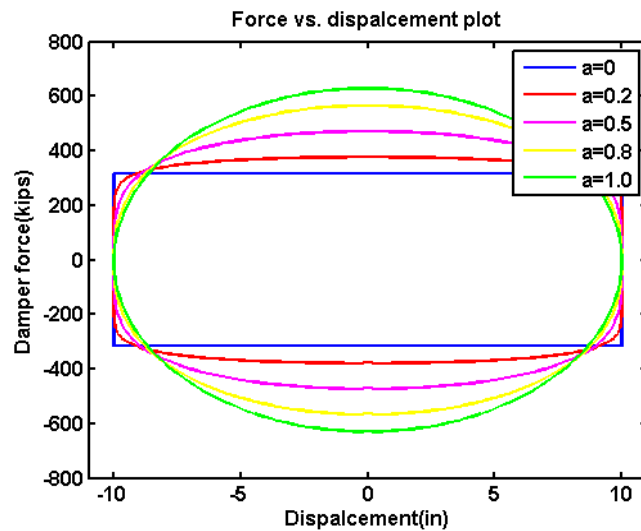
(b) Force vs. displacement

Figure 4.32   Characteristic damper properties with different α values

Schemes using nonlinear dampers with a smaller α value were more effective in reducing peak drift ratios, especially at the most deformed zones; see Figure 4.33. The distributions of peak drifts were similar for different cases in stories 11 and above. On the other hand, the distributions of floor accelerations (Figure 4.34) predicted that linear dampers were more effective than nonlinear dampers in reducing peak accelerations; the case with largest damping nonlinearity (α equals to 0.2) predicted the largest floor accelerations at most floors.

When damper forces are considered, the benefits of using nonlinear dampers are clearer. A nonlinear damper with α equaling 0.2 resulted in a peak force of 1100 kips at floor 3, but a linear damper reached a 1700-kip peak force; see Figure 4.35. The interaction between dampers and columns was also investigated. Despite a significant change in peak damper forces, the column axial *D/C* did not vary much for different cases; see Figure 4.36. The linear dampers produced larger damper forces but had less interaction with structural elements; their impact on column forces compared to nonlinear dampers was similar.

As an overall evaluation, an α value in the range of 0.2 and 0.5 was considered to be most effective in controlling structural response and limiting maximum damper forces; thus, its average value (e.g., 0.35) was used in the study presented herein. Alternatives within this range could be considered.
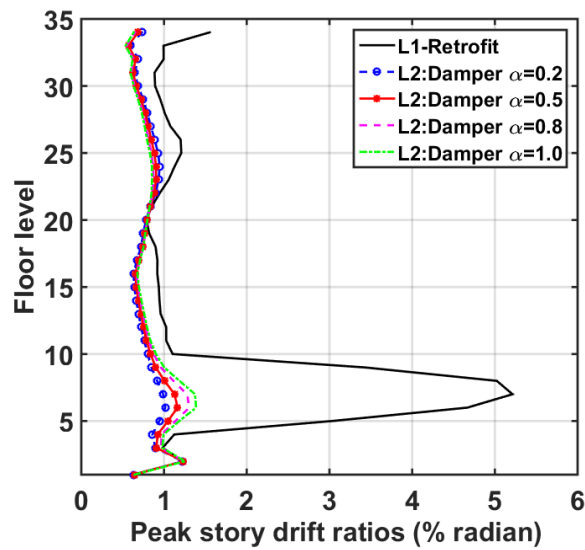
Figure 4.33   Distribution of peak story drift ratios with different α values
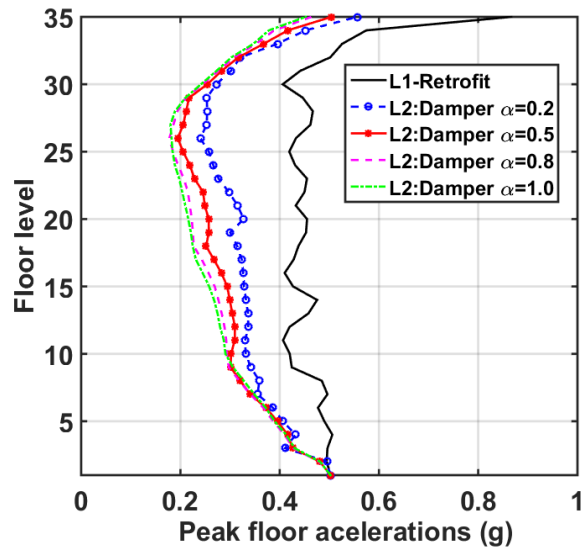
Figure 4.34   Distribution of peak floor accelerations with different α values
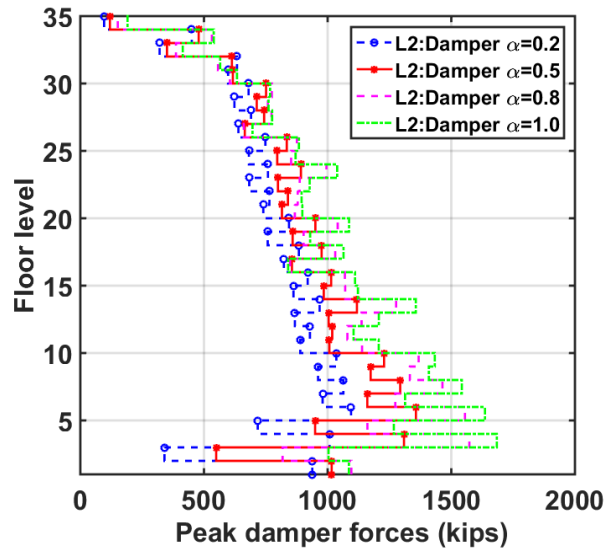
Figure 4.35   Distribution of peak damper forces with different α values
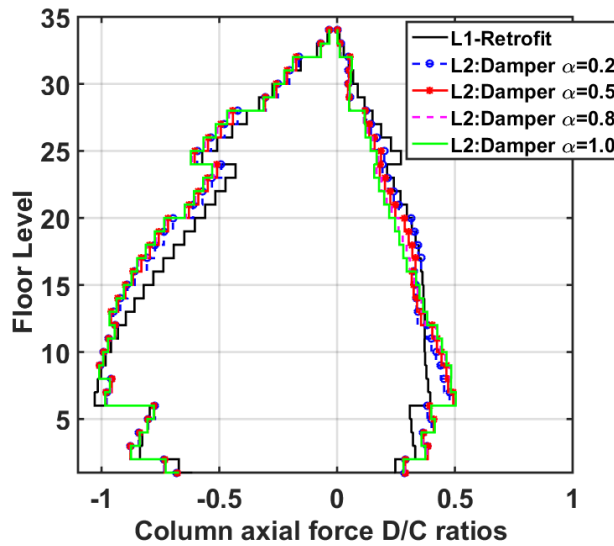
Figure 4.36   **Distribution of peak axial force D/C ratios of Group 1 columns with different α values: (+) tension, (-) compression**

4.4.3 Brace Flexibility

In this sensitivity study, various K_b values were examined, which were selected as a percentage of the frame stiffness K_f at each floor. Two horizontal directions were considered separately. Six cases were selected, varying from the fairly flexible case to fairly stiff case; i.e., $K_b = 0.5K_f$, $1.0K_f$, $2.0K_f$, $3.0K_f$, $4.0K_f$ and $5.0K_f$. The initial damper Scheme III was used as the baseline model.

An observable increase was observed in the story drift ratio distributions in the Y-direction when K_b was doubled from $0.5K_f$ to $1.0K_f$, and from $1.0K_f$ to $2.0K_f$, see Figure 4.37. However, only a marginal increment was observed when K_b exceeded $2.0K_f$. The difference was much smaller in the X-direction.

One damper was selected for detailed examination, and its hysteresis loop under different scenarios were compared; see Figure 4.38. The damper is located at the 5th floor in the X-direction. Comparison of these hysteresis loop indicate that the damper connected with a stiffer brace provided a better hysteresis loop shape. The peak damper force was larger for a damper element with a larger K_b. Additionally, the phase angle between the damper force and the frame force was examined. Figure 4.39 plots the time history of story shear forces for the 1st story for two extreme cases: one with very flexible braces ($K_b=0.5K_f$) and the other with very stiff braces ($K_b=5K_f$) were compared. The change of forces during the free-vibration period was examined. Compared with a flexible brace, a stiff brace suppressed the peak story shears more effectively as well as resulted in a more rapid decay of structural response. A stiff brace was also more efficient to eliminate higher frequency contents. Moreover, a scrutiny of Figure 4.39 (a) and (b) revealed that the phase angles between the peak damper force and peak frame force would be more out-of-phase if a stiff brace was used.

Based on results presented above, a brace with a K_b equal to twice of K_f is suggested as an optimal value for this structure; this value provides an adequate damper effect without requiring excessively large braces. Note: the proposed brace size is fairly large considering the size of this building; the feasibility of constructing the braces and connecting them to existing building is worthy of future study.

(a) X-dir.

(b) Y-dir.
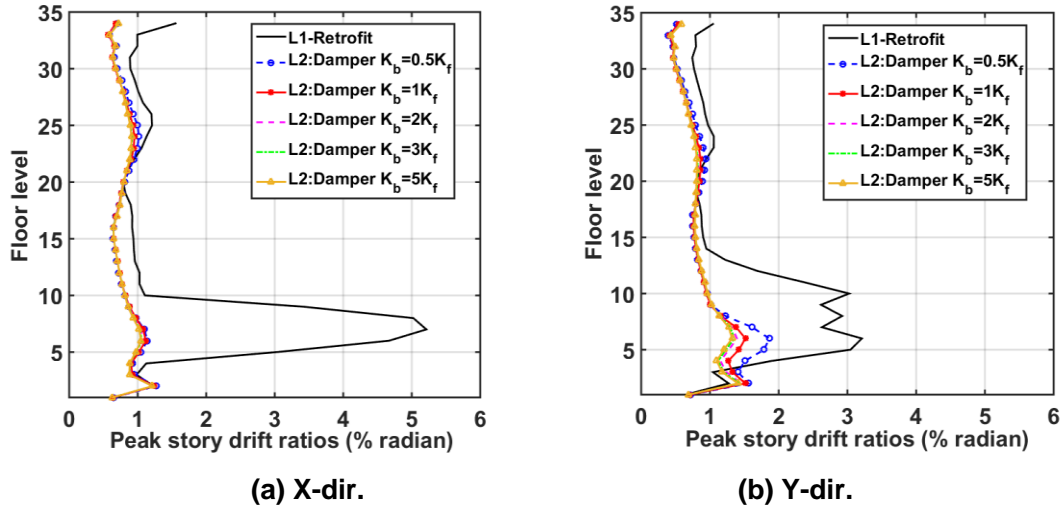
Figure 4.37   Distribution of peak story drift ratios with different K_b

(a) K_b=0.5K_f

(b) K_b=1K_f

(c) $K_b=2K_f$ **(d) $K_b=5K_f$**
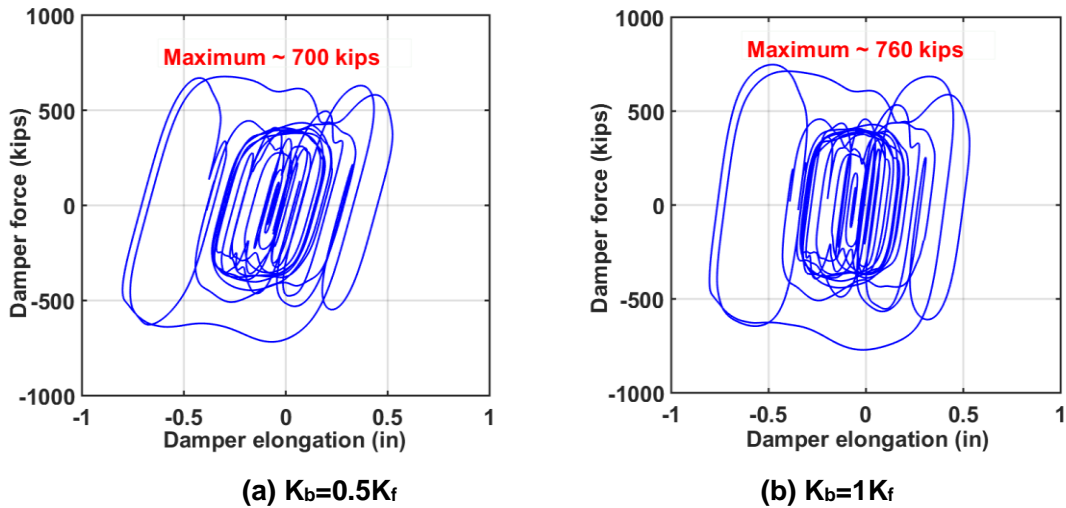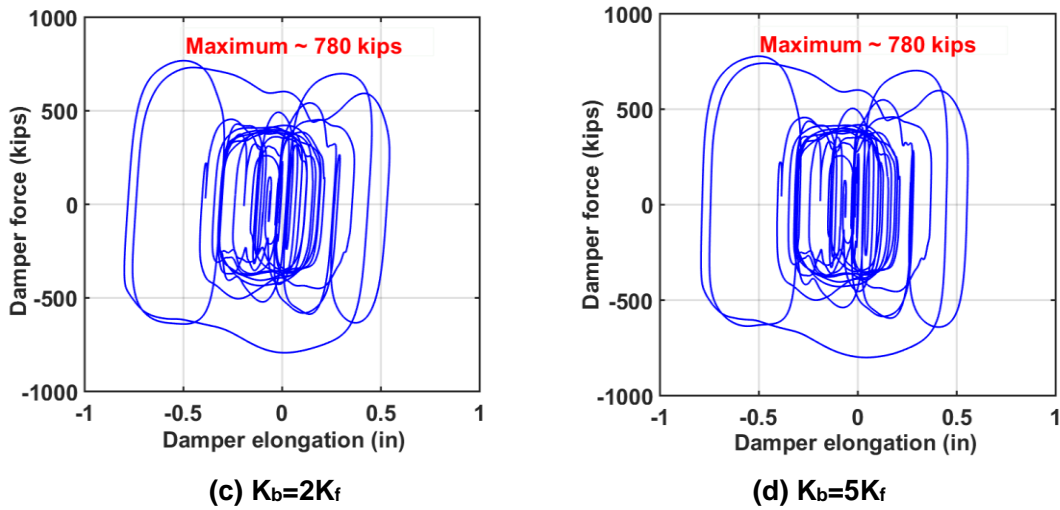
Figure 4.38   Damper hysteresis loops of a typical damper under one ground motion (GM 1) with different K_b

(a) $K_b=0.5K_f$ **(b) $K_b=5K_f$**
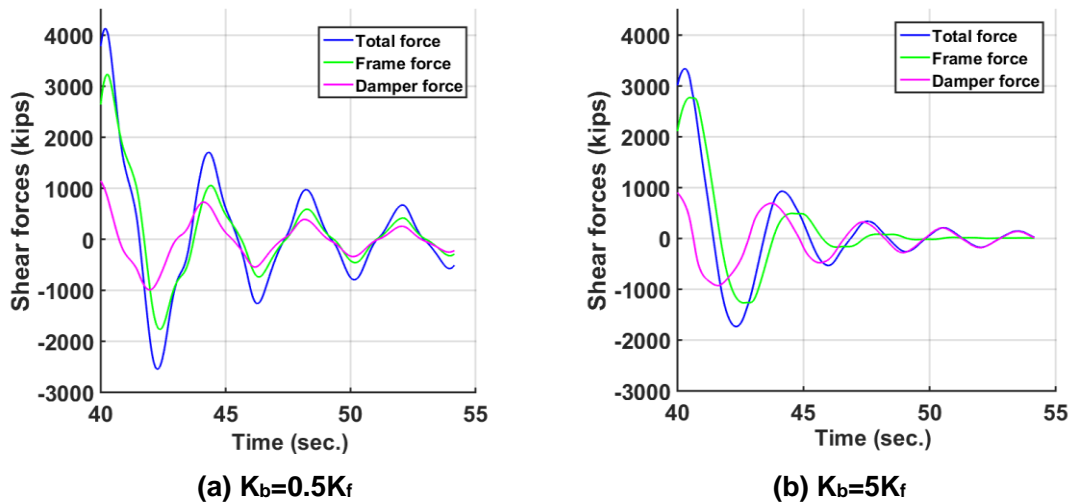
Figure 4.39   Time history of 1st story force under one ground motion (GM 1) with different K_b (free vibration)

4.4.4 Effective Damping Ratio

A target performance goal based on the roof displacement of incipient collapse from a static pushover analysis was selected to estimate the effective damping ratio; see Section 4.3.2. This method is based on a first-mode assumption, and thus used as an approximation of the required damping ratio. In this section, a sensitivity study was conducted to assess how the variation of effective damping ratio could impact structural response.

Scheme III was selected as the baseline case that uses 10% and 15% as the effective damping ratios (denoted as ξ_0). Four cases were compared with ξ_{eff} equaling to: (1) 50% ξ_0; (2) 100% ξ_0; (3) 150% ξ_0; and (4) 200% ξ_0.

When the effective damping ratio ξ_{eff} was as small as half of ξ_0, the case-study building was unable to suppress the peak story drifts from levels 4 to 10 (Figure 4.40) or to control the peak floor accelerations (Figure 4.41). A significant improvement was achieved if ξ_{eff} was increased to 100% ξ_0; the weak story trend was fully eliminated. If ξ_{eff} was increased further (say, 150% ξ_0 or 200% ξ_0), the structural response could be improved even more, although the incremental improvement was small. In terms of peak damper forces, they were proportional with ξ_{eff} (Figure 4.42). Therefore, the optimal case is Case (2) where ξ_{eff} is equal to ξ_0 as it controlled the structural response and avoided large damper forces.
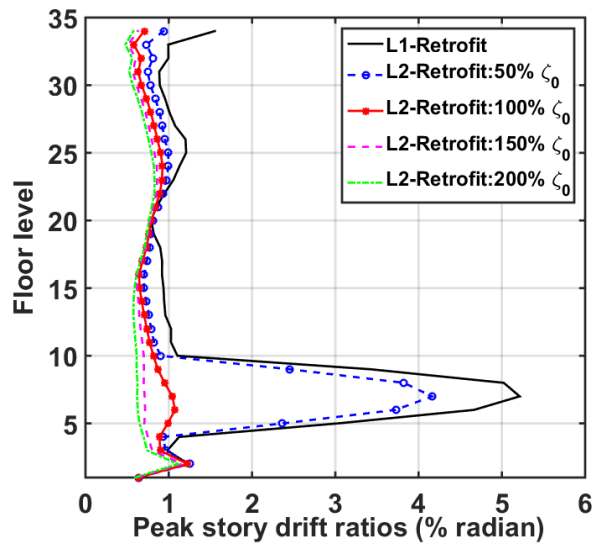
Figure 4.40   Distribution of peak drift ratio with different damping ratios (X-dir.)
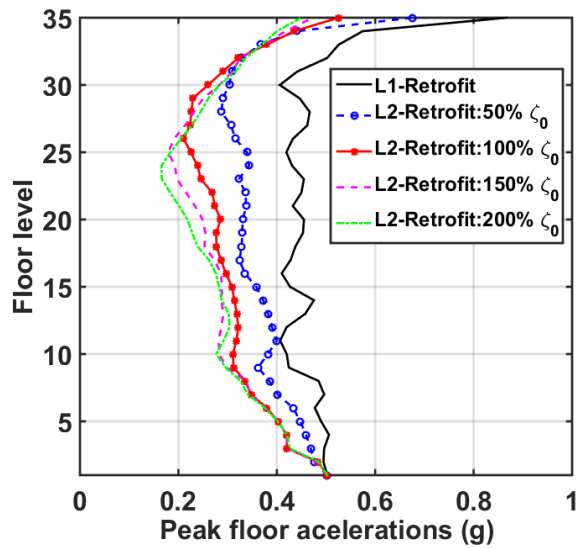
Figure 4.41   Distribution of peak floor accelerations with different damping ratios (X-dir.)
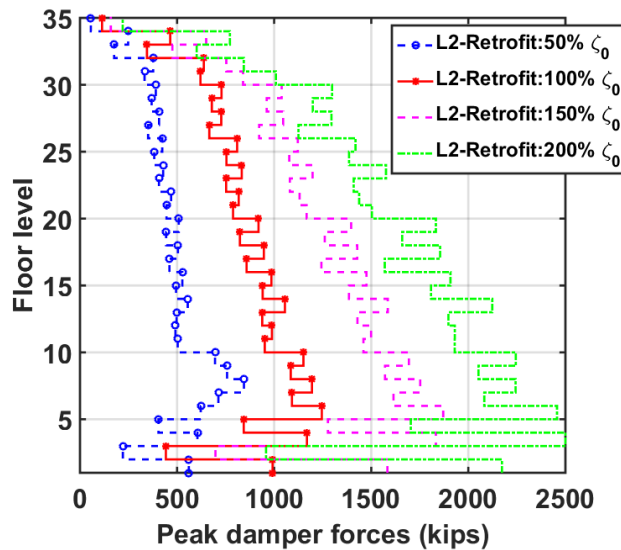
Figure 4.42   Distribution of peak damper force with different damping ratios

4.4.5 Damper Configurations

A damper can be constructed in a building with different configurations. The most commonly used types are a diagonal shape or a chevron/V-shape configuration; see Figure 4.43. The former is considered easier to construct when retrofitting existing buildings [Malley *et al*. 2009]. An examination of the past projects by the author found that use of the diagonal configuration was more than 50% based on the list provided by Taylor Device Inc. [Taylor Inc. 2015]. The advantage of the chevron/V-shape configuration is that it might avoid blockage of the view or

egress, and provide larger damper deformations. Alternatives such as the "toggle-brace dampers" systems [Figure 4.43(c)] could be considered if the system is stiff and relative story deformations are small.

In a tall building, a mega-brace-damper configuration has been used outside of building as the lateral force resisting system. This system was first adopted the Torre Mayor Building at Mexico City (Figure 4.44) to resist seismic load [Taylor and Katz 2004] and is gaining popularity in current high-rise constructions in San Francisco [Brinklow 2017]; see Figure 4.45 for one example building. By arranging dampers across multiple continuous floors, the damper deformations will be amplified, increasing the energy-dissipation capability of the damping system with fewer dampers.

Three configuration types were investigated in this study: (1) diagonal, (2) chevron, and (3) multi-story configuration. The Scheme III$_R$ was selected as a baseline.

(a) Diagonal configuration   **(b) Chevron configuration**

(c) Toggle-brace-damper system

Figure 4.43   Different damper configurations

Figure 4.44   Torre Mayor building in Mexico City (adapted from Taylor and Katz [2004])

Figure 4.45   181 Fremont at San Francisco (photo courtesy of Arup)

Mathematical modeling of a diagonal damper was introduced in Section 4.2.2; however, the case with a chevron configuration added two diagonal braces that connected to the horizontal damper, requiring slight modifications of the numerical model. In each frame where dampers were installed, the two added braces were simulated using *elastic beam column* elements in OpenSees. The axial stiffness of the brace was based on the optimal brace stiffness identified in Section 4.4.3 and back calculated. Because the bending of the braces was not considered, the moment of inertial was set to be a very large number in both strong and weak axis. The mechanical properties of each FVD was kept consistent with the diagonal configuration, but damping constant C was adjusted to account for the angle change (from diagonal to horizontal). Dampers were arranged at top of each frame and linked to the beam-to-column connection. The *viscous damper* material and *two node link* elements were used to model the damper in OpenSees; see Figure 4.46. Note: with two additional braces, the rotations of the beam-to-column connections were slightly restrained, which contributed to a shift of the fundamental period from 4.33 sec to 4.28 sec.
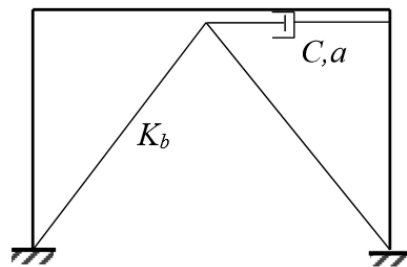
Figure 4.46   Modelling of FVDs with a chevron configuration

In Case (3), the mega-braces were installed across 4 or 5 continuous floors, and each brace has a damper connected in series; see the diagonal blue lines in Figure 4.47. The mechanical properties of each mega-damper were selected based on the average value of these smaller dampers in Case (1) at identical floors. The damper locations were slightly different than other two cases to avoid discontinuity of damper distributions, but the effective damping ratios were kept consistent for all three cases. Case (3) had a total of 44 dampers, whereas both Cases (1) and (2) resulted in a total of 174 dampers.
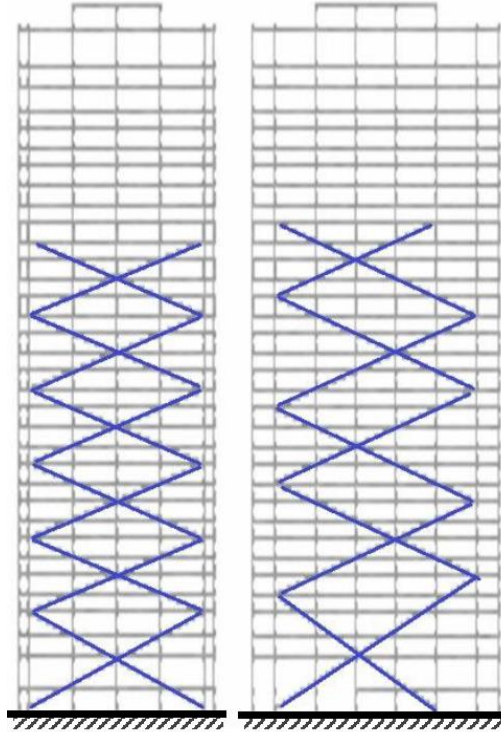
Figure 4.47   Mega-brace system configuration

The distributions of the peak drift ratios in the *X*-direction were similar for the three cases, though slight changes were observed in the mezzanine level [Figure 4.48 (a)]; however, a larger difference was seen in the *Y*-direction, especially at lower stories [Figure 4.48 (b)]. Among these, the diagonal scheme was the most effective in reducing the maximum drift ratio. The chevron configuration was relatively less effective in controlling the drifts at floors 2 to 4. However, an observable concentration of drifts was observed in the mega-brace-damper case at floors 5 to 8, indicating that spanning dampers across multiple stories is a less effective strategy to reduce the number of beam-to-column connection failures.

In terms of controlling the peak floor accelerations (Figure 4.49), the chevron shape scheme was the least effective over most stories, especially in the *Y*-direction. This was mainly due to the additional stiffness due to constraint of beam end rotations in this scheme, which slightly amplified the seismic demand. The mega-brace-damper configuration showed a similar trend in the diagonal configuration but did not adequately reduce accelerations at the lower floors where larger story drift ratios were predicated.

Considering the size of dampers, Cases (1) and (2) with dampers installed at single story had essentially same damper force distributions, although the chevron configuration had slightly larger force; see Figure 4.50. Case (3), however, predicted a larger damper force than the average of dampers distributed in these stories compared to the other two configurations at lower floors, but the trend was reversed above floor 16. This indicated that in lower stories where the damping demand is highest, the distributed damper configuration is more efficient than using a large damper spanning across several floors.

98

To understand the damper's behaviour in different configurations, the hysteresis loops of one damper at 7th floor for Case (1) and (2), and the mega damper spanned from floor 7 to 11 at Case (3) were compared; see Figure 4.51. The shapes of selected three dampers were similar, but Case (2) exhibited a slightly smaller damper force due to its horizontal orientation compared to Case (1). On the other hand, a 30% increase of damper force was seen for Case (3). A more significant difference was the deformation demand, where the mega-brace system predicted a damper elongation as large as 5 compared to Case (1) and (2).

(a) X-dir. (b) Y-dir.
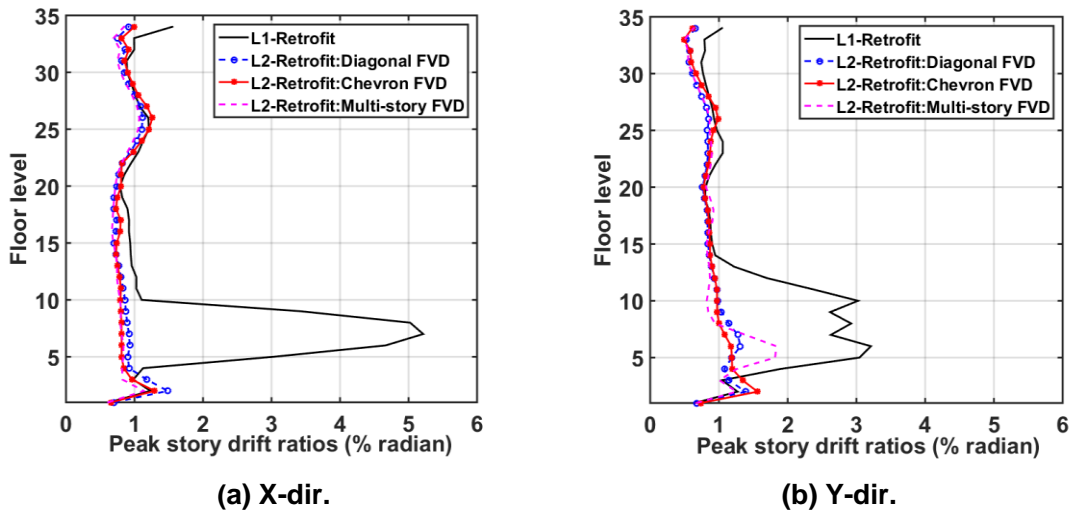
Figure 4.48   Distributions of peak story drift ratios for different damper configurations

(a) X-dir. (b) Y-dir.
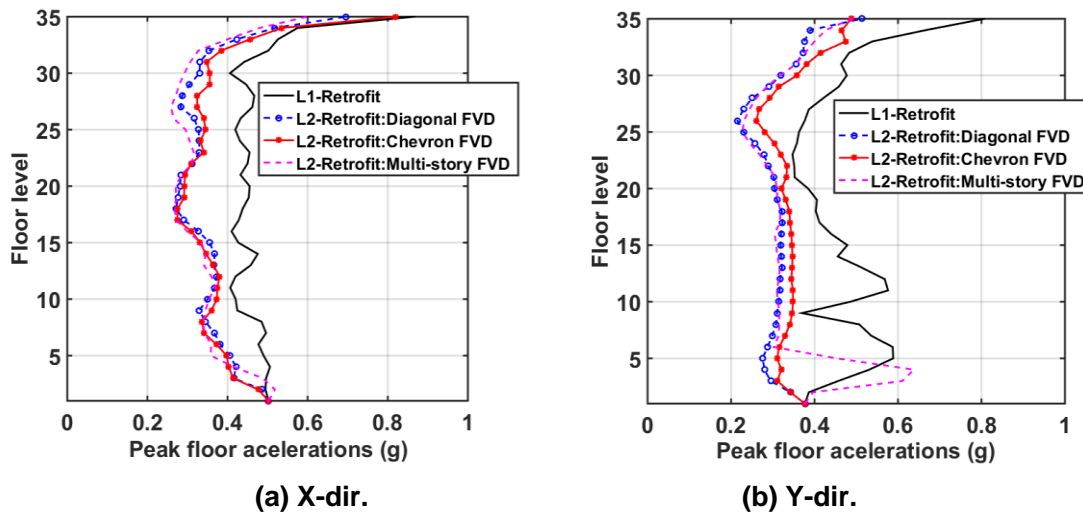
Figure 4.49   Distributions of peak floor accelerations for different damper configurations

99
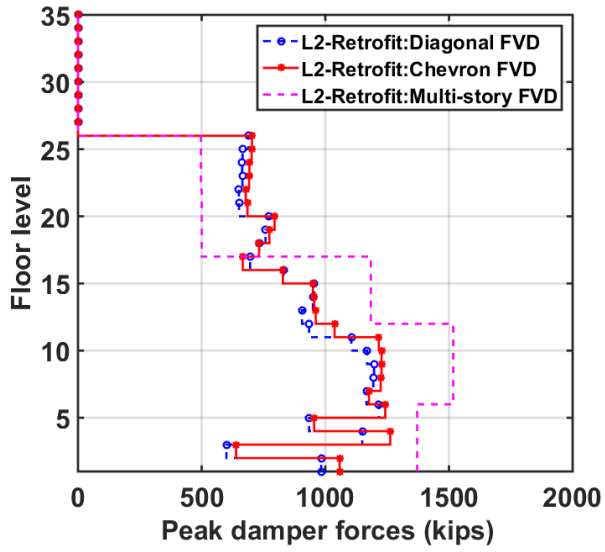
Figure 4.50   Distributions of peak damper forces for different damper configurations
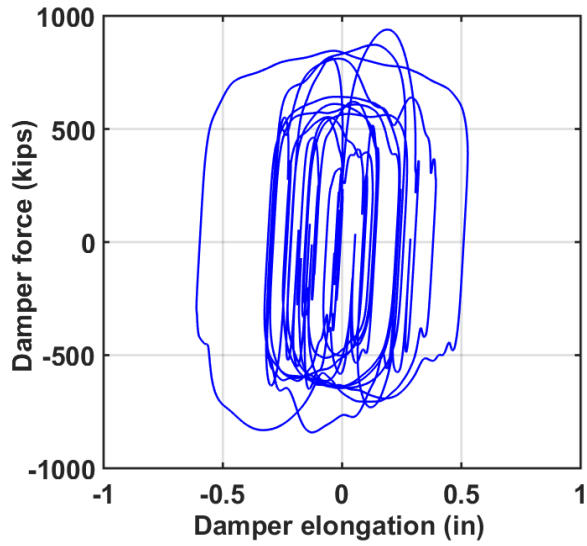
(a) Diagonal configuration
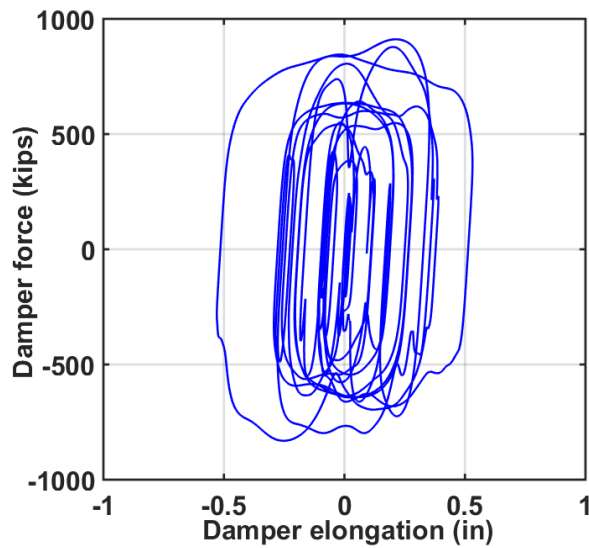
(b) Chevron configuration
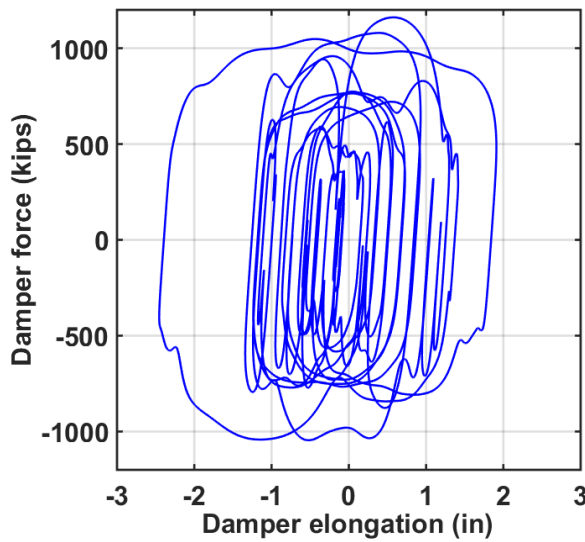
(c) Multi-story diagonal configuration

Figure 4.51   Damper hysteresis loops for different damper configurations

In comparison, Case (2) with chevron configuration predicted similar structural response control and damper force demand as in Case (1), but it increased the floor accelerations due to a light stiffening by the additional braces. In practice, the additional braces in the chevron type configuration might increase the initial cost compared to a diagonal configuration. The mega-brace-damper system was slightly less effective in controlling structural response at lowest floor levels but reduced the total number of dampers to be only a quarter of other two cases. This could be considered as an alternative strategy; but special attention should be paid at most

101

deformed zones, and the trade-off between using fewer dampers versus increased cost of constructing mega-brace should be prudently evaluated.

4.5   CONCLUDING REMARKS

This chapter explored retrofit strategies using FVDs to augment the measures taken in the Level-1 retrofit. The numerical models used were assumed to include the Level-1 upgrades—strengthening brittle column splices and removing exterior heavy cladding.

With the velocity-dependent properties, FVDs are expected to meet the major retrofit goals of providing lateral stiffness and energy dissipation needed to reduce the lateral displacements but at the same time not to increase the demands on structural members significantly. In the study presented herein, FVDs improved significantly the building's performance under the BSE-2E hazard level of excitation by reducing the peak drift ratio by up to 30%, essentially eliminating the localized connection fractures. In addition, FVDs may reduce the floor accelerations up to 50%–thus leading to a more rapid decay of vibrations–thereby reducing damage to structural and non-structural elements and discomfort to occupants.

The analysis results indicated that large damper forces were needed to achieve the desired response, especially in the stories that experienced the most deformation. Extensive upgrading of column splices and other existing features of the building was also necessary. The results showed that damper demands could be significantly reduced by adjusting the configuration of dampers within the building and the careful selection of damper properties. A refined Phase-2 design was proposed to determine the most effective placement of dampers to achieve similar structural control effects with fewer dampers. Other design considerations, with an emphasis on finding feasible strategies/properties to guide the optimization design, include:

- Strengthening columns by boxing the existing column members and filling them with concrete;

- Distributing dampers in multiple bays to avoid accumulating damper forces and favoring the four exterior frames so that there is less interaction with interior office use;

- Targeting a damping exponent α on the order of 0.35 to reduce seismic response of the building without generating excessive damper forces;

- Considering driving braces with sufficient stiffness to achieve the desired control effects of FVDs, which was found to be on the order of twice the story stiffness for this selected building, but efforts to optimize brace sizes to obtain an improved performance-cost ratio are recommended;

- Proposing a method to estimate the total effective damping ratio to provide acceptable results in the design of FVDs, which was in the range of 8% to 15% for the case-study building;

- Considering a diagonal configuration in each frame as the most effective way to design FVDs in an existing building.

The study presented in this chapter demonstrates that installing FVDs is a promising solution to achieve a target performance level. Consideration of important design issues should be accounted for when designing FVDs in an existing tall building.

5 Seismic Retrofit with Supplemental Energy-Dissipation Devices: (II) Viscous Wall Dampers & (III) Buckling Restrained Braces

5.1 INTRODUCTION

A Level-2 retrofit that used fluid viscous dampers (FVDs) was found to satisfy the retrofit criteria of preventing collapse under a BSE-2E seismic hazard event. This chapter now considers the relative effectiveness and economy of other two types of passive energy-dissipation devices: viscous wall dampers (VWDs) and buckling restrained braces (BRBs). To compare the behavior of the selected devices on an equal footing, the numerical models used for all cases with supplemental damping devices are assumed to include the Level-1 upgrades—strengthening brittle column splices and removing exterior heavy cladding. In addition, the locations of the BRBs or VWDs are kept consistent with Phase-2 design scheme of FVDs (Scheme III$_R$), and the mechanical properties for each device are selected to achieve the same overall effective damping ratio. The comparison is based on nonlinear response history analysis (NRHA) and uses three ground motions under BSE-2E hazard event. The selected ground motions are the same as these used in the Phase-1 design of FVDs, and the results reported are based on the maximum of the three analyses. Important design considerations of using VWDs are discussed.

5.2 RETROFIT USING VISCOUS WALL DAMPERS

Compared to a FVD, the advantages of using a VWD include:

(a) Its compact, rectangular configuration provides more architectural versatility;

(b) It could provide larger damping and a larger output force (which could be increased easily by adding another steel tank), thus requiring a smaller number of VWDs to achieve the same damping ratio.

The disadvantages of a VWD compared to a FVD might include:

(a) It has additional stiffening effect, thus increasing seismic force demands on existing structural elements;

(b) The high viscosity material is more sensitive to temperature and frequency variations [Reinhorn and Li 1995]; and

(c) Installing a VWD in the middle of a beam alters a typically assumed inflection point at the mid-span of the beam under a lateral loading; this changes the clear span to depth ratio of a beam, which could bring about special concerns for a building with brittle beam-to-column connections.

5.2.1 Mathematical Modelling

Unlike a FVD, a VWD provides both a viscous damping force and a restoring force [Arima *et al*. 1988]. Various analytical models of differing complexity are available to characterize the behavior of a VWD [Reinhorn and Li 1995]. Since the mechanical properties of a VWD is fairly stable over a wide range of frequencies experienced during an earthquake event, and temperature variation during cyclic loading is typically small [Arima *et al*. 1988], a *Kelvin* model with constant parameters was selected for this study to simulate a VWD. The proposed model has a spring and a dashpot connected in parallel, and the total force of a VWD is thus expressed by the following formula:

$$F_d = Ku + Cv^a \tag{5.1}$$

where K is the spring stiffness, C is the damping constant, and α is damping exponent. This model is appropriate under most seismic excitations based on consultations with experienced engineers. More rigorous modeling is possible if its frequency and temperature dependency needs to be closely examined.

5.2.2 Retrofit of Case-Study Building using Viscous Wall Dampers

The bays where the VWDs have been located are the same as those for the Phase-2 FVDs scheme (Scheme III$_R$). The OpenSees numerical model was modified to account for the points along the beams where the VWDs were attached; see Figure 5.1. One mid-beam node was inserted above and below a damper, respectively. As such, the original beam was divided into two beam elements, and a rigid offset was assigned to each of these two beams at the point of their connection. Such offsets represent the steel plates that fix the VWD to the beams, which are very stiff [DIS Inc. 2011]; as an approximate, they were assumed rigid in this study. The total length of the rigid offsets in the middle of each beam is equal to 3.6 m, which is the width of a typical wall damper [DIS Inc. 2011]; see Figure 5.1 (b). The mid-beam nodes at the upper and lower beams were connected by a *two-node link* element to resemble the VWD, which was assigned with a *Kelvin* material model in the horizontal direction. To insure the same overall effective damping ratio, the damping constant C, and damping exponent α of a VWD were selected to be the same as for the FVD at the same location. The elastic spring K represents a combination of steel plate and the fixed connection between a wall damper and a beam; it provides a restoring force, but not additional damping to the structure when subjected to external excitations. The stiffness of the elastic spring: K was selected based on recommendations from experienced engineers, which is 1000 *kip/in*. The same value of K was used for all VWDs at different locations as a simplification considering the purpose of the current study. Consequently,

the fundamental period of the building being studied was reduced by 5% (from 4.33 sec to 4.10 sec) after the wall dampers were incorporated. Such a change corresponds to results from past experiments [Arima *et al*. 1998; Lu *et al.* 2008; Yeung and Pan 1998], which demonstrated that the installing VWDs typically increased the structural stiffness by about 5% to 15%.

(a) Without a VWD   **(b) With a VWD**   **(c) M-ϕ for potential P.H locations**
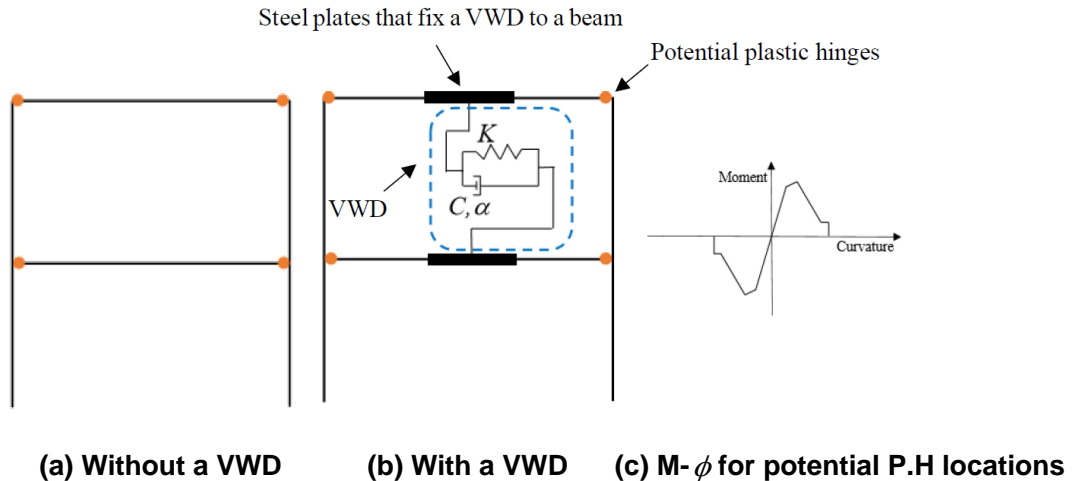
Figure 5.1   **The frame model**

Results were reported for the Level-1 retrofit and Level-2 retrofit with VWDs. One analysis with VWDs had widespread beam-to-column connections failure and excessive drift ratios and thus were numerically unstable. That case was considered to experience global failure according to the current code [ASCE 7 2017], and the analysis was terminated once the peak drift ratio exceeds 10%. The reasons for the undesired behaviors of VWDs will be discussed later.

The distributions of peak story drifts (Figure 5.2) demonstrated that VWDs were far less effective than FVDs in eliminating the concentrated deformations, with a maximum drift exceeding 3% at floor 6. In the *Y*-direction, the maximum drift approached a value larger than 10% due to the numerical instability when subjected to one ground motion. Correspondingly, the VWDs were not able to eliminate a high percentage of beam-to-column connections failure at the BSE-2E event; see Figure 5.3.

(a) X-dir.   **(b) Y-dir.**
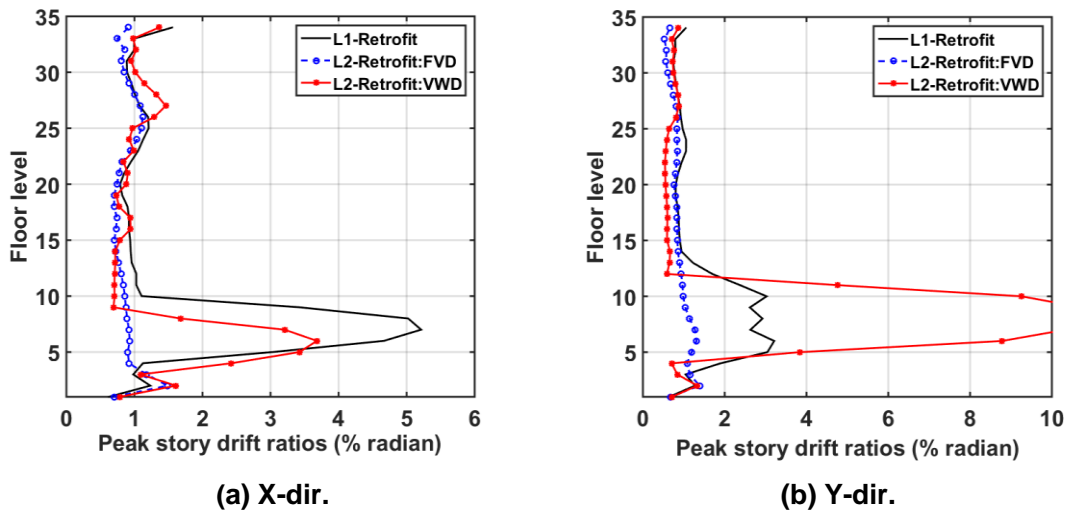
Figure 5.2   **Distributions of peak story drift ratios**
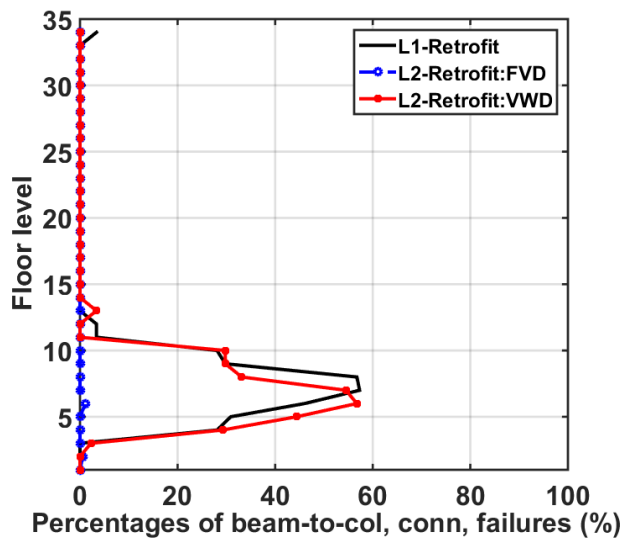
Figure 5.3   **Distribution of peak beam connection failures (as percentage of total number of connections per floor)**

The maximum floor accelerations when VWDs were used were not reduced as much compared to FVDs; this may be associated with the stiffening effect of VWDs [Figure 5.4 (a)]. The maximum acceleration was as high as 0.8 for Level-1 and Level-2 using VWDs. A further check on the acceleration responses during the free-vibration phase indicated that the VWDs were not able to attenuate the roof acceleration any more rapidly than the Level-1 retrofit case [Figure 5.4 (b)]; however, some minor suppression of high-frequency contents were observed.
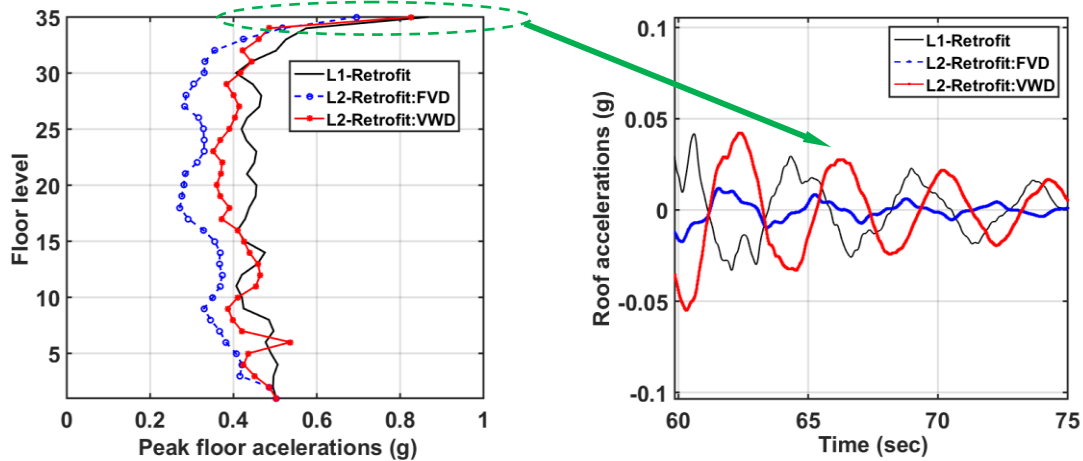
(a) Distributions of peak floor accel. (X-dir.) **(b) Time history of roof accel. under one ground motion**

Figure 5.4   Floor accelerations

When considering the interaction of the supplemental energy-dissipation devices and existing structural members, the corner columns—Group 1—were selected and their axial *D/C* were examined. The overloaded columns became an even bigger concern in the case of VWDs (Figure 5.5): peak values were increased by 15% to 20% compared to the Level-1 case.
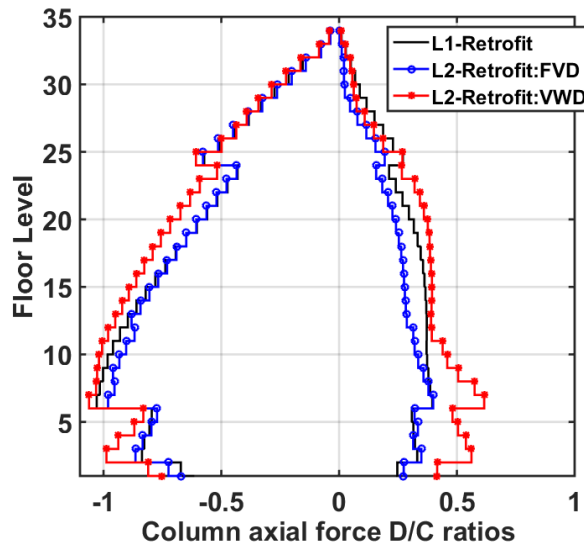
Figure 5.5   Distribution of peak axial force D/C ratios of Group 1 columns: (+) tension, (-) compression

Despite the performance of VWDs was not satisfactory, the predicted peak damper forces were generally larger than FVDs in most stories, which was as large as 2300 kips at floor 4; see Figure 5.6. This was mainly affected by the elastic spring. As shown in Figure 5.7, the behaviour of a VWD showed the typical hysteresis loop of a wall damper at story 8. The total force

108

constitutes a viscous damping force and an elastic spring force, with the former contributing to more than 80% of the total force. The large damper force output of VWDs suggests that the dampers achieved the target damping ratio, but unexpected adverse effects were induced that exacerbated the structural behaviour. This phenomenon is investigated in great detail in Sections 5.2.3 and 5.2.4.
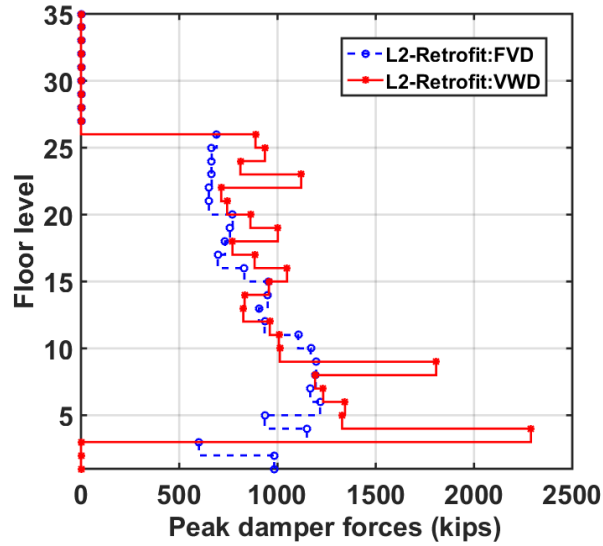
Figure 5.6   Distributions of peak damper forces
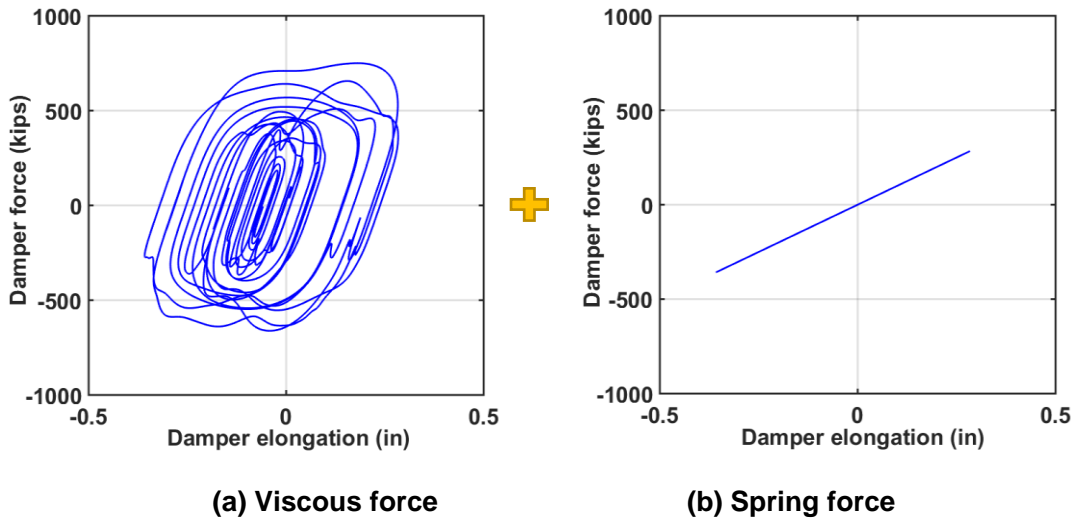
(a) Viscous force   **(b) Spring force**
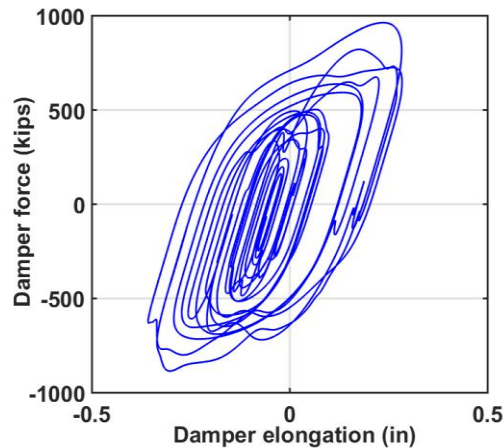
(c) Total force

Figure 5.7   Contribution of a viscous force and a restoring force in a VWD

5.2.3 Special Design Considerations

One issue that emerged from this study that is worthy of further investigation is the failure of the VWD retrofit strategy to achieve the desired performance goal. A scrutiny of analysis results indicated that the deficiency was largely due to the failure of some of the brittle pre-Northridge beam-to-column connections under larger than average displacement demands. The interaction between a VWD and the connecting beams as well as their influence of the system behavior are discussed below.

Figure 5.8 shows how a pair of beams connected to a VWD might behave before and after the fracture of the connections of a beam to the columns. In Case 1 [Figure 5.8 (a)], where beam ends provide full restraint against relative rotation between the beam and column, the two steel vanes (plates) in the VWD develop large relative horizontal movement. The viscosity of the fluid between the plates results in a resisting force and energy dissipation as the structure moves laterally. However, if under continued horizontal motion, the welded joint between the beam's tension flange fractures where it attaches to the column flange, and the connection may behave like a pin. The sudden release of moments at the ends of the beam will result in a dramatic change in the deflected shape of the beam [Figure 5.8(b)] and very high velocities and changes in displacement in the VWD.
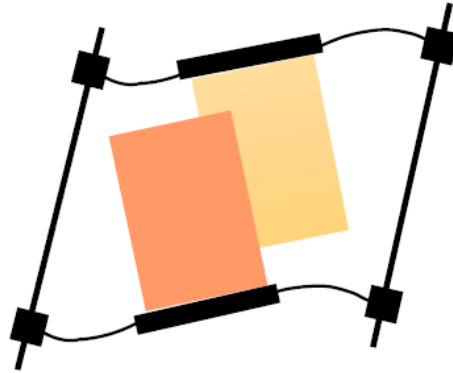
(a) Case 1: full end constraints
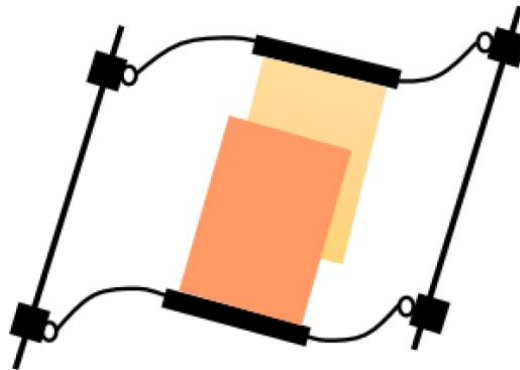
(b) Case 2: pin-end constraints

Figure 5.8   Beam deformed shapes under different boundary conditions

These high velocities result in large transient forces in the VWDs that may physically damage the VWD and result in high-frequency vibrations in the VWD and surrounding framing elements. Numerical simulation of these transient vibrations is very sensitive to details of the numerical model used, and special numerical integration schemes and iteration strategies might be needed to achieve numerically stable results. In buildings like the case-study building discussed herein, brittle pre-Northridge beam-to-column connection details would complicate the use of VWDs and may require measures (e.g., repair of adjacent connections, or the use of lower lateral displacement limits) to reduce the probability of brittle beam-to-column fractures.

Additionally, the shear force demands were increased due to the stiffening of the building and reduced clear beam span. As such, the beam-to-column connections might fracture earlier. To understand the influence of the additional VWD on the shear force transferred to the beam end connections, the aspect ratio of a VWD, i.e., b/h in Figure 5.9, is used to formulate the following expression based on the free-body diagram:

$$V_w = V \frac{h}{2b} \qquad (5.2)$$

The shear forces transferred to the beam ends are amplified by a factor inverse to the aspect ratio b/h. In a scenario where the b/h ratio is small, the shears transferred to the beam-

to-column connection increase substantially, and shear yielding of these connections is likely before forming plastic hinges. Admittedly, the numerical model in this study did not include the shear yielding for the beam-to-column connections; however, we raise this issue because it is relevant for engineers when designing VWDs for use in an existing building.
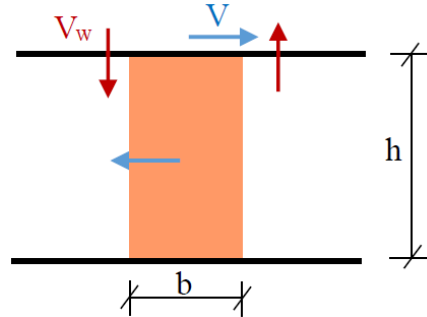
Figure 5.9   The effect of aspect ratio of a wall damper to the shear demand

To understand the interactions between beams, beam-to-column connections and wall dampers, a frame located at 8th floor where concentrated deformations were observed was examined. Figure 5.10 shows the time history of bending moments and shear forces at one beam end (node *i*). The Level-1 retrofit experienced beam fracture around 11 sec, whereas FVDs successfully avoided fracture by decreasing its rotation demand. On the other hand, the VWDs increased the force demand, and the beam fractured sooner than the fracture in the Level-1 retrofit; moreover, an increase of the shear forces was observed. The maximum shear stress was estimated using the following formula, which indicated a potential shear yielding failure mechanism of the beams:

$$\tau_d = \frac{V_d Q}{It} = \frac{460 \times 637}{0.5 \times 21148} = 27.7 kips > \tau_c = 0.6 f_y = 22.2 kips$$

Once the end of a beam broke, its moment-resisting capacity was reduced to be as small as 20% of M_p as suggested by ASCE 41. Therefore, the beam acted similarly to Case (2) shown in Figure 5.8, whereby severely decreasing the energy-dissipation capacity of the wall damper. Worse still, the abrupt change of the deflected shape of the beam brought about very high velocities and changes in displacement, subjecting the VWD to large transient forces in the VWD, which may physically damage the VWD. The response history of the damper force/deformation under one ground motion excitation is plotted in Figure 5.11 for one VWD that failed. An observable increase of both force and deformation was seen upon the beam-to-column connection fracture. Note that: the failure of the viscous material was not modeled in this study. This potential damper failure could not be captured; however, it was clearly shown that the wall damper could not work properly after the failure of the beam-to-column connection. Figure 5.12 shows the hysteresis loop of the investigated VWD where the damper had quite limited capacity to dissipate energy, as evidenced by the small irregular cycles after the beam end fractured.

(a) Moment   **(b) Shear force**
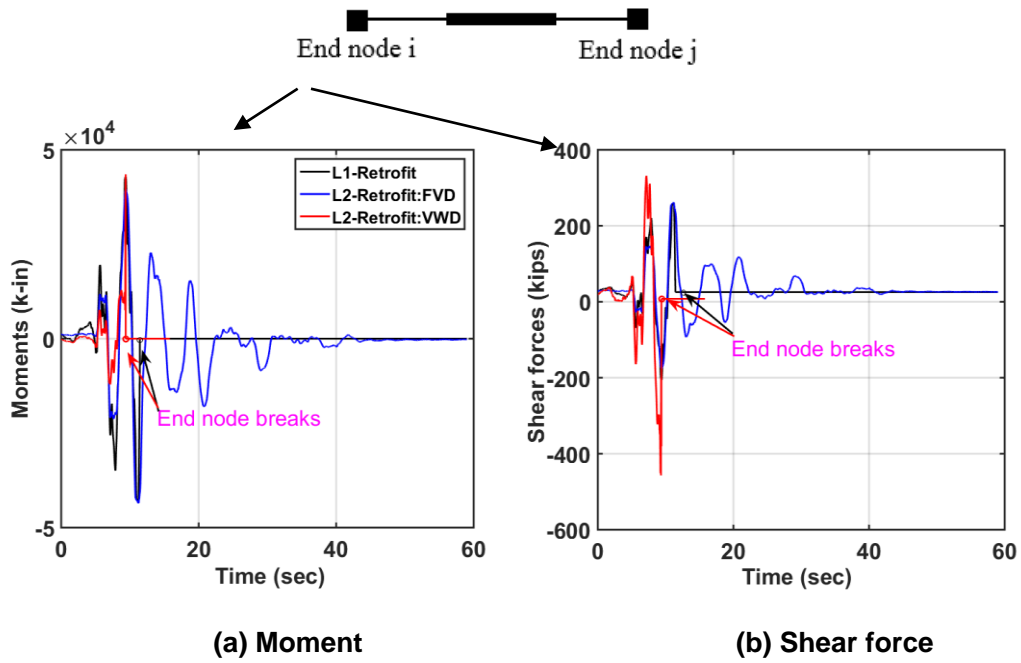
Figure 5.10   Time history of the beam end forces at node i

(a) Deformation   **(b) Force**
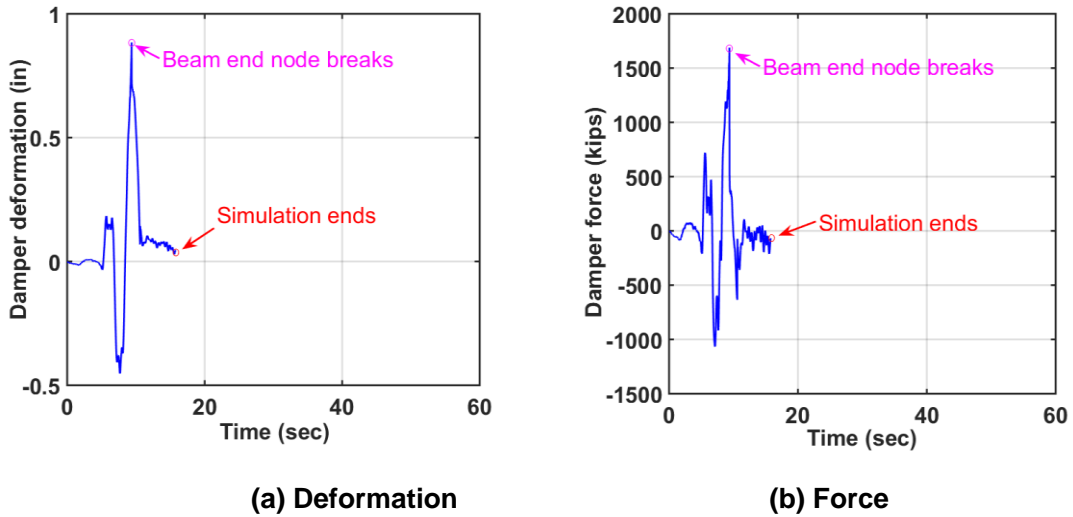
Figure 5.11   Response of a selected VWD
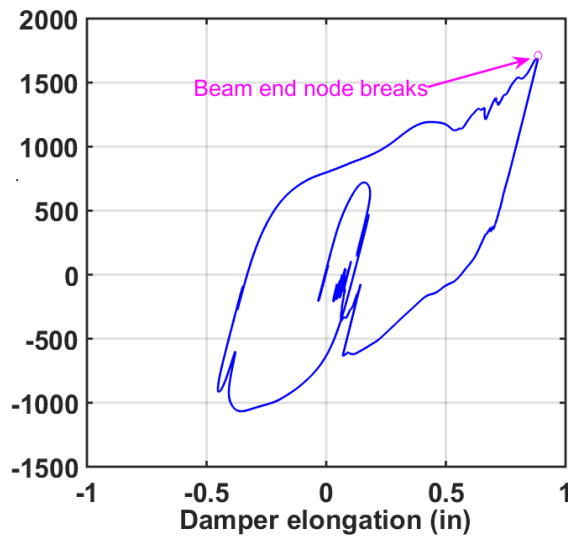
Figure 5.12   Hysteresis loop of a selected VWD

5.2.4 Enhance Beam-to-Column Connections

As demonstrated above, the brittle beam-to-column connections largely inhibited the control effect of VWDs. Next, we examine the performance of VWDs when the beam-to-column connection is not an issue. This could provide insight into how VWDs could contribute to improving seismic performance of a new building. Therefore, a case with all the pre-Northridge beam-to-column connections fixed in the case-study building was examined.

After fixing the brittle beam-to-column connections, the VWDs were able to eliminate the weak-story trend, which resulted in a drift profile closer to FVDs; see Figure 5.13. Nevertheless, the peak drift at the mezzanine level in the *Y*-direction still remained as high as 2.5%, which was partly attributed to the inadequate installation of VWDs in the mezzanine level where vertical irregularity exists. Increasing the damping capacity in this region might improve structural response, although it is worth noting that upgrading beams did not contribute to a reduction of peak floor accelerations; see Figure 5.14.

In terms of peak damper forces, the maximum damper force demands along building height were changed substantially (Figure 5.15). A significant large force demand at floor 3 and 7 was reduced, and the maximum force demand was reduced from 2300 kips to be less than 2000 kips. However, the force demands at floors 10 to 25 were generally larger even after beam ends fixed. An examination of the hysteresis loop of a VWD showed that the damper exhibited a more desirable behavior, eliminating the force spike and dissipating more energy during earthquake excitations (Figure 5.16).

114

(a) X-dir. **(b) Y-dir.**
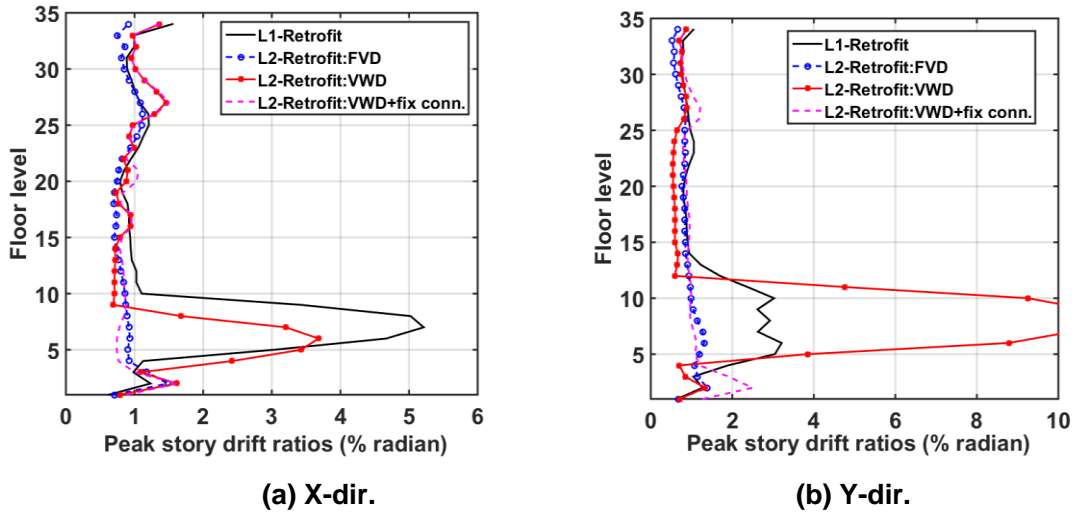
Figure 5.13   Distribution of peak story drift ratios
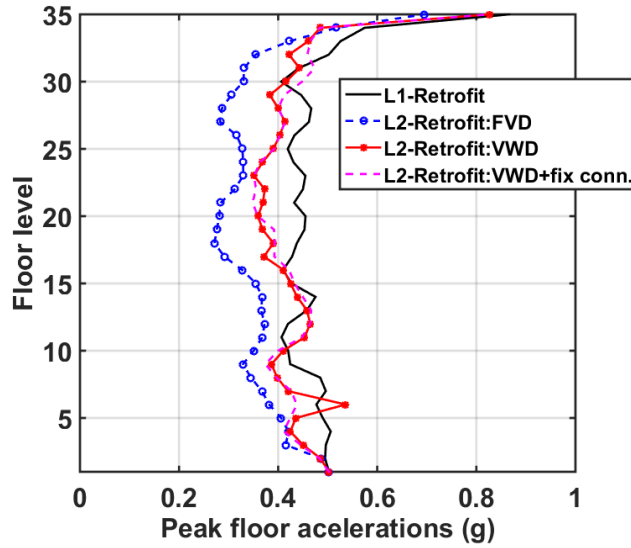
Figure 5.14   Distribution of peak floor accelerations (X-dir.)
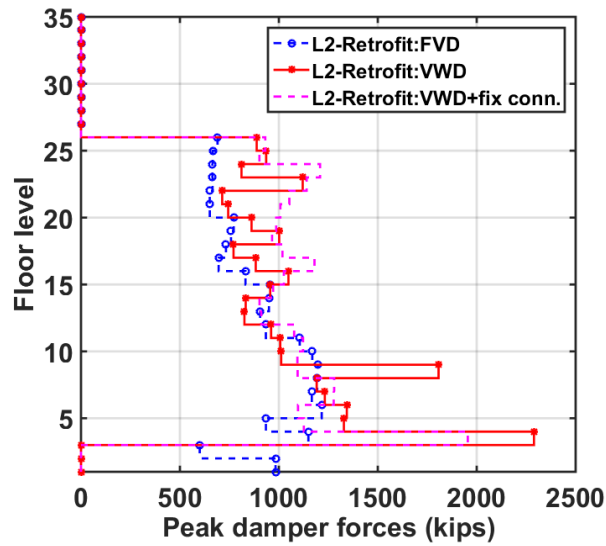
Figure 5.15   Distribution of peak damper forces
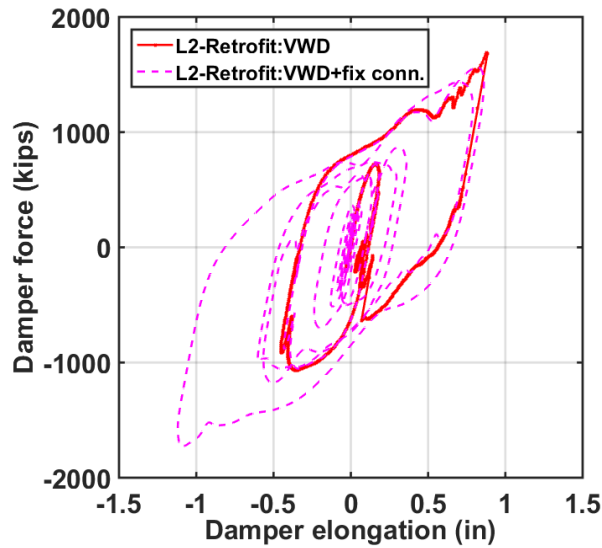
Figure 5.16   Hysteresis loop of a selected VWD

Retrofitting a structure with VWDs highlights the problem that exist between the characteristics of VWDs and beams; this issue is not exclusive to retrofitting projects. For newly constructed buildings, the beams should be carefully designed if wall dampers are used. Experimental testing of the frame-damper system might be needed in order to understand their behavior and insure the adequacy of the connection capacity. If the beam-to-column connections do not pose a problem in a building, however, the effectiveness of VWDs to enhance structural behavior is similar to FVDs in terms of reducing the peak deformations but will likely require larger forces capacities compared to FVDs.

116

5.3 RETROFIT USING BUCKLING RESTRAINED BRACES

The BRB is another energy-dissipation device used worldwide. Application of BRBs began in the early 1970s and have gained widespread practical applications in Japan, the U.S., China, etc. Figure 5.17 shows the number of buildings and the percentages of different damper contributions. Clearly, hysteretic dampers (including BRBs) are the most popular application, which is mainly because they are relatively inexpensive and are effective [Feng *et al.* 2015]. The largest BRBs used in building so far is in the 597-m tall Tianjin Goldin Finance 117 Tower [Shen 2015], which is a 48-m long and 1.5 m×0.9 m brace. It weighs 260 tons and is designed to attain 3600 tons of force before yielding; see Figure 5.18. The addition of braces stiffens the structure, thus increasing the seismic demands; therefore, special concern should be taken when BRBs are used in retrofitting an existing building.

(a) Number of damped buildings   **(b) Percentage of various dampers**

(adapted from Feng et al. [2015])
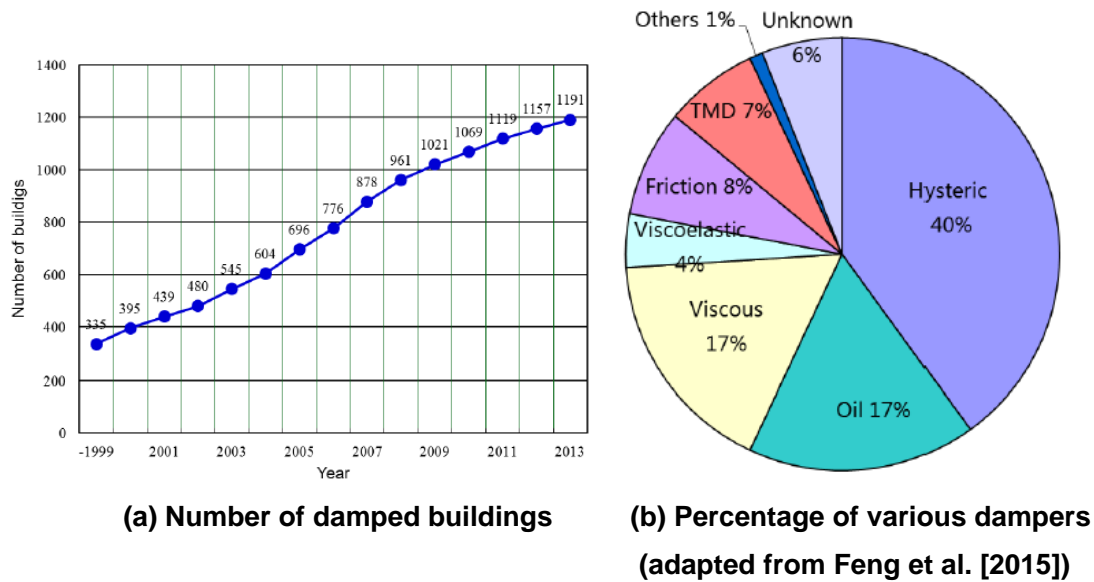
Figure 5.17   Application of buildings with dampers in Japan
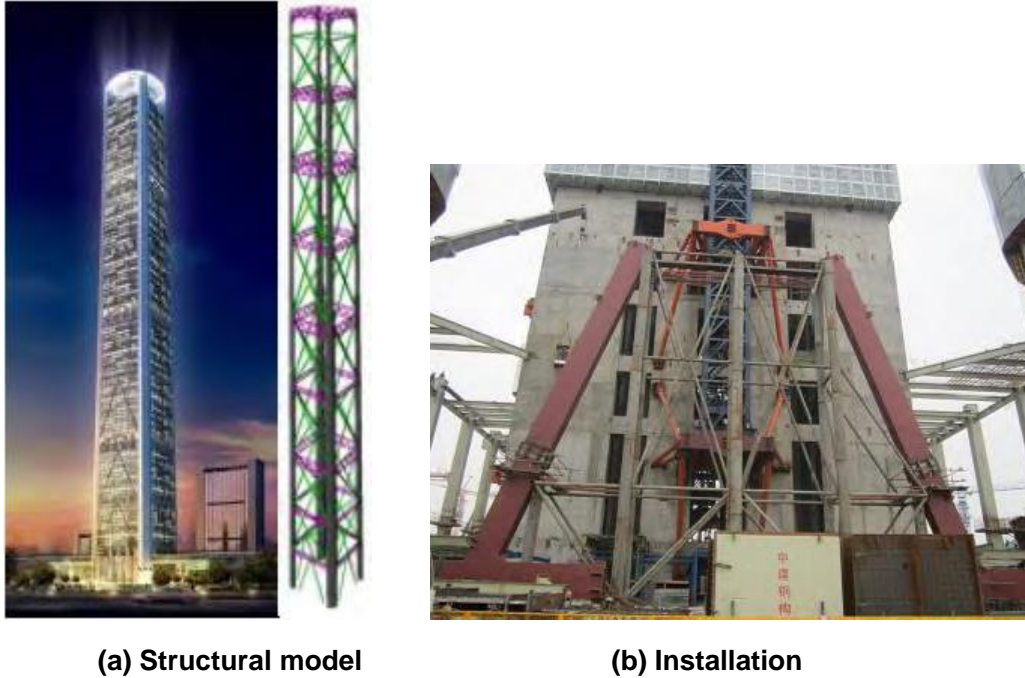
(a) Structural model   **(b) Installation**

Figure 5.18 Mega BRB in Tianjin Goldin Finance 117 Tower (adapted from Shen [2015])

5.3.1 Mathematical Modeling

Typically, a BRB exhibits stable bilinear hysteretic behavior (Figure 5.19) with slightly greater strength in compression than tension. Since the mechanical properties of a BRB are displacement-dependent rather than velocity-dependent, its energy-dissipation characteristics are quite different from those of a FVD or a VWD. To represent the behavior of a BRB in the OpenSees model, simple pin-ended truss elements were employed considering a *Giuffre-Menegotto-Pinto* hysteretic material model and co-rotational geometric nonlinearity. For the purpose of this comparison, following the results of a study of BRB frames by Uriz and Mahin [2008], the yield strengthen was set to 58 ksi in both tension and compression, and strain hardening was taken as 0.3% of the initial stiffness. Other parameters to capture the isotropic hardening properties and to control the transition from elastic to plastic branches were based on values suggested by Filippou *et al.* [1983].

  The sizes of the BRBs were calculated at a location so that a BRB and a FVD would dissipate the same amount of energy if both devices were loaded through an ideal symmetric displacement cycle at the fundamental frequency of the building to the same displacement amplitude u_0. For this steady-state case, the areas within the closed hysteresis loops in Figure 5.20 for a BRB and a FVD are approximately the same, i.e., $W_{FVD} = W_{BRB}$, where W_{FVD} and W_{BRB} denote the energy dissipated by a FVD and a BRB, respectively. For large displacement cycles, these can be represented by Eqn. (5.3) and Eqn. (5.4), respectively:

$$W_{FVD} = \lambda C \omega^{\alpha} u_0^{1+\alpha}$$

(5.3)

$$W_{BRB} \approx 4P_y(u_0 - u_y)$$

(5.4)

The terms in Eqn. (5.3) are the same as previously used in Eqn. (4.2) in Chapter 4; P_y, u_y, u_0 in Eqn. (5.4) are the yield force, yield displacement, and maximum displacement of a BRB; see Figure 5.19. With these equations, P_y can be computed and from this value the effective area A_{eff} of the BRB can be determined for the numerical model. A more refined model could be considered to account for the compression strength adjustment factor, the recoverable elastic stored energy, and the relation between tension and compression strain hardening and plastic strain, if a more refined determination of BRBs sized is desired [Shen 2015]. With the stiffening effect from the added BRBs, the fundamental period of the building reduces from 4.33 sec to 4.05 sec.
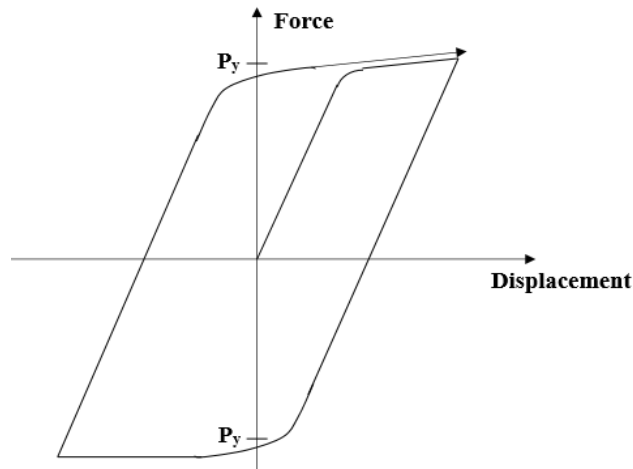
Figure 5.19   Typical load-deformation relation of a BRB
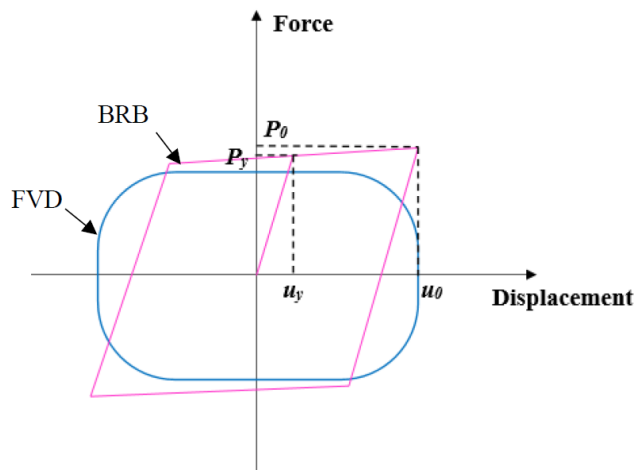
Figure 5.20   Idealized hysteresis loop of a FVD and a BRB with a same energy dissipation

5.3.2 Investigated Schemes

To investigate the feasibility of using BRBs to upgrade the seismic performance of the case-study building, two design schemes were proposed based on Scheme III$_R$ of FVDs.

(a) Replace FVDs from floors 1 to 10 with BRBs, but retain FVDs elsewhere;

(b) Replace FVDs with BRBs everywhere.

For the purpose of this comparison, both Scheme (a) and (b) had the same effective damping ratios as Scheme III$_R$.

Table 5.1 lists the first five periods of structure for the different retrofit schemes. The addition of braces shortened the periods by about 4.3% and 6.7% for Scheme (a) and (b), respectively, which corresponds to 8% and 15% additional stiffness.

Table 5.1 Modal periods of different schemes (sec)

Mode	Baseline	BRB (a)	BRB (b)
1	4.329	4.137	4.045
2	4.179	3.918	3.749
3	3.585	3.192	2.968
4	1.499	1.438	1.407
5	1.451	1.372	1.334

The distributions of peak drift ratios indicated in Figure 5.21 showed that BRBs were much less effective than FVDs in controlling drift, especially when the BRBs replaced all FVDs. Limiting the number of BRBs at lowest 10 stories worked well within these stories, but the weak-story zone moved above to floors 11 to 19 in the *Y*-direction. However, when more BRBs were used, the structural dynamic behavior changed by a larger extent and failed to suppress peak drifts, resulting in multiple weak-story zones from floor 4 to 8, and from floor 11 to 14. Correspondingly, both Scheme (a) and (b) contributed to a larger number of beam-to-column connections failure than the FVDs scheme, with a maximum percentage as high as 28% at two weak-story zones identified for Scheme (b); see Figure 5.22.

(a) X-dir.   **(b) Y-dir.**
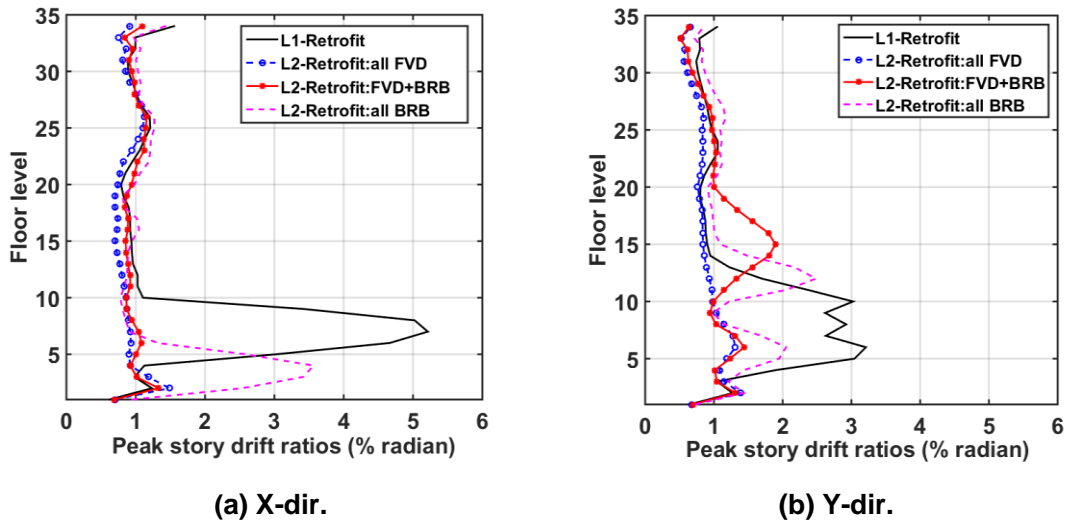
Figure 5.21   **Distribution of peak story drift ratios**
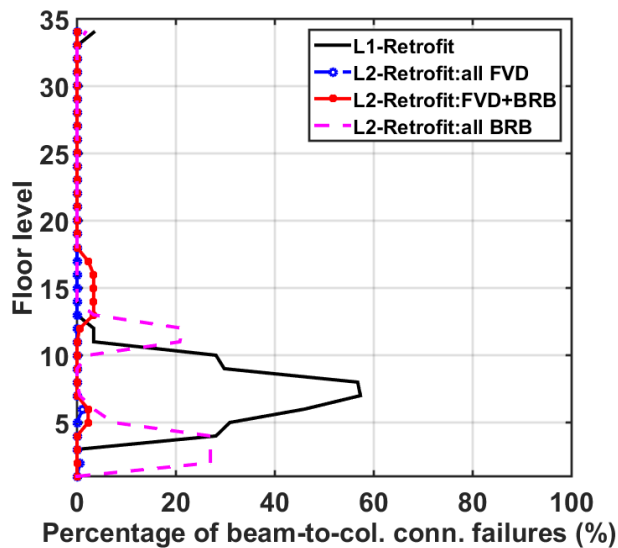
Figure 5.22   **Distribution of peak beam connection failures (as percentage of total number of connections per floor)**

The influence of using BRBs was more obvious when considering the peak floor accelerations (Figure 5.23). When FVDs from floors 1-10 were replaced with BRBs, the accelerations were increased at most floors compared with Scheme III$_R$ of FVDs; the increase was even larger if all FVDs were replaced with BRBs, which exceeded the Level-1 retrofit case. The addition of BRBs stiffened the building and increased the seismic force demand, which contributed to larger accelerations throughout floors. Additionally, BRBs were less effective in attenuating vibration after the excitation ended; see the acceleration history at roof level in Figure 5.23 (b).

121

In a same fashion, the vulnerable columns were more sensitive to failure in the cases using BRBs. See the *D/C* ratio distributions for Group 1 corner columns in Figure 5.24, where a 10% increase was exhibited at most floors.
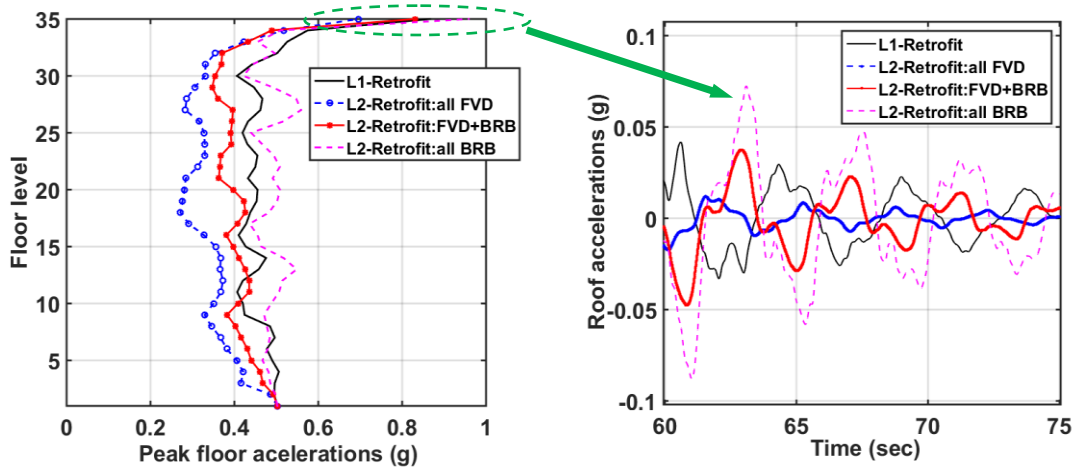
(a) Distributions of peak floor accel. (X-dir.)   (b) Time history of roof accel. under one ground motion

Figure 5.23   Floor accelerations
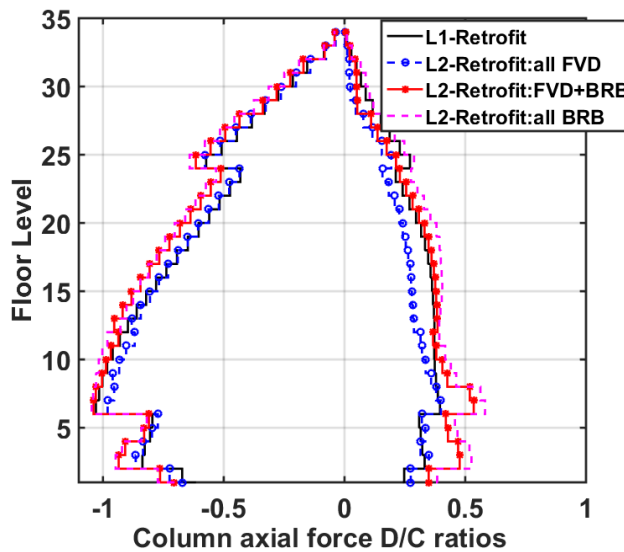
Figure 5.24   Distribution of peak axial force D/C ratios of Group 1 columns: (+) tension, (-) compression

To investigate the behavior of the BRBs, one BRB element located at the 6th story in the *Y*-direction was selected. Its hysteresis loop under both BRB Schemes (a) and (b) were compared with the FVD at the same location in Scheme III$_R$; Figure 5.25, and. The maximum forces of the BRB for Scheme (a) and FVD are similar, although the BRB had slightly larger force. On the other hand, in Scheme (b), where only the lower 10 stories used BRBs, the structure was stiffer

122

in these stories, which in turn inhibited the energy-dissipation capacity of a BRB as evidenced by a much smaller deformation in this scheme. Note: all these cases were designed to have the same energy dissipation per cycle if loaded at the same frequency to the same target displacement. Nonetheless, the ultimate response of a FVD and a BRB in the same location might differ in the peak load, displacement, and energy-dissipation demand.

Figure 5.26 shows the maximum damper force demands at each story for different schemes. For the BRB Scheme (a), the braces at floors 1 to 10 exhibited a decrease of the peak force demands compared to these of FVDs, but an increase was shown from floors 12 to 17. However, BRB Scheme (b) increased the force demands at most stories except from floors above 21. An average increase of 10% was seen for these BRBs, which mainly resulted from the increase in seismic demands.

When designed with the same effective damping ratio, BRBs were demonstrated to be less effective then FVDs in retrofitting the case-study building; this was mainly due to their pure displacement-dependency properties. The additional braces stiffened the structure, thus increasing seismic forces.
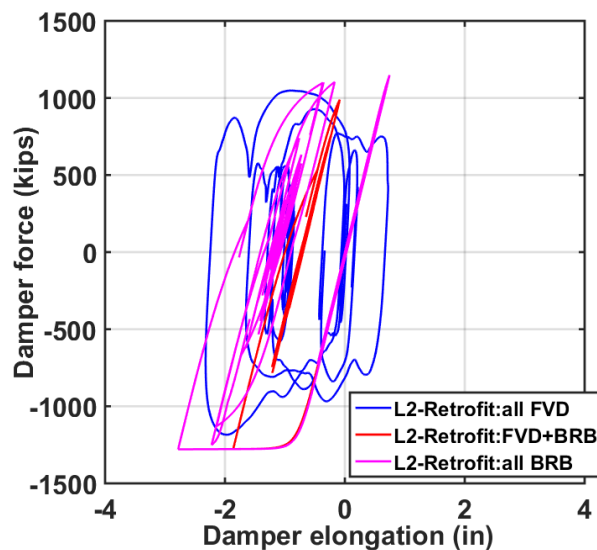
Figure 5.25   Hysteresis loop of a BRB/FVD (floor 6)
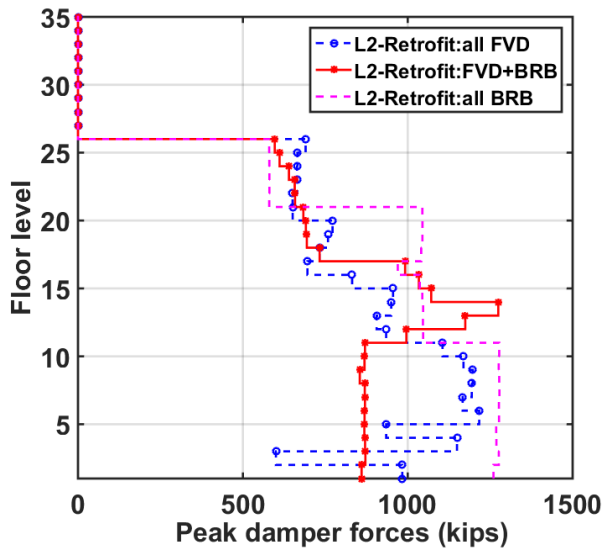
Figure 5.26   Distributions of peak damper forces

5.4   CONCLUDING REMARKS

This chapter explored the characteristics and mechanical properties of two other supplemental energy-dissipation devices: VWDs, and BRBs. To conduct a side-by-side comparison the behavior of the selected devices with the FVDs presented in Chapter 4, the locations where the devices were installed the devices were kept the same and the mechanical properties of different devices were chosen to insure a same effective damping ratio.

The structural analysis indicated that neither of the VWDs nor BRBs were capable of meeting the retrofit objective to ensure the seismic integrity of the selected building under BSE-2E hazard level. Specifically, the addition of VWDs altered the behaviour of existing beam members and significantly increased the existing beams' vulnerability to fracture. Consequently, wall dampers did not behave as expected unless the fragile beams-to-column connections were also upgraded in this building. The BRBs stiffened the building substantially, thus increasing seismic demands and contributed to an undesirable outcome. A comparison of the structural analyses showed that in the case study presented herein, the performance of the FVDs was superior to either BRBs or VWDs. The findings might change if VWDs or BRBs are designed differently, or considered in another building. Further estimates of loss and business downtime interruption will be presented in Chapter 6.

6   Predicted Damage and Loss

6.1   INTRODUCTION

This chapter estimates damage and loss of the case-study building, including two parts: (1) a preliminary comparison that focuses on repair cost alone and (2) an extends comparison that includes business downtime and total financial loss. Part (1) comparison is conducted between three Level-2 retrofit strategies that used fluid viscous dampers (FVDs), viscous wall dampers (VWDs) or buckling restrained braces (BRBs); whereas part (2) compares different levels of retrofit, including the building in its as-built condition, after Level-1 retrofit and after a complete Level-2 retrofit with FVDs. The damage and loss analysis is based on three sets out of twenty ground motions under the basic safety earthquake, level 2 hazard events (BSE-2E). Despite the limited number of nonlinear response history analysis (NRHA) used, this preliminary comparison could help identify economically feasible and cost-effective retrofit methods among three strategies investigated. The most promising retrofit strategy: the scheme that used FVDs is then used in part (2) for a more extensive and informative comparison of potential costs and losses. Three decision variables are used in part (2) comparison: the repair cost, business downtime and total financial losses that include loss due to business interruption. A method developed by Terzic *et al*. [2015] is utilized to assess business downtime with considerations of mobilization factors and the degree of building repairs. A simplified business model is used to assess the total financial loss for different cases. Both BSE-1E and BSE-2E hazard levels are selected, each utilizing 20 NRHA results in part (2) study. However, this study does not include building collapse; had building collapse considered, the building loss under each case would be larger, especially for the as-built condition and the building with only Level-1 retrofit.

6.2   PERFORMANCE ASSESSMENT CALCULATION TOOL

The FEMA P-58 documents [2012a-c] were used as a major resource for the damage and loss estimates, which are outcomes from the ATC-P-58 project. The framework and the Performance Assessment Calculation Tool (PACT) (Version 3.0.2) [ATC 2016], based on the methodology developed in PEER and implemented by Tony *et al*. [2009], was used to formulate repair costs and repair time for this study. PACT performs the probabilistic loss analysis calculations needed to estimate repair cost and repair time based on peak story drifts, residual story drifts, peak floor accelerations and peak floor velocities and the dispersion of these responses. To ensure that results would be more generally applicable, the study used the default fragility and consequence

relations for typical structural and non-structural components in office buildings provided by the program. Residual drifts were estimated using an empirical relation in FEMA P-58 [2012a] between peak transient drift and residual drift.

PACT dollar values are based on 2011 estimates. To account for inflation, a 5% increase on this estimate was applied so that the default values were brought up to represent the current value. A regional cost multiplier was assumed to be 5% above the average of Northern California for the site in San Francisco. A total replacement cost of $475 million and a replacement time of five years were assumed for present-day market conditions for the case-study building [LoopNet 2014]. A maximum number of workers per square foot of 0.001 was assumed based on PACT recommendations [FEMA 2012b], which results in 24 laborers able to work on a typical floor level. Modeling recommendations specific to tall buildings depend on a height factor, see Volume 2, Table 2-1 [FEMA 2012b]. This accounts for increased costs of transporting materials and workers above four floors. Recommendations include an 8% increase for floors 5−10 and 16% thereafter. FEMA P58 [2012b] acknowledges that high-rise buildings may incur significant premiums for some items but combined with elements less sensitive to elevation, and they anticipate only modest increases in most cases for tall buildings. The case-study building is designated as having an office building occupancy with default parameters.

Nonstructural components and contents generally contribute the most to post-earthquake repair costs [Taghavi and Miranda 2003]. In this study, the nonstructural components were assigned through the normative quantities available in PACT [FEMA 2012c] as recommendations for generic buildings based on occupancy. Contents obtained as normative quantities for an office building, see Table 6.1, were modified to reflect the most appropriate options based on given information of the case-study building. Modifications included changing the exterior curtain walls to 4-in precast concrete panels. Structural elements such as beams, columns, and walls are building specific and require user input. Structural plans were used to identify member sizes. Components used in the building model included welded column splices on every other floor, bolted shear tab gravity connections, pre-Northridge welded unreinforced flange, type B (WUF-B) beam–column connections, and steel column base plates on the ground level; see Table 6.2. Note that the building after the Level-1 retrofits removed the exterior claddings and fixed column splices; therefore, the corresponding building model in PACT was modified to reflect the changes. However, the list of generic nonstructural components considered might not fully describe the conditions in the case-study building, and hazardous materials were not considered for this analysis.

Residual drift ratios were included in the damage and loss analysis to account for their effect on the loss estimation. Note: any analyses that exhibited numerical instability were not included in the damage and loss estimates. This is consistent with FEMA P-58 recommendations to discard analysis results when numerical instability occurs [FEMA 2012b].

The analysis results reported below would be dependent on assumptions made within the FEMA P-58 framework since default parameters, damage fragility curves, and cost consequence functions were used unaltered. To the extent that the normative quantity components and structural elements encompass the majority of possible damage and repair costs, the repair scenarios should be reasonable.

Table 6.1   Nonstructural components included in loss estimations

Raised access floor, non seismically rated
Wall partitions
Curtain walls (modified to precast concrete cladding)
Prefabricated steel with steel treads and landings with seismic joints that accommodate drift
Suspended ceiling
Recessed lighting
Independent pendant lighting
Traction elevator
Cold water piping
HVAC
Variable air volume box
Fire sprinkler water piping and standard threaded steel
Motor control center
Low voltage switchgear
Battery rack
Book case
Vertical filling cabinet
Storage rack

Table 6.2   Structural components included in loss estimations

Welded column splices (every other floor)
Bolted shear tab gravity connections
Pre-Northridge WUF-B beam-column joints, beam one side of column
Pre-Northridge WUF-B beam-column joints, beam both sides of column
Steel column base plates, column w>300plf

6.3   OVERALL WORK FLOW

The workflow of Performance Based Earthquake Engineering (PBEE) is illustrated in Figure 6.1. Based on structural analysis presented in Chapters 3-5, this chapter focuses on damage and loss analysis, and was conducted using PACT. In evaluating the decision variables (DVs), a downtime model proposed by Terzic *et al*. [2015] and a simple business model was implemented to estimate the total financial loss considering both business interruption loss and repair cost under two hazard levels of concern (i.e., BSE-1E and BSE-2E); see Figure 6.2. The procedure to estimate the repair cost, business downtime and total financial loss are illustrated below.

Figure 6.1   Flow chart of PBEE
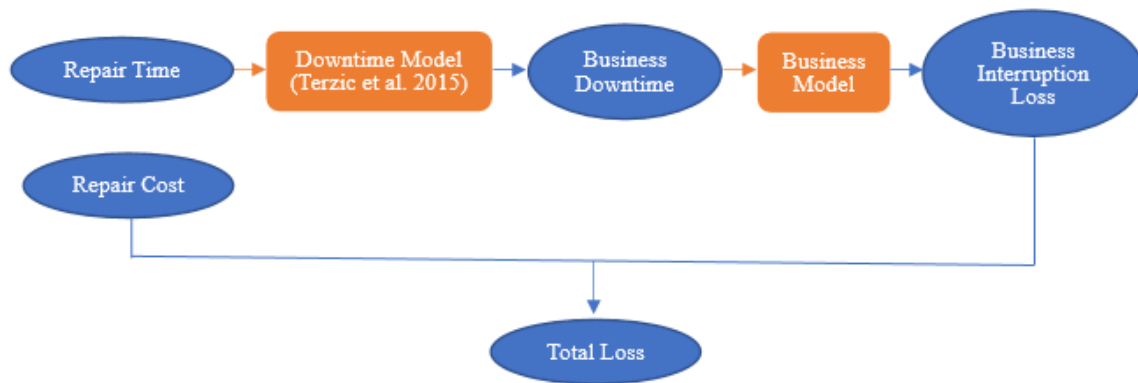
Figure 6.2   Procedure to assess decision variable

6.3.1 Repair Cost

Repair cost of each component could be assessed based on its fragility curve that relates an engineering demand parameter (EDP) with the probability of that item reaching a particular damage state, and the consequence function that associates the repair cost and repair time with that damage state. For every realization of Monte Carlo simulation, the total repair cost was summed up for all components, and consequently a cumulative distribution function of the repair cost for the building under the hazard level of concern was obtained. To better inform designers or clients, the repair cost of the entire building was summed, and expressed in a normalized fashion: the loss ratio (i.e., a ratio between the repair cost and the cost to replace a similar new building).

6.3.2 Business Downtime

In this study, business downtime refers to the periods when a building is unavailable for occupancy. The business downtime could lead to business interruption and correspondingly a significant revenue loss; thus, this is a crucial parameter in the decision-making process.

A business downtime model based on the work of Comerio [2005 a,b] and Terzic *et al.* [2015] was used in this study. Several key mobilization factors were considered in the proposed model, including building inspection, clean up, site preparation, contracting construction services, acquiring materials and financing. In addition, repair work would be invoked if major structural and/or non-structural damage is observed; such repair time needed to restore normal building operations is based on results reported from the PACT analysis. Figure 6.3 presents the flowchart of the proposed business downtime model.

To estimate the above-mentioned mobilization factors, several components that affect building functionality were selected, including the structural components such as the bolted shear tab gravity connections, steel column base plates and pre-Northridge welded unreinforced flange beam-column joint, and non-structural components such as prefabricated steel stairs and fire sprinkler water piping. Their damage states were identified based on the PACT results. To assess the extent of damage and total financial losses of the building under a specific hazard intensity, a simplified procedure was adopted from Terzic *et al*. [2015], as illustrated below. For each Monte Carlo simulation,

1. The average damage state of each performance group was assessed and their damage classes identified based on Table 6.3;

2. The maximum damage class of structural groups and the that of non-structural groups were selected to represent the building damage status.

Based on work by Comerio [2005 a,b], five damage classes were categorized, ranging from minor or aesthetic damage (damage class 0) to complete failure (damage class 4); see Table 6.3.

Once the damage class is known, mobilization factors that contribute to the business downtime can be determined and quantified. Figure 6.3 shows the flowchart of business downtime. If the building is deemed irreparable due to excessive drift ratios or a large loss ratio, a replacement is incurred, and thus the downtime defaults to the replacement duration. If a building is considered repairable, however, the business downtime depends on mobilization factors incurred in the flowchart. The mobilization factors are based on the building's damage status determined through Step 1–2 outlined before. For instance, if there is major structural damage (damage class 2) or extensive non-structural damage (damage class 3), a detailed inspection is required, which is followed by the need for architectural and engineering drawings for the repair strategy and approvals from local building authorities. In the meanwhile, cleaning up the site and making preparations are conducted. Under conditions where structural/non-structural damage is insignificant, business downtime is estimated to be zero.

A lognormal distribution is used to estimate the time needed for each mobilization factor, with a dispersion of 0.3 considering their large uncertainties. The estimated median values and dispersions are proposed on experiences gleaned from past earthquakes in New Zealand, Chile, and Japan [Terzic *et al.* 2015]; see Table 6.4. These values would vary depending on the damage status of structural/non-structural components.

In addition, the repair time needed to restore a building was estimated based on the repair sequence shown in Figure 6.4. It is assumed that enough suppliers and laborers will be available to facilitate simultaneous repair work at multiple floors; the repair time is dominated by the floor

with the longest repair duration. This is the most optimal strategy and gives a lower bound estimate of repair time. A labor density of $0.001/ft^2$ was used based on FEMA recommendations [2012a]. The repair sequence at each floor was based on Figure 6.4 that considers realistic work flow. The repair time estimated for each performance group was based on the PACT analysis.

Table 6.3   Category of damage classes

Damage status (DS)	Damage class	Damage extent
$DS_{ave}=0$	0	None
$DS_{ave}\leq0.1$	1	Minor
$0.1<DS_{ave}\leq1$	2	Major
$1<DS_{ave}\leq2$	3	Extensive
$2<DS_{ave}\leq3$	4	Failure
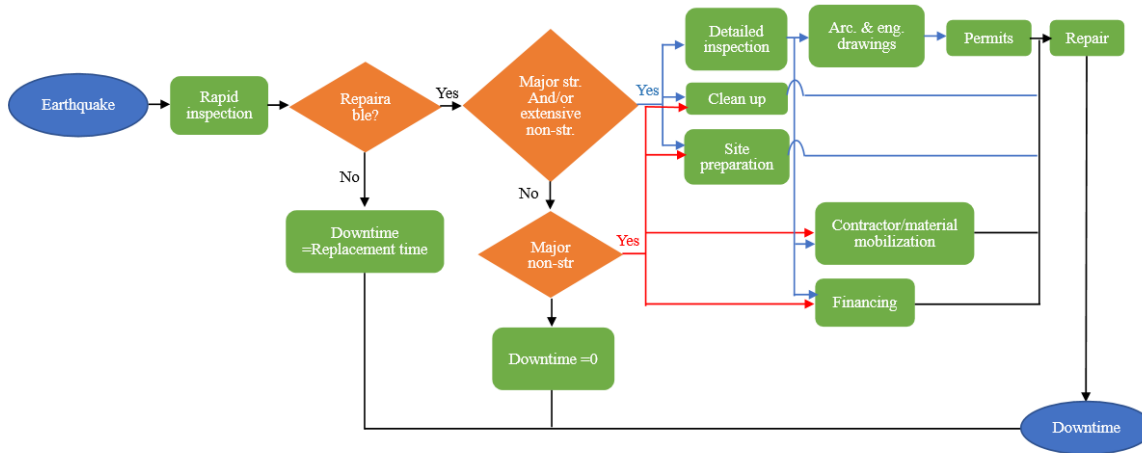
Figure 6.3   Business downtime model

Table 6.4   Median downtime for each mobilization activity (adapted from Terzic et al. [2015])

Factor	Condition	Median Downtime
Detailed Inspection	Max. Structural Damage Class < Damage Class C Max. Non-structural Damage Class ≥ Damage Class D	2 weeks
	Max. Structural Damage Class = Damage Class C Max. Non-structural Damage Class < Damage Class D	2 weeks
	Max. Structural Damage Class = Damage Class C Max. Non-structural Damage Class = Damage Class D	4 weeks
	Max. Structural Damage Class = Damage Class D Max. Non-structural Damage Class < Damage Class D	4 weeks
	Max. Structural Damage Class = Damage Class D Max. Non-structural Damage Class = Damage Class D	6 weeks
Re-issuing Drawings	Max. Non-structural Damage Class = Damage Class D	1 months
	Max. Structure Damage Class = Damage Class C	3 months
	Max. Structure Damage Class = Damage Class D	6 months
Permitting	Max. Non-structural Damage Class = Damage Class D	2 weeks
	Max. Structure Damage Class = Damage Class C	1 month
	Max. Structure Damage Class = Damage Class D	2 months
Clean up	Max. Structural Damage Class < Damage Class C Max. Non-structural Damage Class = Damage Class C	1 week
	Max. Structural Damage Class = Damage Class C Max. Non-structural Damage Class < Damage Class D	2 weeks
	Max. Structural Damage Class < Damage Class C Max. Non-structural Damage Class = Damage Class D	2 weeks
	Max. Structural Damage Class ≥ Damage Class C Max. Non-structural Damage Class = Damage Class D	4 weeks
Site Preparation	Max. Damage Class ≥ Damage Class C	7 days
Financing	5% ≤ Loss Ratio < 10%	1 month
	10% ≤ Loss Ratio < 20%	3 months
	20% ≤ Loss Ratio < 40%	6 months
Contractor and Other Professionals Availability & Mobilization	Max. Non-structural Damage Class = Damage Class C	2 weeks
	Max. Structure Damage Class = Damage Class C	1 months
	Max. Structural or Non-structural Damage Class = Damage Class D	2 months
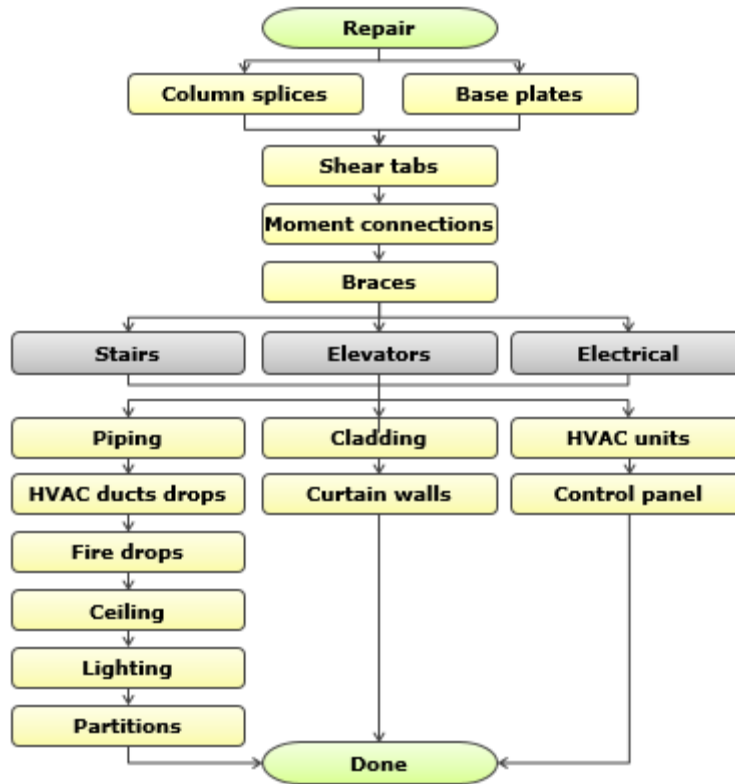
Figure 6.4   Repair sequence (adapted from Terzic et al. [2015])

6.3.3 Total Financial Loss

The total financial loss consists of the losses due to business downtime interruption and the repair cost. To convert the business downtime to business interruption loss, a simplified business model was used by assuming that the loss is due to rental loss during downtime periods. According to several recent real estate market review reports as of writing, the average leasing rate for an office building in San Francisco area is about $65/ft^2/year [Kidder Mathews 2015]. As such, the daily loss is approximately \$145,890 for the 35-story case-study office building. Note that the loss estimates were largely dependent on the selection of business model; the value could be even higher, if other factors such as revenue losses are taken into account.

6.4   ESTIMATES OF REPAIR COST FOR THREE LEVEL-2 RETROFITS

Ideally, an economic assessment of the retrofit schemes should consider costs of: installing the retrofit devices, repairing damage for all seismic events likely during the building's lifetime, and business interruption associated with installing the retrofits and repairing seismic damage. Given the specific objectives of this preliminary comparison, however, emphasis herein is placed on estimates of the cost of the different retrofit strategies, and the presented value of repair costs should a BSE-2E level event occur. Results of the NRHA based on three ground-motion set were

used in PACT to trigger 1000 Monte Carlo simulations so that a probabilistic distribution of repair cost for three Level-2 retrofit strategies under a BSE-2E hazard event could be obtained.

Table 6.5 presents the values estimated by PACT for probability of being irreparable and having unsafe tag after a BSE-2E earthquake; the major contributors to these conditions are identified as well. The fragility curve in PACT related to residual drift indicates that if a building has a residual drift ratio more than 2%, repair work is essentially infeasible and replacement should occur [FEMA 2012a]. As such, the residual drift was used as the criterion to identify the irreparable condition.

The building with only Level-1 retrofits implemented was expected to experience large residual drifts, which made repair difficult. Consequently, this limited retrofit resulted in a building with more than a 90% chance of needing to be torn down after a BSE-2E event. After adopting the Level-2 retrofit measures, the residual drifts were expected to be significantly reduced; thus, reducing the probability of being irreparable or receiving an unsafe tag. Among the three cases, the FVD retrofit scheme was the most efficient in eliminating large residual drifts, reducing the probability of the building being irreparable to less than 1% and of being red tagged to about 27%. In contrast, the retrofit measures developed herein using VWDs or BRBs did not bring down residual drifts to a satisfactory level, with a 66% and a 46% chance of demolition, respectively, and of 71% and 61% of receiving a red tag, respectively, following a BSE-2E event. The unsafe placarding of the building was due mainly to the dispersion of story drifts in the lower ten stories of the building for some BSE-2E events that resulted in fracture of some of the pre-Northridge welded beam-to-column connections and damage to stairways needed for egress.

To further assess the different retrofit schemes, an economic loss ratio was computed, which is defined as the expected repair cost normalized by the building's estimated replacement cost ($475 M). The likelihood that this ratio exceeds a given value is shown in Figure 6.5(a). Previous work indicated that the expected median loss ratio for the as-built structure was 100%, and that the Level-1 retrofit scheme reduced losses substantially for moderate earthquake excitations (i.e., BSE-1E). However, the Level-1 scheme was not especially effective at reducing loss at the BSE-2E level, and predicted a median loss ratio of 100%. The median loss ratio for the Level-2 scheme with FVDs was estimated to be only 4.8% at the BSE-2E level. Similarly, it was estimated that there was less than a 10% chance that the losses for the FVD scheme would exceed 7.2%. By comparison, the Level-2 retrofit scheme with VWDs resulted in the need to demolish and construct the building even at a median probability level; the Level-2 retrofit scheme with BRBs brought down the median loss ratio to about 8.4%, but was unable to achieve a 90% confidence of being able to avoid the need for demolition and replacement.

A further check on the median loss ratios was conducted to disaggregate the values into the contributions from structural components or non-structural components; see Figure 6.6. Most repair costs were due to damage observed of non-structural elements; the structural elements contributed to about 7.2% to 19.3%. The most efficient retrofit plan—Level-2 retrofit with FVDs—had a smallest repair cost ratio from structural components, indicating only limited damage was observed for structural members. It should be pointed out that for the cases that required complete replacement, the disaggregation was based on a new construction, e.g., 18% construction fees due to structural components, and 82% from non-structural components for a typical office building [Taghavi and Miranda 2003].

Table 6.5   Probability of irreparability and unsafe tagging

Case	Prob. of irreparbility	Prob. of unsafe tagging (primary contributors)
Level-1	94.3%	98.3%: (Residual drift, prefabricated steel stairs)
Level-2: FVDs	0.6%	26.9%: (Pre-Northridge beam-to-column connections, prefabricated steel stairs)
Level-2: VWDs	66.0%	70.6%: (Residual drift, Pre-Northridge beam-to-column connections, prefabricated steel stairs)
Level-2: BRBs	45.5%	60.6%: (Residual drift, Pre-Northridge beam-to-column connections, prefabricated steel stairs)
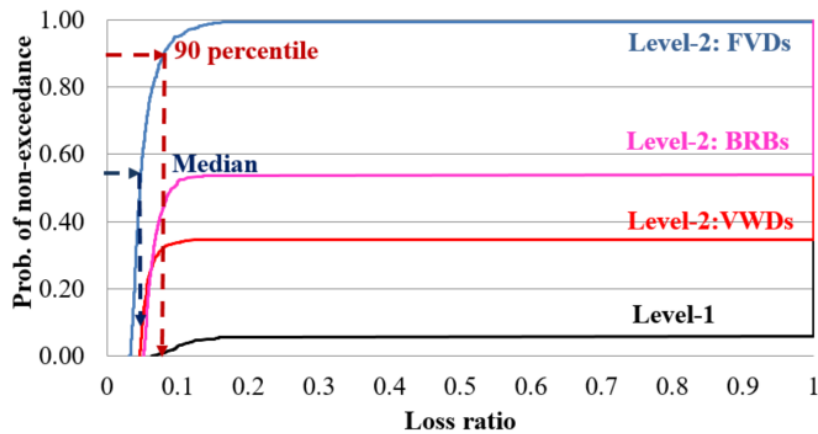
(a) Cumulative distributions of loss ratios
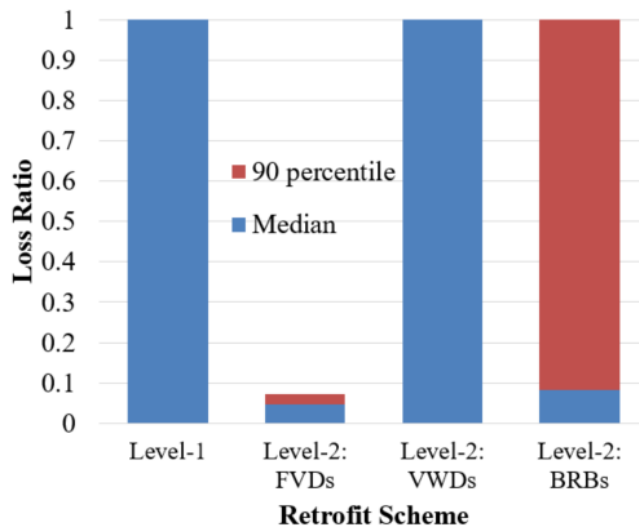
(b) Median and 90-percentile

Figure 6.5   Loss ratios
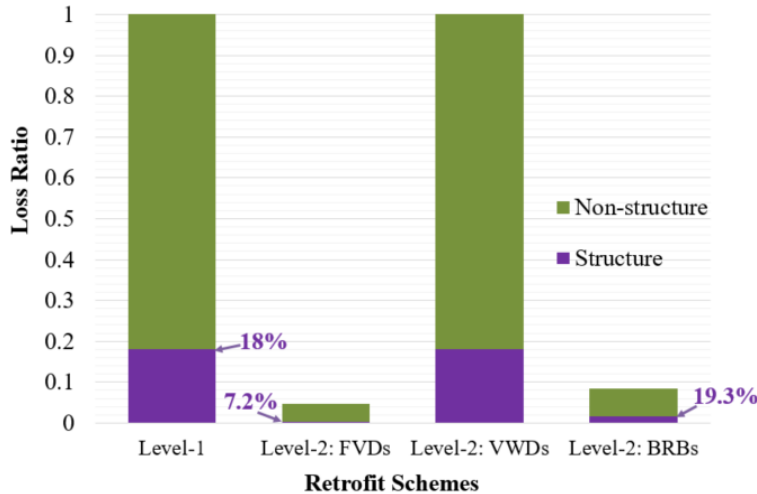
Figure 6.6   Disaggregation of median loss ratios

Construction costs for installing the Level-1 and 2 retrofits, and the unit cost for a FVD based on its force and stroke capacity (Table 6.6) were developed in consultation with design engineers experienced with the retrofit of tall buildings. Cost estimates are listed in Table 6.7. The Level-1 retrofit measures costed about $86 M, or about 18% of the building's replacement cost. The incremental cost of the Level-2 retrofits was comparatively modest, but brought total costs up to about $110.8 M (23.4% of the replacement cost) for the FVD scheme. The unit costs for the BRBs were significantly smaller than for either the FVDs or VWDs, with the unit cost of the VWDs being the most expensive. However, the cost of the supplemental energy-dissipation devices themselves was relatively small: less than 1% of the total replacement cost. The total cost of the Level-2 retrofits included the substantial cost of the Level-1 retrofit measures, and the additional cost of components needed to attach the devices to the structure and to drag the distributed inertial forces in the structure to the devices. These supplemental costs were particularly large for the retrofit with FVDs due to the significant costs of the required gusset plates and driving braces. While the BRB scheme also required gusset plates, it did not require the hefty driver braces needed for the FVDs. The relatively expensive VWD did not require either gusset plates or driving braces, but spacers were needed to connect a VWD to upper and lower beams, at a similar cost to that for gusset plates. Note that these construction-cost estimates are approximate, and factors such as design and permit fees, abatement of hazardous materials (asbestos, etc.), moving or protection of equipment and furnishings, modernization of telecommunications, internet and other services and finishes, and surging of building occupants, were not accounted for in these estimates.

Table 6.8 compares the cost of implementing the various retrofit schemes and the cost of repairs in the event of a BSE-2E level earthquake as predicted using PACT. Repair costs are presented in the format of median losses and 90-percentile losses. The Level-1 retrofit costed about $86M to implement and was expected to result in a median repair cost of $475 M, which corresponded to building demolition and replacement. Supplementing the Level-1 retrofit using FVDs increased the total retrofit costed by an additional $24.8 M, but significantly reduced the median and 90th percentile repair costs to $23 M and $34 M, respectively. The cost of the BRB

retrofit scheme was \$14.9 M less than that of the FVD scheme, but median repair costs were \$17 M greater. However, the response of the building retrofitted with BRBs was characterized by large dispersions and by large peak (and thereby residual) drifts in the lower part of the building. Consequently, the 90th percentile repair cost for the BRB retrofit corresponded to full replacement of the building. Since the lateral drifts predicted for the VWDs were also high near the bottom of the building and the VWDs exhibited problematic behavior as discussed later, its median repair costs corresponded to full replacement of the building as well even though the retrofit cost was in between that of the FVD scheme and the BRB scheme.

Table 6.6   Estimate of unit cost for a FVD

Fd (kip)	Stroke (in)	Cost (\$1,000)
300	± 5	10
500	± 5	15
800	± 5	25
1000	± 5	30
1200	± 5	45
1500	± 5	60

Table 6.7   Cost of different retrofit measures

Items	Cost (\$M)
Remove existing cladding	25
Install new curtain wall system	45
Fix column splices	16
Initial cost of FVDs	4.7
Initial cost of VWDs	7.5
Initial cost of BRBs	1.7
Gusset plates for FVDs/BRBs	8.2
Diagonal braces to drive FVDs	11.9
Spacers to connect VWDs to beams	9.0

Table 6.8   Comparison of cost-benefit

Scheme	Investment (\$M)	Median repair loss after a BSE-2E event (\$M)	90% repair cost after a BSE-2E event (\$M)
Level-1	86	475	475
Level-2: FVDs	110.8	23	34
Level-2: VWDs	102.5	475	475
Level-2: BRBs	95.9	40	475

6.5   SCENARIO-BASED DAMAGE AND LOSS ESTIMATES

The retrofit scheme using FVDs was identified as the most promising solution and was selected for more in-depth analysis of damage and loss. Three cases were evaluated: the as-built condition, the building after Level-1 retrofit, and the building after complete Level-2 FVDs retrofit. Structural analysis results were presented in Chapters 3-4, evaluated under BSE-1E and BSE-2E hazard events, with each hazard level containing 20 analyses. In the as-built case, 9 out of 20 analyses at BSE-1E and 13 out of 20 analyses at BSE-2E hazard encountered numerical instability; these analyses results were disregarded in the structural analysis as well as in damage and loss estimates presented in this chapter. As such, the results were likely conservative, and provided lower bonds to the estimated loss.

The probabilities of the irreparability and unsafe placarding of the building under different conditions are presented in Table 6.9, the primary contributors included. The building in its as-built condition had a 60% to 70% probability of being torn down or being red-tagged under BSE-1E hazard events. Moreover, when the hazard was increased to the BSE-2E level, replacing the building became a near certainty. After the Level-1 retrofit, a large improvement was observed under a BSE-1E event that brought down the probabilities to be around 30% to 40%. This proved to be insufficient under BSE-2E events, whereby the probabilities ranged between 87% and 91% for re-construction and the possibility of being red-tagged, respectively. With complete two-level retrofits, however, the safety level of the building was enhanced significantly under both BSE-1E and BSE-2E hazard events. Excessive residual drift was the major contributor to the unsafe factors of the building, particularly for those cases exhibiting a large probability of being tagged. The large transient drifts in the as-built or Level-1 retrofit cases have fractured some of the pre-Northridge welded beam-to-column connections and caused damage to stairways.

Table 6.9   Probability of irreparability and unsafe tagging

	Case	Prob. of irreparbility	Prob. of unsafe tagging (primary contributors)
BSE-1E	As-built	63.8%	71.7% (Residual drift, welded column splices)
	Level-1 retrofit	38.6%	44.2% (Residual drift, prefabricated steel stairs)
	Level-2 retrofit with FVDs	3.1%	6.8% (Pre-Northridge beam-to-column connections)
BSE-2E	As-built	100%	100% (Residual drift)
	Level-1 retrofit	86.6%	91.1% (Residual drift, prefabricated steel stairs, pre-Northridge beam-to-column connections)
	Level-2 retrofit with FVDs	30.2%	50.3% (Residual drift, pre-Northridge beam-to-column connections, prefabricated steel stairs)

6.5.1 Repair Cost

Repair costs were estimated for the three cases listed above under both BSE-1E and BSE-2E events, and expressed in the form of loss ratio (Figure 6.7). The as-built condition had a high probability of needing full replacement under both BSE-1E and BSE-2E events. Note that under BSE-2E hazard, the probability of the as-built case having a loss ratio of 1.0; as such, the probability curve is represented by a single point at a value of. To better inform the comparison, the median loss ratios were extracted and are presented in Figure 6.8. The as-built case hit a loss ratio of 1.0 at both BSE-1E and BSE-2E hazard events. Level-1 retrofits improved the building performance under a BSE-1E event, but were inadequate when the hazard was increased to BSE-2E. The histogram in Figure 6.8 clearly shows that Level-2 retrofit with FVDs was very effective in reducing the median loss ratio to 0.02 and 0.05 under BSE-1E and BSE-2E events, respectively. According to FEMA P-58 [FEMA 2012a], a 40% loss ratio is typically selected by the building owners as the threshold for replacing a building, as indicated by the red dashed line in Figure 6.8. Only by adopting a complete two-level retrofit could the loss ratio drop below this line, even in the event of a large earthquake.

Based on results of the PACT analysis, the median loss ratios could be disaggregated into contributions from structural and non-structural components (Figure 6.9). As noted, most repair costs are due to non-structural elements. The complete Level-2 retrofit with FVDs had zero contributions from structural elements, indicating only minor damage was observed and no repair work was required. The cases requiring complete reconstruction were predicted to have an 18% contribution from structural elements and the remainder from non-structural components or contents, based on studies on new office buildings [Taghavi and Miranda 2003].

(a) BSE-1E   (b) BSE-2E
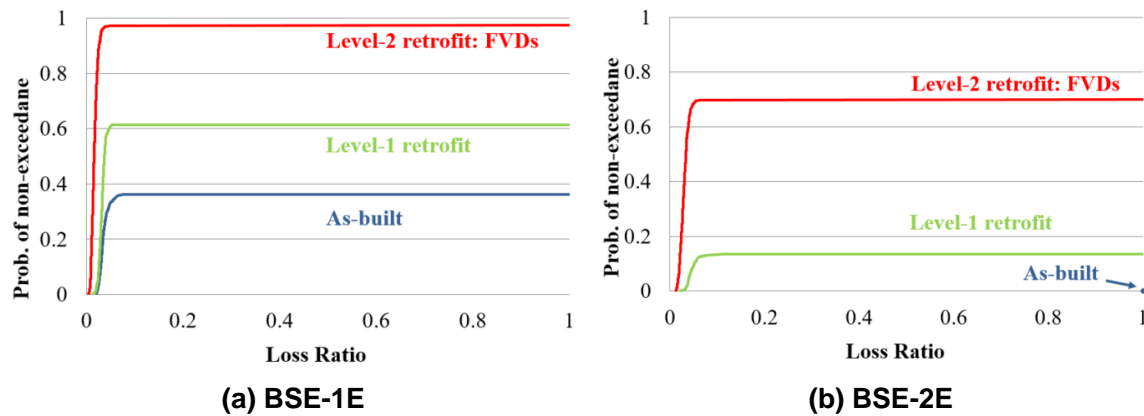
Figure 6.7   Cumulative distributions of loss ratios
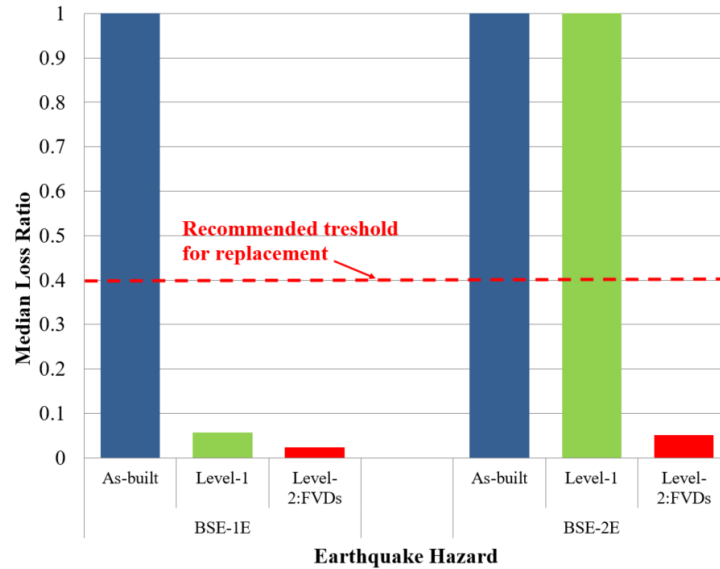
Figure 6.8   Median loss ratios

(a) BSE-1E   **(b) BSE-2E**
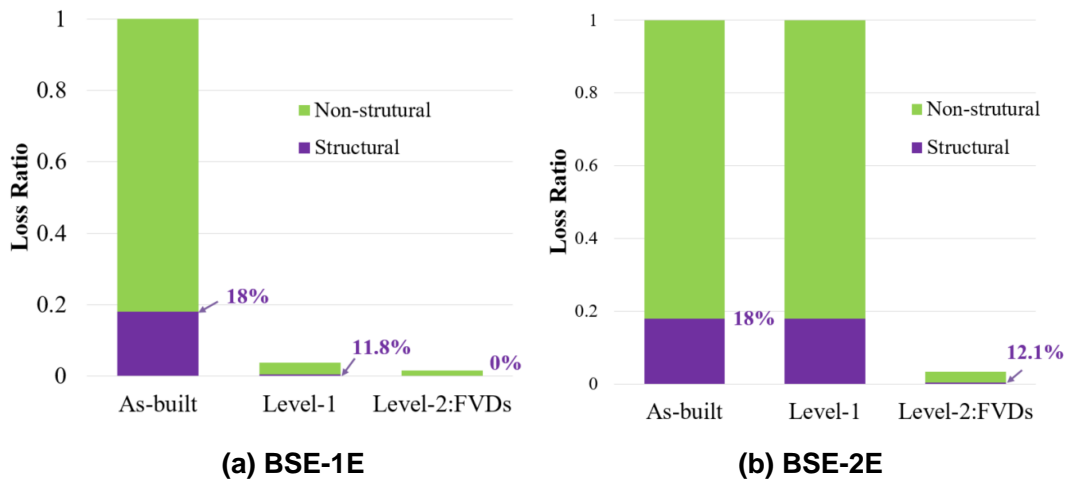
Figure 6.9   Disaggregation of median loss ratios

6.5.2 Business Downtime

The business downtime was estimated based on the procedures outlined in Section 6.3.2. Figure 6.10 shows the median business downtime for three different cases under BSE-1E and BSE-2E hazard events. Under a BSE-1E event, the as-built case had more than a 50% chance to trigger a full replacement; thus, the median business downtime defaulted to 5 years, which represented the duration necessary to construct a new similar building. The Level-1 retrofit reduced the median downtime by about 92%, to 22 weeks under a BSE-1E event; but its median downtime was as high as the as-built case under a BSE-2E event. Further augmenting the building by adding FVDs (Level-2 retrofit) contributed to a significant reduction in business downtime and essentially eliminated business interruption under a BSE-1E event.

Likewise, the median business downtime of each case is disaggregated to help understand the contributions from repair time and mobilization time; see Figure 6.11. If replacement is required (e.g., the as-built case), a duration to reconstruct a new similar building is used as total business interruption. On the other hand, if a building is within the repairable range, the downtime is triggered from both mobilization factors and the time to conduct repairs. After the Level-1 retrofit, the building had a median downtime of 22 weeks under a BSE-1E event, where 85% time was due to mobilization activities and only 15% was due to repairs. A similar finding was found for the building undergoing a two-level retrofit plan under a BSE-2E event. For a BSE-1E hazard event, the building after Level-2 retrofit had limited damage and no business interruption was likely.
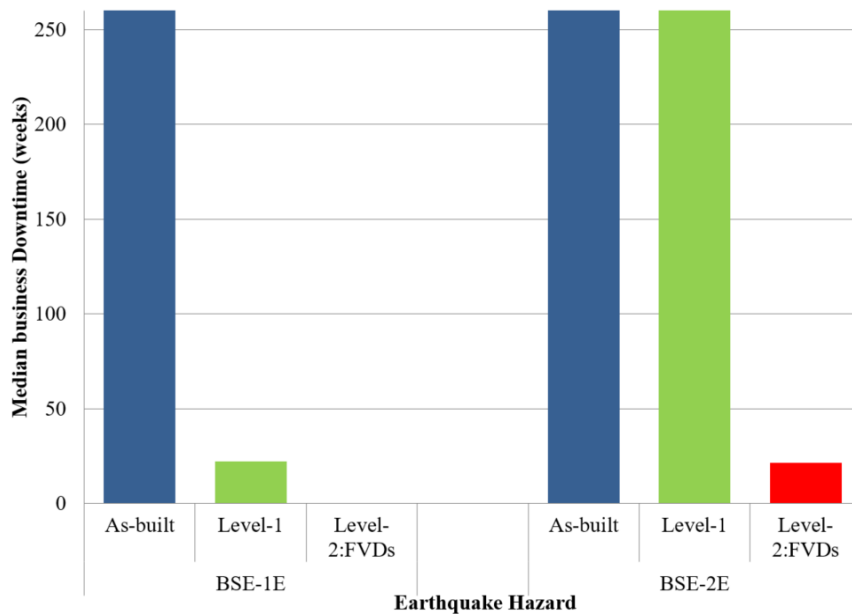
Figure 6.10   Median business downtime
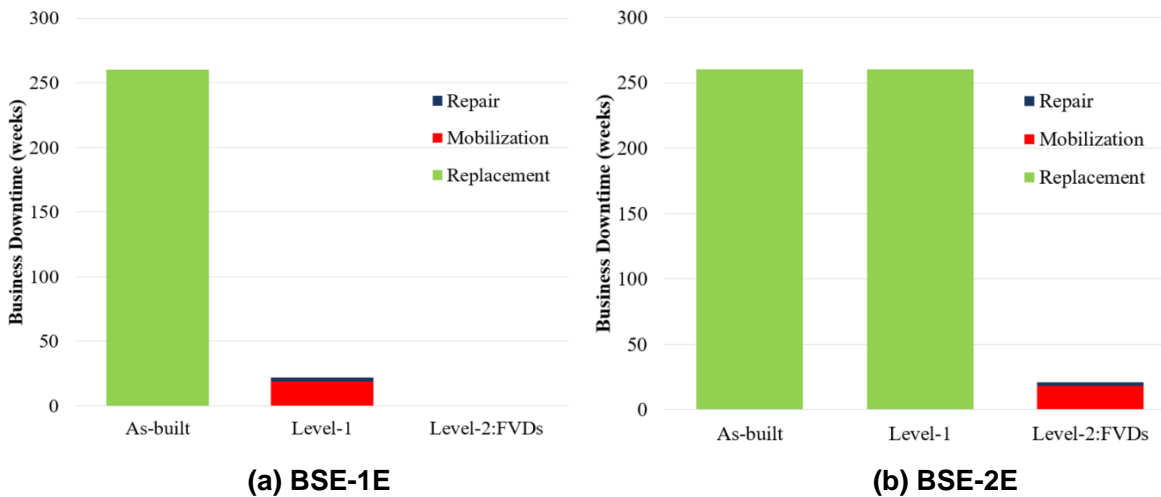
(a) BSE-1E   **(b) BSE-2E**

Figure 6.11   Disaggregation of median downtime

140

6.5.3 Total Financial Loss

The total financial loss combines the loss due to business interruption and repairs. The probability of non-exceedance of financial loss is shown in Figure 6.12 under BSE-1E and BSE-2E hazard levels. The median values were disaggregated into dollar loss from business interruption or repair work, as illustrated in Figure 6.13. For a building considered irreparable, the total loss is a combination of the cost to reconstruct a new similar building (replacement cost) and the business interruption loss. Under a BSE-1E hazard event, the benefits of implementing retrofit strategies were clear: with Level-1 retrofits, the median financial loss was dramatically reduced from $740 M to less than $40 M; after completing the two-level retrofits, the building performance was so improved that there was no interruption of business, and only $7 M was predicated due to minor repair work. When the earthquake intensity increased to the BSE-2E hazard, limiting the total financial loss at a smaller value of $40 M was only possible with the complete two-level retrofit, which represented a more than 90% reduction compared to the as-built or Level-1 retrofit cases.

(a) BSE-1E   (b) BSE-2E
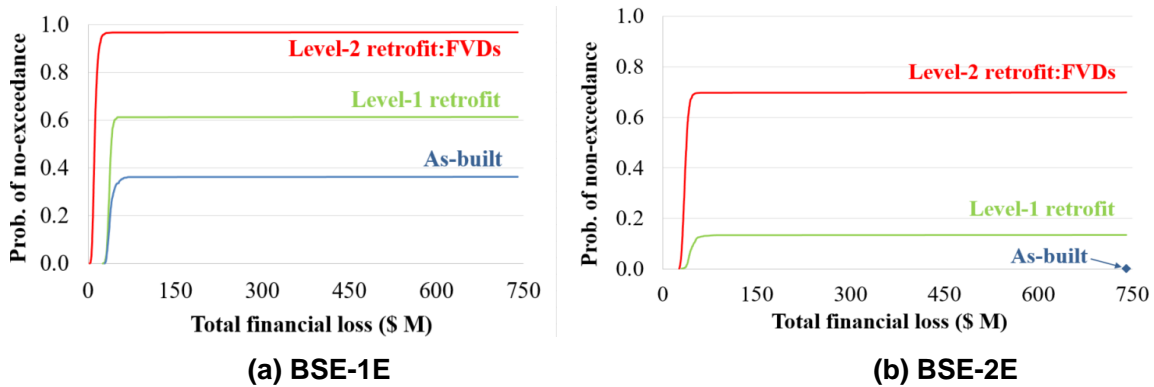
Figure 6.12   Cumulative distribution of total financial loss

(a) BSE-1E   (b) BSE-2E
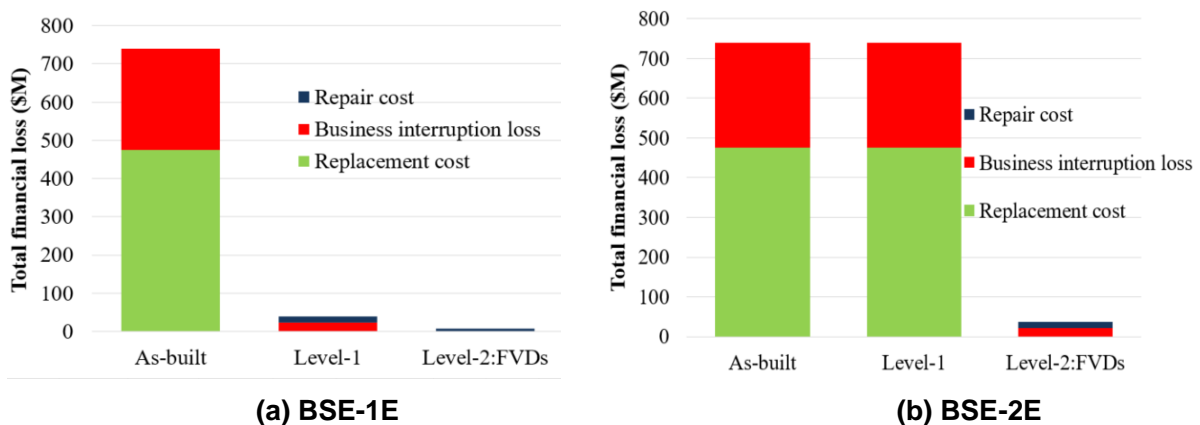
Figure 6.13   Median financial losses and disaggregation

6.6   CONCLUDING REMARKS

This chapter reported on the results of a damage and loss analysis conducted in the PBEE framework, following the structural analysis presented in Chapters 3 to 5. A PACT analysis was utilized for the probabilistic assessment procedure, using the default fragility and consequence curves for structural and non-structural components. The PACT analysis provided the repair costs and repair time of all building components under each hazard intensity. Based on those results, the business downtime and financial loss was further estimated using a simplified downtime model and a business model.

As a first trial, a preliminary damage and loss analysis was conducted for three retrofits at Level-2, i.e., using FVDs, VWDs or BRBs on top of Level-1 retrofits. Results from three NRHA were used in this preliminary examination, and the repair costs were compared between these retrofit methods. The results demonstrated that the FVDs scheme had the smallest chance of triggering unsafe factors and the smallest repair loss ratio among investigated schemes. It had more than 90% confidence of reducing the repair loss ratio to be as little as 0.08, which was significantly better than the Level-1 retrofit case or other Level-2 retrofit cases. Moreover, the disaggregation of the median repair loss indicated that the retrofit using FVDs corresponded to the smallest contribution from structural component repair. Therefore, the Level-2 retrofit with FVDs scheme was considered as the most promising solution of those considered herein to improve the structural response of the case-study building, and achieve the target retrofit intent. Refinements of the schemes or alternative schemes considered, the resulted loss predictions might be different.

The second part of the study focused on evaluating the cost-effectiveness of different levels of retrofit, including the building in its as-built condition, with Level-1 retrofit alone, and after complete two-level retrofit using FVDs. Two hazard levels: BSE-1E and BSE-2E were included in the scenario-based assessment. Each hazard used twenty structural analysis results obtained from NRHA, but excluded any analysis that exhibited numerical instability in the numerical model representing the as-built condition. Repair costs, business downtime, and total financial losses were assessed under each hazard level. The results indicated that the as-built building had a more than 60% chance of requiring reconstruction under a BSE-1E event; this was a certainty under a BSE-2E event. The Level-1 retrofit improved the building's seismic behavior under a BSE-1E event and contributed to more than a 90% reduction in total business downtime and financial loss. Under the BSE-2E hazard, however, additional retrofit methods were deemed necessary to meet the limited safety performance goal under a BSE-2E event. The seismic response of the case-study building after the Level-2 retrofit by using FVDs improved significantly, and the economic loss was reduced by more than 90% under both BSE hazard events.

.

7 Overview of Automated Optimization Procedure

7.1 INTRODUCTION

Chapters 7 to 9 constitute the second part of this dissertation, and focus on optimal design of fluid viscous dampers (FVDs) in selected tall buildings. In this chapter, a literature review on relevant studies on optimally design supplemental energy-dissipation devices in a building is provided in Section 7.2. The algorithm and gradients of the optimization procedure used in this study are reviewed, as well as proper selections of three basic ingredients: the design variables, objective functions and constraint functions. The work flow of the proposed automated design procedure is discussed in Section 7.3; the optimization solver and high-performance computers resources are introduced. A built-in function in Matlab (Version R2016a) [Mathworks 2016a] considered appropriate for this study is selected to link the optimization engine and the structural analysis program OpenSees. A series of nonlinear response history analysis (NRHA) is conducted each time the objective function and constraint functions are evaluated.

7.2 LITERATURE REVIEW OF OPTIMAL DESIGN OF DAMPERS IN A BUILDING

The introduction of passive energy-dissipation devices in seismic design prompted the rapid development of code-oriented procedures to design supplemental energy-dissipation systems. Considerable research in the 1990s have resulted in at least five such procedures [Ramirez *et al.* 2001]. These design provisions provide methods to select effective damping ratios needed to achieve the basic performance goals, but do not prescribe specific methods to optimally and efficiently find locations and tune parameters of dampers. However, these and other design considerations have significant impact on structural behaviour and the cost of supplemental devices [Soong and Dargush 1997]. As such, much research has been undertaken to help identify optimal damper design strategies.

7.2.1 Algorithm

Several pioneering works were conducted in the 1980s and early 1990s to identify locations and sizes of passive energy-dissipation devices in a building. Constantinou and Tadjbakhsh [1983] proposed a first-story damping system for multi-story shear buildings, and derived the optimum

damping coefficient by evaluating the maximum displacement under stationary white-noise excitations. Although the first-story damping was effective for short buildings, later work by Hahn and Sathiavageeswaran [1992] found that for a 10-story shear building with uniform story stiffness, dampers needed to be added to the lower half floors for maximum response reduction after several parametric studies. De Silva [1981] used a gradient-based algorithm that sought a set of preassigned values for modal damping and natural frequencies to optimally design passive vibrational controllers for flexible systems. Ashour and Hanson [1987] suggested locating dampers where the first mode damping ratio would be maximized. Masri *et al.* [1981] used a simple yet efficient optimal active control method for pulse control of flexible structures subjected to arbitrary deterministic or stochastic excitations. Although it was intended for active control technology, the result was informative to the development in passive optimal control theory. Gürgöze and Müller [1992] proposed an energy criterion to find the optimal positioning of one viscous damper in a linear, multi-degree-of-freedom (MDOF)system using an analytical procedure. Milman and Chu [1994] used a simulated annealing strategy to determine the optimum placement of devices and a sequential quadratic programming method to tune the parameters of these devices. Similar studies were conducted when designing optimal isolation systems. For example, Inaudi and Kelly [1993] studied the optimal damping needed in a base-isolation system to minimize the acceleration response subjected to stationary random vibrations.

These pioneering works have provided insight into selection of the optimal design parameters of special devices when designing a building. Nevertheless, most of these works were confined to simple and regular linear structures, as constrained by the hardware and software capabilities at that period of time. Later, more rigorous optimization approaches have been proposed using more systematic methods or algorithms. From the author's point of view, these methods fall in to five categories:

(1) *Sequential search algorithm (SSA).* This algorithm is perhaps the most direct approach among all the different algorithms. Zhang and Soong [1992] developed this method based on the concept of controllability index, which was able to determine one optimal location corresponding to the maximum story drift at each time and repeated until all pre-sized dampers were placed. More investigations based on this method were conducted and verified: Shukla and Datta [1999] verified *SSA* for a shear frame model; and Wu *et al.* [1997] applied *SSA* to a three-dimensional structure where translation-torsion coupling effects were a major concern. An improvement of *SSA* was developed by Lopez-Garcia [2001] a few years later, which was termed as the simplified sequential search algorithm (*SSSA*). With a simplification to compute the optimal location indices, *SSSA* essentially achieved all the advantages of the conventional *SSA* but was even less complicated, making it quite appealing to practicing engineers. *SSSA* was proven to be efficient using a few steps to optimally design dampers for regular buildings having different heights, natural periods and level of damping, etc. [Lopez-Garcia and Soong 2002]. Lopez-Garcia [2001] also demonstrated that for linear structures having linear viscous dampers, *SSSA* is as efficient as more complex methods such as the gradient-based method [Takewaki 1997] and optimal control algorithm [Gluck *et al.* 1996] to control story drift ratios. Nevertheless, the algorithm was formulated within the framework of linear matrix inequalities; thus, its applicability is limited. In addition, the results are sensitive to the characteristics of the selected ground motions, especially if the damping ratio in the system is low [Lopez-Garcia and Soong 2002], and it lacks a specific performance indicator [Whittle *et al.* 2012]. Another criticism is

144

that this method is not efficient in reducing floor accelerations, especially for non-uniform stiffness buildings [Singh and Moreschi 2002].

(2) *Fully stressed analysis/redesign procedure*: the previous work by Lavan and Levy [2005] on optimal design of viscous dampers on nonlinear structures provided insight into optimal damper distribution that led to subsequent development of the fully stressed design method [Levy and Lavan 2006]. With a basis on the principle of fully stressed design of truss member, this algorithm is relative simple to implement and uses a recurrence relationship to "fully-stress" the influence of dampers on the performance index. The optimal locations of dampers would be selected based on whether or not a performance index reaches an allowable value. They verified this method by comparing it with the gradient-based method and applying it to both a two-dimensional shear frame [Levy and Lavan 2004] and a three-dimensional irregular building [Lavan and Levy 2005]. A comparison to the active control approaches in Levy and Lavan [2009] indicated that the fully stress analysis/redesign procedure was more effective in reducing the story drift ratios based on multiple structures. This method is easy to implement from scratch and is considered as the most efficient method among three optimization algorithms investigated to reduce the story drift ratios [Whittle *et al.* 2002]. Despite its straightforward procedure, the method has not been rigorously proven to be the optimal design for viscous dampers [Levy and Lavan 2006]; these investigations are limited in that story drift ratios were the sole performance objective evaluated.

(3) *Gradient-based approach*: Takewaki [1997 and 2000b] used a gradient-based algorithm for the optimal design of viscous damping in order to minimize the sum of the amplitudes of transfer function for story drift ratios evaluated at undamped fundamental frequency of a structure. Since the damper placement was based on dynamic behaviour of the structures, it could be independent from ground motions, nonlinearity of structures, and damping systems. To avoid potential negative damping, Takewaki and Yoshitomi [1999] augmented this method with a new algorithm via parameter switch method. Takewaki [2009] continued developing this method by extending it to more complex structures using multiple objective functions. Singh and Moreschi [2001] utilized this algorithm to find the minimum viscous and viscoelastic damping required for the desired structural response reduction with a non-classical damped response spectrum approach. To efficiently use gradient-based optimal analysis incorporated with Maxwell dampers, Singh *et al.* [2003] developed a symmetric, self-adjoining system of equations that eliminated the need to work with two sets of eigenvectors and corresponding derivatives. Lavan and Levy [2004] proposed procedures to reduce computational effort by using the gradient-based algorithm: the optimization problem was solved for one "active" ground motion record first and continued with additional ground motions one by one until the optimum was reached. Note that all these works were confined to regular linear structures with linear dampers. Later work by Lavan and Levy [2005] extended the procedure to the irregular shear frames with the presence of yielding and used an energy-based global damage index. Lee *et al*. [2004] used the gradient-based algorithm to select the gradient of eigenvalues to optimally distribute damping and stiffness of viscoelastic dampers for target modal properties. They found that locations with large story drift ratios or flexible edges of asymmetric buildings had larger gradients of eigenvalues, requiring more damping.

As the name indicates, the nature of such an algorithm is to identify the gradients for the objective function and constraint functions. However, in most engineering problems, it is hard to devise closed-form expressions for such functions or to identify their gradients. This is especially true if velocity-dependent devices are incorporated that increase the discontinuities in gradient functions. A practical approach uses finite difference methods to approximate the gradients of the functions. Such a procedure requires evaluating the functions at each iteration point as well as adjacent points to estimate gradients, and the level of computation needed would be increased exponentially. This might not be a concern nowadays considering the wide applicability of high-performance computer resources. However, it should be noted that the objective function and constraint functions are likely non-convex, and no global optimum is guaranteed using this method.

(4) *Active control theory based algorithm*: Gluck *et al.* [1996] adapted the optimal linear control theory using a linear quadratic regulator (LQR) to design systems with passive devices, and proposed several options to determine the resultant added stiffness and damping matrices using Riccati's equation. Similarly, Agrawal and Yang [1999a and 1999b] presented two methods—the constrained static output LQR method, and the suboptimal LQR method—to determine the capacities and locations of passive dampers, respectively. They extended Gluck's work to consider more than one mode. Agrawal and Yang [1999b] found that two intelligent search algorithms, namely "*worst-out-best-in*" method and "*exhaustive single point substitution*" method, were quite effective in improving the optimal locations determined through *SSA*. Yang *et al.* [2002] used other two design methodologies based on active control, namely H_2 and H_∞ control strategies, to find both the optimal passive damper locations and capacities. Xu and Teng [2002] used an increment algorithm, based on the linear quadratic performance index for the optimal placement of active/passive control devices in a structure. These works were confined to linear structures with linear dampers. Later, Lavan *et al.* [2008] used a nonlinear active control procedure for seismic weakening and damping of inelastic structure with a two-phase design approach. Soltani and Hu [2014] extended the use of LQR algorithm to nonlinear viscous dampers and found that a variable damping system exhibited better performance than a linear damping system. This method is appealing due to its simplicity, with no requirement for nonlinear analysis and less sensitivity to the loading characteristics. However, some of the methods presented here utilized a single mode approach to transform the control forces to dampers forces, which makes their applicability constrained within the scope of relative short buildings. Finally, this analytical approach devises an objective function in an integral form, which prevents the concentration of added damping in a building, thus resulting in a design unable to reduce concentrated deformations [Levy and Lavan 2009].

(5) *Genetic algorithm*: Holland's research [1975] formed the basis for this algorithm, which has been applied to design linear dampers in linear structures. This research was expanded on by several researchers: Furuya *et al.* [1998] attempted to identify the best damper locations so that the optimal control effect would be achieved for a 40-story building with a constraint on the total cost; Singh and Moreschi [2002] used genetic algorithm to determine both the optimal number and distribution of dampers for seismic response control of a 10-story linear building; and Park *et al.* [2004] adopted this method to minimize the life-cycle cost of a viscoelastically damped system by considering the structure and dampers as an integrated system.

The main advantage of this type of algorithm is its wide applicability to different types of systems (linear or nonlinear), damper types (linear or nonlinear), and analysis methods (static or dynamic). For example, later work by Moreschi and Singh [2003] successfully applied this method to yielding structures for a suite of four synthetic earthquakes; Wongprasert and Syamns [2004] identified the locations to install dampers that most effectively minimize frequency-domain objective functions evaluated at the linear state of a seismic benchmark building; and Dargush and Sant [2005] considered alternative damper types to robustly design nonlinear structures under an uncertain seismic environment. This algorithm has been extended to more versatile problems, e.g., Lavan and Dargush [2009] investigated multi-objective framework that enabled the evaluation of the trade-offs between two important damage-measuring parameters and provided key information for the decision makers; Apostolakis and Dargush [2010] found optimal locations and sizes of different types of passive dampers to retrofit steel moment resisting frames using multi-level optimization. Other advantages of this algorithm include its reduced chance to converge to a local optimum, no requirements for calculating/estimating gradients of complex functions to guide the search, straightforward computer implementation, convenient use of probabilistic transition rules instead of deterministic transition rules, and use discrete design variables [Moreschi 2000]. Nevertheless, a major deficiency with this algorithm is that it requires a tremendous amount of computational effort, which is more than 10 times or more compared to other types of algorithms. If a building model is complicated and several sets of NRHA are needed to evaluate function values, the amount of time it takes to perform the analysis would prevent it from being widely applicable in practice. On the other hand, a global optimum point is not essential if local optimum results is sufficient for the optimization study.

In addition to the methods discussed above, alternatives such as these utilized the topological theory [Natke and Soong 1993], finite element perturbation [Cao *et al*. 1995], and capacity spectrum [Kim *et al*. 2003] were also investigated for optimization studies.

Generally, the above-mentioned work would be comparable to identify a solution if the objective function such as the maximum drift ratio is used [Whittle *et al*. 2012]. Thereby, the most important considerations when formulating the optimization design problem are simplicity, efficiency, and practicality.

Comparisons were made between different algorithms. For example, Whittle *et al*. [2012] compared three methods: Lopez-Garcia's *SSSA* [2001], Takewaki's *gradient-based approach* [1997] and Levy/Lavan's *fully stressed analysis/redesign method* [2006]. It was found that the Levy/Lavan's method achieved the best performance while being the least complex and requiring the least amount of computational effort. Cimellaro [2007a] modified three methods: Takewaki's *gradient-based approach* [2007], Gluck's [1996] *active control based theory* and Lopez-Garcia's *SSSA* [2001] to find optimal retrofit solutions by softening and adding viscous dampers to reduce absolute floor accelerations and story drift ratios, and found that the *active control based* method was relatively simpler, non-iterative and less computational demanding based on investigations of two short buildings. Levy and Lavan [2009] compared their own method (*fully stressed method* [2006]) with *active control tools* based on Gluck *et al*. [1996], and demonstrated that the latter could not truly optimize added damper schemes and led to unsatisfactory response reduction. Duerr and Tesfamariam [2012] compared the *genetic algorithm* and Zhang and Soong's *SSA* [1992], in terms of the resultant solution and the number

of required iterations. They found that although the *genetic algorithm* was equal or superior for several retrofit schemes, it required significantly more computational effort when the complexity of the problem increased.

Based on an evaluation of the feasibility and efficiency of different algorithms presented above, and the availability of software, this study selected a built-in optimization function in Matlab (Version R2016a) [Mathworks 2016a] that is based on an approximate gradient-based algorithm. More details are provided in Section 7.3.1.

7.2.2 Optimization Ingredients

The key step in the optimum design procedure is the formulation of the design problems in a minimax optimization format [Austin *et al*. 1987]. The basic ingredients include: a continuous or discrete objective function; a set of well-defined constraint functions; and a vector of multiple design variables. Selecting appropriate parameters of these ingredients is a major challenge in formulating the optimization problem.

Objective function

The most straight-forward objective function is to use an engineering demand parameter (EDP) directly. For instance, the maximum of the peak story drift ratios provides an important measure to quantify the performance of primary structural systems and a few non-structural components; the maximum of the peak floor accelerations affects many non-structural components and contents in a building and could contribute significantly to the economic loss after an earthquake [Tghavi and Miranda 2003]. Either of these EDPs could be used as an objective function. Moreover, alternative parameters such as an aggregated structural damage index would provide insight into the extent of damage when yielding occurs. However, there is usually a trade-off between different parameters, e.g., reducing drift usually is accompanied by increasing the acceleration, and vice versa. As such, a better way to consider multiple aspects of a design is to devise an objective function by integrating multiple EDPs through a weighted function.

Commonly used objective functions in previous studies include: peak displacement or peak drift ratio [Constantinou and Tadjbakhsh 1983; Wu *et al.* 1997], amplitude of transfer function of displacement [Takewaki 1997], base shear force [Aydin *et al.* 2007], or a combination of different responses [Cimellaro, 2007b]; other more complicated objective function include relative performance index [Apostolakis and Dargush, 2010], integral of a quadratic form of structural responses [Gluck *et al.* 1996], the H_∞ or H_2 norm of the transfer function [Milman and Chu 1994; Yang *et al*. 2002; Wongprasert and Syamns 2004], energy form [Gürgöze and Müller 1992], damping ratios for selected modes [Milman and Chu 1994; Agrawal and Yang 1999b], total stiffness [Tsuji and Nakamura 1996], life-cycle or initial cost [Park *et al*. 2004; Puthanpurayil *et al*. 2015], and a function combining repair cost and structural damage [Koduru and Haukaas, 2010]. Given that different objective functions can lead to quite different optimal designs [Wongprasert and Syamns 2004; Liu *et al*. 2004; Moreschi and Singh 2003 etc.], an alternative is to consider the multi-objective framework [Lavan and Dargush 2009]. The multi-objective framework provides a more robust way to select optimal designs where an improvement in any one objective can be realized by accepting a degraded performance in at

least one other objective. In the end, an entire family of solutions in the Pareto front design will be provided.

Given that the target of the optimum design focuses on improved structural performance, this study focused on two major EDPs as design objective functions. To assess the sensitivity of an objective function has on the optimal design results, two types of objective functions were investigated in this study: (1) a single EDP (the maximum of peak story drift or the maximum of peak floor acceleration); and (2) a function that relates two EDPs to the total building loss (decision variable, *viz.* DV). The objective functions are evaluated under a BSE-1E hazard event or a BSE-2E hazard event, respectively.

Constraint functions

The second ingredient of the optimization problem is a series of constraint functions, which may come in either equal or unequal formats. In most previous studies, a constraint is usually imposed on the sum of damping coefficients of the dampers, while minimizing the structural responses. A reverse method would be to impose constraints on the maximum story drift (linear system) or an energy-based global damage index (nonlinear systems) [Lavan and Levy 2004 and 2005], while minimizing the added damping. Other strategies impose constraints on the total expected loss [Furuya *et al*. 1998 and Puthanpurayil *et al*. 2015], a constraint that could be valuable in terms of the decision-making process in the event of a damaging earthquake.

In this study, constraint functions were selected to reflect performance in a quantitative manner. Several unequal constraint functions were investigated that intended to limit the average structural responses and to constrain the maximum damper response. Note that the formulation of constraint functions differed slightly when considering different objective functions and earthquake intensities.

Design variables

Lastly, several design variables were selected. The number of function evaluations depends on the number of design variables and constraints. The more design variables used and more constraints defined, the more trial points need be evaluated at each iteration. The total evaluated time is exponentially increased when a larger number of design variables and constraints is used for a non-convex problem [Nocedal and Wright 2006]. Considering the complexity of the numerical model and the efforts needed to obtain function values at each evaluated point, it is desirable for practical reasons to limit the total number of design variables.

The problem in this study focused on specific design considerations: identifying optimal locations for installing FVDs and their mechanical properties (e.g., damping constant C, damping exponent α). Properties of elements linked to the dampers, such as the stiffness of the driving braces K_b could serve as another set of design variables [Takewaki and Yoshitomi 1999; Singh *et al*. 2003; Park *et al.* 2004; Chen *et al.* 2011]. For newly constructed buildings, damper parameters could be optimized simultaneously with the elements of the main frame, e.g., the story stiffness. Research on simultaneous optimization of damping and frame stiffness have been conducted by Takewaki [1999 and 2000a], Park *et al.* [2004], Tsuji and Nakamura [1996] and Cimellaro [2007b]. Other design variables, such as the damper configuration in selected frames, are viable topics for optimization.

For the purposes of this study, which examines a single existing building, it is more practical to focus on the most critical parameters, thus limiting the number of design variables to a reasonable range. In this study, damping constant *C* — the parameter most relevant in sizing a damper and its story-wise distribution — were used as the design parameters. Dampers at several continuous floors were assigned with a same property (design value) for practical reasons. Other parameters of the dampers, including the damping exponent α, driving brace stiffness K_b, damper locations, and configurations used, were based on values obtained from sensitivity studies presented in Chapter 4. Dampers oriented in the two horizontal principal directions of the building were designed separately. As a result, the total number of design variables used in this study was 10 or less. In practice, the number of different dampers used in a project is usually limited, and thus this approach aligns with engineering practice. It is pointed that if the configuration of damper groups (design variables) changes, the optimization results might differ.

7.3   AUTOMATED DESIGN PROCEDURE

Matlab (Version R2016a) was used as the optimization platform. The flowchart of the automated design procedure and high-performance computer resources used are presented below.

7.3.1 Nonlinear Optimization Solver

Matlab contains a built-in optimization tool, with a variety of solvers that cater to problems with differing complexity (e.g., constrained or unconstrained, continuous, or discrete, linear or nonlinear, etc.). One solver—*fmincon* —was selected in this study; it is able to solve a constrained nonlinear optimization problem while accepting multiple design variables [Mathworks 2016b].

Considering the nonlinearity nature of this problem, it is very likely that the objective function and many constraint functions are non-convex. As such, identifying "global minimum" would be very difficult or impractical. The goal of this optimization is to find an optimal damper design scheme that achieves a target performance goal. Therefore, a local optimal point within a feasible region might be an acceptable engineering solution. Efforts to find a strict "global optimal" might provide little incremental improvement, require substantially more computation time, or be infeasible.

Different functions are provided in the Matlab optimization toolbox [Mathworks 2016b] to minimize or maximize objectives under constraints, including those for linear programming, quadratic programing, nonlinear optimization, and nonlinear least squares. Three functions are usually considered for constrained nonlinear problems: (1). "*fminbnd*"; (2). "*fmincon*"; and (3). "*fseminf*". Of these, "*fminbnd*" is only applicable to single-variable function problem, and "*fseminf*" is intended for semi-infinitely constrained multivariable nonlinear function. Only the "*fmincon*" is suitable for this problem: it is targeted at finding the minimum of constrained nonlinear multivariable function. The problem is formulated as follows:

$$\text{Minimize } f(x) \text{ , } x \in R^n \text{ , when subject to } \begin{cases} c(x) \le 0 \\ c_{eq}(x) = 0 \\ lb \le x \le ub \end{cases}$$

where $f(x): R^n -> R$ is the objective function; $c(x): R^n -> R^m$ and $c_{eq}(x): R^n -> R^p$ describe unequal and equal constraints, lb, $ub \in R^n$ are vectors designating the lower and upper bounds of variables $x \in R^n$; n is the number of design variables; m is the number of unequal constraints; and p is the number of equal constraints.

Based on this solver, a sequential quadratic programming (SQP) algorithm was used as the numerical method to solve the problem. The SQP algorithm is an iterative procedure that models the nonlinear optimization problem for a given iteration point $x_k, k = 1,...N$ by a Quadratic Programing (QP) subproblem [Nocedal and Wright 2006]. The subproblem should reflect the local properties of the nonlinear optimization problem with regard to the current iteration x_k, which is solved to obtain a new iterate x_{k+1}. Specifically, the objective function f and constraints: c, c_{eq} are replaced by the local approximations:

$$f(x) \approx f(x_k) + \nabla f(x_k)(x - x_k) + \frac{1}{2}(x - x_k)^T Hf(x_k)(x - x_k)$$

$$c_{eq}(x) \approx c_{eq}(x) + \nabla c_{eq}(x_k)^T (x - x_k)$$

$$c(x) \approx c(x) + \nabla c(x_k)^T (x - x_k)$$

Setting $d(x) = x - x_k, B_k = Hf(x_k)$, then the QP subproblem becomes:

$$\text{Minimize } f(x_k)^T d(x) + \frac{1}{2}d(x)^T B_k d(x) \text{ , } d(x) \in R^n$$

$$\text{subject to } \begin{cases} c_{eq}(x) + \nabla c_{eq}(x_k)^T (x - x_k) = 0 \\ c(x) + \nabla c(x_k)^T (x - x_k) \le 0 \end{cases}$$

The procedure iterates until the first order necessary optimality conditions and second order sufficient optimality conditions are satisfied, so that a local minimum x^* is resulted [Nocedal and Wright 2006].

A limitation of this method lies in its gradient-based nature, which requires that the objective and constraint functions are both continuous and usually have continuous first derivatives. The requirement of continuous first derivatives is difficult to satisfy in the problem presented herein. Therefore, in the studies presented in this dissertation, we assume that the functions and their gradients are all continuous in the range of concern, and the gradients are estimated based on the forward finite difference method.

7.3.2 Flowchart of an Automated Procedure

The flowchart of optimization procedure is illustrated in Figure 7.1. It starts once the initial conditions are identified, which includes the initial design variables $DV^{(1)}$ and their lower and upper bounds. Several optimal criteria that determine the termination of the procedure are defined, including: *TolX* (tolerance for change of two successive design variables)*, TolFun* (tolerance for change of two successive objective function) and *TolCon* (tolerance for change of two successive constraint functions), and *MaxIter* (maximum number of iterations) and *MaxFuncEval* (maximum number to evaluate function). The imposed values for these criteria are summarized in Table 7.1. To speed up the search in a wider range, and to avoid spurious estimated gradients if two points are too close, a finite difference step of *1e-1* is arbitrarily selected.

The objective function and constraint functions are evaluated at the design point $DV^{(1)}$ and then starts the iterative procedure. At each iteration, the functions are evaluated at several points in the vicinity of that iteration point so as to solve the QP subproblem and move in the direction of the negative gradient [Nocedal and Wright 2006]. These adjacent points are denoted as $DV_i^{(k)}$ (i=1,2,…,n_k), where k is the iteration sequence, and n_k is the number of function evaluations at k^{th} iteration. At each $DV_i^{(k)}$ (i=1,2,…,n_k), function values have been obtained from NRHA results using OpenSees. OpenSees is linked to Matlab and returns the values of objective or constraint functions of every evaluated point to the optimization engine in Matlab once the structural analysis is completed. The optimization engine will estimate the gradients of objective or constraint functions, and identifie next "best" design point: $DV^{(k+1)}$ for evaluation. The procedure will repeat until the difference of design variables or function values between $DV^{(k)}$ and $DV^{(k+1)}$ is smaller than the minimal value defined in the optimality criteria. Additionally, to limit the maximum computational efforts anticipated, the maximum number of iterations and the number of function evaluations are also pre-defined, and the procedure will be terminated if either of them reach the pre-defined threshold.

Table 7.1   Optimal criteria used in Matlab

Parameter	*TolCon*	*TolFun*	*TolX*	*MaxIter*	*MaxFunEval*
Values	1e-3	1e-3	1e-5	10	100
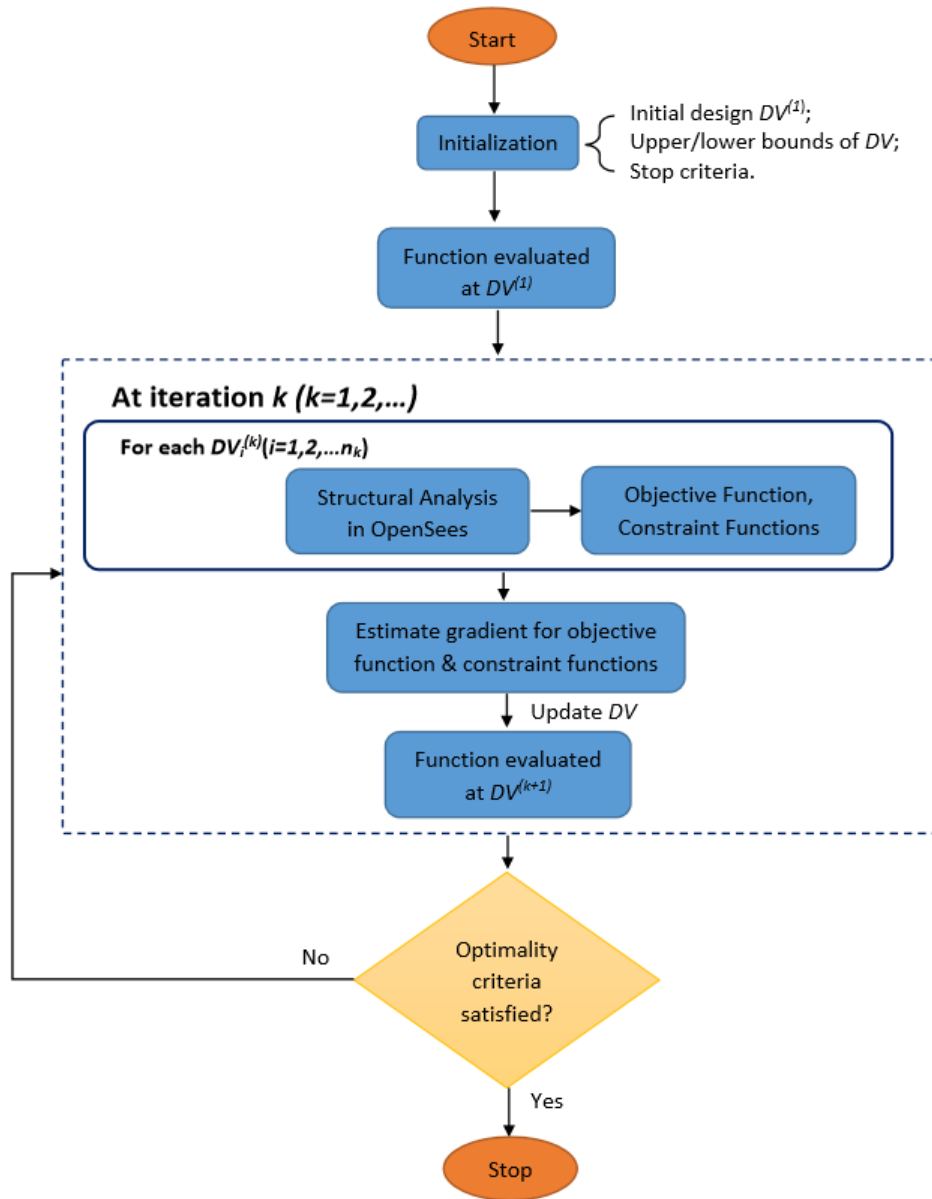
Figure 7.1   Flow chart of automated optimization procedure

7.3.3 Utilizing High-Performance Computers to Speed Optimization Workflow

As we can see from this flowchart (Figure 7.1), it takes several trials at each iteration point to solve the QP subproblem, and the number of trials depends on the number of design variables and constraints. Note that if the objective function or any constraint is non-convex, the problem may have multiple feasible regions and multiple locally optimal points within such regions. Consequently, the optimization process can take time exponential in the number of variables and constraints [Nocedal and Wright 2006]. In the meanwhile, at each trial point, a series of NRHA

are needed to obtain the function values. For example, if it takes 8 iterations to find a local minimum, and each iteration evaluates 10 trial points on average to solve the QP subproblem, then a total of $8 \times 10 = 80$ points are evaluated. Furthermore, each evaluated point requires N sets of NRHA, which gives a total of $80N$ evaluated points. Considering the computational time needed for one set of NRHA for a complicated model (e.g., 2 hours), the total computational time is in the order of $160N$ hours if runs are performed sequentially. Such a high demand in computational time was not possible in the past when computers and techniques were not as advanced as now. Nowadays, with the advent of High Performance Computers (HPC), and parallel processors, such a computation-demanding optimization problem has become feasible at much reduced time and cost.

This study used the Stampede System of Texas Advanced Computing Center (TACC), which is funded by National Science Foundation (NSF); it has a 6,400+ node cluster of Dell PowerEdge server nodes featuring Intel Xeon E5 Sandy Bridge host processors and the Intel Knights Corner (KNC) coprocessor [TACC 2017]. It was used in this study to conduct the optimization procedure. The software Matlab and OpenSees (parallel) were provided by the TACC. The remote computer was accessed through the Secure Shell (SSH), a cryptographic network protocol for operating network services securely over an unsecured network [Wikipedia 2017]. A batch script that contained all the commands necessary to run the program, i.e., the path to the executable, program parameters, number of nodes and tasks, and environmental variables, etc., were submitted to a queue and then managed by the scheduler [TACC 2017]. At each function evaluation, eleven ground motions were used under the hazard level of concern and run on multiple cores in a parallel fashion. The speed of the supercomputer and parallel processing function while conducting NRHA reduced the computational time tremendously. The optimization procedure presented in this study is limited since each trial point is evaluated sequentially. Investigations of optimization engines and algorithms that allow for multiple level of parallel work are worthy of future study.

7.4   CONCLUDING REMARKS

This chapter presented a comprehensive literature review that studied optimizing the design of buildings that incorporate supplemental energy-dissipation devices. The review covered the most crucial aspects in an optimization study, including the type of solving methods and three basic ingredients: design variables, an objective function, and sets of nonlinear constraints. Appropriate selection of the methods and ingredients in this engineering problem were proposed.

The flowchart of this automated procedure was presented in detail, which requires significant computational effort. The automated procedure relies on HPC and parallel processors to achieve its ultimate goal within a reasonable time frame and cost. The platform, software and HPC used to facilitate the automated design procedure were introduced.

8 Automated Damper Optimization in Retrofit of an Existing Tall Building

8.1 INTRODUCTION

This chapter investigates the feasibility of an automated design procedure to identify optimal damper schemes of the case-study existing building. The optimization procedure centers on framework of the Performance Based Earthquake Engineering (PBEE), and utilizes high-performance computers (HPC) and parallel processors to enable a great number of nonlinear response history analyses (NRHA). Two performance levels are considered: (1) collapse prevention for a BSE-2E hazard event and (2) damage control for a BSE-1E hazard event. For the first performance level, three cases are investigated using different objective functions, whereas the second performance level only examines one case that focuses on economic loss after an earthquake event. The efficiency of the automated design procedure is determined by comparing the response with a manual design strategy. At the end of this chapter, a procedure to design dampers in a tall building is suggested, and general design patterns for a moment frame are proposed.

8.2 AUTOMATED DESIGN PROCEDURE

8.2.1 Optimization Problem Design

Chapter 7 reviewed the objective function, constraint functions, and decision variables commonly used in similar optimization problems as in this study, and then selected components suitable for this problem. More details are presented below.

The goal of this optimization is to find an optimal damper arrangement pattern that minimizes the objective function values while conforming to all constraints. Eleven ground motions out of twenty entire ground motion set under either BSE-1E or BSE-2E hazard level (Section 3.1.3) were used in the analysis and return function values to the optimization solver. These eleven ground motions were selected to meet the requirements for the number of ground motions used in NRHA based on current ASCE 7 guidelines [2016] (equal or larger than seven) and to conform to the 16 core limits of each node in the super computer used in this study. These

eleven ground motions were selected so that their median structural responses were close to the median responses from the entire twenty analyses. The results used in the objective function were the median values of the eleven NRHA set.

Objective function

Two types of objective functions were used: (1) a single engineering demand parameter (EDP); and (2) a function that relates multiple EDPs to the financial loss (decision variable). For consideration of number 2, EDP-DV functions proposed by Ramires and Miranda [2009] were constructed. These functions could help facilitate the optimization procedure and avoid holistic loss and damage analysis at each evaluation point, whereas obtaining DV directly through EDPs obtained from structural analysis. The construction of such building-specific EDP-DV functions are outlined below.

EDP-DV functions are constructed through integration of the structural analysis, damage, and loss analysis steps of the PBEE framework (Figure 8.1). One method to formulate the EDP-DV function is to integrate the fragility curves and consequence functions of every component in a single story or an entire building. This method has been applied to construct story-based EDP-DV functions for a new building in Chapter 9.

This chapter proposes an alternative method by utilizing the results obtained in Chapter 6. Loss and damage prediction of the case-study building has resulted in a probabilistic evaluation of repair cost, business downtime, and total financial loss after an earthquake event. Such analysis was carried out for the as-built case as well as retrofitted case. A feasible way to reflect the relation between the total financial loss and EDPs is to construct a smooth curve that fits the scattered points using a regression function. This study assumed that the fitted regression function was log-normally distributed and used a least squared error method to fit the data. As a result, several EDP-DV functions were obtained; each of them increases monotonically, with the *Y*-axis representing the expected financial loss of this building after a BSE-1E or BSE-2E hazard event. Note that the collapse of the building was not considered in these functions, and that the estimated loss is more optimistic than realistic. This method basically is an express "backward" process that relies on already obtained results. In cases where loss and damage analysis has not been performed, this process might not be a preferred method.

Given the different seismic sensitivity of various components in a building, the EDP-DV functions are generated for three performance groups (PGs), including:

- PG$_1$: drift-sensitive structural components;
- PG$_2$: acceleration-sensitive structural components;
- PG$_3$: acceleration-sensitive non-structural components and contents.

The focus of the study is to optimally arrange FVDs in a high-rise steel building. The loss and damage analysis results of two retrofits schemes under a BSE-1E or a BSE-2E hazard event were used to design the EDP-DV functions. The total losses constituted from three contributing parts; each was represented by a specific EDP-DV curve; see Figure 8.2 and Figure 8.3. The *Y*-axis represents the normalized loss (i.e., a total building loss under a BSE-2E event divided by $740.5M—the total economic loss due to a new building construction and business downtime

interruption—and *X*-axis is either a maximum peak story drift or a maximum peak floor acceleration.

The fitted functions (solid lines) and the original data (scattered points) are included in Figure 8.2 and Figure 8.3. Under a BSE-1E hazard event, drift-sensitive structural components— PG_1 (blue) induce smaller damage and loss than the non-structural components, and PG_2 (red) when the peak drift is smaller than 2%—but this trend is reversed when the peak drift exceeds 2% [Figure 8.2 (a)]. Due to the probabilistic nature of the PBEE procedure, there is a large dispersion of PG_1 and PG_2 around a drift ratio of 2%. Consequently, the fitted curve for PG_1 has a sharp increase after 2% and tends to stabilize at 0.036 after the drift exceeds 3%. However, PG_2 doesn't exhibit a clear stabilization as the drift increases. Under a BSE-2E event, the data shifts to a larger drift ratio range. Similarly, PG_1 contributed smaller loss than PG_2 to the total loss when a drift is smaller than 3%, but the trend is reversed after this point. Unlike that under a BSE-1E event, the data has relatively smaller dispersion at the drift range of concern, and both PG_1 and PG_2 curves stabilize around 0.024 and 0.018 at a drift of 6% [Figure 8.3 (a)]. Note that the EDP-DV curves for PG_1 and PG_2 are valid for the peak drift ratio smaller than 6%. Should this threshold be exceeded, the residual drift would be too large to the repair the building based on recommendations from FEMA P-58 [2012a-c]. FEMA P-58 suggests that a 2% residual drift is likely to trigger full replacement of the building, and that value is equivalent to a 6% peak drift ratio based on a relation between peak drift ratio and residual drift ratio. Consequently, the normalized loss is set to 1.0 if the drift ratio exceeds 6%.

The acceleration-sensitive non-structural components and contents (PG_3) might induce larger building losses than other two groups based on the distribution of the scattered points [Figure 8.2 (b) and Figure 8.3 (b)]. The EDP-DV curve for PG_3, after data fitting, stabilizes at a normalized loss of 0.018 and 0.055 under a BSE-1E and BSE-2E event, respectively. However, the incremental change is smaller than both PG_1 and PG_2 based on the fitted curves.
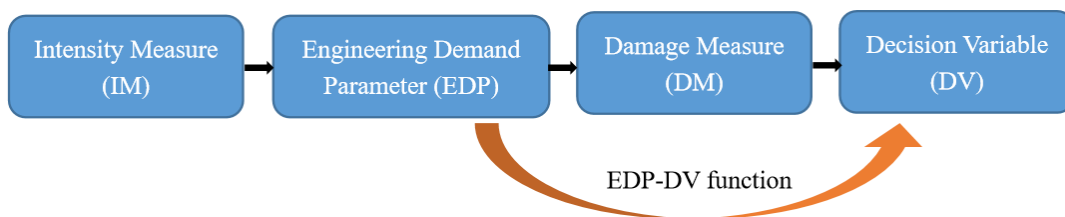
Figure 8.1   PBEE framework and EDP-DV functions
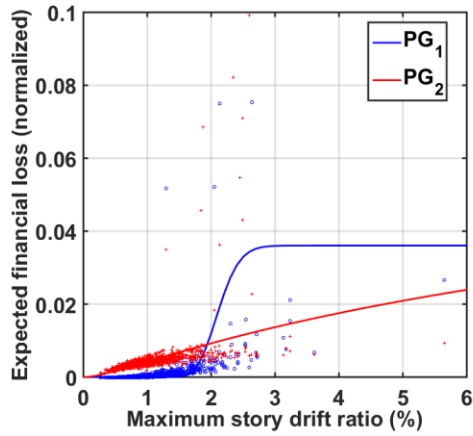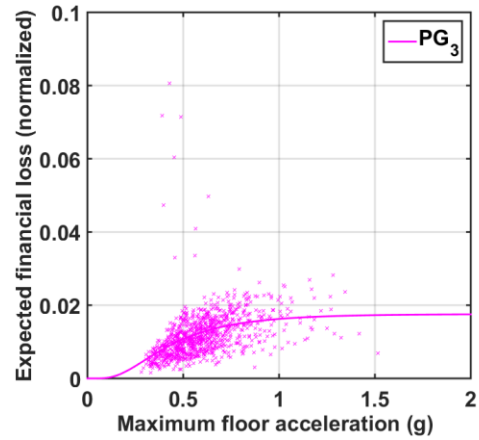
(a) Drift-sensitive PGs
(b) Accel-sensitive PGs

Figure 8.2   EDP-DV functions for different PGs under BSE-1E events
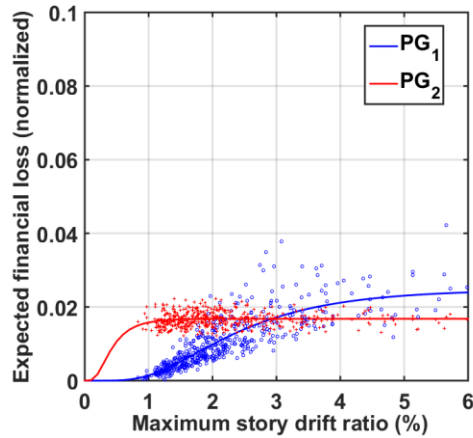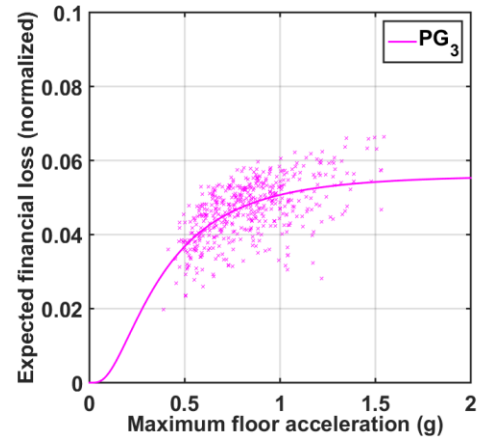
(a) Drift-sensitive PGs
(b) Accel-sensitive PGs

Figure 8.3   EDP-DV functions for different PGs under BSE-2E events

Constraint functions

In this study, the maximum structural responses were used as the objective function, and the average structural responses were used for constraints to complement the objective function. Meanwhile, the allowable peak force and stroke of a FVD were constrained based on the range of feasible designs presented in Chapter 4 and other practical considerations to limit the cost of the dampers. Consequently, four constraints were used but differed under a BSE-1E event or a BSE-2E event.

- Average peak inter-story drift ratio < 0.6% (BSE-1E) or 1.0% (BSE-2E);
- Average peak floor acceleration <0.25g (BSE-1E) or 0.3g (BSE-2E);
- Maximum damper force < 1000 kips (BSE-1E) or 1500 kips (BSE-2E);
- Maximum damper stroke < 2.0 in (BSE-1E) or 5.0 in (BSE-2E).

158

Design variables

The damping constant, the parameter most relevant to the size of a damper, and its distribution pattern over stories were used as the design parameters in this study. The results from structural analysis indicated that continuous floors usually have similar responses (e.g., peak story drift, and floor acceleration). As such, dampers at several continuous floors were assigned with the same property (design value), which also helped further reduce the number of design variables. Dampers at two horizontal directions were designed separately considering their different damping demands. Consequently, six design parameters were used in selecting damper locations; see Figure 8.4. The initial values and the range of design variables were selected based on a suggested range for the effective damping ratio that would efficiently alleviate or eliminate the weak stories in this building and were based on results from the sensitivity study conducted in Section 4.4.4; they are summarized in Table 8.1. Note that the optimal sizes of dampers might change if the damper zones are grouped differently.

The optimization began with the lower bound of design values. Note: stories 17 to 25 require smallest dampers, and their damping constant C_x and C_y (representing damping constant C for two directions) were used as the design variables directly. For the middle or bottom stories, however, the design variables determined the relative damper sizes with regard to these at stories 17 to 25 in consideration of their relations. The actual damper size with regard to the design variables are summarized in Table 8.2. During optimization, all design variables were scaled to a same magnitude to accelerate the procedure. Additionally, 16 smaller dampers were used in the top two stories to control the peak roof acceleration since these values would impact the objective function. These dampers added two additional design parameters: cx_0 and cy_0. Note; in engineering practice, limiting the number of types of dampers used is typical. The design variables and their ranges were kept consistent under a BSE-1E and a BSE-2E event.

Results are presented below, initially focusing on the BSE-2E hazard level, followed by results obtained for BSE-1E hazard level excitations and a discussion of the results obtained, and a suggestion for an ideal automated design process.
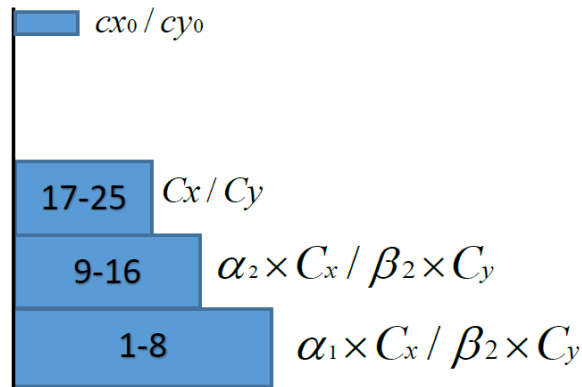
Figure 8.4   Design variables

Table 8.1   Initial value and range of design variables

159

Design variable	C_x kip·(sec/in.)$^{0.35}$	C_y kip·(sec/in.)$^{0.35}$	α_1	β_1	α_2	β_2	c_{x0}	c_{y0}
Initial value	1000	1500	1.4	1.4	1.0	1.0	200.0	200.0
Range	[1000, 3000]	[1500, 3000]	[1.4, 2.0]	[1.4, 2.0]	[1.0, 2.0]	[1.0, 2.0]	[200.0, 500.0]	[200.0, 500.0]

Table 8.2   Size of FVD in different groups

Story zone	1-8	9-16	17-25	34-35
Size	$C_x \times \alpha_1$ $C_y \times \beta_1$	$C_x \times \alpha_2$ $C_y \times \beta_2$	C_x C_y	c_{x0} c_{y0}

8.2.2 Case Studies Under BSE-2E Hazard Events

Case 1: Maximum of the peak story drift ratios as objective function

Peak story drift ratio provides an important damage measure and the maximum value was selected as the objective function for the first study case. The maximum responses of *X*- and *Y*-directions at each iteration were selected for results reported below. The changes of objective function values at iteration points (red dots) and trial points around each iteration point (blue lines) are shown in Figure 8.5. A significant improvement was observed from the first to the second iteration, with a reduction of the maximum of peak drift by more than 50%. Nevertheless, the improvement became quite limited afterwards, and the objective function value fluctuated between 1.05% to 1.08%. The optimization procedure was terminated at the fifth iteration when the difference of objective function values at subsequent iteration points became smaller than the tolerance.

To better understand how the design parameters were tuned during the optimization process, design variables at iterations 1, 2, and 5 are presented in Figure 8.6. The results shown in the following figures were based on the median results out of eleven NRHA. As a general trend, the sizes of FVDs needed to be increased to reduce the maximum story drift ratios. Moreover, a larger increase was seen in the *X*-direction considering a slightly larger peak drift and smaller initial values in this direction (see Figure 4.48). Correspondingly, the C_x were increased by a factor of 2–3 at iteration 2. In subsequent iterations, a small increase of C_y was more effective than an increase in C_x to achieve incremental improvements.

Consistent with the changes of objective functions, a significant improvement of the peak drift ratios from the first iteration to the second iteration was seen, bringing down the maximum drift from 2.6% to about 1.1% (Figure 8.7). Nevertheless, only slight improvements were obtained from second iteration to the final design point. Note that the mezzanine level had a

stiffness deficiency, and was not fully addressed in Level-1 retrofit. As such, the drift at that level became a bottleneck for continued improvement of drift profiles and the optimization procedure.

The peak floor accelerations (Figure 8.8) did not exhibit a significant change after several iterations. Other than an observable change of responses at the final design, the first and second design points were essentially the same. This is due to the fact that additional damping is more effective at controlling drifts compared to floor accelerations. In particular, if dampers are already large, the efficacy of additional damping is limited, whereas increased damper forces would continue to impact the story forces. The final design had a maximum value of $0.5g$ at the roof and an average value smaller than $0.3g$. The acceleration of base floor or the top floor was always the largest. However, note that dampers were only distributed across lower 25 stories in this case; the addition of dampers around roof might help reduce maximum floor accelerations. As such, in the case studies below, where floor accelerations were part of the objective function, two additional design variables were introduced (e.g., c_{x0} and c_{y0} in Table 8.1); they represent 16 small dampers at top two stories of the building as a means to control roof vibration and improve optimization efficiency.

In terms of damper responses, the peak damper forces were increased by more than 70% from the first iteration to the final design. The maximum value was increased from 920 kips to about 1450 kips at mezzanine level (Figure 8.9). The damper strokes were closely link to the peak story drift ratio distributions (Figure 8.10), but they were well below the 5-in limit, and thus not likely influence the size of the dampers.

Figure 8.5   Evolution of objective function values

Figure 8.6   Design variables at selected iteration points

Figure 8.7   Distribution of peak story drift ratios at selected iteration points (median of eleven analyses)
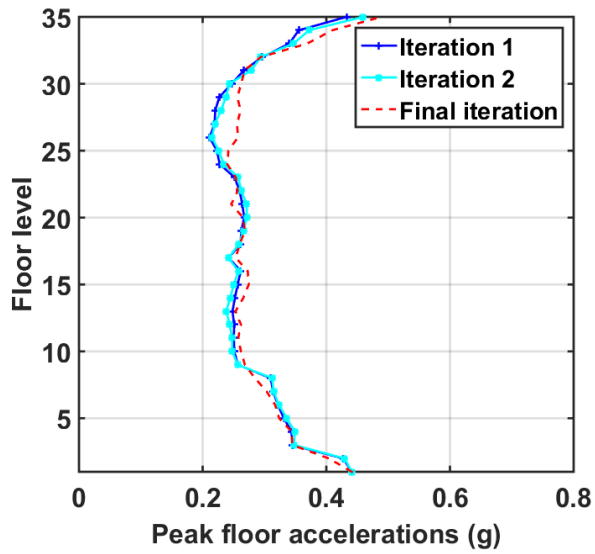
Figure 8.8   Distribution of peak floor acceleration at selected iteration points (median of eleven analyses)
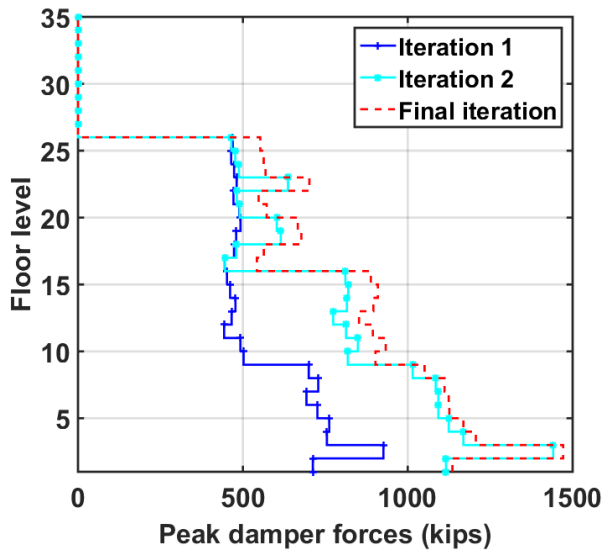
Figure 8.9   Distribution of peak damper forces at selected iteration points (median of eleven analyses)

163
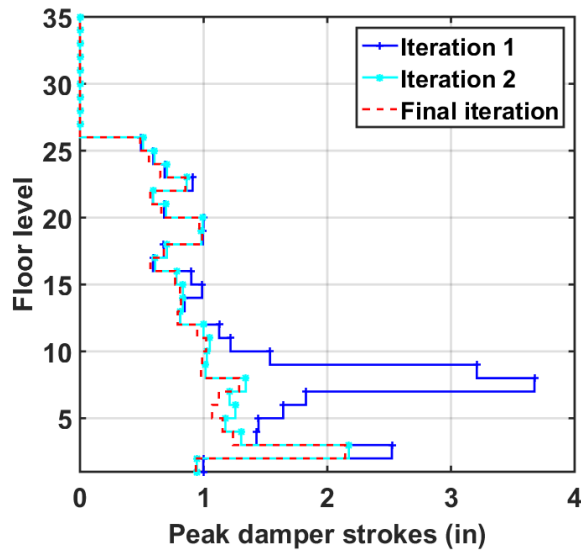
Figure 8.10   **Distribution of peak damper strokes at selected iteration points (median of eleven analyses)**

Case 2: Maximum of the peak floor accelerations as objective function

A wide range of building components are sensitive to floor accelerations, such as the mechanical, electronical and plumbing components (MEP), and thus the maximum of peak floor accelerations was selected as the objective function for the investigation in this case. Two modifications were made in this case from Case 1: (1) an additional 16 dampers were installed at story level 34 and 35 to control the roof vibrations, which generally dominated the objective function; and (2) the floor acceleration at base was a constant, and thus excluded in the objective function to avoid a constant being the objective function.

The evolvement of the objective function is presented in Figure 8.11. A gradual decrease was observed over successive iterations although overall changes were small. From the first to the second iteration, a 4% reduction was observed, i.e., the maximum acceleration was brought down from $0.433g$ to $0.416g$. and the changes afterwards were even smaller. The fifth iteration point was chosen for the final design, and all the constraint functions conformed to the pre-selected limits. Additionally, the changes of design variables at three selected iteration points showed a continuous increase in both directions (Figure 8.12). The changes were larger for C_x from iteration 1 to 2, but larger for C_y in subsequent designs after iteration 2.

In terms of the global structural responses, significant reductions of the peak story drift ratios were predicted when the designs were updated (Figure 8.13). The final design had a maximum drift of 1.0% at mezzanine level, which was equivalent to that in Case 1. Interestingly, the reduction in floor accelerations was insignificant even though maximum acceleration was the objective function (Figure 8.14). The inefficient control over floor acceleration might be attributed to a saturation effect of additional damping on reducing floor accelerations. Adding supplemental damping to a structure may help control floor accelerations when the original damping is small, but as the damping increases, continued increases in damper sizes would

164

increase the damper forces transferred to the main frame, thus compensating for the added damping effect. Moreover, it is likely the design variables need to be reduced to increase the objective function, but this case arbitrarily started with the lower bound, which inhibited the optimization to go in the opposite direction. Given that the weak-story trend is one of the most seismic vulnerabilities in the case-study building, cutting the damper sizes below the lower bounds is not suggested. However, it is worth investigating if it is possible to modify the initial values and the range of design variables. Note: although a few smaller dampers were installed at roof in order to control the large acceleration, it is not a guarantee that the overall floor accelerations could be reduced.

The distributions of peak damper forces are displayed in Figure 8.15. A significant increase of damper forces was seen when the design was updated from the first to the second iteration. A slight increase was possible from the second to fifth iteration, but it was very limited due to the proximity of the damper force at the mezzanine level to the 1500-kip limit. The peak damper stroke distributions (Figure 8.16) reflected the distributions of the peak story drift ratios, and followed the same trend of drift distributions at different iterations.
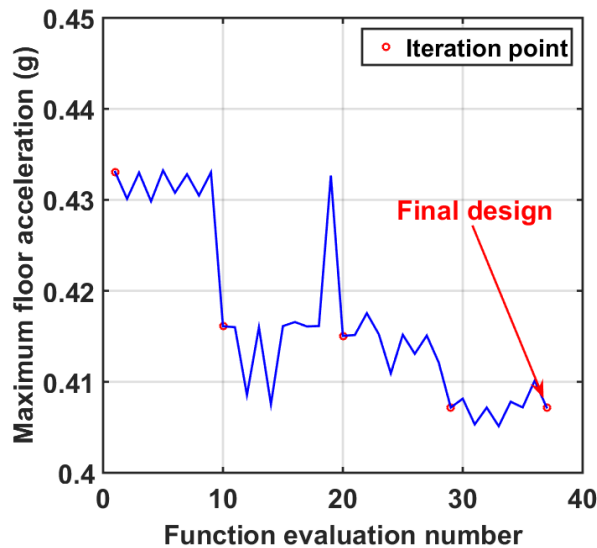
Figure 8.11   Evolution of objective function values
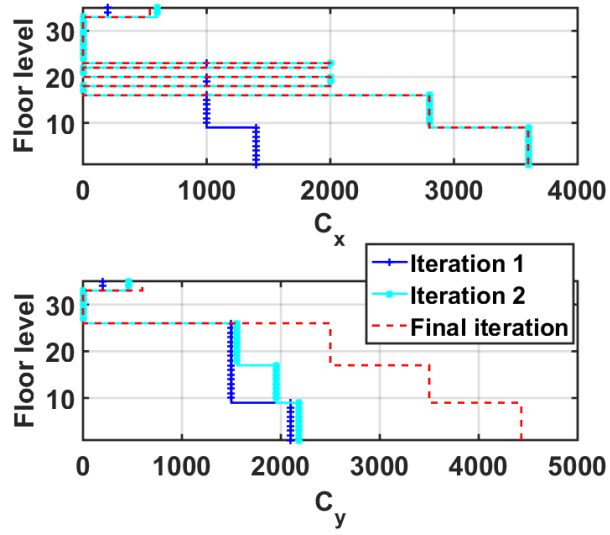
Figure 8.12   Design variables at selected iteration points
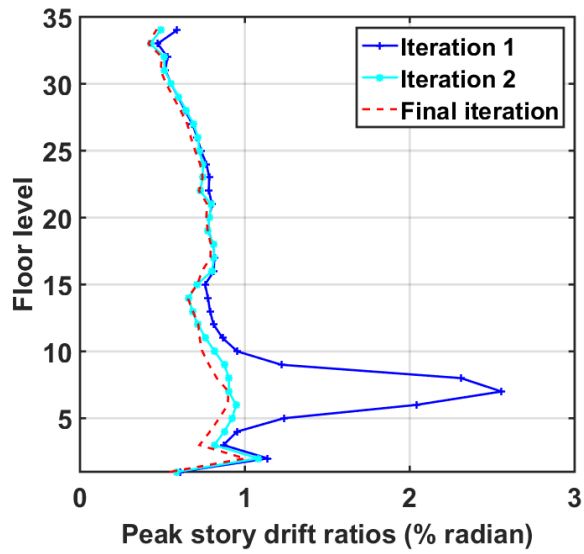
Figure 8.13   Distribution of peak story drift ratios at selected iteration points (median of eleven analyses)
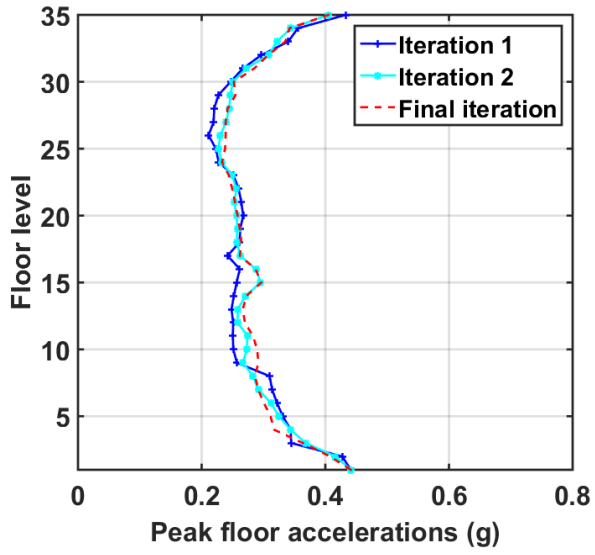
Figure 8.14   Distribution of peak floor accelerations at selected iteration points (median of eleven analyses)
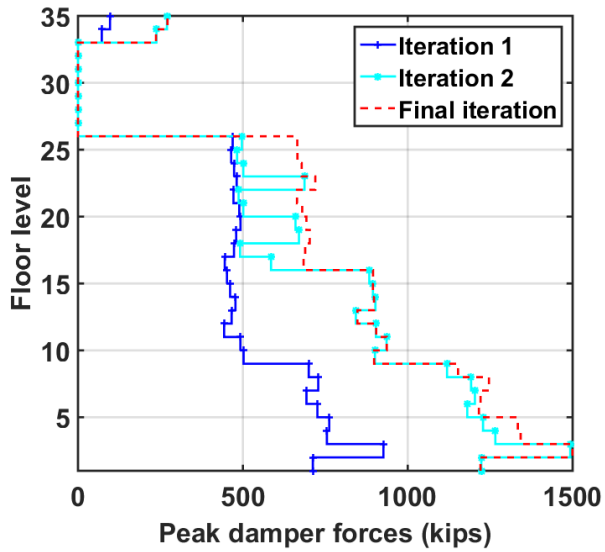
Figure 8.15   Distribution of peak damper forces at selected iteration points (median of eleven analyses)

167
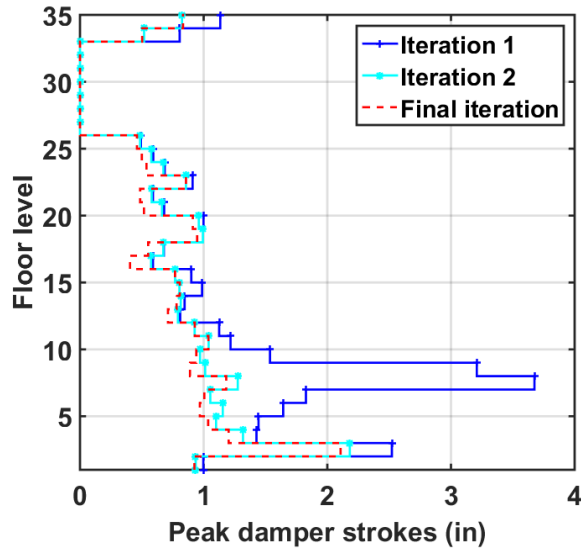
Figure 8.16   Distribution of peak damper strokes at selected iteration points (median of eleven analyses)

Case 3: EDP-DV functions as objective function

For this case, the summation of three EDP-DV functions under a BSE-2E hazard event was used as the objective function, i.e.:

$$f=f\,(\text{DV}|\text{EDP=story drift ratio, PG=PG}_1) + f\,(\text{DV}|\text{EDP=story drift ratio, PG=PG}_2) + f$$
$$(\text{DV}|\text{EDP=floor acceleration, PG=PG}_3) \tag{8.1}$$

Similar to Case 1 and Case 2, a significant change occurred from iteration 1 to 2, reducing the objective function value (the building loss after a BSE-2E hazard event, normalized by \$740.5 M, the total cost to construct a new similar building) from 0.0451 to 0.0196 (Figure 8.17). After this change, the reduction of objective function became very limited, with only 3% incremental changes from the second iteration to the final iteration. Design variables at iterations 1, 2, and 5 are illustrated in Figure 8.18. The damper sizes were increased more in *X*-direction when the design was updated from the first iteration to the second iteration, but larger increase was imposed on dampers at *Y*-direction for the remainder of iterations. Overall, increasing damper sizes in *X*-direction appears to be more effective than increasing the size of the damper in the *Y*-direction.

The changes of peak story drift ratio distributions are illustrated in Figure 8.19, where a large reduction of the responses was exhibited from the first iteration to the second iteration, bringing down a peak drift ratio from 2.6% to about 1.1%; only slight improvements were seen after the second iteration. Although a slight increase of peak floor accelerations at a few stories were observed from the first iteration to the final iteration (Figure 8.20), it was not significant enough to impact damage or loss.

Given the large reduction of peak story drift ratio from the first to the second iteration, a 50%-90% increase of peak damper forces was observed at floor 1 to floor 14, and a maximum

168

force was reaching 1400 kips at mezzanine level; see Figure 8.21. In the final design, a further 10%–15% increase of peak damper force was predicted, but the reduction of peak drift ratio was smaller than 5%. As such, additional damping would provide smaller incremental benefit if the dampers were already large. In the final design, the maximum damper force reached the limit of 1500 kips at the mezzanine level. The peak damper stroke demands in Figure 8.22 showed a similar trend to the peak story drift ratio distributions.
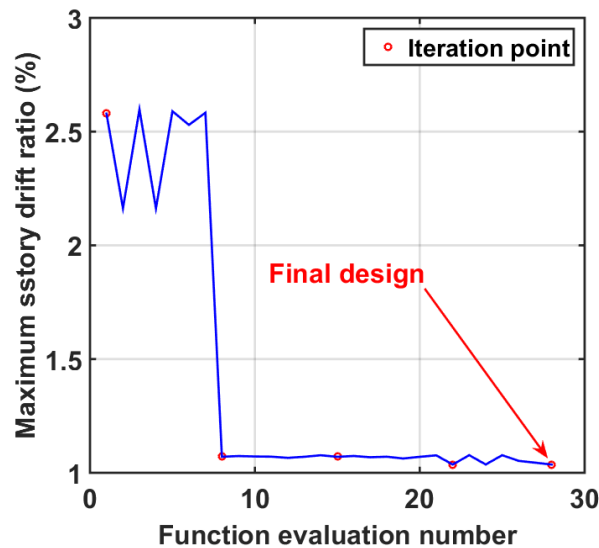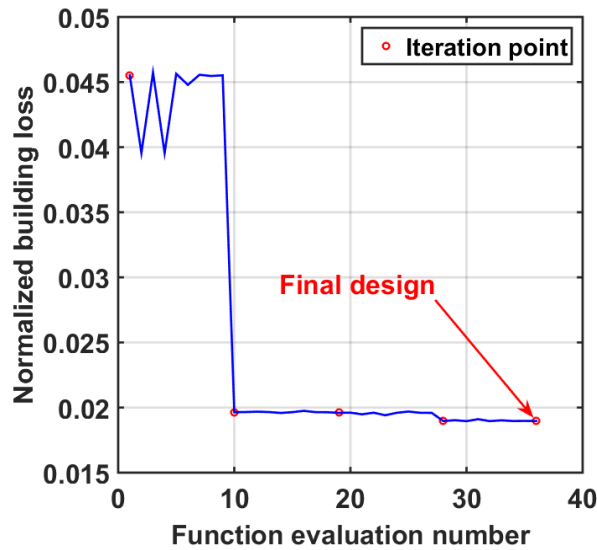

Figure 8.17   Evolution of objective function values
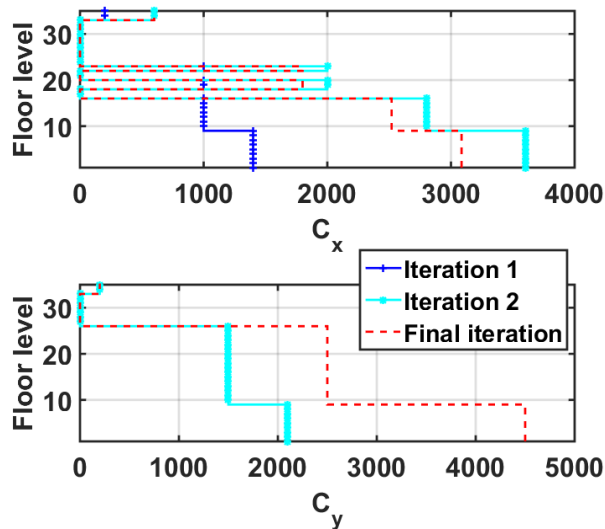
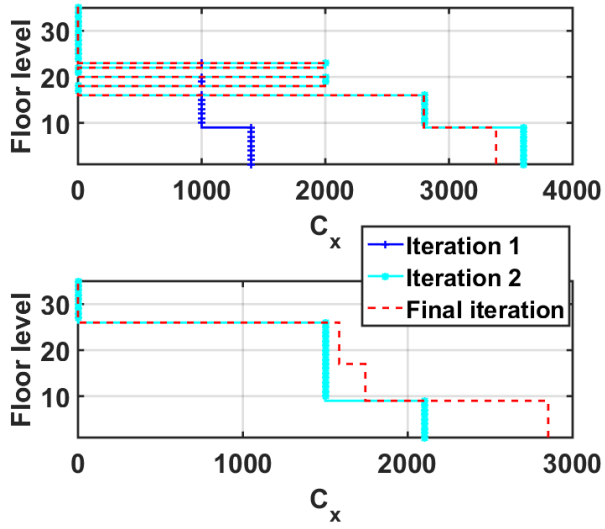**Figure 8.18   Design variables at selected iteration points**
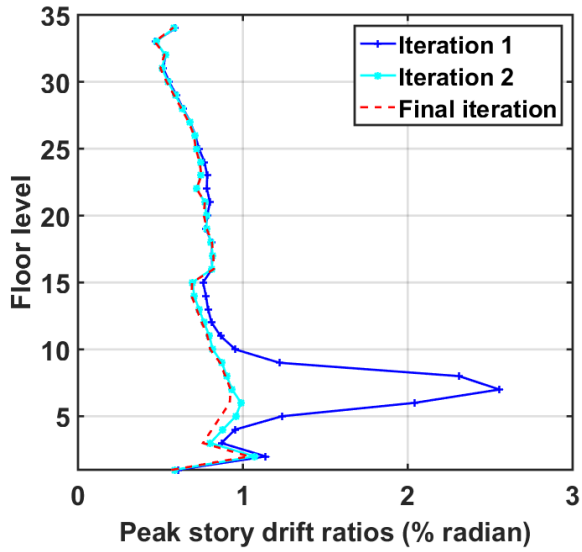
169
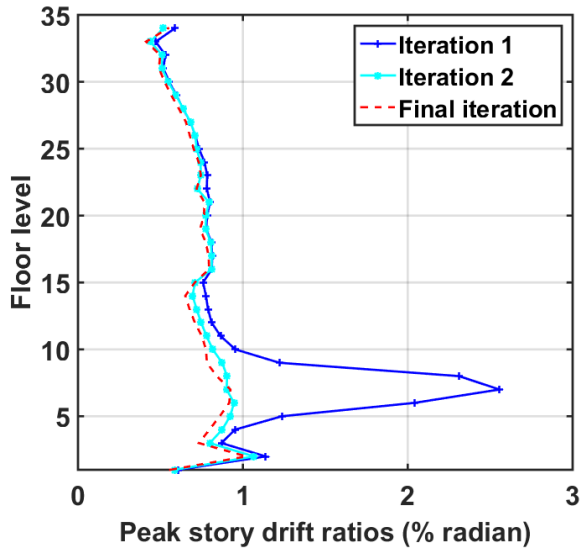
Figure 8.19   Distribution of peak story drift ratios at selected iteration points (median of eleven analyses)
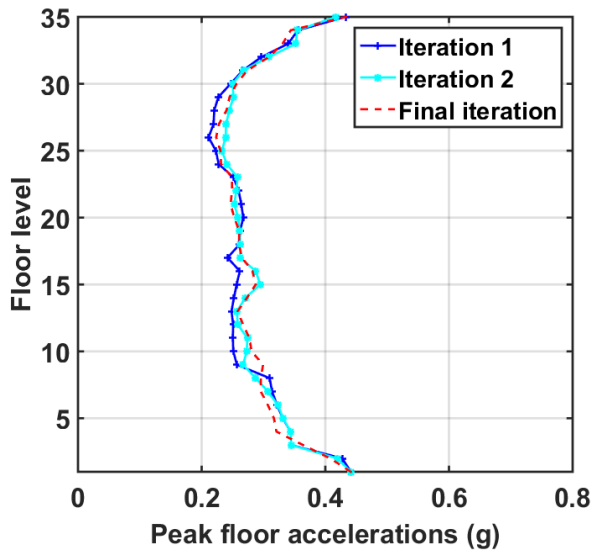
Figure 8.20   Distribution of peak floor accelerations at selected iteration points (median of eleven analyses)
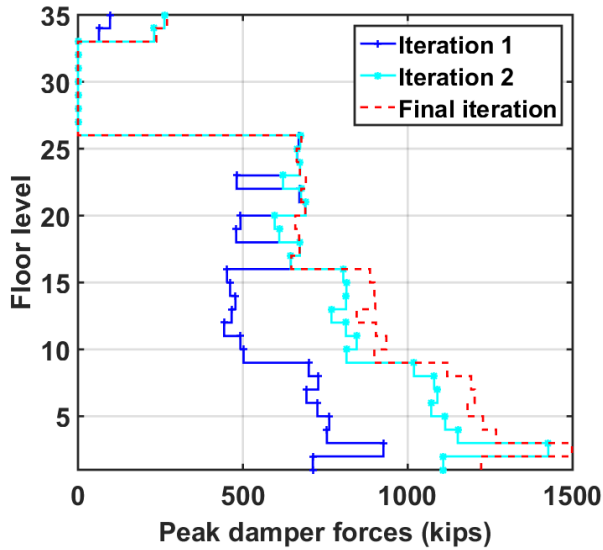
Figure 8.21   Distribution of peak damper forces at selected iteration points (median of eleven analyses)
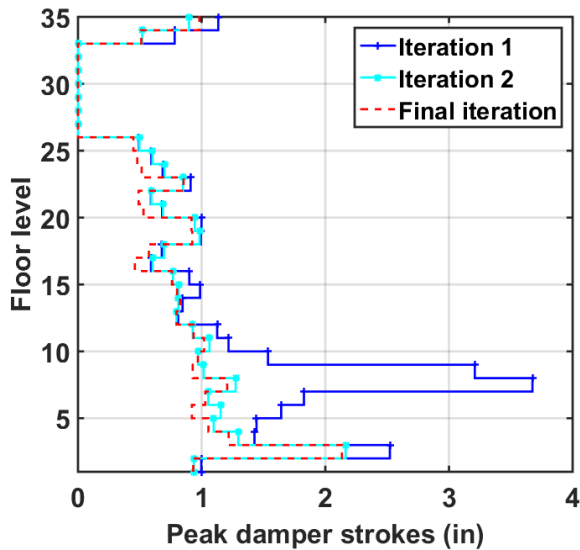
Figure 8.22   Distribution of peak damper strokes at selected iteration points (median of eleven analyses)

Three automated optimization cases under a BSE-2E event were investigated; all of them were targeted to meet the performance goal of limited safety under this hazard level. The design variables and constraints were kept the same, but different objective functions were used. Similar trends were observed for investigated three cases:

171

- The automated optimization procedure was very efficient to reach an optimal solution with limited number of iterations, and the increase was most efficient during the first update;

- Reductions of the distributions of the peak story drift ratios were large at most deformed zones when the optimization was efficient; however, the peak floor accelerations did not change much at different iterations;

- A large increase of peak damper forces was exhibited, and incremental benefits of enlarging dampers became limited once dampers sizes were already large; and

- Variations of peak damper stroke demands were consistent with the change of the peak story drift ratios.

To compare the efficiency of different automated cases, the building without FVDs (e.g., Level-1 retrofit), and final design schemes of three automated cases were selected for comparison. Additionally, a refined damper scheme (Scheme III$_R$) using a manual procedure in Chapter 4 was included. The median values out of eleven analyzes at BSE-2E hazard, which were selected in automated optimization, were used for all cases.

The design variables of final schemes are listed in Table 8.3, including the initial values. The initial design started with the lower bounds and was updated by increasing damper sizes. The three automated designs increased the dampers sizes by a factor of 2 or more compared with the initial design at X-direction. In the Y-direction, the increase in damper size was smaller, ranging from 10% to 35% for Case 1, and 67% to 133% for Case 2 and 3. Similarly, the effective damping ratio in each direction was increased in proportional to the damper sizes; see the right-most columns in Table 8.3. The effective damping ratio was estimated based on an elastic strain energy method [Soong and Constantinou 1994]; refer to Chapter 4 for details. For the case-study building to achieve a desired performance level, a total effective damping ratio of 12% to 13.5% was determined for X-direction; a slightly larger value was suggested for Y-direction (that ranged from 13.0% to 19.3%). However, the average sizes of FVDs and the effective damping ratio of Scheme III$_R$ were smaller than these automated schemes, indicating that the manual design could be further refined to achieve better performance.

The distributions of peak story drift ratios (Figure 8.23) demonstrated that although all damper designs could eliminate the concentrated deformations at floor levels 4 to 7, the effectiveness of the different schemes might differ. The automated procedure proved to be more effective than the manual procedure, which brought down the maximum drift to about 1.0%; the manual design predicted 1.48%. All schemes reached maximum values in the mezzanine level due to a deficient of the stiffness in that region. Nevertheless, the overall control efficacy of drift ratios was similar in other floors.

Contrary to the peak drift ratio distributions, the manual design pattern proved to be the most effective to suppress the floor accelerations (Figure 8.24). It used different sizes of FVDs at every story, and thus likely to be more adaptive to maintain the out-of-phase properties of each FVD and added smaller forces to the main frame compared with other cases. In terms of automated designs, Case 1 was slightly worse than the other two cases, especially in top floors,

where the roof acceleration reached $0.500g$ given that no dampers were installed there. Case 2 and 3 exhibited similar behavior, with both achieving a maximum acceleration larger than $0.4g$.

In terms of damper response, the manual design procedure used resulted in relative small dampers at the mezzanine level, which was less efficacious in reducing the story drift ratios (Figure 8.25). The deficient of stiffness in the mezzanine level became a bottleneck for continued improvement, and affected the manual design since Scheme III_R sized FVDs based on story stiffness. This drawback was unique for the existing building where some structural inadequacies were not fully addressed before incorporating the dampers. The damper forces at Case 1 were the smallest, whereas Case 2 predicted the largest damper forces among three automated cases. Regarding the peak strokes, different automated schemes did not differ much, with a peak value smaller than 2.5 in. (Figure 8.26). Nevertheless, the manual design showed that a much larger stroke of 3.5 in. in the mezzanine level, as observed earlier with larger drift ratios (Figure 8.23).

The maximum values of above results could be extracted to determine the total building loss under a BSE-2E hazard event, which was estimated using the EDP-DV functions; see Table 8.4. Note: the total construction cost of a new similar building is $740.5 M, and the building losses listed in row four were obtained by converting the normalized loss to the actual number. In the meanwhile, the costs associated with purchasing the damper devices could be assessed considering unit prices provided in Table 6.6, which were estimated by consultations with experienced engineers.

The maximum of peak residual drifts was used to determine whether a building should be demolished based on a fragility curve provided in FEMA P-58 [FEMA 2012]. The Level-1 retrofit without introducing dampers resulted in very large residual drift ratios after a BSE-2E hazard event, and a replacement was very likely, as seen by the 99.9% probability to replace the building in the first row of Table 8.4. Incorporating FVDs dramatically reduced the vulnerability of the building and brought down the probability of the building being irreparable to be almost zero. Correspondingly, the dampers reduced the total building loss from $740.5 M to $20 M using a manual design procedure. When using the automated design procedure, the loss was even smaller: about $14 M. The difference in the cost of dampers between the manual case and different automated cases was less than $0.6 M, and was far smaller than the difference of reduction of total loss between these designs.

Table 8.3   Comparison of design variables

Design variable	Cx kip·(sec /in.)$^{0.35}$	Cy kip·(sec /in.)$^{0.35}$	α_1	β_1	α_2	β_2	cx_0	cy_0	ζ_{eff}	
									X	Y
Initial value	1000	1500	1.4	1.4	1.0	1.0	200.0	200.0	6.2%	11.2%
Case 1	1997	1584	1.69	1.80	1.40	1.00	/	/	12.9%	13.0%
Case 2	2000	2500	1.80	1.77	1.40	1.40	600	600	13.5%	19.3%
Case 3	2000	2200	1.71	1.80	1.40	1.00	600	200	12.0%	17.7%
Manual	1200	1800	1.78	1.58	1.39	1.45	/	/	8.5%	11.8%

173

Figure 8.23   **Comparison of peak story drift ratios (median of eleven analyses)**

Figure 8.24   **Comparison of peak floor accelerations (median of eleven analyses)**

Figure 8.25   Comparison of peak damper forces (median of eleven analyses)

Figure 8.26   Comparison of peak damper strokes (median of eleven analyses)

Table 8.4   **Cost-effectiveness of various schemes under BSE-2E hazard level**

Scheme	W/O damper	W/ damper			
		Manual design	Case 1	Case 2	Case 3
Prob. of irreparability	99.9%	0.24%	0.003%	0.001%	0.002%
Maximum story drift ratio (%)	5.21%	1.48%	1.04%	1.00%	1.02%
Maximum floor acceleration (g)	0.628	0.438	0.500	0.407	0.438
Total building loss ($M)	740.0	19.8	14.2	13.9	14.1
Damper price ($M)	N/A	6.4	6.3	7.0	6.8

8.2.3 Case Studies Under BSE-1E Hazard Events

In this section, the automated procedure was investigated for the case that focused on reducing the building loss after a BSE-1E hazard event to achieve enhanced performance of the building.

Case 4: EDP-DV functions as objective function

The objective function used in this case was the summation of three EDP-DV functions under a BSE-1E hazard event; see Eqn. (8.1). The value was normalized by the maximum financial loss, which represents the cost to construct a new similar building and is $740.5M.

The biggest change of the objective function occurred at the first update (Figure 8.27), that reduced the normalized building loss by more than 17%. No significant changes were observed during the update from the second to the third iteration. However, as will be demonstrated later, these two design points violated one of the imposed constraints; as such, subsequent updates involved a compromise between reducing the design variables and increasing the objective function values. The optimization was terminated when the number of evaluations reached the maximum value defined. The final design point met all constraints.

Three iteration points were selected to track the changes of design variables: first, third, and final design (Figure 8.28). A significant increase of C was observed from iteration 1 to iteration 2, and such an increase was much larger in the X-direction than the Y-direction. However, C_x were reduced by 20% from the third iteration to the final design in order to meet the constraint requirements. Nevertheless, there were no significant changes of C_y during the updates.

The distributions of the peak story drift ratios of the selected three iterations are illustrated in Figure 8.29. The overall drift ratios were reduced by about 30% at all floors from iteration 1 to 3, and the maximum value was reduced from 0.8% at the mezzanine level to 0.7%. A slight increase of the damper sizes at the final design led to a corresponding larger drift values at floor levels 1 to 10, although not significantly.

As was observed in Case 1-3 under a BSE-2E hazard event, the peak floor acceleration distributions were only slightly influenced by the optimization in this case as well (Figure 8.30), for reasons discussed before. Considering the limited changes of the maximum floor acceleration,

it was predicted that the drift-sensitive PGs played a more important role than acceleration-sensitive PGs in reducing the loss during the optimization procedure.

In terms of the peak damper responses, the peak damper forces exhibited an average of 40% increase spanning from floor 1 to 15 when the design was updated from the first to the third iteration point (Figure 8.31). Nevertheless, to meet the maximum damper force constraint of 1000 kip, the final design reduced the damper sizes by about 10% and increased the peak drift ratios by less than 5% from level 5 to 10. The peak damper stroke demands in Figure 8.32 were below the 2-in limitation; this was less of a concern than the damper forces while selecting appropriate damper sizes. Note: the reductions of drift ratios at mezzanine level (Figure 8.29) were relatively inefficient considering the increase rate of the damper forces at that region. The is partly due to the design variables selected: the dampers had a uniform size from floor 1 to 8, which could not capture the special needs of damping demands in the mezzanine level. Further investigations of assigning different design variables at such and other unique stories would be a fruitful area of study.
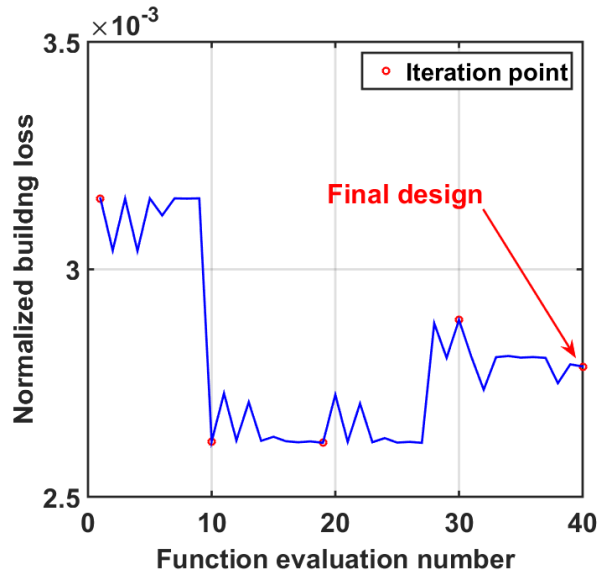
Figure 8.27   Evolution of objective function values
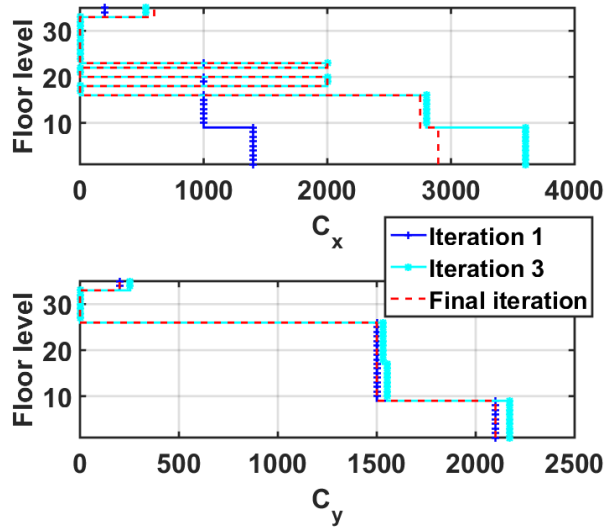
Figure 8.28   Design variables at selected iteration points
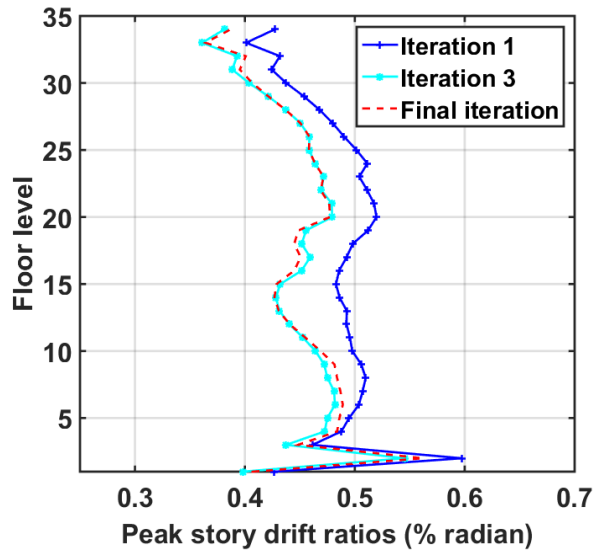
Figure 8.29   Distribution of peak story drift ratios at selected iteration points (median of eleven analyses)
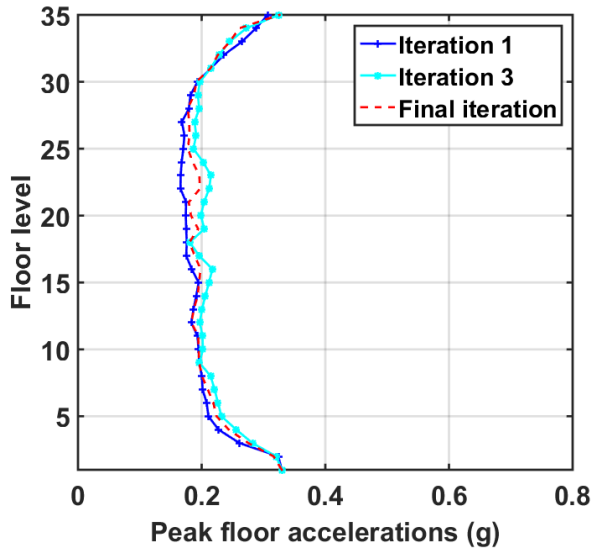
Figure 8.30   Distribution of peak floor accelerations at selected iteration points (median of eleven analyses)
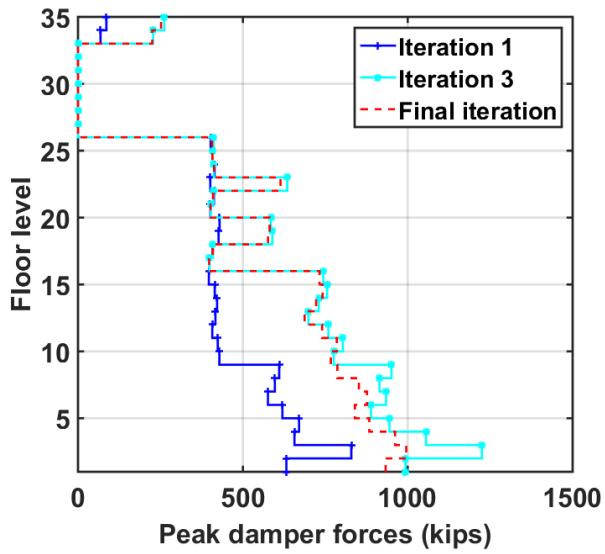
Figure 8.31   Distribution of peak damper forces at selected iteration points (median of eleven analyses)

179
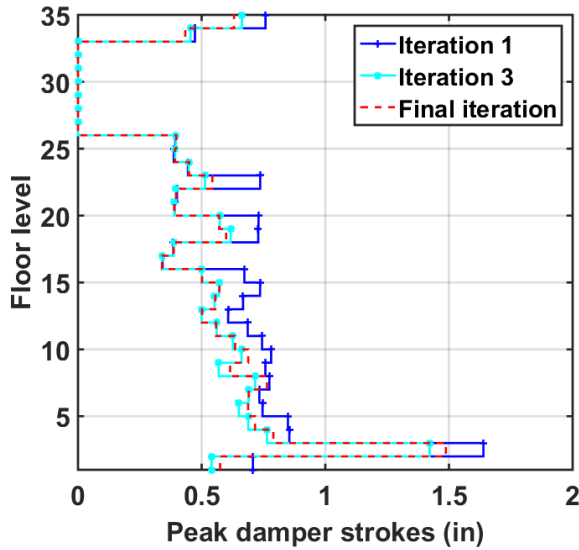
Figure 8.32   Distribution of peak damper strokes at selected iteration points (median of eleven analyses)

A comparison was made between the automated design procedure and manual procedure under a BSE-1E hazard event. Two cases were selected: the automated design Case 4, and the manual design case Scheme III$_R$; see Table 8.5. The initial design values of Case 4 were the same as previous study cases that evaluated under a BSE-2E event, which provide effective damping ratios of 6.2% and 11.2% in the X- and Y-directions, respectively. Although the initial design was considered insufficient to achieve the limited safety performance level under a BSE-2E hazard event, it was adequate when the hazard intensity was reduced to BSE-1E level, as demonstrated by the smaller increase of damper sizes at the final designs. Moreover, a larger increase was needed for C_x than C_y for the automated design. In terms of Scheme III$_R$, a smaller damping ratio in X-direction was needed compared to Case 4, but the design required slightly larger damping in Y-direction. Note: Scheme III$_R$ was kept the same as that used in BSE-2E event, but the damper force demanded changed under a different hazard.

Table 8.5   Final design variables

Design variable	Cx kip·(sec /in.)$^{0.35}$	Cy kip·(sec /in.)$^{0.35}$	α_1	β_1	α_2	β_2	cx_0	cy_0	ζ_{eff} X	ζ_{eff} Y
Initial value	1000	1500	1.4	1.4	1.0	1.0	200	200	6.2%	11.2%
Case 4	1890	1500	1.52	1.4	1.4	1.0	600	210	11.8%	11.2%
Manual design	1200	1800	1.78	1.58	1.39	1.45	/	/	8.5%	11.8%

The distributions of peak story-drift ratios (Figure 8.33) indicated that both the manual scheme and the automated schemes were capable of reducing the drift ratios by 25% to 35% at different floor levels; however, the manual design was relatively less efficient than the automated case at floors above 11, as well as in the mezzanine level. When consider the effect of controlling the peak floor accelerations, the difference between two schemes were negligible (Figure 8.34). The reduction of story-wise floor accelerations was about 50% for both cases. Such a large reduction of structural vibrations under a moderate earthquake provides a huge incentive to use FVDs considering its benefits to reduce occupants' discomfort and fear during a seismic event.

The damper force distributions (Figure 8.35) showed difference of damper force demands at different stories. Although the overall damper demands were similar between the manual scheme and the automated design, scrutiny revealed that the former was not able to provide sufficient dampers at mezzanine for the reasons discussed before. As such, the manual design had an observable larger drift in the mezzanine level and larger damper strokes; see Figure 8.33 and Figure 8.36.
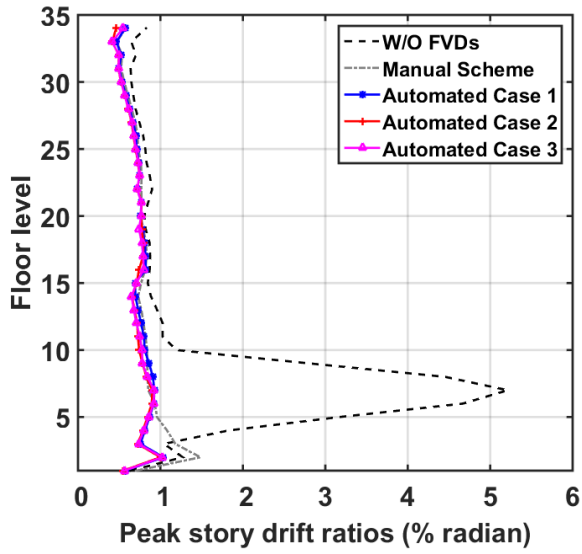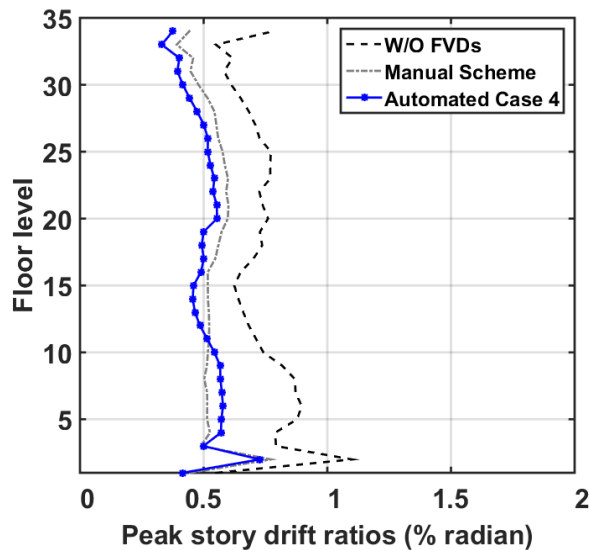

Figure 8.33   **Comparison of peak story drift ratios (median of eleven analyses)**
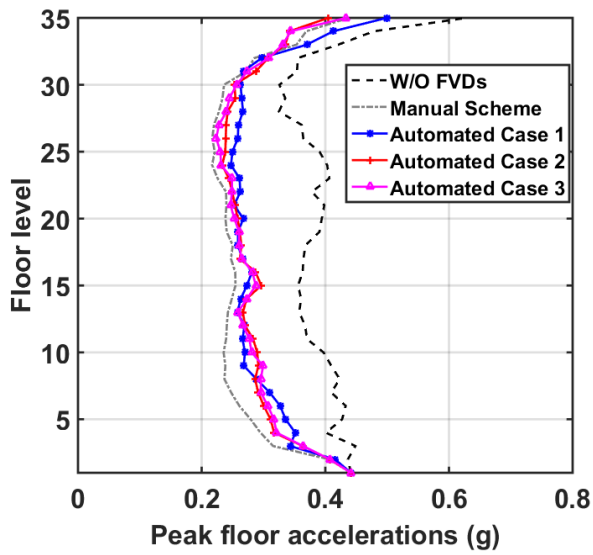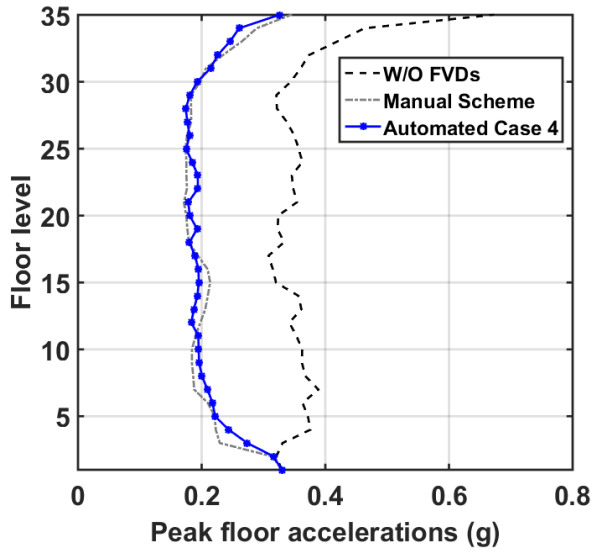
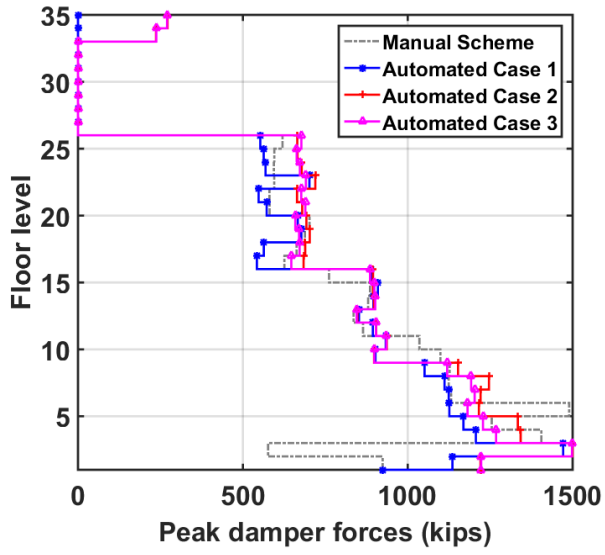**Figure 8.34   Comparison of peak floor accelerations (median of eleven analyses)**
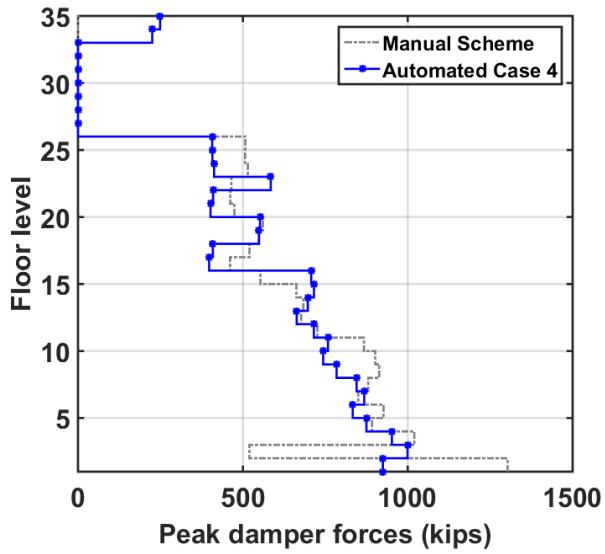
Figure 8.35   Comparison of peak damper forces (median of eleven analyses)
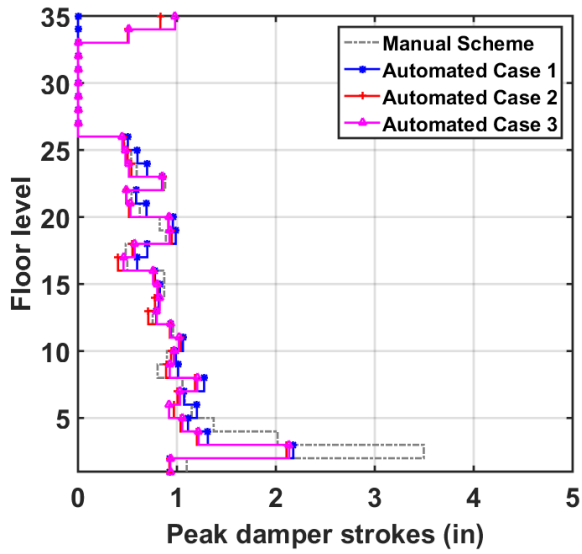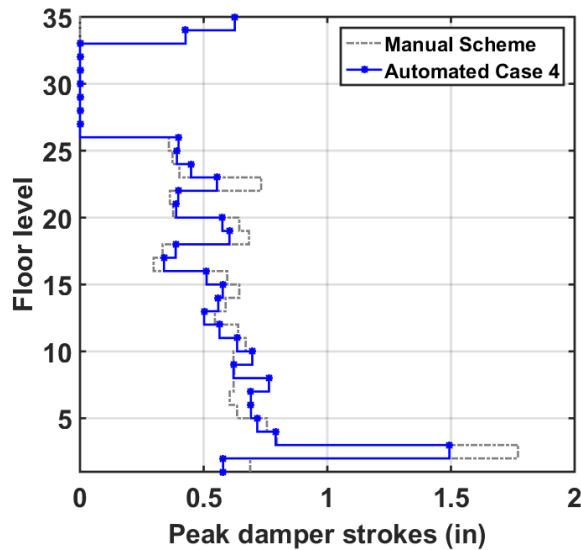
Figure 8.36   **Comparison of peak damper strokes (median of eleven analyses)**

The maximum values of the peak responses are listed in Table 8.6, which were used to estimate the total building loss under a BSE-1E hazard event using the EDP-DV functions. The building with only Level-1 retrofit behaved reasonably well under a BSE-1E hazard event, with a peak drift ratio in the order of 1.1% and a peak acceleration of 0.671*g*. This resulted in a total building loss of $3.48 M. Incorporation of FVDs on top of the baseline building further improved structural response and reduced the building loss to be slightly larger than $2 M. The automated design scheme was slightly more effective than the manual design, which predicted ha loss of $2.07 M compared to the $2.22 M for the manual design.

The initial costs of purchasing dampers were $3.7 M and $ 3.8 M, for the manual design and Case 4, respectively, based on the unit damper force/stroke demand under a BSE-1E earthquake event; see Table 6.6 for unit damper price. Note: the damper price is dependent on the maximum force stroke, and the failure of a damper is not considered in this study. The cost-benefit of using FVDs at a moderate earthquake event was less promising than under a major earthquake. However, the incentives of such a retrofit could not be considered in a sole event, and a life-cycle analysis would be a fruitful area for future study to better understand the cost-benefit and return on investment.

Table 8.6   **Cost-effectiveness of various schemes under BSE-1E hazard level**

Scheme	W/O damper	W/ damper	
		Manual design	**Case 4**
Maximum story drift ratio (%)	1.10%	0.77%	0.73%
Maximum floor acceleration (g)	0.671	0.344	0.330
Total building loss ($M)	3.48	2.22	2.07
Damper price ($M)	N/A	3.7	3.8

8.3   ADVANTAGES OF AUTOMATED DESIGN PROCEDURE

In Section 8.2, the automated optimization design procedure was applied in the case-study building, with the aim of identifying optimal damper arrangement patterns based on the objective functions selected. The procedure was evaluated separately for the two earthquake hazard levels and identified a set of parameters that significantly improved the structural behavior and reduced the total building loss with only a few iterations. The resulted final designs were compared with a manual design pattern designed previously in this dissertation, and showed that the design solutions of the automated procedure were superior compared to the manual case.

A key feature of the automated design is its much-reduced engineering effort compared to the manual procedure. In engineering applications, design of these dampers mainly relies on trial and error, which is both repetitive and labor intensive. The alternative, using high-performance computers (HPC) and parallel processors, enables streamlining the design effort and saves significantly on labor costs. The analysis is conducted at multiple cores simultaneously, and each design is automatically refined using a gradient-search algorithm. To quantitively compare the time input for each procedure, a rough estimation is provided in Table 8.7.

Consider a building model of similar complexity that requires a similar amount of analysis: a manual damper design procedure would require determine the initial scheme, analyse the structural responses, and refine the design based on a consistent criterion. Each of these steps might require a week or so for the case under consideration. Note the design-analysis process is repeated at least a couple of times until a satisfactory design is reached. As such, the entire duration of a manual procedure could be a few months. In contrast, the major effort in the automated procedure is designing the loop. Based on optimization packages provided by most software, the optimization algorithms are readily available. As such, additional labor savings are possible. The optimization problem is set up with a link between different software, which is straightforward and doesn't require intensive programming. A duration of half a week is considered for such an initialization.

Next, the design-analysis job is handed over to the optimization engine, which runs the analysis, post-processes the results and refines the design parameters in an automated manner. For the scenario considered here, it took about three to five days for the software to identify a good design solution. It is worth noting that if the numerical model is simpler, the computational time for both manual and automated procedures would be reduced proportionally. Note: the automated design in this study used six to eight design variables and four nonlinear constraints. If the number of design variables or constraints is increased, the time needed to identify a refined solution would increase.

Clearly, the automated design strategy is superior compared to a common design approach since it significantly reduces the design duration, and, more importantly, saves on labor. Nowadays, HPC resources are widely accessible at minimal or no cost. Consider an on-demand hourly cost of $0.251 for a 16-CPU core machine available at Amazon EC2 Cloud [Amazon 2017], a computation time of 5-day costs roughly $30, which is negligible compared to the overall project budget. Therefore, engaging HPC resources to help streamline the optimization efforts and identify design parameters is a practical and promising way for both research and engineering practice.

Table 8.7   Efficiency comparison

	Design initial scheme	Structural analysis	Update design
Manual procedure	1 week	1week	1 week
	Automated loop	**Optimization engine**	
Automated procedure	Half week	3-5 days	

8.4   GUIDANCE OF IDENTIFYING OPTIMAL DAMPER DESIGN IN A TALL BUILDING

In Chapter 4 of this dissertation, several important design parameters of dampers were investigated, including determined the optimum locations to install dampers, the damping exponent α, and the stiffness of spring to drive the dampers K_b. Another design parameter, damping constant C and its story-wise distributions, were selected for refinement. This section integrates these efforts and outlines a step-by-step procedure to design FVDs in a high-rise building from scratch. Based on results identified in this chapter, several suggested damper arrangement patterns are suggested for preliminary design. This procedure starts with the case that the original building model without dampers is already designed and focuses on designing dampers. As such, it is applicable to both a new construction as well as a retrofit case.

8.4.1 Identify Damper Locations

Selecting appropriate locations to accommodate dampers is usually restricted to functional and architectural requirements. For example, putting devices inside a building that avoids blocking a view or changing a building's aesthetic appearance might result in interfering with office use or egress. Interference with a building's functionality could be reduced if dampers were placed in the outside of an existing building. Another important concern is the interruption of building's normal use during construction. By putting dampers in the exterior frame, the need to empty the building during construction could be avoided, which significantly reduces business downtime and business interruption cost. As such, exterior frames may provide a better location to install dampers, especially when a retrofit case is considered. Additionally, other constructability considerations, such as delivery of devices to high-level floors and the need to strengthen existing members/connections would influence the location selection and need to be accounted for.

Aside from aesthetic considerations, dampers should be installed at locations with relative large shear deformations to maximize the efficiency of dampers in a structure. For instance, in a moment-resisting frame that provides larger stiffness at top floors, installing dampers there would inhibit their effectiveness. Thus, dampers are more effective if installed at middle and bottom floors where relative deformations are larger.

To find specific locations at each floor to install dampers, the study in this dissertation used an equivalent frame method proposed by Kasai *et al.* [2002 and 2006], which imposed a code-conformed lateral force pattern to the building to estimate the stiffness of each story. The same lateral force pattern was assigned to the building after installing dummy "rigid" element at selected locations. If a story's stiffness increases significantly after "rigid" elements are added there, it has the potential to undergo large shear deformation and thus able to provide better control.

Additionally, the interaction between dampers and existing structural elements should be considered when selecting locations to install dampers. As has been demonstrated, distributing dampers in multiple bays is a better option than stacking them in one or two bays in order to avoid large accumulations of damper forces to the columns connected with dampers.

Taking all these variables into consideration, a preliminary scheme to install damper could be devised.

8.4.2 Estimate Effective Damping Ratio

The total effective damping ratio needed to reduce overall drifts or drift concentrations to an acceptable level need to be estimated before selecting damper sizes and number of damper needed. A rough estimate could be obtained by comparing the current displacement demand and a target displacement.

One quantity to consider is the roof displacement. The current demand could be obtained by evaluating the displacement spectrum under a certain earthquake hazard level. The spectral displacement could be obtained for each mode and then converted to the roof displacement demand by considering nonlinearity, SDOF to MDOF conversion, etc. [ASCE 41 2013]. In the preliminary design stage, the first mode is usually sufficient to get a reasonable estimate of a damping ratio. On the other hand, the target displacement depends on the target performance level. In this study, a target roof displacement was based on the pushover curves and chosen to avoid a sudden strength deterioration of the building.

After obtaining the displacement demand and target, an estimation of effective damping can be conducted based on a damping modification factor that is related to the ratio between the two displacements. Design guidelines [ASCE 7 2010] suggest B_D and B_M values to account for modification of the design response spectrum with damping values other than 5%. Alternative methods could be used based on relevant research [Rezaeian *et al*. 2012]. In practice, an effective damping ratio between 8% to 20% is considered reasonable for a building based on consultation with experienced engineers.

8.4.3 Design Parameters

The mathematical model for a damper-brace-frame assembly was discussed in Section 4.2.2. Three critical parameters for this model are: (1) brace stiffness K_b; (2) damping exponent α; and (3) damping constant *C*. A review of previous studies on each of these parameters were presented in Section 4.2.3; more specific and applicable suggestions are provided below.

186

(1) Stiffness of the brace (K_b)

To ensure that the energy-dissipation capacity of a FVD is maximized, K_b should be fairly large to control the damper effect and insure the force of a damper stays out of phase with structural displacements. As noted previously, other elements in the load path such as the beam-to-column connection and the damper device itself are flexible and could contribute to the flexibility of the assembly if they are in series with a FVD. However, this study focused on the driving brace flexibility since it is the most critical component (e.g., K_b denotes the brace stiffness herein).

A separate parametric study presented in Section 4.4.3 was undertaken to help determined the design. Several analyses were done to identify a minimal value of the K_b for the purpose of maximizing damper effect. The results indicated that the in-line braces should be sized to be twice as stiff as that of the frame in the same bay, i.e., $K_b = 2K_f$. Consequently, in each floor with FVDs, the sum of each K_b should be equal to twice of its floor stiffness. Assuming this is achievable in practice, the damper force output could be expressed by Eqn. (4.5). Note: the brace needed to achieve this criterion could be very large, especially for a tall building. Worth considering for engineering practice are alternatives that study achieving a smaller damper effectiveness but use smaller braces.

(2) Damping exponent (α)

The damping exponent α of a FVD characterizes its nonlinearity and has significant impacts on its hysteresis behavior, peak force, and the interaction with the structural elements. A sensitivity study was undertaken in Section 4.4.2 that investigated how this parameter influenced the behavior of a FVD and the control effect of dampers to improve structural performance. The results indicated that an α value in the range of 0.2 to 0.5 was optimal to provide adequate structural control without inducing excessive damper forces. Although this finding is mainly used for the case-study building, it agrees with past practices where nonlinear fluid viscous dampers with a damping exponent varying between 0.35 to 0.5 were used to protect buildings or bridges from an earthquake shaking. [Asher *et al*., 1996; Rodriguez *et al*., 1996].

(3) Damping constant (C)

Another design parameter is the damping constant C, which is the primary influence on determining the size of the damper. It is suggested that C distributions over stories proportional to story stiffness is an optimal pattern; an automated optimization procedure might use these findings to select the design variables and their ranges

8.4.4 Prototype Design Pattern of FVDs In a Steel Moment Frame

Group of FVDs

In practice, a preliminary damper design scheme is proposed by structural designers. Then the physical dampers are provided by a damper manufacture to satisfy the damper force/stroke requirements. Usually, the same type of damper is used where a similar force and stroke demands are required in a building. Consequently, only a few types of dampers will be used in one project. To align with this practical consideration, dampers are categorized into a few groups,

with each group having identical mechanical properties. Stories with a similar plane layout and dynamic behaviors could be categorized into a same damper group. The total number of damper groups could be selected based on the number of design variables used for optimization. Additionally, if two horizontal directions utilize different structural systems, or exhibit different structural performances, dampers could be treated separately. Besides, if some floors exhibit different structural responses, it is advised to group them separately. The optimal scheme would be different when considering different group methods.

Proposed design patterns of FVDs

Optimal design patterns of dampers were proposed for the case-study steel moment frame based on the type of objective function used, as summarized in Table 8.8. These schemes suggest installing dampers at lower two-thirds floors where additional damping is more effective than other locations. For this case-study building, dampers were grouped into three layers, from stories 1 to 25. The optimal design patterns are expressed by the relation between damper sizes at each location to the smallest damper group (upper-level group) in Table 8.8.

The optimal patterns of damper distributions in the building showed a similar trend regardless of the objective function used. Although the largest damping demand was found at low-level group (stories 1 to 8), different schemes required different level of damping. For instance, if the objective function focused on reducing the maximum drift ratio or maximum floor acceleration with the goal of achieving life safety at a BSE-2E hazard, a ratio of 3:2:1 for damper sizes from bottom to upper group was suggested. However, an increased weight for lower-story damping was found for other two cases, where the objective was centered on reducing economic loss under either a BSE-1E or BSE-2E event. An effective damping ratio in the range of 12% to 20% was determined for different optimal schemes, which is close to the values suggested before (10%-20%).

Table 8.8   Optimal patterns of *C* over story height

Group of FVDs	Objective function		
	Life safety at BSE-2E	Economic loss at BSE-2E	Economic loss at BSE-1E
C at upper-level group	1	1	1
C at mid-level group	2	2	2
C at low-level group	3	4	5
Effective damping ratio ζ_{eff}	13%-18%	12%-20%	12%

The specific *C* values at each damper group can be calculated based on an expression [e.g., Eqn. (4.6)] that relates the effective damping ratio to the structure's key parameters (ϕ, θ, *A*) and damper properties (*C*, α).

Note that the suggested pattern for placing the dampers is most applicable for a steel moment frame or a similar structural system type that is flexible at bottom and stiff at top, and

more suited for a site located in a far-field region. Its applicability to other structural types and different hazard characterizations need further investigation.

8.4.5 Verify Design

Following the steps listed above, an appropriate design pattern of FVDs in a tall building is obtained; the design is expected to achieve in a cost-effective manner the target performance objective. Rigorous NRHA is necessary to evaluate and validate the design by checking the adequacy of both dampers and existing elements based on ASCE 41 [2013] requirements. For the purpose of this check, analysis methods other than HRHA are not realistic for a tall building since higher modes are not taken into account. In addition, other methods are unable to capture accurately damper behaviours and their interactions with structural members.

The structural global responses, element responses, and damper responses must be evaluated. Special attentions should be given to existing members that are connected with FVDs directly, such as the beam-to-column connections. Additionally, columns at lower floors are usually fragile in an existing building and require rigorous checks to ensure they will not fail after dampers are installed. Note: this study focused on designing dampers based on limited scenarios; the properties of existing structural members were not changed from the as-built condition.

The economic impact could be assessed by a loss and damage analysis under a certain earthquake scenario. A more in-depth analysis to estimate the business interruption and total financial loss should be conducted based on a downtime model and a financial model. The cost-benefit of using dampers following optimal design strategy could be estimated by comparing the savings due to loss under an earthquake scenario and the additional costs to purchase and install these dampers. The return on investment, if needed, could be examined by conducting the loss analysis under different earthquake scenarios to obtain an annualized loss.

8.5 CONCLUDING REMARKS

An automated design procedure to tune damper parameters in a tall building was proposed and applied to an existing high-rise building. The basic ingredients included the design variables, an objective function, and several constraints, which were chosen to define the optimization problem. This automated design procedure was evaluated under two seismic hazard levels: BSE-1E and BSE-2E. The design variables were kept consistent for all case studies, but different objective functions were used, including the cases that used a single EDP and these based on comprehensive EDP-DV functions. Constraint functions were modified slightly under different cases.

Results indicated that the automated PBEE procedure was able to identify design parameters that improve a structure's seismic performance efficiently with a limited number of iterations. Despite of slight differences in the final design, all cases under investigation indicated that the additional damping demand was maximum for lowest stories where a weak-story trend was observed; however, the damper sizes in middle to upper stories were much smaller, and no dampers at top stories were required in order to achieve the stated performance targets.

189

Compared with a manual design procedure, the automated design procedure has great advantages. It not only provides better design strategies to control structural responses and reduce economic loss under a moderate or a major earthquake, but more importantly, it streamlines the design process by substantially reducing time and engineering efforts.

A systematic procedure for designing FVDs in a high-rise building was outlined. Geared toward engineering practice, the procedure includes selecting locations to install dampers, estimating the effective damping ratio needed to achieve a target performance level, characterizing design parameters of a FVD, and suggesting patterns for arranging dampers of different sizes over building height. After the preliminary design, NRHA should be used to verify the adequacy of existing structural elements and damper elements, and damage and loss estimates are needed to assess the cost-effectiveness of proposed damper scheme. This procedure could apply to both an existing or a newly-designed tall building, but it is most suitable for a steel moment-resisting frame.

9 Automated Damper Optimization in the Design of a New Tall Building

9.1 INTRODUCTION

This chapter extends the automated optimization procedure of dampers to a newly-designed tall building. A hypothetical 61-story mega-brace steel frame system is selected as a study case. This case-study building is based on an actual building, but the structural configuration and other properties have been substantially modified for simplicity in this study. Section 9.2 provides a detailed introduction of the building, including basic information about the building and its structural system, code-based performance objectives, selection of ground motions, and modeling techniques. In Section 9.3, the ability of the case-study building to satisfy code-based performance objectives is examined. Results indicate that the building could meet the collapse prevention performance level under the risk-adjusted maximum considered earthquake (MCE$_R$) hazard level. The ability of fluid viscous dampers (FVDs) used in parallel with the original building's mega-brace system to enhance its seismic performance is then examined. Several design considerations related to the installation of the FVDs, including selecting their locations, configurations, and mechanical parameters, are investigated in Section 9.4. The efficacy of proposed method to achieve enhanced performance is demonstrated by a trial damper scheme. In Section 9.5, an automatic procedure is used to streamline the effort to tune damper parameters in selected installation locations. Four cases are studied, each having a different objective function. Optimal design patterns are proposed for a mega-brace type building in Section 9.6.

9.2 CASE-STUDY NEW BUILDING

9.2.1 Building Description

The case-study building (Figure 9.1) is based on a newly-designed building located in San Francisco. It consists of two tall towers for mixed use: one 61-story-tall tower with residential floors over office space, with a total height of 850 ft; and one 54-story-tall tower with residential floors over a hotel, with a height of 605 ft. Its structural system was designed by engineers from Magnusson Klemencic Associates Inc. (MKA) in 2015, and the building is currently under construction.

Given that the primary goal of this study is to select optimal damper sizes in the case-study building, for simplicity, the structural layout of the original building was modified to be more regular in shape. The original building was un-symmetric [Figure 9.2(a)], but for the purpose of this study, a simplified doubly symmetric plane was assumed; see Figure 9.2(b). The information of the original building is mainly based on a numerical model in ETABS (Version 15.2) [Computers & Structures Inc. 2016], shared by MKA designers.

The main lateral force-resisting system of the building is an exterior steel mega-frame "kite-bracing" system, which consists of large mega-columns connected by inclined steel braces and horizontal tie-beams [Figure 9.3(a)]. The mega-columns are large steel box columns filled with concrete. All inclined bracing elements use buckling restrained braces (BRB) except these in the lowest level that use same sections as columns. Additionally, although the office section and the residential sections differ slightly, there are a few secondary lateral force-resisting systems [Figure 9.3(b)] inside the building. Specifically, in the office levels (Levels 1 to 43), a floor-by-floor lateral force-resisting frame, comprised of special BRB frames, is designed to close the box of the exterior mega-frames and provide floor-wise bracing between primary nodal floor where exterior BRBs intersect with exterior columns. At the residential floors (floor 43 and above), seven inter-nodal bracing trusses span vertically to provide lateral resistance for each floor level. These secondary lateral force-resisting systems are designed to span between the mega-node locations for proper transfer of inertial floor loads into mega-frame system. The gravity loads are taken by both the lateral force-resisting systems and a few gravity columns inside the building.

Figure 9.1   The exterior view of the case-study building (photo courtesy of MKA, Inc.)
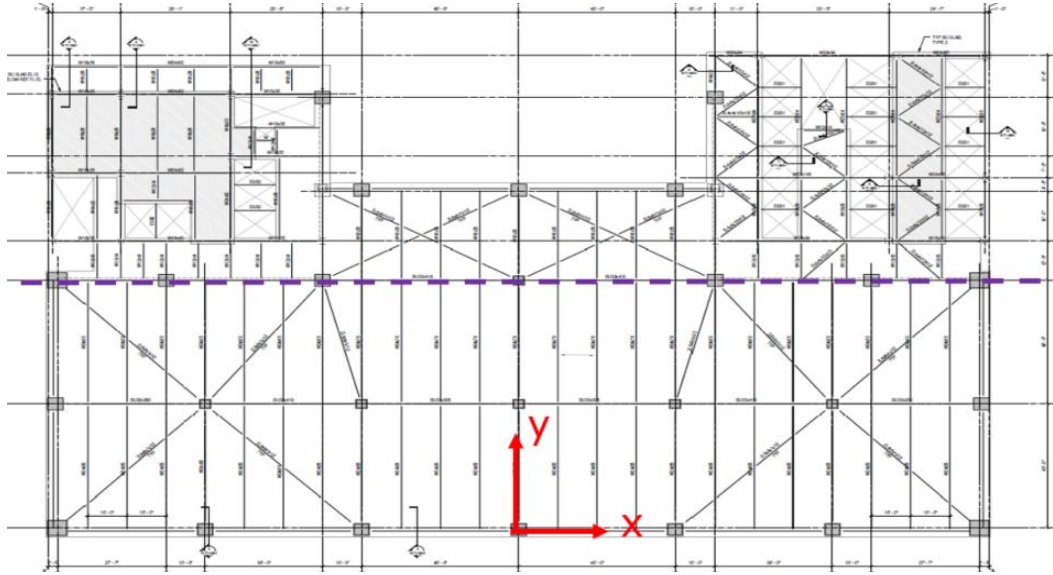
(a) Original floor plan
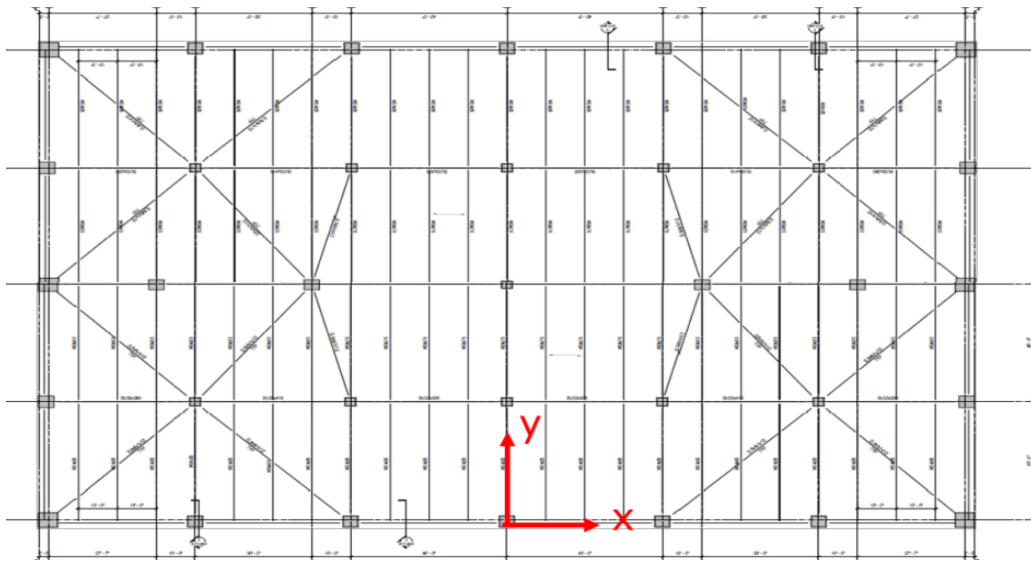
(b) Simplified floor plan

Figure 9.2   Plan view of a typical floor

(a) Exterior mega-frame brace system

(b) Secondary lateral force-resisting system
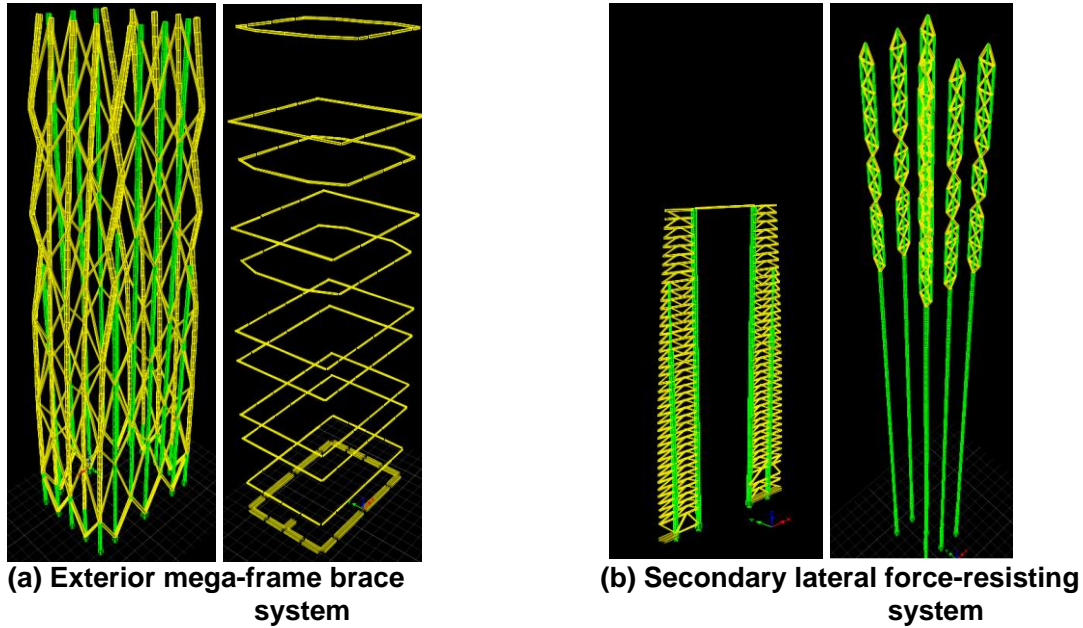
Figure 9.3   Lateral force-resisting system of the simplified building model

9.2.2 Performance Objective

One of the main considerations in a design is to select the appropriate performance objective matrix. ASCE 7-10 provides guidance on selecting the basic performance objectives of a new building depending on its risk category [ASCE 2010]. The building selected herein is a mixed-use high-rise building located in downtown San Francisco. Given its functional and geographical importance, the number of occupants, a risk category III is considered suitable for the purpose of this study. As such, the basic performance objectives required by the code are that it remains fully operational under a service level earthquake (SLE), life safe under a design earthquake (DE), and satisfies the collapse prevention limit state under a risk-adjusted maximum considered earthquake (MCE_R); see Table 9.1. Specific requirements of each performance level are listed in Table 9.2. Under a SLE and a DE event, modal response spectrum analyses (RSA) were conducted by engineers from MKA for the original building per ASCE 7 [2010]. At these hazard levels, response spectra with 2.5% and a 5% damping, respectively, were used. Additionally, nonlinear response history analysis (NRHA) was conducted under the MCE_R hazard level [MKA 2016].

Table 9.1   Performance matrix

Seismic hazard level	Fully Operational	Life Safety	Collapse Prevention
Service Level Earthquake (**SLE**) 50%/30yrs, MRP* = 43 yrs	✓		
ASCE 7 Design Earthquake (**DE**)		✓	
ASCE 7 Risk-Adjusted Maximum Considered Earthquake (**MCE$_R$**)			✓

* MRP: mean return period

Table 9.2   Description of performance objectives (extracted from MKA Inc. [2016])

Seismic hazard level	Earthquake performance objective
SLE	Structure should remain essentially elastic with only minor yielding of structural elements; minor cracking of concrete, but no spalling; minor damage to non-structural elements
DE	Moderate structural and non-structural damage which does not pose a significant danger to life-safety; extensive repairs may be required.
MCE$_R$	Structural has an acceptable low probability of collapse (6% per ASCE 7-10 Sec. C1.3.1) and has stable and predictable responses without losing gravity load carrying capacity or substantially decreasing lateral resistance; extensive structural damage may occur and repairs to structural and non-structural system are required and may not be economically feasible.

9.2.3 Ground Motion Selection

Ground motion selection and scaling were conducted by geotechnical engineers from Langan Engineering & Environmental Services, Inc. [MKA Inc. 2016]. They developed conditional mean spectra (CMS) under different periods, including 1.00, 2.25, 5.25, and 7.50 sec using the software: EZ-FRISK^{TM} (Version 7.65) [Furgo Inc., 2015]. The envelope of the CMS for 1.00 sec and 2.25 sec were selected as the short-period spectrum, while the envelope of 5.25 sec and 7.50 sec CMS represented the long-period spectrum. Adjustments were applied so that the CMS spectra would not fall below 75% of the target MCE$_R$ spectrum per ASCE 7-16. In this study, only the long-period CMS and corresponding ground motions were used since it is closer to the fundamental period of the case-study building.

Based on the CMS, eleven ground motions were selected by Langan Engineering & Environmental Services, Inc. out of 200 ground motion records from PEER NGA West 2 project. Three criteria were applied in the selection procedure, including:

- Moment magnitude is greater than or equal to 6.9;
- Rupture distance is less than 40 kM;
- Vs$_{30}$ is less than 800 m/s.

QuakeManager (Version Beta 2d) [Earthquake Solutions Inc. 2015] was used to help select specific records using the role of least sums of the squared error between the target spectrum and the maximum direction spectrum (D$_{Rot100}$). Proper adjustment was made to account for the near-field effect of building site. Table 9.3 summaries the time series used to match the long-period CMS. Seven out of the eleven records represent pulse-type motions, which was considered a reasonable portion for this site based on Shahi and Baker [2011] and Hayden *et al*. [2014].

Scaling of ground motion records were performed based on a draft of ASCE 7-16, Chapter 16 [MKA Inc. 2016], which requires that the average D$_{Rot100}$ of the eleven ground motions should generally match or exceed the target response spectrum over the period range of interest. As such, each pair of time series was scaled so that the average of eleven set of D$_{Rot100}$

spectra would be equal to the target CMS spectrum at each period from 0.2*T* to 2.0*T*, where *T* is the fundamental period of the building. The scale factors differ at all periods; see Figure 9.4. All set of scaled ground motion records, the average of scaled records, and the target CMS are illustrated in Figure 9.5.

Table 9.3   Selected ground motions

No.	NGA #	EQ	Station	Mag.	R_{rup} (km)	*Vs*30 (m/sec)	Com.	PGA (*g*)	Pulse Period[1] (sec)
1	827	Cape Mendocino	Fortuna	7.01	20	457	0 90	0.12 0.11	-
2	838	Landers	Barstow	7.26	35	370	0 90	0.13 0.14	9.13
3	900	Landers	Yermo File Station	7.28	24	354	270 360	0.24 0.15	7.50
4	1176	Kocaeli Turkey	Yarimca	7.51	5	297	270 360	0.23 0.32	4.95
5	1483	Chi-chi Taiwan	CHY101	7.65	10	259	60 150	0.34 0.40	5.43
6	1501	Chi-chi Taiwan	TCU063	7.65	10	476	E N	0.18 0.13	6.55
7	2114	Denali Alaski	TAPS Pump Station #10	7.90	3	329	47 317	0.33 0.30	3.16
8	5831	El Mayor-Cucapah Mexico	Ejido Saltillo	7.20	17	242	0 90	0.15 0.15	-
9	5975	El Mayor-Cucapah Mexico	Calexico FS	7.20	20	231	90 360	0.27 0.26	-
10	6952	Darfield N.Z.	Papnui HS	7.00	19	263	S33W S57E	0.21 0.18	-
11	6966	Darfield N.Z.	Shireley Library	7.00	22	207	S40W S50E	0.17 0.19	8.76

[1] (-) denotes non-pulse record

196
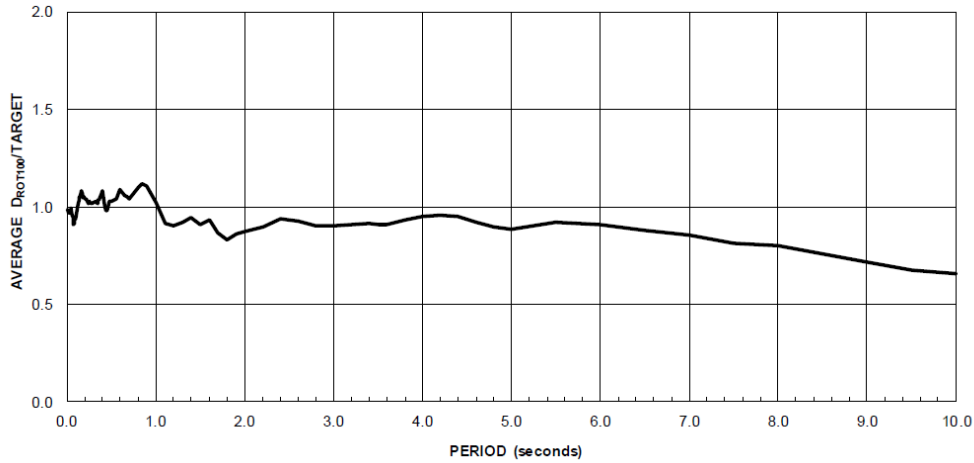
Figure 9.4   Scale factors of selected records at different periods (adapted from MKA Inc. [2016])
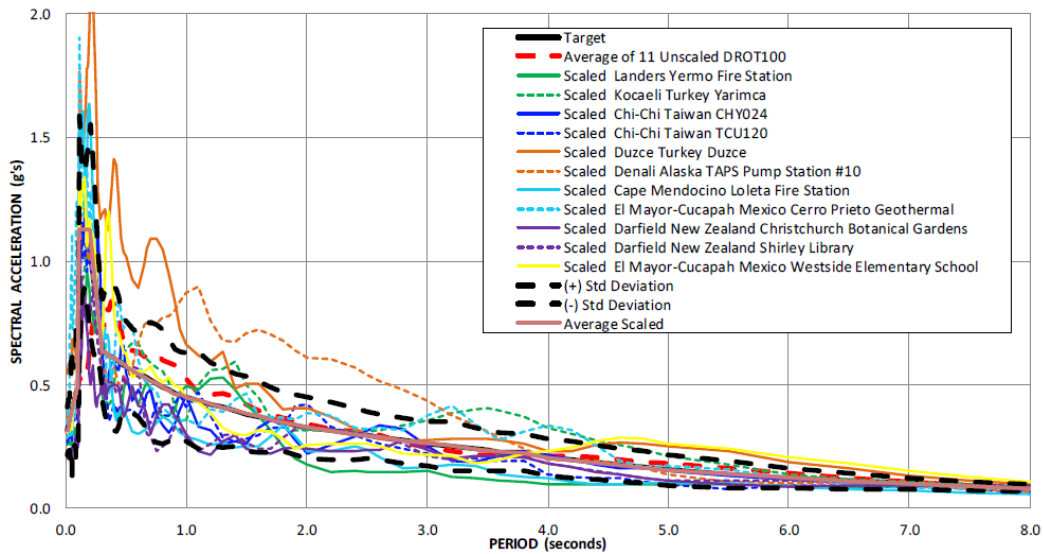
Figure 9.5   Scaled ground motion records for long-period CMS (adapted from MKA Inc. [2016])

9.2.4 Numerical Modeling

A three-dimensional (3D) numerical model was developed using OpenSees [McKenna *et al.* 2010] based on the original ETABS model. Nonlinear response history analysis was conducted under MCE$_R$ hazard events, using eleven records selected based on the long-period CMS. All main framing members in the superstructure that contribute to the seismic lateral force resisting system and gravity load-resisting systems were included in the model.

197

Considering that the primary study goal is to identify optimal sizes and locations of FVDs in a newly designed high-rise structure that consisted of exterior mega-framed brace system, a few modeling simplifications were made for the numerical model, including:

- Basement levels were disregarded;

- Ground level was assumed to be fixed;

- Composite floor slabs, that consisted of 3-1/4' in. light-weight concrete and 2 in. steel decks were assumed to be rigid in-plane, and their contributions to the flexural behavior of beams were not included;

- Any contribution of the non-structural elements—including the perimeter concrete façade—to the strength and stiffness of the structure was ignored;

- Panel zones were not explicated modeled, and center line model was used instead, as permitted by FEMA 451 [FEMA 2006]; and

- Inertial and kinematic soil-structure interaction effects were not considered.

Dead loads and 25% design live loads were included in the seismic analysis based on PEER TBI guidelines [PEER 2010]. Seismic masses were lumped at the joints in proportion to tributary area, considering element self-weight, concrete slab weight, superimposed dead loads, and 25% of live loads. The inherent damping was represented by Rayleigh damping, and the damping coefficients were derived so that the damping ratio around the fundamental period is 1.5% at MCE$_R$ hazard earthquakes.

The material, section type and section size of all structural members were modeled based on the design model provided by MKA engineers. Specifically,

- Columns in the exterior perimeter braced frames are built-up steel box columns, infilled with high-strength concrete. In the secondary lateral-force resisting systems, columns use either built-up box sections or rolled wide-flange steel sections. Exceptions are found in the base level where columns used reinforced concrete. In the numerical model, displacement-based nonlinear beam-column elements with fiber sections were used, and each column at one story was discretized into five elements to better reflect the possible yielding behaviors, especially at potential plastic hinge locations [Vesna 2011]. Seven integration points were used along element length. Each section had a mesh size of 4×4 for the concrete core and was divided into four layers along length of steel plate on each side [Figure 9.6(a)]. Similarly, wide-flange steel column sections used 12 fibers, with each flange or web divided into 4 layers along the length; see [Figure 9.6(b)]. The columns in the exterior braced frame are not necessarily vertical, while some are designed at an inclined angle to meet the architectural requirements. A zero-tensile strength concrete material model (*Concrete01*) was used for infilled concrete, and a bilinear steel model (*Steel01*) was used for both steel cover plates and longitudinal rebar.

- Beams exist in the primary and secondary lateral force-resisting systems, and have wide-flange sections. The original ETABS model only considered beams in the lateral-force resisting system, and beams in the gravity-only load resisting systems were not explicitly modeled. However, the weights of gravity beams were accounted for by distributed uniform slab loading and lumped seismic nodal masses. Displacement-based nonlinear beam–column elements with fiber sections were used for beams. The mesh for different section types followed these of wide-flange column sections [Figure 9.6(b)].

The axial-bending interaction of these sections could be captured by the fiber model, whereas the shear or torsional yielding were not considered in this study for simplicity. For concrete-filled sections, the contributions from steel plates to shear or torsion capacities were not included considering their relative small contributions.

The first three elastic modal periods are 6.19 sec (X-translation), 5.89 sec (Y-translation), and 3.51 sec (rotation about the Z-axis). Modal participation factors are 69% and 72% for the first mode and second mode, respectively.

(a) Concrete-filled tube section   (b) W-section
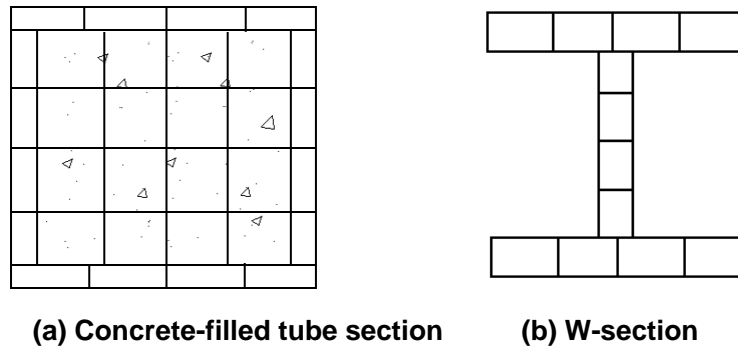
Figure 9.6   Illustration of typical sections and discretized fiber element

9.3   SEISMIC ASSESSMENT OF BUILDING RESPONSE

Nonlinear response history analysis was conducted to better understand the seismic behaviors of the case-study building. Eleven two-component ground motion records under MCE$_R$ hazard level were selected based on a target CMS at long periods; see Section 9.2.4.

9.3.1 Global Response

The distributions of the peak story drift ratios over the height of building at MCE$_R$ hazard are shown in Figure 9.7 for both horizontal directions, including eleven analyses results (blue solid lines representing the median values). The peak drift ratios increased steadily from floors 1 to 10, becoming more uniform above floor 10. No observable weak-story trend was found for the X-direction, where the peak median drift was about 1.1% at floor 56. However, in Y-direction, a larger dispersion was observed at floor 40, and the median value was around 1.1%.

The floor acceleration distributions indicated that the peak accelerations were larger for stories below level 40; see Figure 9.8. The peak median values were quite uniform throughout floor levels, in the order of 0.2g. Nevertheless, a larger dispersion was seen at Y-direction at floors below 12, with a maximum value approaching 0.55g.

In general, the building exhibited a stable, predictable response under MCE$_R$ level excitations. The global responses indicated that the structural has a low probability of collapse and is capable of meeting the basic performance objectives per ASCE 7 [2010] for a risk category III building.

(a) X-dir. (b) Y-dir.
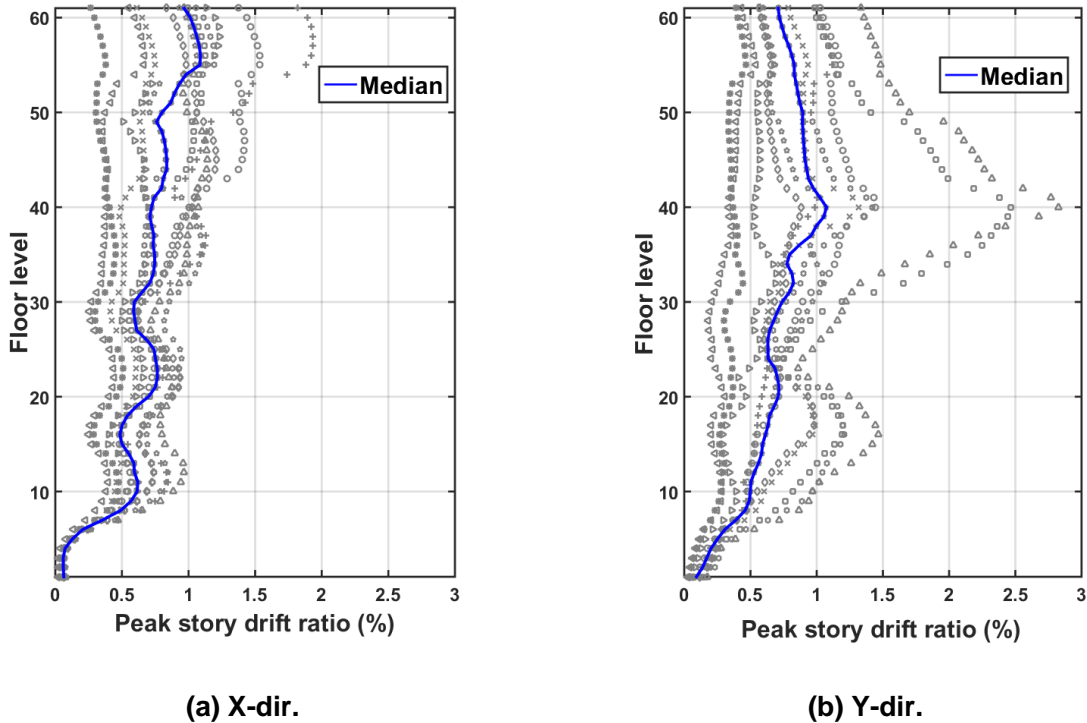
Figure 9.7   Distribution of peak story drift ratios

(a) X-dir.   (b) Y-dir.
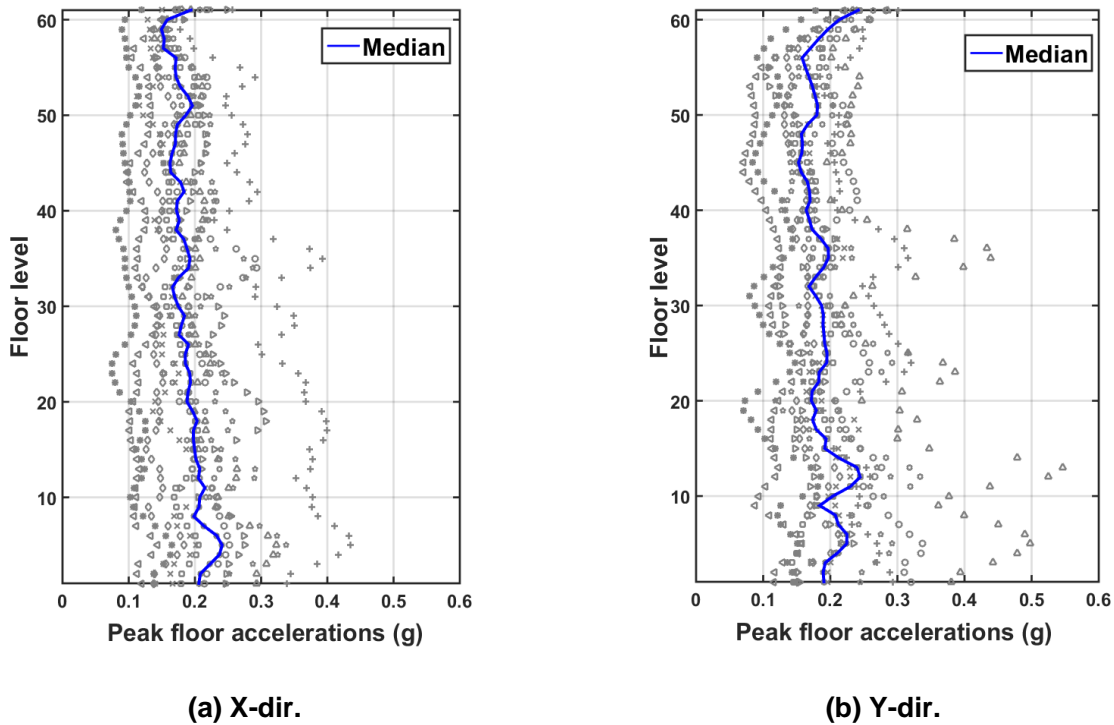
Figure 9.8   Distribution of peak floor accelerations

9.3.2   Local Response

To more closely examine the structural responses, a few elements were selected, including representative columns and buckling restrained braces (BRBs) at different floor levels.

Three columns along a column line in the southeast corner of the building are selected for this investigation, which are located at floor levels 1, 30, and 50, respectively. Their response considering combined axial-bending (*P-M*) interactions were examined; see Figure 9.9. The column at floor 1 used reinforced concrete, whereas other two (located at floor 30 and 50) used concrete-filled steel tubes. The *P-M* interaction capacity diagram of selected column members are identified in red in Figure 9.9, which were estimated using the program: XTRACT (Version 3.0.9) [TRC Inc. 2015]. The seismic demands under one ground motion input are designated in blue. The reinforced concrete column at the base of the simplified case-study building showed inadequate capacity in tension and was thus insufficient to resist combined tension and bending loading; see Figure 9.9 (a). Other two selected columns located on a middle or an upper floor, displayed adequate capacity to avoid yielding.

Three mega braces at the exterior of the building, which span from floor level 7 to 15, 31 to 39 and 54-61, were investigated. They are located in either *X*- or *Y*-direction, and are buckling restrained. The relative shear deformations between floor 7 and 15 and 54 and 61 in *X*-direction was small, and, consequently the selected BRB at these floor ranges remained elastic essentially during the earthquake excitation, although a slight yielding was observed [Figure 9.10 (a) and Figure 9.10 (c)]. However, larger deformations were seen around floor level 40 in the *Y*-direction

201

(Figure 9.7), which corresponded to a significant yielding of a BRB spanned from floor 31 to 39; see [Figure 9.7 (b)].
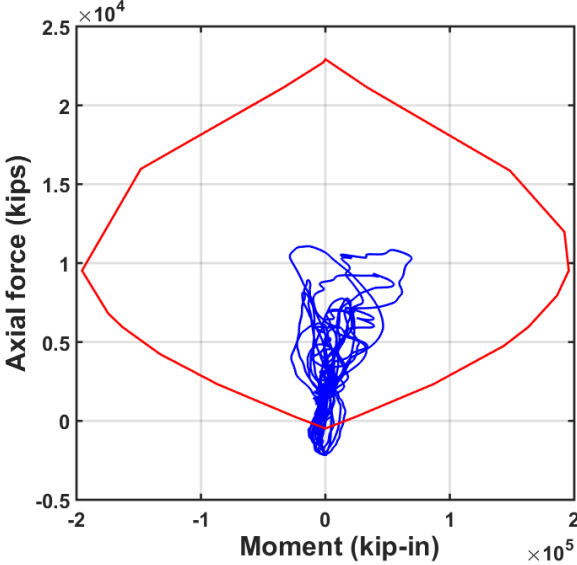
(a) Floor 1
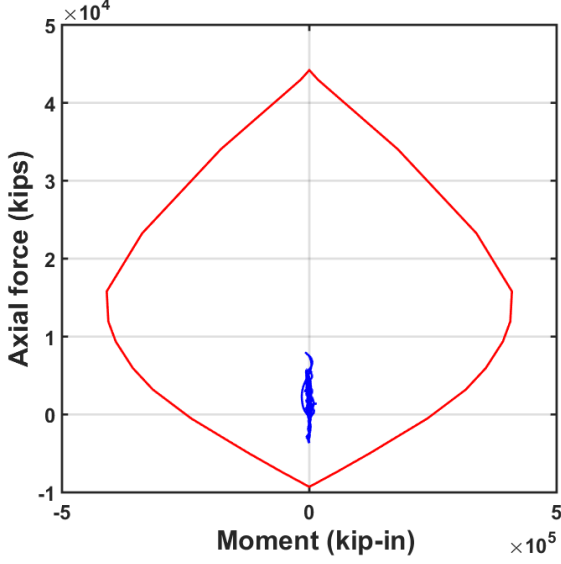
(b) Floor 30
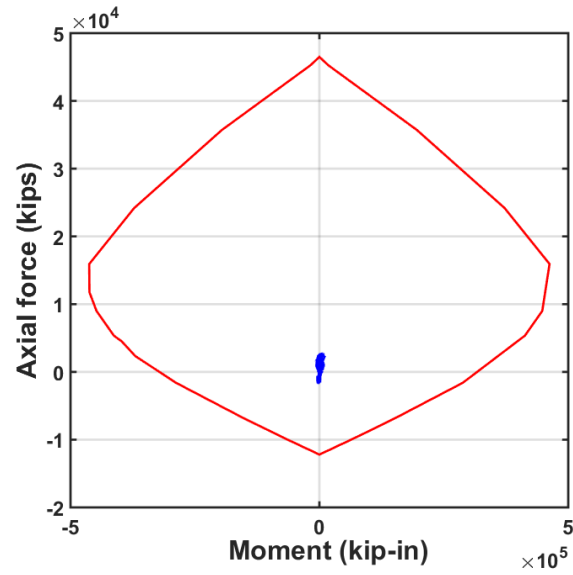
(c) Floor 50

Figure 9.9   Column P-M relations under one selected ground motion (GM8)

(a) Floor 7-15

203
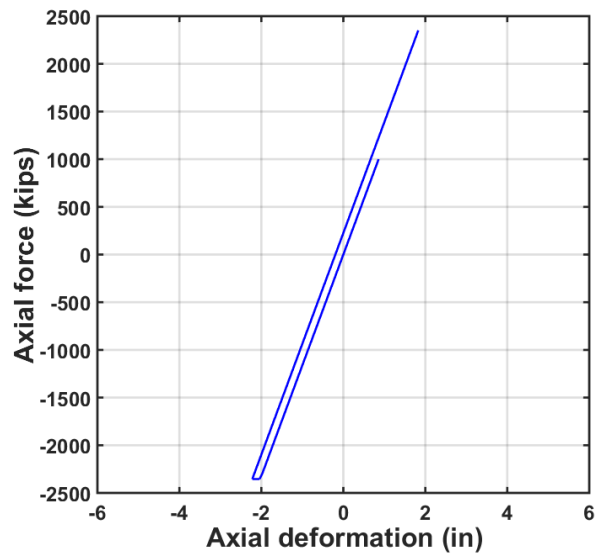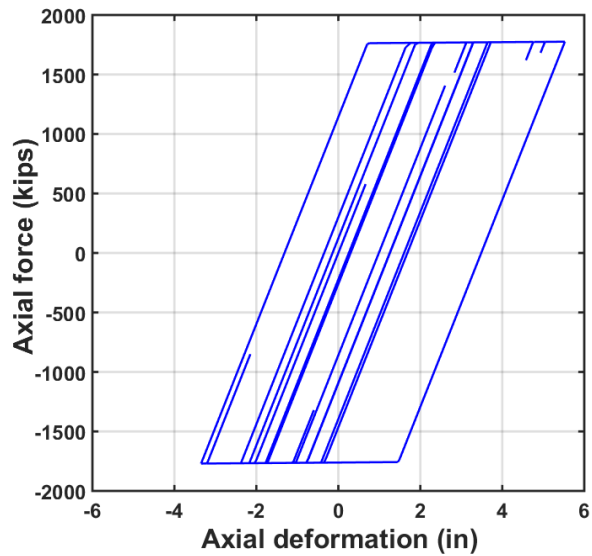
(b) Floor 31-39
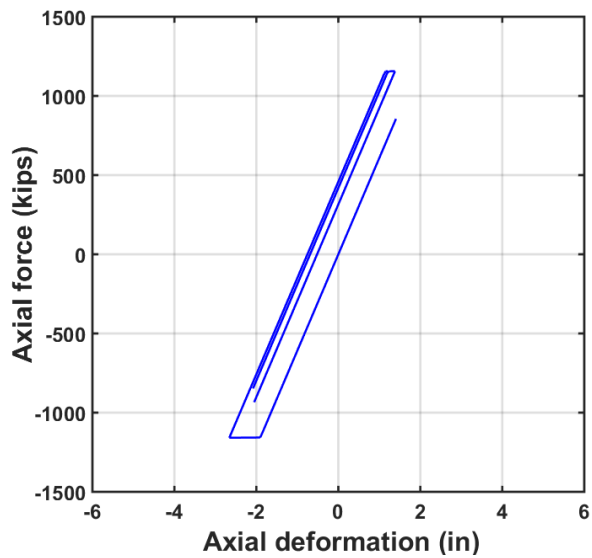
(c) Floor 54-61

Figure 9.10   BRB axial hysteresis loops under one selected ground motion (GM8)

9.4   IMPROVE STRUCTURAL PEFRORMANCE WITH FLUID VISCOUS DAMPERS

Evaluating the seismic performance of the case-study building indicated that the building complies with the performance objectives suggested by ASCE 7-10, with a low probability of collapse under a MCE$_R$ event. Yielding was exhibited at columns of the base floor and BRBs at most deformed stories under a MCE$_R$ hazard event. However, ensuring life safety does not

necessarily avoid extensive structural damage, and nonstructural failure; repair work is usually inevitable and contributes to a great amount of economic loss.

As such, an improved design that targets at enhancing seismic resilience and reducing economic loss after an earthquake event was explored. A method utilized FVDs was explored in terms of enhancing its seismic performance. Selecting damper locations and design parameters were carried out, and one trial design was proposed to investigate the efficacy of this method.

9.4.1 Damper Locations

In Section 4.3.5, a method based on an equivalent frame model [Kasai *et al*. 2002 and 2006] was used to identify effective locations in which to install dampers. This building utilizes a mega-frame brace as its lateral force-resisting system, and larger deformations were found at upper stories (Figure 9.7). As such, dampers are expected to be more effective if located at floor levels above 20. Following a same procedure outlined in Section 4.3.2, K_R^i / K_N^i ratios were identified for different mega-brace locations; see Table 9.4. The bottom seven floors have the largest original stiffness and thus are not considered as effective damper locations. The improvement of stiffness from state *N* to state *R,* at floor level 7 to 19 were not as significant as that for upper stories in both *X*- and *Y*-directions. Consequently, the floors with the largest K_R^i / K_N^i ratios were selected to install dampers, as indicated in grey in Table 9.4. FVDs were installed in parallel with mega braces and distributed across several bays, as indicated in colored lines in Figure 9.11. Each of the floor ranges had eight dampers in both directions.

Table 9.4   Calculations of frame parameters

Story	X-direction			Y-direction		
	K_N^i (k/in)	K_R^i (k/in)	K_R^i / K_N^i	K_N^i (k/in)	K_R^i (k/in)	K_R^i / K_N^i
1-7	16405.0	19251.7	1.2	13015.5	11305.8	0.9
7-15	1908.9	14567.8	7.6	2845.0	7455.2	2.6
15-19	4720.9	36912.4	7.8	5135.6	23006.5	4.5
19-27	1472.2	24884.2	16.9	2065.7	12774.8	6.2
27-31	5013.7	39924.5	8.0	3885.5	19945.9	5.1
31-39	1748.1	22083.9	12.6	1420.0	11092.3	7.8
39-43	3453.1	31600.2	9.2	2563.5	16536.5	6.5
43-50	3897.2	33267.1	8.5	2073.7	15121.5	7.3
50-54	1954.2	11426.2	5.8	1655.3	7477.8	4.5
54-61	679.6	9206.3	13.5	521.9	3704.6	7.1

Note: shaded boxes are selected locations to install dampers
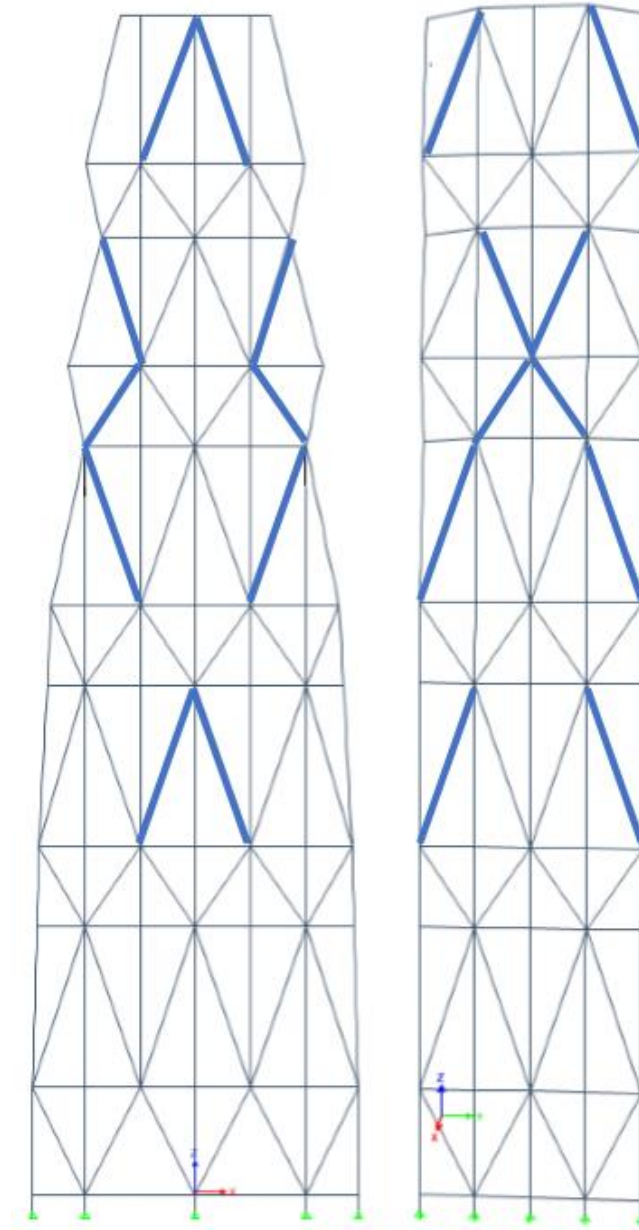
Figure 9.11   Selected locations to install fluid viscous dampers

9.4.2 Design parameters of FVDs

Several design parameters need to be characterized for FVDs installed in a high-rise building; see detailed discussions in Chapter 4. Considering a variety of parameters and a wide range of each of these variables, this study used a same procedure as that in Chapter 8, that is, selecting the damping constant C and their story-wise distributions as the design variables for the automated optimization design. Other mechanical properties of FVDs were selected prior to the automated procedure based on previous knowledge, as summarized below:

- Nonlinear FVDs with a damping exponent α equaling to 0.5 were used in this study. A sensitivity study in Section 4.4.2 of this dissertation indicates that a range of α between 0.2 to 0.5 was effective in controlling structural response, while also limiting the peak damper force for a high-rise steel building. The reason for selecting a relatively large value in this range is to ensure a larger phase angle between the velocity-dependent FVD and the displacement-dependent BRB, so that a FVD and a BRB could, in turn, take effect and active the energy dissipation mechanism in a longer duration. A better choice of α is possible but would require more detailed sensitivity study of this building.

- The stiffness of driving braces K_b was sized based on findings of Section 4.4.3, that demonstrated that the brace in series with a FVD should have a stiffness on the order of twice as that of the lateral force-resisting frame to insure adequate damper deformation. This finding, applied in the case-study building where FVDs are installed across multiple stories, is equivalent to having driving braces with stiffness equal to twice the multi-story stiffness provided by the mega braces across the same levels. Considering that the exterior mega-BRBs are the main lateral force-resisting system in this building, an assumption was made that the total lateral stiffness provided by these BRBs of the same direction represent multi-story stiffness; thus, K_b are sized accordingly.

9.4.3 Trial Design Scheme

The effectiveness of using FVDs as a means of improving the structural performance of the case-study building was examined through a trial scheme. A total of 40 FVDs were used; the distributed locations are illustrated in Figure 9.11. Selection of the damping exponent α and driving brace stiffness K_b were discussed previously; the damping constants C at different floor levels were the major parameters considered in this study. For a preliminary design, a list of C, ranging from 1000 to 2500 kip (sec/in.)$^{0.5}$ was used, which resulted in an approximate 10% damping based on Eqn. (4.6); see Table 9.5 for a detailed C value of each FVD. Global and local response of the bare frame and the building with FVDs were compared.

The distributions of the peak maximum displacements are compared in Figure 9.12 for the two scenarios. All eleven NRHA results are shown as dots, and the median values are indicated by solid lines. The blue represents the bare frame, and the red indicates the building after installing FVDs. In this proposed damper design, a majority of dampers were located at floor levels above 30. As such, no observable reductions of peak displacements were shown at lower part of the building compared with the building in its as-built condition, whereas a 20% reduction was observed from floor levels 30 and above. Both directions showed a similar trend. A clearer demonstration is through the distributions of peak story drift ratios (Figure 9.13): FVDs helped reduce the drift ratios by 30% – 40%. In the *Y*-direction, a larger reduction was seen at floor levels above 35.

The additional damping was ineffectual in controlling peak floor accelerations; see Figure 9.14. The FVDs contributed less than 10% toward reducing the accelerations as an overall trend; at floor levels 30 to 50 in *Y*-direction they were relatively more efficient, reducing peak floor accelerations by 20%. Stories without FVDs did not show any observable reduction.

The effect of dampers was further examined by discretizing the shear forces into those resisted by the main frame and additional dampers. The time history of shear forces is plotted in Figure 9.15 under one ground motion excitation for two floors: 20 and 50. For the case with additional FVDs, the contributions to the total shear forces due to dampers (red dashed lines) or main frames (pink dashed lines) were identified. The total shear forces were almost identical under the two scenarios, but the forces in the main frame were reduced slightly. The maximum damper forces at peak of each cycle were about 20% – 30% of the maximum forces; but these peaks occurred at different times. The observed phase lag between the maximum damper force and the maximum total force was larger at initial cycles with large pulses. Additionally, it was also noted that the building with FVDs decayed more rapidly than otherwise.

The maximum damper force required was checked. The median of the peak damper force is shown in Figure 9.16, indicating a need for fairly large dampers. The peak force ranged from 1600 kips to 3100 kips in this mega-brace system. Considering the difficulty in manufacturing mega dampers, an alternative would be to use multiple smaller dampers in parallel for each mega-brace to provide a same force capability. To estimate the initial damper cost, it was assumed that several smaller dampers would be used to represent one large damper. Based on the damper price quote listed in Table 6.6, the initial damper cost was estimated to be $4 million for this design scheme. This value, when compared with the total project cost of the original building (about $1.6 billion for the original case-study building), is insignificant, especially when considering that the dampers are likely to significantly reduce economic losses after a major earthquake event.

Table 9.5   Parameters of FVDs

Story level	19-27	31-39	39-43	43-50	54-61
C $kip{\cdot}(sec/in)^{0.5}$	2000	1500	1500	1000	1000
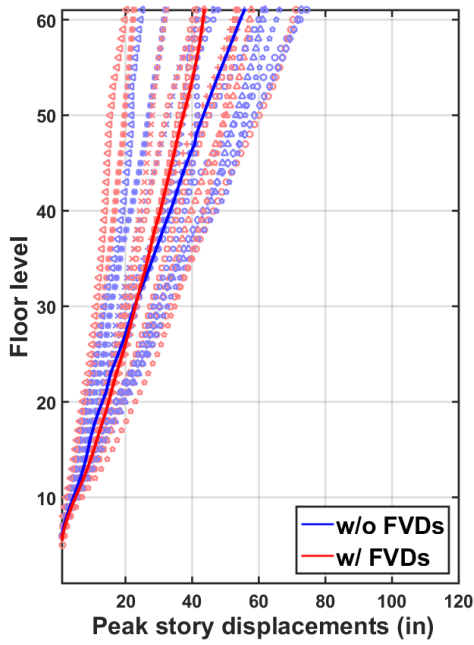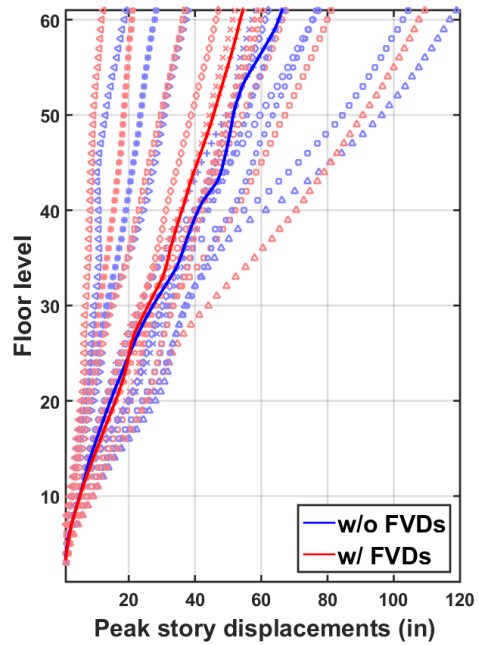
(a) X-dir. **(b) Y-dir.**

Figure 9.12   Distribution of peak story displacements
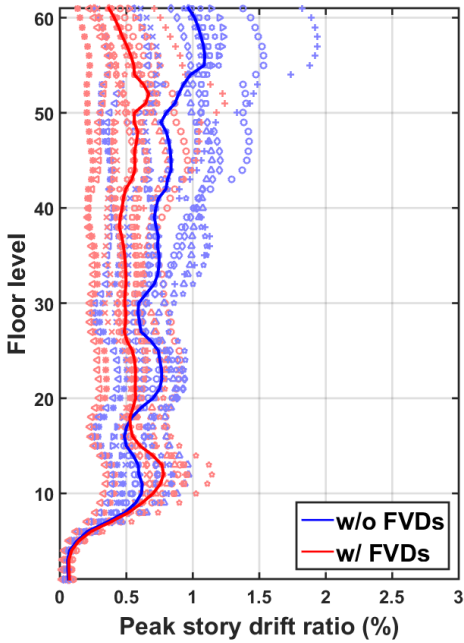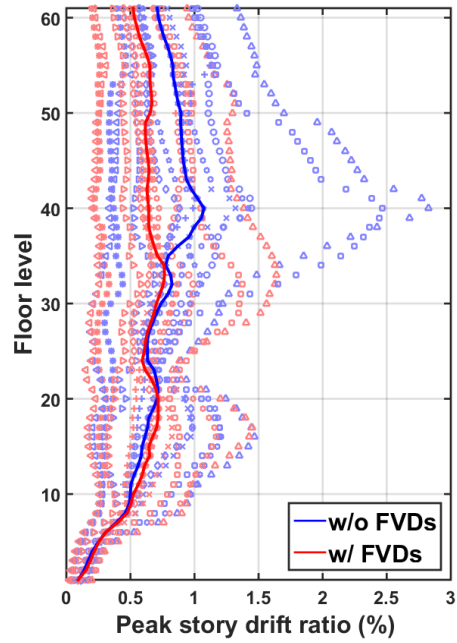
(a) X-dir. **(b) Y-dir.**

Figure 9.13   Distribution of peak story drift ratios

209
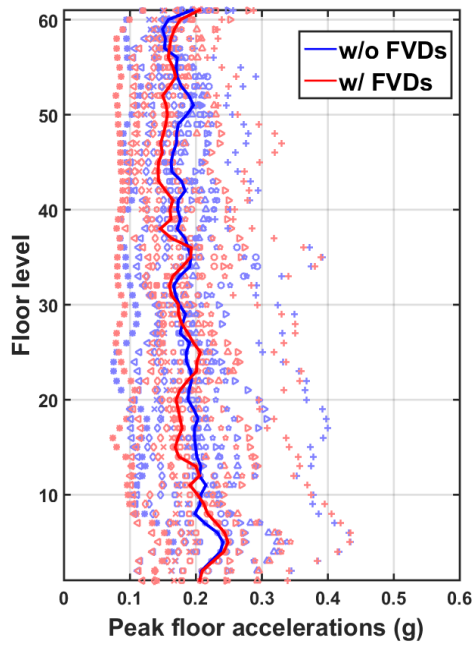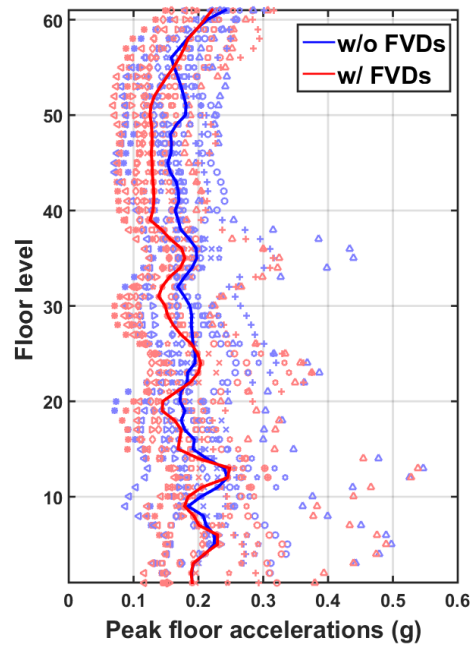
(a) X-dir.   (a) Y-dir.

Figure 9.14   Distribution of peak floor accelerations
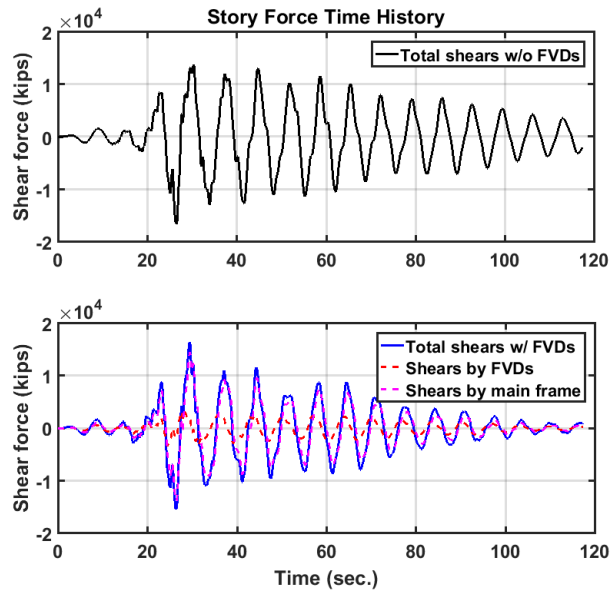
(a) Floor 20
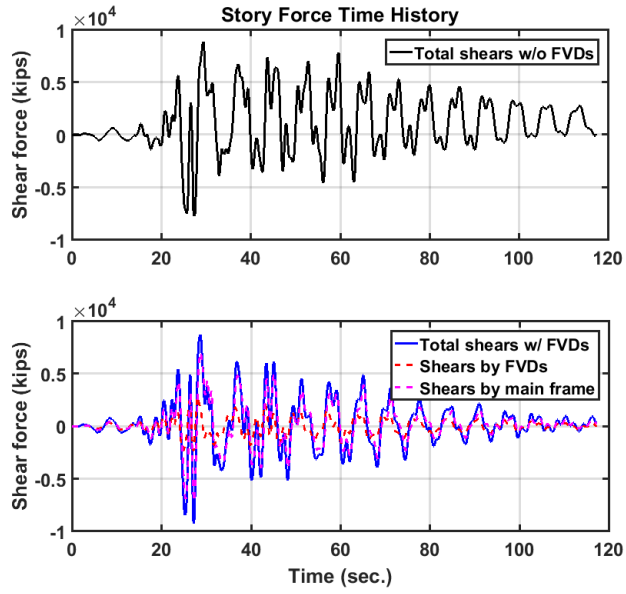
(a) Floor 50

Figure 9.15   Time history of story shear forces under one selected ground motion (GM8)
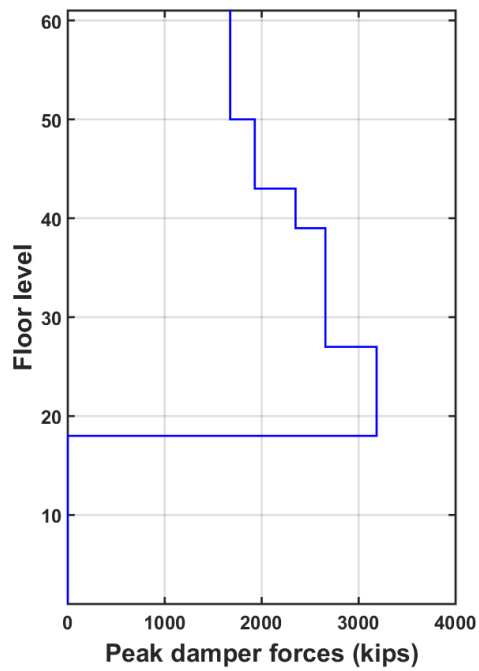
Figure 9.16   Distribution of peak damper forces

9.5 AUTOMATED DESIGN PROCEDURE

9.5.1 Optimization Problem Design

A same procedure as that outlined in Chapter 8 was used to set up the automated optimization design of FVDs for this new tall building. Objective function, constraint functions, and decision variables were selected in a same manner, with slight modifications from the existing building case. The optimization objective is to enhance the seismic performance of the case-study building under a MCE$_R$ hazard event. Eleven ground motions at this hazard level were used, as discussed in Section 9.2.3, and the median results were used in the objective function and constraint functions.

Objective function

As was done previously, two types of objective functions were investigated: a single EDP and a EDP-DV function. Chapter 8 proposed using a "backward" strategy to construct the EDP-DV functions of the entire building based on results obtained from loss and damage estimates. In this chapter, however, given that no holistic damage and loss estimates were performed previously, a "forward" process is more appropriate for the purpose of this study. Since the functionality of the building differs over floor height, constructing a story-specific loss function to account for this discrepancy seems more appropriate. As such, two story-specific EDP-DV functions were proposed for an office floor loss and a residential floor, respectively. The procedure was based on fragility curves of structural, nonstructural, and contents, and their consequence functions provided in PACT fragility specification manger [FEMA 2012c]. The fragility curves were assumed log-normally distributed.

To develop an EDP-DV function, the intermediate step of damage analysis is compensated for by integrating the fragility and consequence functions of all components of concern [Ramires and Miranda 2009]. The fragility information of each component at different damage states were consolidated to obtain the expected repair cost; see Eqn. (9.1). Considering that collapse is not likely for this building under a MCE$_R$ hazard event, the expected loss was conditioned on non-collapse status only.

$$E[L_j \mid EDP_k] = \sum_i E[L_j \mid DS_i] \times P[DS = ds_i \mid EDP_k] \tag{9.1}$$

where L_j is the loss of jth component; EDP_k: EDP k; DS_i: i^{th} is the damage state; $E[L_j \mid EDP_k]$ is the expected loss of jth component conditioned on EDP_k; $E[L_j \mid DS_i]$ is the expected loss of jth component under damage state i; and $P[DS = ds_i \mid EDP_k]$ is the probability of jth component having damage state DS_i with respect to EDP_k.

The total expected story loss is the summation of all individual component losses for an entire story of the building:

$$E[L_{story} \mid EDP_k] = \sum_j E[L_j \mid EDP_k] \tag{9.2}$$

212

where $E[L_{story} | EDP_k]$ is the expected loss of a story with regard to EDP_k.

The structural, non-structural components, and contents and their quantities were estimated based on the normative quantities suggested by FEMA P-58 [FEMA 2012c] and area of each floor. The office floors (below level 43) have a combined exterior mega-framed brace and interior moment frames as major structural systems. Therefore, the structural components considered in this study were selected based on these two systems, e.g., the moment frame connections and BRBs. Nonstructural components considered included exterior curtain walls, interior finishes, and HVAC systems. Contents such as desks, computers, and bookcases contribute a great deal to the total cost of offices and are fully accounted for. Tables 9.6 lists all performance groups (PG) considered for an office floor.

The residential floors are designed to be upscale condominiums; therefore, their nonstructural components are more expensive to replace compared to that found in a typical office floor. For example, superior marble interior finishes and high-quality fire protection covers are used in each apartment, which would significantly increase the replacement cost. Other non-structural components, such as exterior curtain walls, partition walls, HVAC system and electric systems, were also included in this study. The main structural system of residential floors consists of an exterior bracing system and interior intra-nodal trusses. See Table 9.7 for PGs considered for a residential floor.

The PGs were divided into three parts: PG1, which is the drift sensitive structural performance group; PG2, which is the drift sensitive non-structural performance group; and PG3, which is the acceleration sensitive non-structural performance group. Each PG contains one EDP-DV function. Consequently, three EDP-DV functions were developed for an office floor and a residential floor, respectively.

As noted, the simplified case-study building under investigation is based on an actual project in downtown San Francisco, with a total cost is estimated to be $1.6 billion according to *San Francisco Business Times* [Kilpatrick 2016] for the original building. To obtain a rough estimate for the cost of each floor, it was assumed that the modified structure in this study has a same value as the original one, and floors have the same functionality (e.g., office and residential use) with identical costs. Since a residential floor is likely to be more expensive than an office floor, a total construction cost of $25 million was assumed as an office floor cost, and $30 million as the residential floor cost. The average floor areas for office levels and residential levels, respectively, were used when selecting the quantities of each PG.

Each floor cost was further disaggregated into contributions from different PGs based on a database developed by Taghavi and Miranda [2003]. The database considers difference in various functionalities, e.g., the cost for structural components, nonstructural components, and contents, which constitute 18%, 62%, and 20% of the total cost for an office building, but 13%, 70% and 17% for a hotel. Taghavi and Miranda [2003] also found that by breaking down the cost of nonstructural components, mechanical systems and interior constructions were found to be the most expensive items regardless of the type of building. Table 9.6 and Table 9.7 list PGs considered for an office floor and a residential floor, respectively, including the EDP each PG is sensitive to and the normalized cost (percentage of repair cost to the total floor construction cost) of every PG. The fragility information in PACT is not exhaustive. Thus, estimates were needed

to fill the missing information. One major assumption was that the expected loss of computers at different damage states, which were estimated based on a price range found at different stores.

The resulted EDP-DV functions are presented in Figure 9.17 and Figure 9.18. The *Y*-axis denotes the expected damage loss of that floor, which is normalized by the initial floor construction cost. Clearly, the PG_3 constituted a large portion of the total floor value, and damage of these components would likely induce a significant economic loss after an earthquake event. The normalized loss for PG_3 increased quickly at an acceleration level of 0.4*g*, but stabilized when the acceleration reaches 4.0*g*. The two drift sensitive groups—PG_1 and PG_2—had similar sensitivity to drift ratios. PG_1 contributed a smaller portion to total loss when the drift ratio was smaller than 3.0%, but this trend was reversed when the drift ratio exceeded 3.0%. The losses saturated around 0.20 and 0.15 for PG_1 and PG_2, respectively.

Likewise, for a residential floor, PG_3 possessed the most valuable components and contents. Therefore, it was most likely to contribute to the total loss, especially when the floor acceleration became large. The total normalized loss reached 0.76 when the floor acceleration was larger than 5.0*g*. The damage sensitivity of PG_1 and PG_2 to the story drifts were close, and both reached a loss of 0.11 when the drift ratio was about 6.0%. Nevertheless, a large discrepancy was seen between these two groups when the drift ratio was smaller than 4%. Note: the curves in Figure 9.17 and Figure 9.18 only present the drift ratio up to 6%, and the acceleration up to 6.0*g*; it is unlikely that either of these values would be exceeded in this building.

Table 9.6   Performance groups considered for an office floor

Performance group	Seismic sensitive EDP	Normalized cost	
B. SHELL			
B10 Superstructure			18%
Bolted shear tab gravity connection	DR	1.3%	
Buckling restraint braces	DR	5.4%	
Special concentric braced frame with WF braces	DR	3.8%	
Post-Northridge welded steel moment connections	DR	7.5%	
B20 Exterior enclosure			10%
Curtain wall	DR	5.4%	
C. INTERIORS			16%
C10 Interior construction			
Wall partition	DR	2.4%	
C20 Stairs			
Stairs	DR	1.0%	
C30 Interior finishes			
Wall partition finishes	DR	0.1%	
Raised access floor	Accel	0.2%	
Suspended ceiling	Accel	5.2%	
Recessed lighting in suspend ceiling	Accel	0.8%	
Floor covering	Accel	6.3%	

D. SERVICES			
D10 Conveying			7%
Traction elevators	Accel	7.0%	
D20 Plumbing			2%
Cold & hot water service	Accel	1.1%	
Sanitary waste piping system	Accel	0.9%	
D30 HVAC			15%
HVAC steel sheet metal	Accel	2.5%	
HVAC drops	Accel	4.0%	
Variable air volume	Accel	8.5%	
D40 Fire protection			3%
Fire sprinkler water piping	Accel	3.0%	
D50 Electrical			9%
Electrical service	Accel	3.0%	
Emergency light & power system	Accel	6.0%	
E. EQUIPMENTS & FURNISHINGS			
E20 Furnishings			20%
Modular office work station	Accel	5.8%	
Vertical filing cabinet	Accel	1.3%	
Bookcases	Accel	1.6%	
Computers	Accel	11.3%	

$$\sum = 100\%$$

Table 9.7   Performance groups considered for a residential floor

Performance group	**Seismic sensitive EDP**	**Normalized cost**	
B. SHELL			
B10 Superstructure			13%
Bolted shear tab gravity connection	DR	1.6%	
Buckling restraint braces	DR	3.6%	
Special concentric braced frame with WF braces	DR	2.6%	
Post-Northridge welded steel moment connections	DR	5.2%	
B20 Exterior enclosure			5%
Curtain wall	DR	5.0%	
C. INTERIORS			20%
C10 Interior construction			
Wall partition	DR	3.7%	
C20 Interior construction			
Stairs	DR	2.3%	
C30 Interior finishes			
Wall partition finishes	DR	0.7%	
Floor covering	Accel	5.3%	
Suspended ceiling	Accel	7.7%	
Pendant lighting	Accel	0.3%	
D. SERVICES			

D10 Conveying			4%
Elevators	Accel	4.0%	
D20 Plumbing			3%
Cold water service	Accel	0.5%	
Hot water service	Accel	1.2%	
Sanitary waste piping system	Accel	1.3%	
D30 HVAC			25%
Chiller	Accel	5.0%	
Compressor	Accel	1.5%	
HVAC steel sheet metal	Accel	2.5%	
HVAC drops	Accel	3.5%	
Variable air volume	Accel	8.5%	
Air handling unit	Accel	4.0%	
D40 Fire protection			5%
Sprinkler water supply	Accel	5.0%	
D50 Electrical			8%
Electrical service	Accel	3.0%	
Emergency light & power system	Accel	5.0%	
E. EQUIPMENTS & FURNISHINGS			
E20 Furnishings			17%
Home entertainment equipment	Accel	9.6%	
Electronic equipment	Accel	3.9%	
Bookcases	Accel	1.6%	
Computers	Accel	1.9%	

$$\sum = 100\%$$
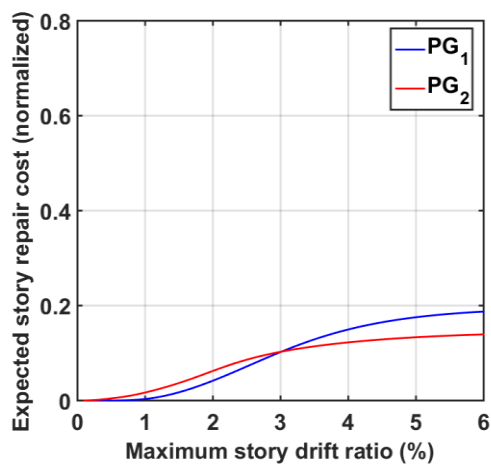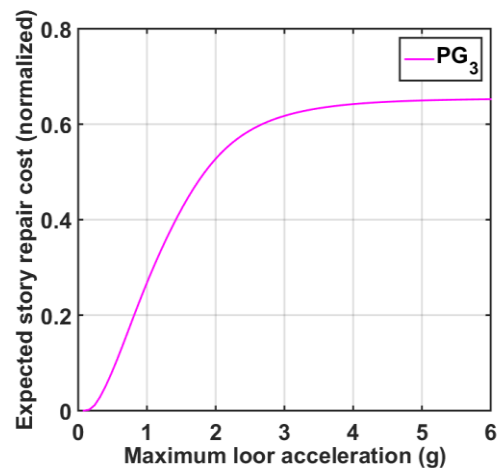
(a) Story drift-sensitive PGs   (b) Acceleration-sensitive PGs

Figure 9.17   EDP-DV functions of an office floor

216
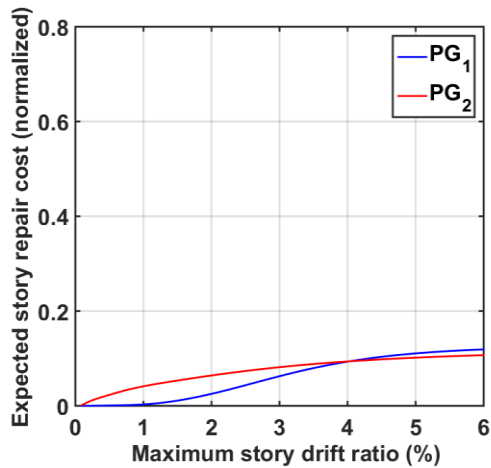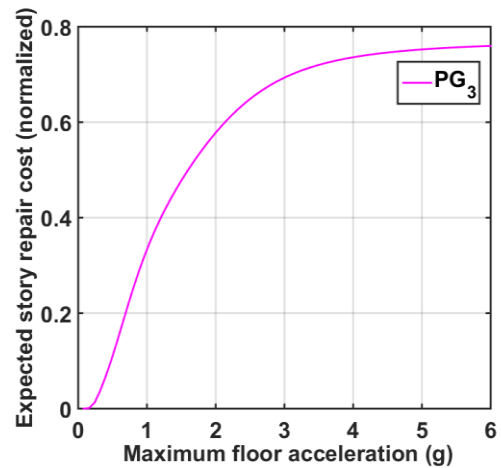
(a) Story drift-sensitive PGs **(b) Acceleration-sensitive PGs**

Figure 9.18   EDP-DV functions of a residential floor

Constraint functions

Four constraints were used that align with the specific performance levels under a MCE$_R$ seismic event:

- Average peak story drift ratio $< 0.8\%$;
- Average peak floor acceleration < 0.3 g;
- Maximum damper force < 3000 kips;
- Maximum damper stroke < 5.0 in.

Design variables

Damping constant C at selected damper installation locations were selected as the design variables. The dampers connected with the mega braces at floor levels 31-43 use an identical damper size considering their close responses; floors 43-50 and 54-61 use another design variable. Two horizontal directions were considered separately for a total of six design variables for this study; see Figure 9.19. Without any preliminary efforts to narrow down the damper selection, the optimization process selects a wide range for each design variable, as listed in Table 9.8.
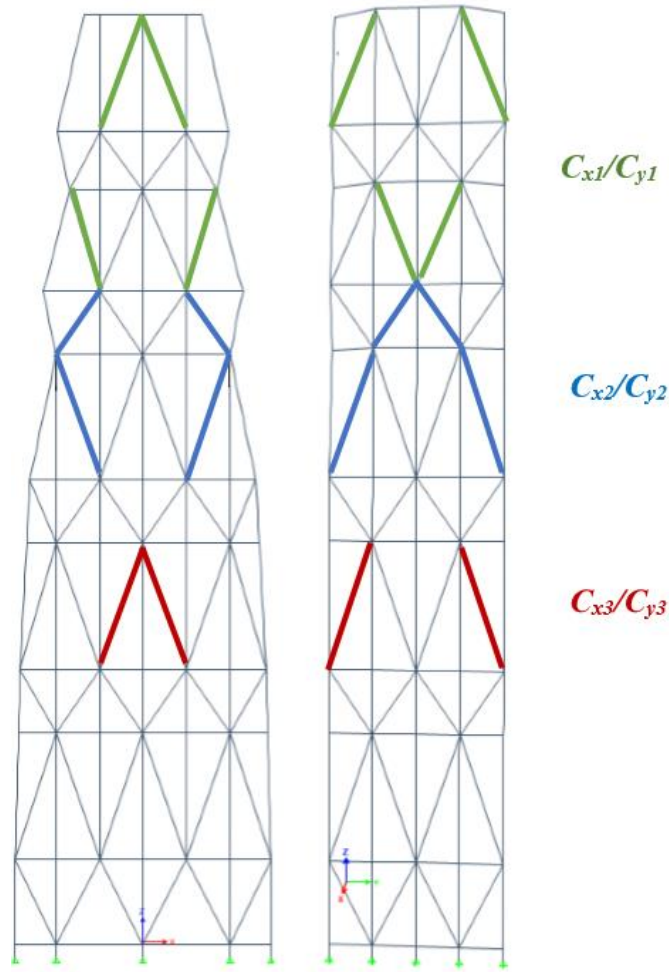
Figure 9.19   Distributions of design variables (damping constant *C*) over story height

Table 9.8   Initial value and range of design variables

Design variable	Cx_1 $kip·(sec/in.)^{0.5}$	Cy_1 $kip·(sec/in.)^{0.5}$	Cx_2 $kip·(sec/in.)^{0.5}$	Cy_2 $kip·(sec/in.)^{0.5}$	Cx_3 $kip·(sec/in.)^{0.5}$	Cy_3 $kip·(sec/in.)^{0.5}$
Initial value	200	200	200	200	200	200
Range	[500, 6000]	[500, 6000]	[500, 6000]	[500, 6000]	[500, 6000]	[500, 6000]

9.5.2 Case Studies Using a Single EDP as the Objective Function

Case 1: Maximum of the peak story drift ratios as objective function

The maximum of the peak story drift ratios was selected as the objective function for this investigated case. The maximum responses of *X*- and *Y*-directions at each iteration were selected for results reported below. The objective function was evaluated over six iterations (red dots) and the points near them (blue line); see Figure 9.20. A gradual decrease of the objective values was observed from the iteration 1 to 4, followed by a slight increase at the fifth and sixth iterations that corrected for exceedance of constraint functions. The efficiency of optimization reduced after the fourth iteration due to imposed constraints, and iteration 6 was selected as a final design that met all constraints.

The successive changes of design variables, distributions of global response, and damper response were investigated for selected three points: the first, fourth, and sixth iterations. The first design distributed dampers uniformly at selected damper locations, which was found inadequate around floor level 40. The damping demands were thus increased at both *X*- and *Y*-directions at following iterations; the increase was much larger in the *Y*-direction (Figure 9.21). This change successfully brought down the peak story drifts by about 20% at floor levels 35 to 50 from iteration 1 to 4 (Figure 9.22), although the reduction in peak floor accelerations was insignificant (Figure 9.23).

Correspondingly, the peak damper forces demand (Figure 9.24) doubled at iteration 4 compared to iteration 1, and the maximum value exceeded the constraint of 3000 kips. Such an exceedance was penalized by reducing the design variables, e.g., C_y at floor level 30 to 50, by about 20% from iteration 4 to 6, whereby the final design (iteration 6) conformed to the target values. Interestingly, this adjustment barely impacted the global structural response from iteration 4 to iteration 6, indicating a trend of saturated damping effect. In terms of the damper stroke, the multi-story configuration spans each damper over continuous four or eight stories, which correspondingly increased the damper stroke by a factor of four or eight compared to a one-story configuration. As such, the aggregated damper stroke demands could be very large if story drifts over these spanned floor levels were generally large, as demonstrated by the peak damper stroke at floor levels 43 to 50 at iteration 4 (Figure 9.25). However, the 5-in limit was satisfied in all designs.

Figure 9.20   Evolution of objective function values

Figure 9.21   Design variables at selected iteration points

Figure 9.22   Distribution of peak story drift ratios at selected iteration points (median of eleven analyses)

Figure 9.23   Distribution of peak floor accelerations at selected iteration points (median of eleven analyses)

Figure 9.24   Distribution of peak damper forces at selected iteration points (median of eleven analyses)

Figure 9.25   Distribution of peak damper strokes at selected iteration points (median of eleven analyses)

Case 2: Maximum of the peak floor accelerations as objective function

This case focused on the maximum of the peak floor acceleration. It revealed that the optimization was insensitive to changes in damper size. As is seen in Figure 9.26, the objective functions were reduced from $0.252g$ at the first iteration to $0.248g$ at the final iteration. The iteration was terminated at the fourth point when the incremental changes of objective functions were smaller than the tolerance. All the constraints were met in the final design. Unlike Case 1

where the peak drift was the objective function, this case required cutting the size of dampers in order to reduce the maximum floor acceleration (Figure 9.27). Both C_x and C_y were reduced from the first iteration to the second iteration, but C_y were increased in subsequent two iterations.

Since the damper size was reduced to optimize the objective function, the peak drift ratios exhibited an obvious increase for those floor levels above 38 (Figure 9.28). In the last iteration, the damper sizes at *Y*-direction increased from floor level 31 to 51, which in turn reduced the peak drift ratios at these floors. The peak floor accelerations (Figure 9.29) were reduced slightly for floor 10 to 15, and 25 to 30. Note that the roof acceleration, which seemed was at the maximum, was insensitive to the changes of additional damping.

The peak damper forces were reduced at different floors from the first iteration to the second iteration but were increased at all floors except at floor level 52 to 61, when reaching the final design (Figure 9.30). The distributions of the peak stroke of FVDs shown in Figure 9.31 had a similar trend with that of the peak story drift ratios (Figure 9.28), and the peak strokes for the final design were barely within the 5-in. limit.

Figure 9.26   Evolution of objective function values

Figure 9.27   Design variables at selected iteration points

Figure 9.28   Distribution of peak story drift ratios at selected iteration points (median of eleven analyses)

Figure 9.29   Distribution of peak floor accelerations at selected iteration points (median of eleven analyses)

Figure 9.30   Distribution of peak damper forces at selected iteration points (median of eleven analyses)

Figure 9.31   Distribution of peak damper strokes at selected iteration points (median of eleven analyses)

9.5.3 Case Studies Using a Story-Based Cost as the Objective Function

Case 3: Story-based repair cost for an office floor as objective function

The story-based repair loss of an office floor based on the three EDP-DV functions obtained in Section 9.5.1 was used in this case. The objective function used the summation of three function values based on the maximum structural responses among office floors from floor 1 to 43.

The evolvement of the normalized floor loss is presented in Figure 9.32, showing a significant improvement from iteration 1 to 3. A 7% reduction was observed from the first iteration to the second iteration; and a 25% reduction was shown from the second to the third iteration. However, the updates were much slower after iteration 3, with only 2% incremental improvements at each successive iteration. The optimization ended when the maximum evaluation time (40) was reached, with iteration 6 being the final design.

Meanwhile, the design parameters at first, third, and sixth iterations are shown in Figure 9.33. C_x were much less effective in limiting damage and costs for the office level, and thus were kept constant over all iterations; C_y were increased continuously at selected iteration points, indicating better control effect of dampers in Y-direction.

A consistent increase of C_y brought down the peak drift ratios, especially at floor levels 35 to 50 (Figure 9.34). The peak drift was initially 0.89% at floor 40, but was reduced to 0.75% at iteration 6; such a reduction was compromised by an increase in drift at several other floors. Incremental reduction of the peak story drift ratios from the iteration 3 to 6 were negligible for most stories expect floor level 38. A corresponding change pattern was observed for the damper peak stroke distributions (Figure 9.37), where a peak reduction was about 15% from level 31 to 50. Peak damper forces increased gradually as the design updated (Figure 9.36). It is interesting to note that the reduced of peak story drift ratios were limited to a few floors where the dampers

226

distributed across different floor levels increased in size. The peak floor accelerations were not influenced much by the update (Figure 9.35). As such, the drift sensitive PGs were more likely to reduce the damage costs of the office floor cost during an earthquake event than the acceleration sensitive PG even though the latter PG constitutes more costly components.
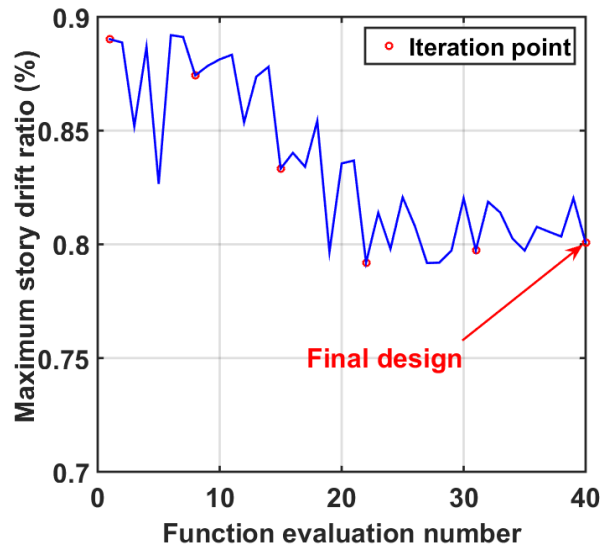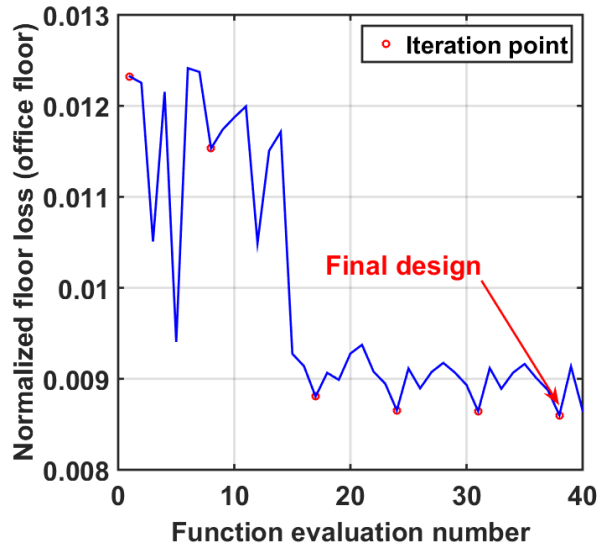

Figure 9.32   Evolution of objective function values
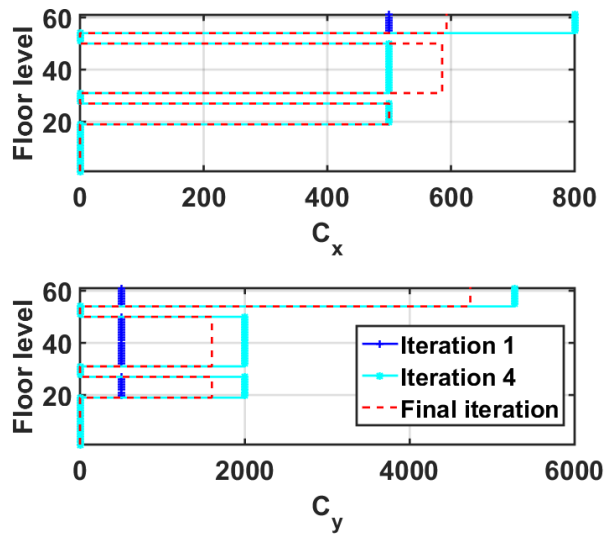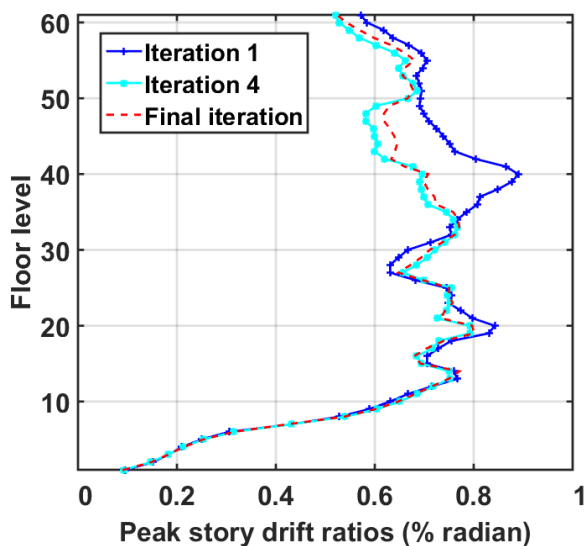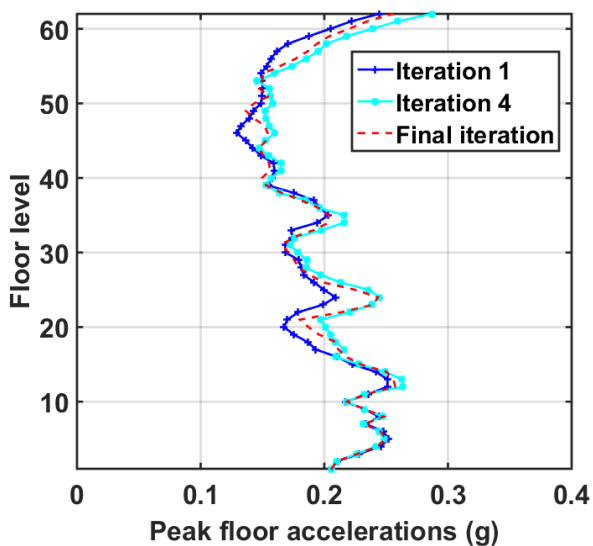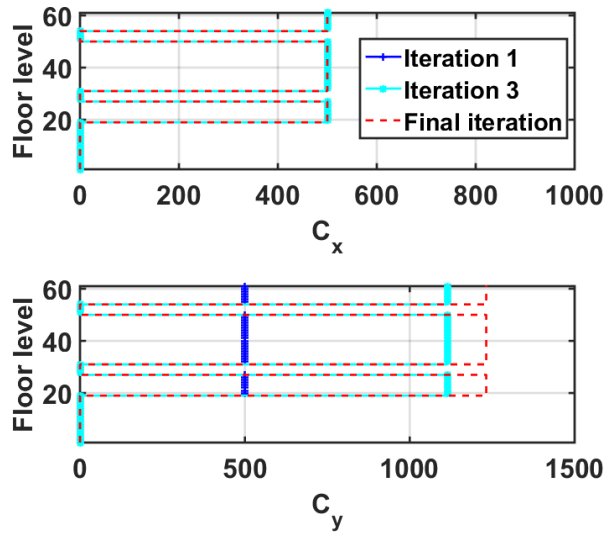

Figure 9.33   Design variables at selected iteration points

227
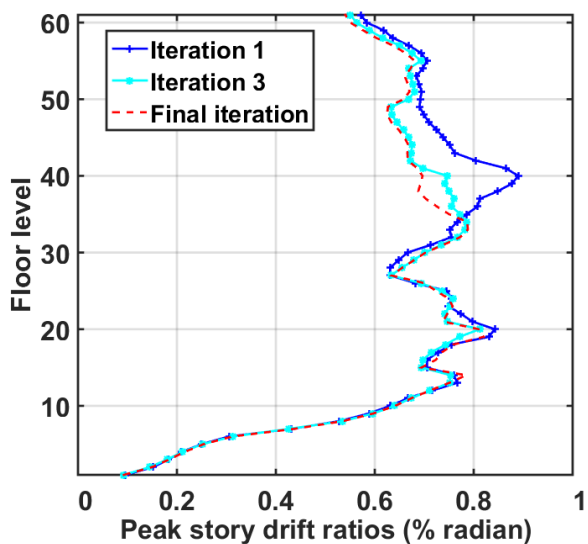
Figure 9.34   Distribution of peak story drift ratios at selected iteration points (median of eleven analyses)
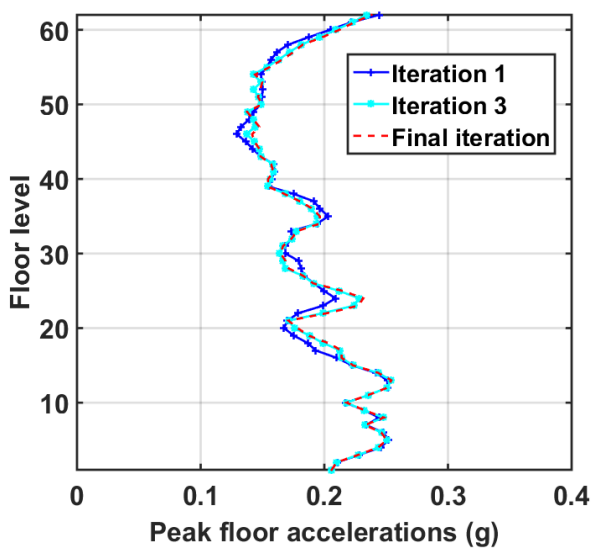
Figure 9.35   Distribution of peak floor accelerations at selected iteration points (median of eleven analyses)
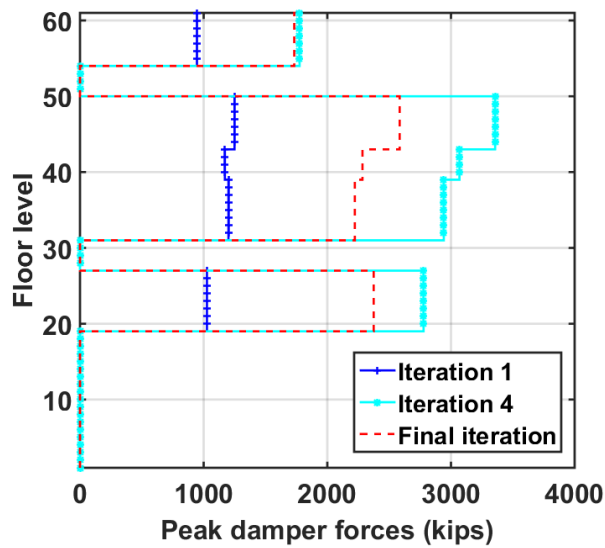
228
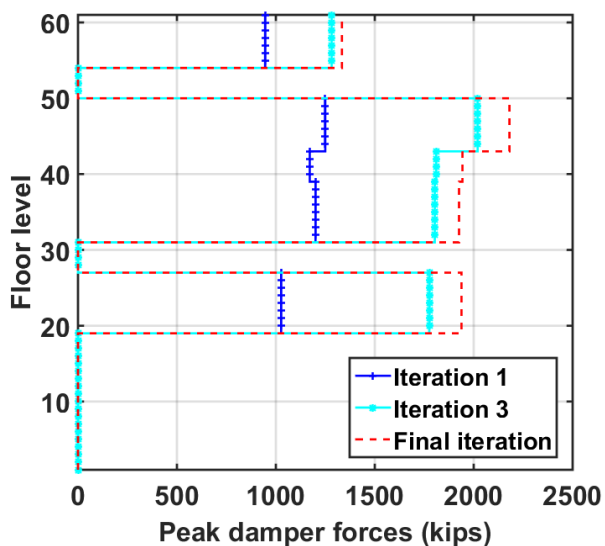
Figure 9.36   Distribution of peak damper forces at selected iteration points
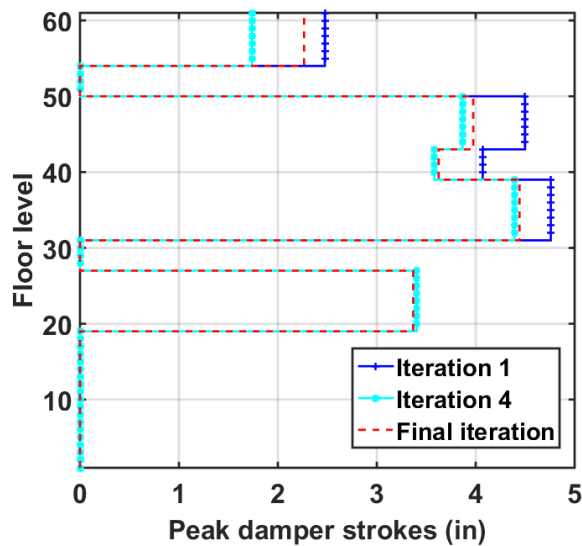(median of eleven analyses)
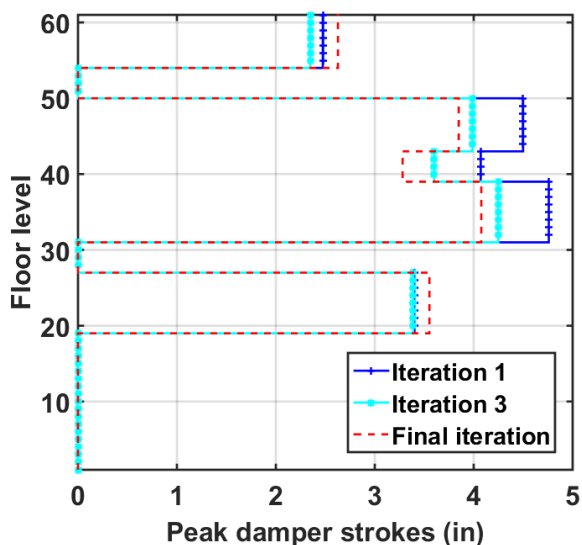
Figure 9.37   Distribution of peak damper strokes at selected iteration points
(median of eleven analyses)

Case 4: Story-based repair cost for a residential floor as objective function

In this case, the likely cost of a residential floor after an earthquake was selected as the objective function. Three EDP-DV functions for a residential floor developed in Section 9.5.1 were used to obtain the objective function.

The objective function was gradually decreased from 0.0317 to 0.0292 over iterations (Figure 9.38), representing an 8% overall reduction. However, a significant increase of C_x and C_y (Figure 9.39) were necessary to achieve this reduction. For example, C_x were increased from 500 kip·(sec/in.)$^{0.5}$ to 2600 kip·(sec/in.)$^{0.5}$, and C_y were increased from 500 kip·(sec/in.)$^{0.5}$ to 5500 kip·(sec/in.)$^{0.5}$ from the first iteration to the third iteration. Given the obvious oversized dampers, and an exceedance of the damper force limit, the sixth iteration reduced C_x and C_y. Yet such a reduction still resulted in a slight reduction of the objective function. As such, the sixth design was selected as the final design and met all constraints.

Considering that the optimization was focused on reducing loss on a residential floor, the third iteration successfully brought down the maximum drift from floor levels 34 to 41. However, the peak drift ratios from floor levels 8 to 20 were increased considering a lack of dampers installed at most of these floors (Figure 9.40). An observable increase was seen for floor acecelrations from iteration 1 to 3 (Figure 9.41), which was reflected in a large increase in damper size. The final design used much reduced damper sizes, and consequently the peak floor accelerations were smaller than iteration 3.

In terms of the peak damper responses, the third iteration exhibited the maximum damper forces exceeding the 3000-kip limit (Figure 9.42) and was adjusted subsequently to meet this constraint. The peak damper strokes (Figure 9.43) had a maximum stroke of 3.2 in in the final design, which was well below the 5-in limit.
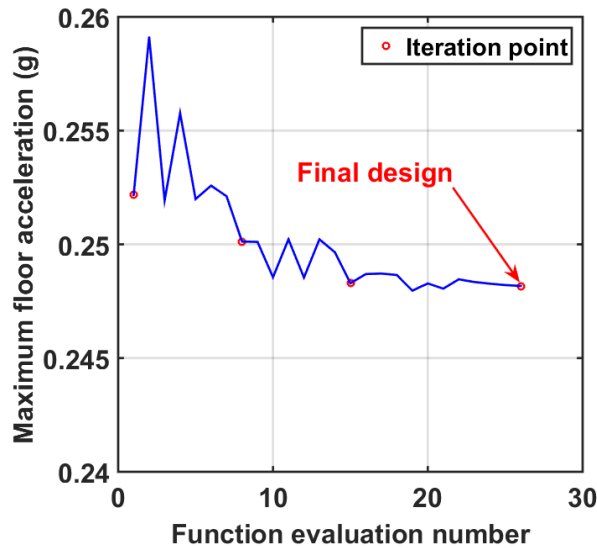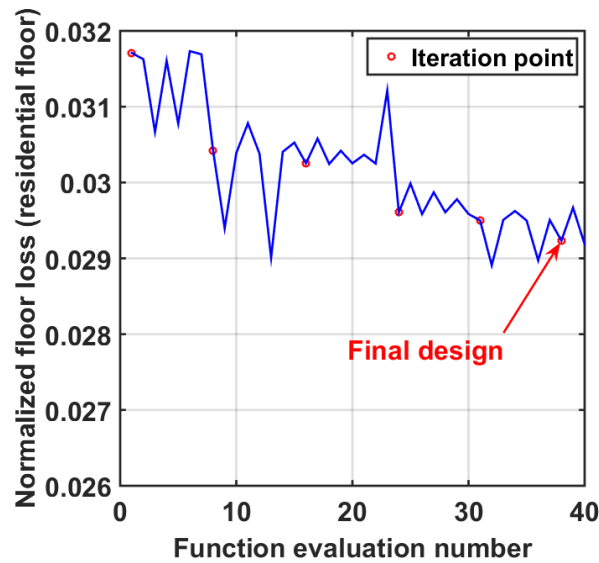

Figure 9.38   Evolution of objective function values
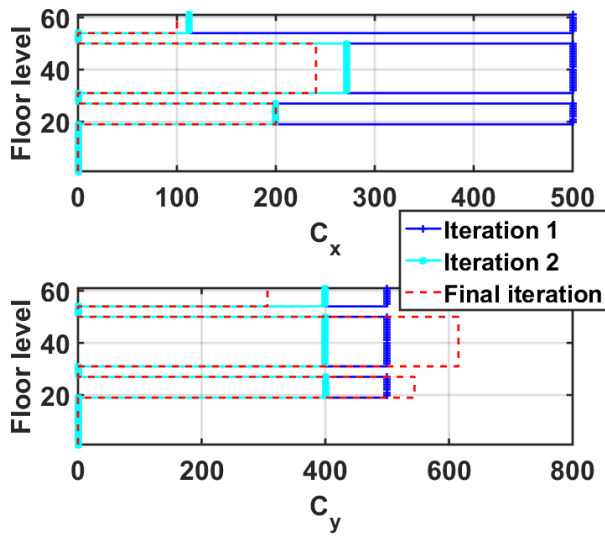
230
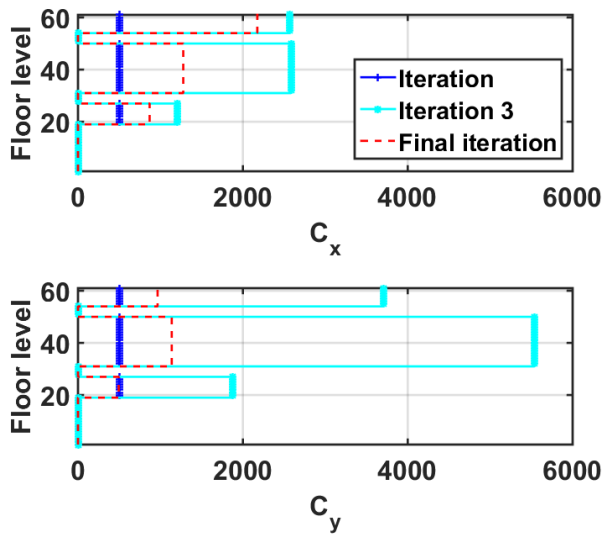
Figure 9.39   Design variables at selected iteration points
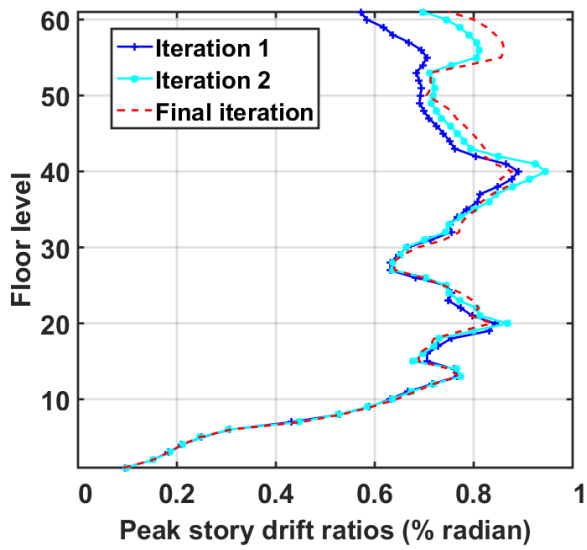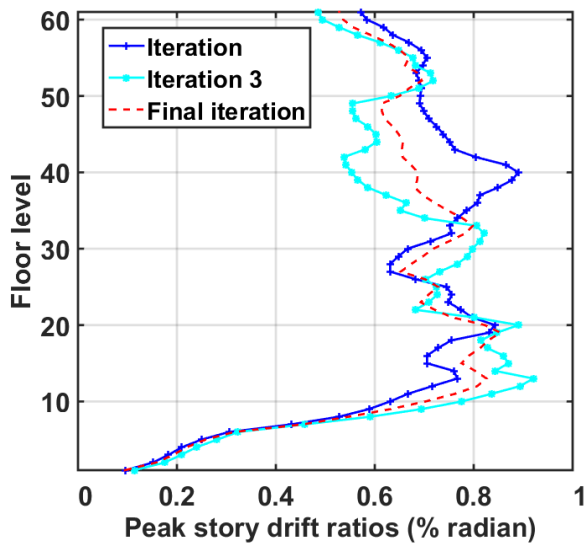

Figure 9.40   Distribution of peak story drift ratios at selected iteration points (median of eleven analyses)
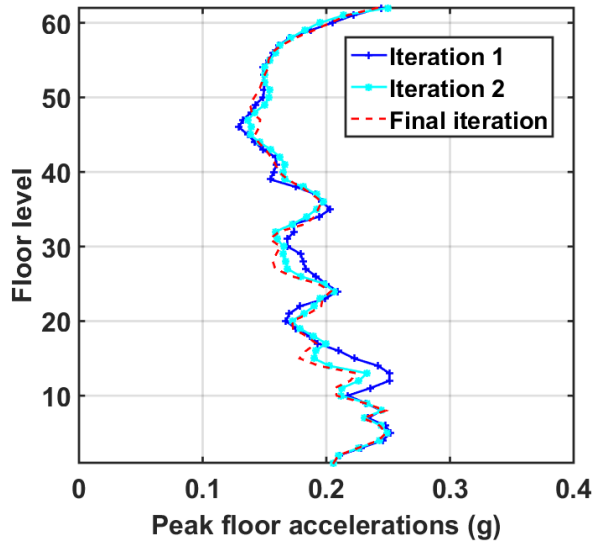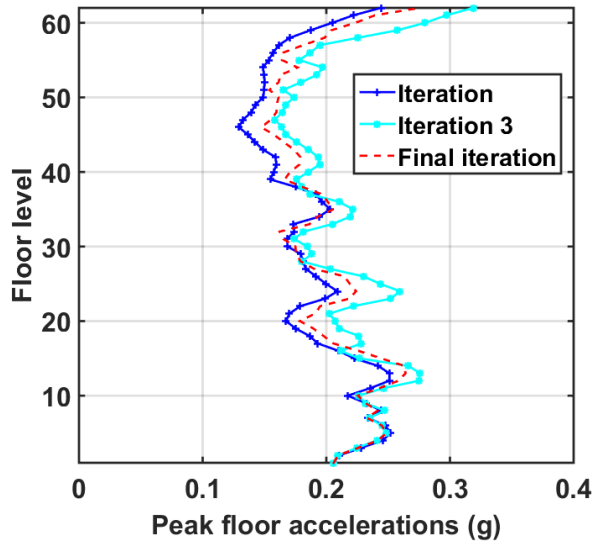
Figure 9.41 Distribution of peak floor accelerations at selected iteration points (median of eleven analyses)
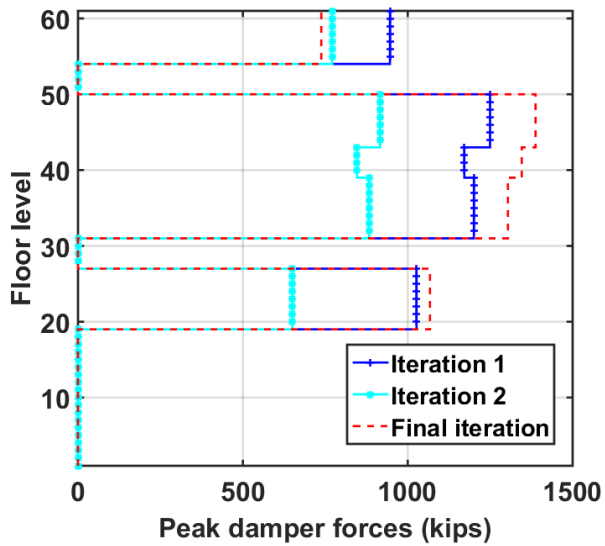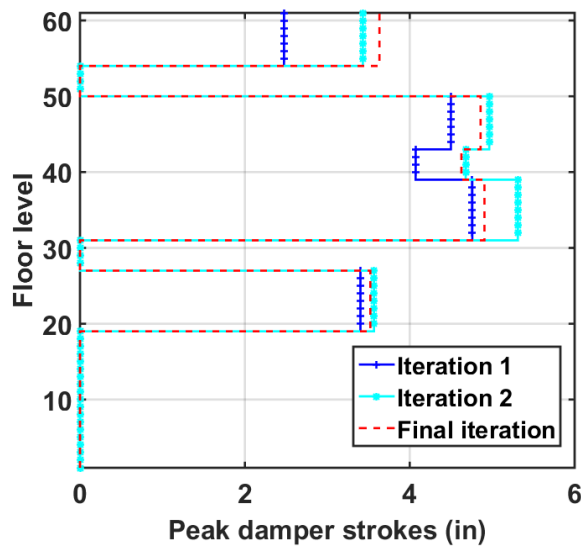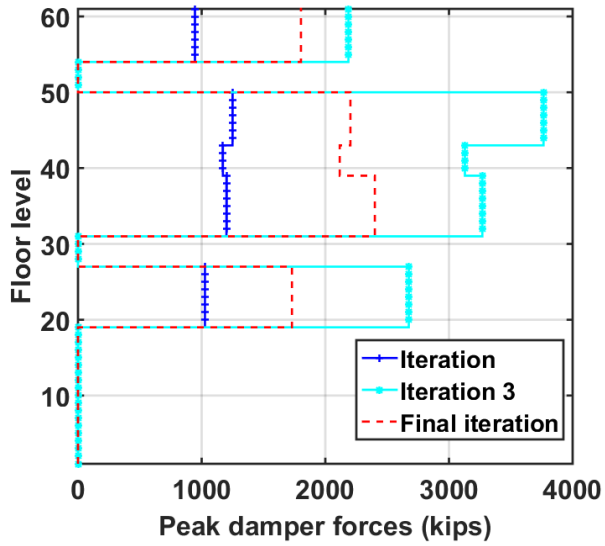

Figure 9.42 Distribution of peak damper forces at selected iteration points (median of eleven analyses)
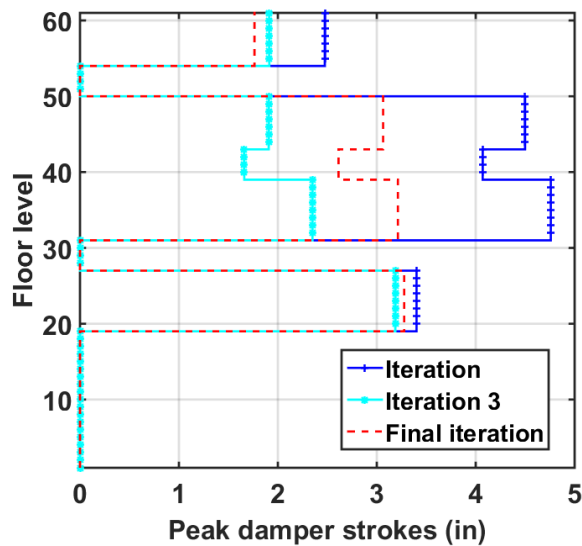
Figure 9.43   Distribution of peak damper strokes at selected iteration points (median of eleven analyses)

9.5.4 Observation and Comparison

Four cases using different objective functions were investigated to achieve an optimal damper scheme in the case-study building. As an overall trend, the automated design effectively updated the design parameters, thereby enhancing the seismic performance and resilience of the new building. Nevertheless, the changes were not significant, and incremental improvement of adjusting the damper properties were much smaller than these observed in the existing case-study building investigated previously. This is mainly due to the fact that this new building is likely to perform well under a MCE$_R$ hazard event and meets the basic performance level suggested by ASCE 7 [2010], limiting the benefit of adding supplemental dampers in this building. In most cases, the optimization procedure increased the sizes of FVDs in the selected locations in order to reduce the objective function values; but in Case 2, where the maximum floor acceleration was selected as the objective function, the damper sizes were reduced. Thus, its optimization was least efficient among all investigated cases. Moreover, it was found that incremental benefit of increasing damper size was offset by a possible contribution to a larger floor-based loss (e.g., Case 4).

To compare optimal design procedure using different objective functions, the above-mentioned four cases were compared herein. The design variables—damping constants over story heights—are listed in Table 9.9. The initial design started with a value of 500 kip·(sec/in.)$^{0.5}$ at locations where dampers were distributed, but the final schemes differed significantly among these cases. Fairly small additional damping was required in all cases, ranging from 2.3% to 9.0%. The *Y*-direction required a larger damping demand than *X*-direction in most cases, and generally larger dampers were needed at the middle to upper floors.

The distributions of the peak story drifts are presented in Figure 9.44. The building without FVDs had larger deformations at floor levels 35 and above. Installing FVDs in parallel with mega braces successfully brought down the drifts in these floors, which could be up to 40% in most cases, with the exception of Case 2, where the peak acceleration was the objective function. The target performance level of limiting the average peak drift ratio within 0.8% was satisfied for all four cases. Although the dampers were relative less effective in reducing peak floor accelerations, a 30% reduction at floor level 50 was observed although the roof acceleration seemed insensitive to additional damping (Figure 9.45). A slight increase of floor accelerations was observed in the lower stories where no dampers were installed.

The peak damper forces varied significantly for different cases, but all predicted the largest demand at floor levels 31 to 50. The maximum force was about 1300 kips for Case 2, but became more than 2500 kips for Case 1. (Figure 9.46). Considering the larger cost associated with large-force dampers, replacing a large damper with a few smaller dampers might be more economical. The mega-brace configuration provides physical feasibility to employ a few dampers in parallel with the brace. As such, the initial damper cost was estimated based on the median peak damper forces shown in Figure 9.46, but assumed that two smaller dampers were used to provide the required damper force demand. A range between $1.8 M to $3.7 M was obtained for different cases according to the unit price listed in Table 6.6.

The maxima of the peak median responses are summarized in Table 9.10 for a quantified comparison, and typical floor loss and total building loss were also estimated based on median structural responses. The total building loss was $54.4 M for the original building, which was reduced to between $24.4 M to $32.4 M when FVDs were introduced. Case 1, where the maximum drift was used as the objective function, controlled the structural response and reduced the economic loss of the building after a MCE$_R$ event most effectively; it also required the largest dampers. For Case 2, which used the maximum floor acceleration as the objective function, had a total economic loss of about $8 M more than Case 1 although the initial damper price was only half of Case 1 ($1.8 M compared to $3.7 M). In those cases where a story-based loss was used as the objective, Case 3 was slightly more cost-effective for the office floor since its building loss was smaller, and it required a smaller damper cost compared to Case 4. This was mainly due to fact that larger than required dampers were used in Case 4 in upper stories, whose objective was to reduce residential floor loss. Note that the results presented in Table 9.10 do not account for building collapse or irreparable residual drift ratios. This is a reasonable simplification considering the good structural response of the case-study building under investigation.
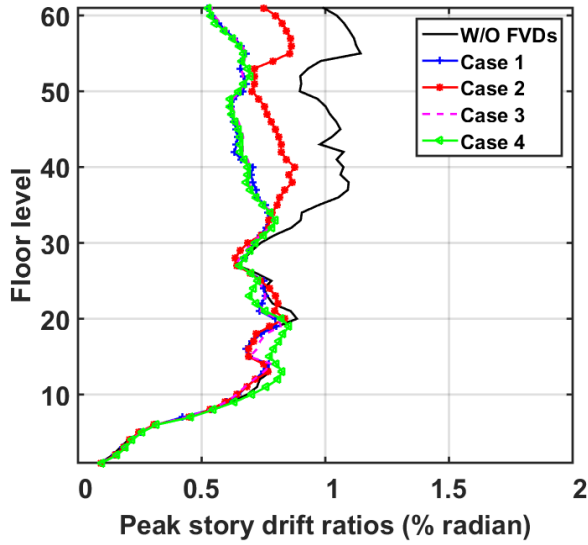
Figure 9.44   Comparison of peak story drift ratios (median of eleven analyses)
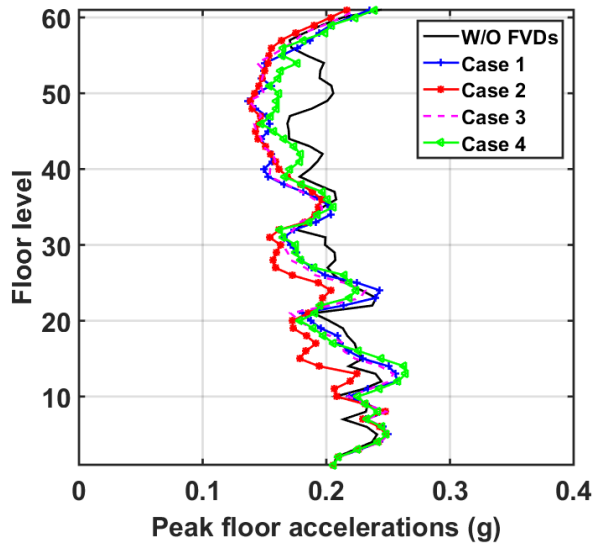
Figure 9.45   Comparison of peak floor accelerations (median of eleven analyses)

235
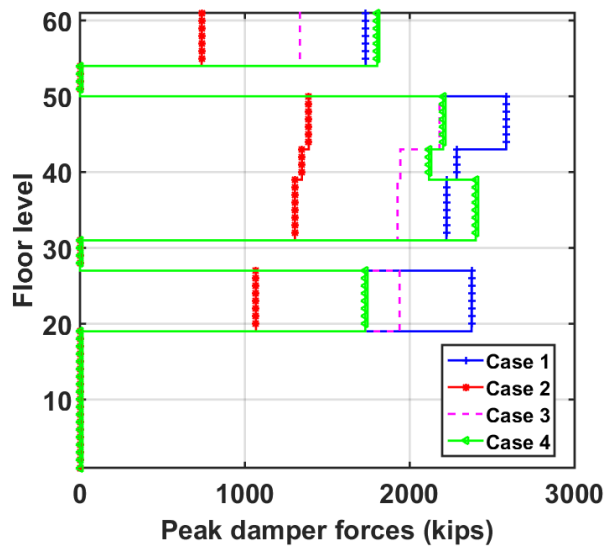
Figure 9.46   Comparison of peak damper forces (median of eleven analyses)

Table 9.9   Design variables

Design variable	Cx_1 kip·(sec /in.)^0.5	Cy_1 kip·(sec /in.)^0.5	Cx_2 kip·(sec /in.)^0.5	Cy_2 kip·(sec /in.)^0.5	Cx_3 kip·(sec /in.)^0.5	Cy_3 kip·(sec /in.)^0.5	ξ_{eff} X	ξ_{eff} Y
Initial value	500	500	500	500	500	500	2.9%	3.3%
Case 1	590	4730	585	1600	500	1600	3.0%	9.0%
Case 2	100	305	240	615	200	540	2.3%	3.2%
Case 3	500	1230	500	1230	500	1230	2.9%	5.3%
Case 4	2175	965	1275	1140	870	490	4.7%	4.5%

Table 9.10   Cost-effectiveness of various schemes under MCE_R

Scheme	W/O damper	W/ damper Case 1	Case 2	Case 3	Case 4
Prob. of irreparability	1.14%	0.80%	0.88%	0.82%	0.85%
Maximum story drift ratio (%)	0.300	0.257	0.248	0.254	0.275
Maximum floor acceleration (*g*)	0.632	0.208	0.296	0.228	0.260
Total building loss ($M)	1.509	0.857	1.096	0.857	0.883
Damper price ($M)	54.4	24.4	32.4	25.2	27.1
Prob. of irreparability	N/A	3.7	1.8	2.7	3.4

236

9.6 GUIDANCE ON OPTIMAL DESIGN PROCEDURE OF FVDS IN A MEGA-BRACE-TYPE STEEL TALL BUILDING

Chapter 8 outlines a step-by-step procedure to guide the design of FVDs in a high-rise building with an optimal configuration, which is applicable to both an existing tall building and a newly-designed tall building. As such, it is not repeated herein. However, two considerations should be accounted when a new building is considered.

For a new building designed in compliance with current code requirements, the basic performance goals are usually well defined. As such, the additional damping ratio needed to target for an enhanced seismic performance or resilience of the building could be much smaller than that for an older building whose seismic performance is likely problematic. Given that the initial damping ratio was usually smaller than 2% for a tall building [Smith *et al*. 2010; Cruz and Miranda 2016], a total effective damping ratio slight larger than 2% to 9% is suggested based on resulted presented before.

Additionally, the dampers are grouped based on plan and vertical configurations of the building and structural response. etc. The total number of different groups depends on the number of design variables used. For example, in a building with about 60 stories like the building considered herein, four groups could be used. In the case-study tall steel mega-brace building, the story-wise distributions of dampers differed considerably for a steel moment frame (Chapter 8). Table 9.11 provides a summary of optimal patterns of damping constant *C* for four story groups, from bottom stories (first group) to top stories (fourth group). Basically, additional damping is not needed for the lowest level since the original structural system provides adequate stiffness and strength to avoid large deformations. In other parts of the building, the above groups require different levels of effective damping, and the distribution patterns vary depend on the type of objective function used. For example, in the case where the maximum peak floor acceleration is the objective, the additional damping demand is essentially identical, whereas the other cases usually require larger damping in the middle to upper stories.

Table 9.11   Optimal patterns of *C* over story height

Group of FVDs	Objective function			
	Maximum drift ratio	Maximum floor acceleration	Maximum office floor loss	Maximum residential floor loss
C at 4th group	1.5	0.6	1.0	2.2
C at 3rd group	1.0	1.2	1.0	1.9
C at 2nd group	1.0	1.0	1.0	1.0
C at 1st group	0	0	0	0
Effective damping ratio ζ_{eff}	6.0%	3.0%	4.0%	4.5%

9.7   CONCLUDING REMARKS

A newly-designed mega-braced steel frame was selected for an in-depth investigation of its structural response. The original building layout was simplified for the purpose of this study, and a numerical model was designed in OpenSees. Systematic evaluations of the building responses under a MCE_R earthquake hazard were conducted, which indicated that the building could perform reasonably well and meet the basic performance level of life safety according to the current code requirements. However, it is possible to further improve its performance by using FVDs in parallel with exterior mega braces. An initial damper design was investigated and its efficacy was demonstrated.

After the feasibility study, the automated procedure was used to identify and tune the design parameters of FVDs in selected locations in order to effectively improve the seismic performance and resilience of the building. Four study cases with different objective functions were investigated, including two cases that used a single EDP and another two cases that based on EDP-DV functions. The automated procedure, aided by HPCs, helped identify design patterns of FVDs in this new building and enhanced significantly the seismic performance of the building with limited number of iterative designs. The required additional damping was small, although a slightly larger demand was shown in the middle to upper stories. Several optimal patterns of damper distributions were suggested for new high-rise buildings that use mega-braces as their lateral force-resisting system.

10 Conclusions and Recommendations

The objectives of this dissertation are to explore the use of supplemental energy-dissipation devices and modern computer-aided engineering tools to improve the safety and performance of existing and new tall buildings. The dissertation constitutes of two parts. Part 1 focused on examining cost-effective retrofit measures to improve the seismic performance of an existing high-rise building that had a variety of seismic vulnerabilities. A retrofit strategy that incorporated fluid viscous dampers (FVDs) was found to be the most cost-effective to upgrade the 35-story steel moment frame, and thus selected for continued study. Part 2 of this dissertation explored a strategy to automate the design of FVDs in high-rise buildings by utilizing high-performance computers (HPC) and parallel processors. The target for the design is to enhance the seismic performance of new and older tall buildings by optimally distributing FVDs and identifying their mechanical properties. This study not only highlights economic implications for improved design strategies for an individual tall building, but more importantly, it has the potential to enhance seismic resilience by practically and economically reducing seismic damage and the cost and time needed for repair. This study also illustrates the benefits of utilizing advanced HPC to streamline time-consuming analyses and workflows for both practitioners and researchers.

10.1   SEISMIC RETROFIT OF AN EXISTING TALL BUILDING

A majority of tall buildings constructed in California between 1960 and 1990 are steel moment-resisting frames. This type of buildings has been demonstrated to exhibit a variety of seismic vulnerabilities from past earthquakes and previous and more recent analytical studies. Moreover, building codes at the time of construction of these buildings did not adequately address many seismic deficiencies. Although modern building codes have addressed many of these deficiencies, questions linger about the seismic performance of buildings built before 1990.

The building selected for study is a 35-story steel moment-resisting space frame building designed and constructed around 1970 with typical pre-Northridge beam-to-column moment connection details and PJP weld column splice details. This building addresses several key concerns regarding the safety and performance of existing tall buildings during future earthquakes. Structural evaluations of the case-study building were carried out following procedures contained in three modern codes or guidelines: ASCE 41-13, FEMA 351, and FEMA

P-58. All assessment results predicted similar outcomes, indicating that the building had a great many seismic deficiencies, with a more than 90% confidence of collapsing at either BSE-1E or BSE-2E hazard level, leading to significant economic loss in the event of a moderate or a major earthquake.

After reviewing past retrofit strategies, a two-level retrofit method was proposed to improve the seismic performance of the case-study building. The Level-1 retrofit, which significantly reduced the weight of the structure by replacing the heavy cladding with lightweight substitutes and upgrading all column splices in the building, was able to achieve a greater than 90% confidence of preventing collapse under BSE-1E seismic events according to procedures in FEMA 351. In addition, the retrofit limited repair costs for this level of shaking to less than 6% of the buildings replacement cost according to methods described in FEMA P-58. When shaking increased to the BSE-2E level, collapse prevention could not be assured and demolition and replacement were expected even after the Level-1 retrofit.

As such, retrofit strategies that additionally incorporated FVDs were explored and were proved to greatly improve the performance of the case-study building at both the BSE-1E and BSE-2E hazard levels. A two-phase manual design procedure was proposed to select and refine the size and location of the FVDs as a first trial. The design began with selecting locations to install dampers, assessing additional damping ratio needed to achieve a target performance level, and selecting dampers sizes to achieve the required damping ratio. In design Phase 1, dampers were distributed throughout the stories, and three alternate damper distribution schemes were compared. Phase 2 required selecting the best of the three schemes considered in Phase 1. This scheme was adjusted to remove a large number of dampers and refine individual damper characteristics without compromising structural responses.

Several important design considerations were investigated, including the damper parameters: damping exponent α, and the stiffness of brace in series with dampers K_b. Other factors, such as the saturation of supplemental damping and configurations of devices in each frame were explored. Additionally, several design considerations such as the vulnerability of columns, sensitivity of additional damping, nonlinearity, and driving brace flexibly were examined. The results indicated that the final solution of the retrofit addressed the most critical seismic vulnerabilities in the case-study building, which achieved a more than 85% confidence level of avoiding collapse according to the procedures contained in FEMA 351 under the BSE-2E shaking, thus satisfying the performance goal suggested by ASCE 41.

Additionally, two other methods that used viscous wall dampers (VWDs) or buckling restrained braces (BRBs) were compared with FVDs in terms of their efficacy to improve the seismic performance of the case-study building. Both schemes installed devices at the identical locations as those used to install FVDs; all three schemes had a same effective damping ratio. The results revealed that although VWDs or BRBs provided certain control effects to improve structural behaviors, they did not achieve the performance level of preventing building collapse, nor did they reduce with high confidence economic losses under a BSE-2E hazard event. Several design issues to incorporate different energy-dissipation devices in an existing building were discussed, in particular, their interactions with existing structural members such as vulnerable columns and brittle beam-to-column connections. The results indicated that fairly large dampers and driving braces would be needed to achieve the desired control effect.

The retrofit study continued with a damage and loss estimation based on the framework of Performance Based Earthquake Engineering (PBEE). The cost-benefit of different retrofit measures were first compared by examining the repair cost alone. In addition, an in-depth analysis was conducted for the most promising retrofit strategy used in this study, which considered the repair cost, repair sequence, and business interruption loss. The results were presented for the as-built building, the building had Level-1 retrofit, and the case with a complete two-level retrofit with FVDs. The two-level retrofit significantly reduced the financial loss from more than $740 M to under $40 M when subjected to a BSE-2E event. The benefit of using supplemental FVDs would be much larger if a larger earthquake was considered compared to a moderate earthquake.

10.2   OPTIMAL DESIGN OF FLUID VISCOUS DAMPERS TO IMPROVE THE SEISMIC PERFORMANCE OF TALL STEEL BUILDINGS

While the first part of this dissertation demonstrated the ability of supplemental energy-dissipation devices, especially FVDs, to improve the performance of an existing tall steel moment frame building, the trial and error design process typically used in practice is time consuming and is not likely to find a complete optimum because of time limits placed on most projects. Thus, the second part of this dissertation proposed an automatic design procedure to tune the parameters of FVDs in an efficient manner by using HPC and parallel processors.

After reviewing past research related to identifying optimal damper design, a gradient-based algorithm was selected to solve this problem. Several candidates for three key components for optimization problem were suggested. An automated tool was set up based on the Matlab optimization toolbox, using a gradient-based algorithm to refine the design variables and find an optimal solution. The gradients of objective function and constraint functions were estimated based on the finite element difference considering the non-convex nature of these functions. Despite this and other limitations of the algorithm, the reported results have demonstrated the efficacy of this method to achieve the optimization target and was deemed more feasible compared with other much more computational-demanding algorithms (such as the genetic algorithm).

The design variables, an objective function, and constraint functions were selected based on the target performance level, complexity of the problem and feasibility of computation efforts. Specifically, this study focused on optimizing one mechanical property of a FVD—damping constant C and its story-wise distribution. Different C values at various story zones in a high-rise building were selected as design parameters to be tuned during the optimization. Two types of objective functions were investigated, including one type that used a single engineering demand parameter (EDP) directly, and another type integrated several EDPs in a function format that informed the decision variable (financial loss). The constraint functions were designed to reflect the target performance levels and to limit the maximum damper responses.

This automated design procedure was first applied to an existing high-rise steel moment frame that examined in Part 1 of this dissertation. The optimization problem was studied under BSE-1E and BSE-2E hazard events, respectively, and focused on different optimization goals. It was shown that the proposed automated procedure identified design parameters effectively after

a few iterations, and the refined design improved the seismic resilience of the building remarkably. Several cases were investigated using different objective functions, and all of them identified that the damping demand was larger in the lower one-third floors in this building. Optimal patterns of damper distributions for a tall steel moment frame were suggested.

The procedure was further extended to a newly-designed tall steel building. The building selected for examination used exterior mega-braces as its main lateral-force resisting system and was able to meet the code-required performance level of collapse prevention under a MCE_R seismic event after assessment. A strategy that used FVDs was explored and results indicated that installing FVDs in parallel with exterior mega-brace were able to augment the seismic performance and resilience of the building effectively. As such, the automated procedure of identifying design parameters and patterns of FVDs was applied in this case-study building. This procedure worked efficiently, identifying optimal design schemes of FVDs to improve the building's seismic performance in a cost-effective manner. Optimal patterns of sizing and distributing FVDs in a brace-type tall steel building were suggested.

The efficiency of the automated procedure was demonstrated by comparing it with the design that relied on manual trials and errors. The comparison study was conducted for the existing building case that used FVDs as a retrofit strategy. The manual update method could improve the damper scheme, but not as efficiently as that using the automated procedure. More importantly, using the automated design significantly reduced the engineering effort and refined the design parameters in a more efficient way. Therefore, this proposed design procedure would be a promising approach for the design and analysis of an engineering problem, especially considering the widely accessible HPC resources in this era.

10.3 RECOMMENDATIONS FOR FUTURE STUDIES

10.3.1 Alternative Retrofit Strategies

A series of retrofit strategies to improve the seismic performance of the case-study building have been explored, including:

> (a) Fixing vulnerable column splices;
>
> (b) Replacing heavy exterior cladding with a lightweight substitute; and
>
> (c) Adding supplemental energy-dissipation dampers or buckling restrained braces.

One strategy that incorporates (a), (b) and (c) that used FVDs was the most cost-effective strategy among those investigated to achieve the target performance objectives for the existing building examined in this study. A list of alternative retrofit methods for the case-study building that are worthy of future studies are listed below.

Adding steel plate shear walls

Several interior frames in this office building would be suitable for the addition of steel plate shear walls, thus increasing the strength of the building and alleviating the concentrated deformations in the lower levels. Steel plate shear wall systems are lightweight and are easy to construct compared to concrete materials. Moreover, if additional steel plate shear walls are confined within a few floors, the force increased on existing structural elements and the impact on the occupants during construction could be limited.

Adding structural columns

An interesting feature of the case-study building is that dummy "architectural" columns exist in the cladding around the perimeter of the building between every two adjacent structural columns. The typical span of a frame bay between two structural columns is 30 ft. As such, a viable strategy might be to replace the dummy "architectural" columns with structural columns, which would increase the number of bays with a smaller span for each bay. This could reduce the story drifts and increase story strength.

Removing existing floors

The Level-1 retrofit replaced the heavy exterior cladding with a lightweight substitute that helped to reduce the displacement demands and alleviate the P-Δ effect of the building. The seismic weight of this building could be further reduced by removal of a few upper stories. The applicability of such a strategy should be fully evaluated, especially considering the significant social and economic impact if the functionality of this office building is diminished.

Mid-story isolation

The response of the building in its as-built condition exhibited a significant weak-story trend at the bottom stories, which unintentionally provided an isolation effect as it protected the stories above the weak-story zone. Therefore, installing isolation at weakest story and selectively strengthening nearby stories might provide an alternative to address the weak-story problem, while also reducing the seismic demands for the upper stories. Mid-level isolation will introduce substantial changes to the architectural components, elevators, stairs, utilities, and structure near the isolation plane, and need more close investigations if used.

Mega-column system

The mega-column system (or "mega-frame system" or "space truss system") is an efficient and economical way to provide stiffness for a tall building to resist seismic and wind-induced lateral forces [Gunel and Ilgin 2014]. These systems usually consist of reinforced concrete or composite columns with large sections. These mega columns span throughout floor height and are connected with belts or mega braces to form a closed lateral force-resisting system. One viable solution to incorporate mega-column system in the case-study building would be to add mega columns in the four corners that are connected by diagonal mega-braces on the exterior faces of the building, thus forming an "exoskeleton" for this building. Such a method would change significantly the building's architectural aesthetic, but it concentrates retrofit efforts on the outside of the building.

10.3.2 Remaining Retrofit Issues

The two-level retrofit measures to upgrade the existing 35-story building satisfied the collapse prevention performance level of the building under a BSE-2E event, thus reducing significantly economic loss after a moderate and a major earthquake event. However, inadequate axial load capacities of columns in compression remains to be solved. These vulnerable columns are not exclusive for the case-study building under investigation, but also apply for other tall steel buildings constructed decades ago.

Although supplemental viscous damping helped alleviate the overloaded columns in compression due to a reduction of the drifts caused by overall structural bending, these large dampers would elevate the force demands on columns, especially when a building enters the inelastic range and damper forces act more in-phase with structural displacements. Moreover, if displacement-dependent devices are used, it is likely the resultant forces in existing columns would be even larger. Additional methods such as adding steel plates to column exteriors and then filling critical columns with concrete might be viable solutions to add the strength of these vulnerable columns; further investigation is warranted.

10.3.3 Alternative Methods of Arranging Fluid Viscous Dampers

Using FVDs provides an effective and versatile means of improving the seismic performance of a tall building regardless if the building was constructed decades ago or recently built. Despite of their promising features, several design problems might limit their widespread use and are worthy of further investigations.

One of the major problems is the size of the dampers required in such a large building. Large forces generated by these dampers impose great strains on other structural elements in the load path, such as the connections between dampers to frames and the columns connected to dampers. One alternative strategy would be to use additional smaller dampers distributed throughout the building, which would simplify the connection between dampers and the existing structure and the transfer of inertial loads from the structure to the damper system. Another approach worth studying is to use a perimeter mega-truss system that has fewer large dampers where the braces used to drive them extend over several stories. In such a mega-truss system, the effect of additional damping might be further enhanced by combining a FVD with a BRB in a parallel fashion.

10.3.4 Cost-Benefit Estimates

Damage and loss was estimated for the existing case-study building under a scenario-based seismic event. Repair cost and repair time for each component and the entire building were estimated using the computer program Performance Assessment Calculation Tool (PACT). Additional analysis was carried out to assess the business interruption and total financial loss by utilizing a simple business interruption model and a business model. These estimations could be improved if a more robust business interruption model is used. For example, a model to account for the functionality limit state, a more realistic repair sequence and labor allocation, resource scheduling, etc. should be examined. Given that the disruption and cost of retrofit of tall

buildings can be considerable, conducting the damage and loss analysis under multiple hazard events and estimating the annualized loss and return on investment would be fruitful to inform the decision-making process. More work is needed to study the logistics and costs of retrofit or repair, and the business impacts of these interruptions.

10.3.5 Selection of Design Variables

In this study, one design parameter of a FVD—damping constant C, and its story-wise distributions—were selected as the design parameters to be optimized. An additional assumption made was that dampers at several continuous floors were assigned with a same-size damper. One limitation of such a pre-determined damper style was that it might obscure unique demands at special floor levels. For example, the case-study building exhibited a vertical irregularity at the mezzanine level, and the damper demands were larger at that floor than other adjacent floors. Nevertheless, using a uniform damper demand at that level with its adjacent floors might lead to larger dampers than needed at other floors. Studies to consider other arrangement patters of design variables to more efficiently distribute dampers are fruitful areas for continuing study.

This study identified the damper locations before performing the automated optimization, which might limit the applicability of resultant design patterns to other types of structural systems. It is suggested to include the locations of dampers as part of design variables and increase the number of dampers groups so that unique stories could be distinguished.

In terms of selecting design variables, there are several other alternatives that could be considered. These choices include, but are not exclusive to, the damping exponent α and the stiffness of the brace in series with a damper K_b. When designing a new building, the story stiffness K_f could also be considered as another type of design variable to allow for simultaneous optimization of damping and stiffness.

10.3.6 Selection of Objective Function and Constraints

One fruitful area for future study is to investigate other types of objective functions or/and constraint functions. For instance, other EDPs such as the maximum of peak velocity, average structural responses, story-based response could be used or integrated as part of these functions.

Constraint functions were selected in such a way to reflect the performance levels with specific numbers. For each case, the constraints could be used to complement the objective function, that is, to regulate those parameters not fully accounted by the objective. In this case, the damper responses were confined by putting a limit on the maximum force and stroke demands to avoid excessively large dampers and damper costs. Other alternative constraints to consider could be the maximum forces on columns, and the dollar loss considered in the decision-making process, etc.

10.3.7 Sensitivity of Optimal Damper Patterns to the Ground Motions

The current study selected the objective function based on median analysis results out of eleven nonlinear response history analysis. These selected ground motions provided median results

close to these of the entire twenty ground motion set used in Chapter 3 under each hazard level of concern; however, if the ground motion excitations changes, the optimization process and thus the optimal damper patterns might change accordingly. Additionally, if the records selected contain an irregular pulse or if a near-field site is considered, the results might become more sensitive to the ground motions selected. As such, future studies to assess the sensitivity of optimal design to the ground motion input would be suggested.

10.3.8 Selection of Optimization Engine

This study used the Matlab optimization package to design the automatic procedure. A gradient-based algorithm was used to tune the design parameters. At each trial point, the structural analysis was conducted in a parallel fashion so that the eleven set of ground motions were evaluated simultaneously. However, continued study to facilitate parallel-computing of other modules in the procedure would be necessary to fully engage the HPC resources. For instance, if an algorithm could allow several trial points at each iteration to be evaluated independently, the evaluation procedure would be further condensed; the numerical model could be divided to different parts to allow for another parallel processing etc.

Besides, the use of Matlab requires calling an external structural analysis program, thus limiting the efficiency of the optimization. An alternative strategy of employing an open-source optimization package that could be integrated in the structural analysis program directly would be more efficient, speed up the optimization, and allow the use of a larger number of design variables or/and constraint functions.

REFERENCE

Agrawal, A.K. and Yang J.N. (1999a). Design of passive energy dissipation systems based on LQR control methods. *Journal of Intelligent Material Systems and Structures*, 10, 933-944.

Agrawal, A.K. and Yang J.N. (1999b). Optimal placement of passive dampers on seismic and wind-excited buildings using combinatorial optimization. *Journal of Intelligent Material Systems and Structures*, 10, 997-1014.

AISC (2010). *Specifications for Steel Structural Buildings*, 4th Edition, American Institute of Steel Construction, ANSI/AISC 360-10, Chicago, IL.

Amazon web services (2017). Amazon EC2 reserved instances pricing. Accessed Mar. 6th, 2017, from *https://aws.amazon.com/ec2/pricing/reserved-instances/pricing/*.

Antonellis, G. and Panagiotou, M. (2014). Seismic response of bridges with rocking foundations compared to fixed-base bridges at a near-fault site. *Journal of Bridge Engineering*, 19(5): 04014007.

Apostolakis, G. and Dargush, G.F. (2010). Optimal seismic design of moment-resisting steel frames with hysteretic passive devices. *Earthquake Engineering & Structural Dynamics*. 39, 355-376.

Applied Technology Council (ATC) (2016). Performance Assessment Calculation Tool (PACT) (Version 3.0.2) *[computer software]*, Applied Technology Council, Redwood City, CA. Software available at *https://www.fema.gov/media-library/assets/documents/90380*.

Arima, F., Miyazaki, M., Tanaka, H. and Yamazaki, Y. (1988). A study on buildings with large damping using viscous damping walls. *Proceedings of Ninth World Conference on Earthquake Engineering*, Tokyo-Kyoto, Japan, V, 821-826.

ASCE (2003). *Seismic Evaluation of Existing Buildings*, American Society of Civil Engineers, ASCE/SEI 31-03, Reston, VA.

ASCE (2007). *Seismic Rehabilitation of Existing Buildings*, American Society of Civil Engineers, ASCE/SEI 41-06, Reston, VA.

ASCE (2010). *Minimum Design Loads for Buildings and Other Structures*, American Society of Civil Engineers, ASCE/SEI 7-10, Reston, VA.

ASCE (2013). *Seismic Evaluation and Retrofit of Existing Buildings*, American Society of Civil Engineers, ASCE/SEI 41-13, Reston, VA.

ASCE (2017). *Minimum Design Loads for Buildings and Other Structures,* American Society of Civil Engineers, ASCE/SEI 7-16, Reston, VA.

Asher, J.W., Young, R.P. and Ewing, R.D. (1996). Seismic isolation design of the San Bernardino County Medical Center replacement project, *Journal of Structural Design of Tall Buildings*, 5: 265-279.

Ashour, S.A. and Hanson, R.D. (1987). Elastic response of buildings with supplemental damping. *Report UMCE 87-1*, Department of Civil Engineering, University of Michigan, Ann Arbor, Michigan.

Astaneh-A., A. (2000). Steel Plate Shear Walls. *Proceedings of U.S.-Japan partnership for advanced steel structures*, U.S.-Japan workshop on seismic fracture issues in steel structures, Feb. 2000, San Francisco.

ATC 17-1 (1993). *Proceedings on seismic isolation, passive energy dissipation, and active control*, Applied Technical Council, Redwood City, CA.

Austin, M.A., Mahin, S. and Pister, K.S. (1987). CSTRUCT: an interactive computer environment for the design and analysis of earthquake resistant steel structures. *UCB/EERC report, Report No. UCB/EERC-87/13,* University of California, Berkeley, CA.

Aydin, E., Boduroglu, M.H. and Guney, D. (2007). Optimal damper distribution for seismic rehabilitation of planar building structures, *Engineering Structures,* 29, 176-185.

Baker W. J., Shahi K. S., Jayaram N. (2011). New Ground Motion Selection Procedures and Selected Motions for the PEER Transportation Research Program, *PEER Report No. 2011/03*, Pacific Earthquake Engineering Research Center, University of California, Berkeley, CA.

Beker C. T., Yamamoto, S., Hamaguchi, H., Higashino, M., and Nakashima, M. (2015). Application of isolation to high-rise buildings: a Japanese design case study through a U.S. design code lens. *Earthquake Spectra*, Aug. 2015, 31(3): 1451-1470.

Brinklow, A. (2017). Mapping the 20 high-rises under construction in San Francisco right now. Retrieved May 12, 2017, from: *https://sf.curbed.com/maps/tower-highrise-construction-map-sf.*

Blaney, C., Uang, C-M., Kim, D-W., Sim H-B., and Adan, M.S. (2010). Cyclic testing and analysis of retrofitted pre-Northridge steel moment connections using bolted brackets, *Proceedings of SEAOC 2010 Convention*, Indian Wells, CA

Bruneau, M. (2005). Seismic retrofit of steel structures, *Proceedings of 1st Canadian Conference on effective design of structures*, Hamilton, Ontario, Canada, July 10-13, 2005.

Bruneau, M., Mahin, S. and Popov, E. (1987). Ultimate behavior of butt welded splices in heavy rolled steel sections, *Report No. UCB/EERC-87/10*, Earthquake Engineering Research Center, University of California, Berkeley, CA.

Building Center of Japan (BCJ) (2002). *Report on new building technologies–approvals, applications and certification*, Tokyo, Japan: BCJ. (in Japanese).

Cao, X., & Mlejnek, H-P. (1995). Computational prediction and redesign for viscoelastically damped structures, *Computer Methods in Applied Mechanics and Engineering*. 125,1-16.

CBSC (2013). *California Building Code, California Code of Regulations, Title 24, Part 2, Volumes 1 and 2*, California Building Standards Commission, Sacramento, CA.

Comerio, C.M. (2005a). Estimating downtime in loss modeling, *Earthquake Spectra* 22(2), 349-365.

Comerio, C.M. (2005b). Downtime modeling for risk management, safety and reliability of engineering systems and structures, G.Augusti, G.I.Schueller, and M.Ciampoli, eds., *International Conference on Structural Safety and Reliability (ICOSSAR)*, Millpress Scientific Publishers, Rotterdam.

Comerio, C.M., Tobriner, S., and Fehrenkamp, A. (2006). Bracing Berkeley. A guide to seismic safety on the UC Berkeley campus, *PEER Report No. 2006/01,* Pacific Earthquake Engineering Research Center, University of California, Berkeley, CA.

Computers & Structures Inc. (2016). ETABS (Version 15.2) *[computer software]*, Berkeley, CA.

Chen Y.-T., Chai Y. H. (2011). Effects of brace stiffness on performance of structures with supplemental Maxwell model-based brace-damper systems, *Earthquake Engineering & Structural Dynamics,* 40(1): 75–92.

Cimellaro, G.P. & Retamales, R. (2007a). Optimal softening and damping design for buildings, *Structural Control and Health Monitoring*, 14:831-857.

Cimellaro, G.P. (2007b). Simultaneous stiffness-damping optimization of structures with respect to acceleration, displacement and base shear, *Engineering Structures*, 29, 2853-2870.

Chi, B., Uang, C-M., Chen A. (2006). Seismic rehabilitation of pre-Northridge steel moment connections: A case study, *Journal of Constructional Steel Research*, 62: 783-792.

Constantinou, M. (1994). Application of fluid viscous dampers to earthquake resistant design: research accomplishment, 1986-1994, *The National Center for Earthquake Engineering Research*, Buffalo, NY, pp: 73-79.

Constantinou, M.C., Fujii, S., Tsias, P. and Okamoto, S. (1992), University at Buffalo-Taisei Corporation Research Project on Bridge Seismic Isolation Systems, *Proceedings of 3rd NSF Workshop on Bridge Engineering Research in Progress*, 235, La Jolla, CA.

Constantinou, M.C., Symans, M.D. (1992). Experimental and analytical investigation of seismic response of structures with supplemental fluid viscous dampers, *NCEER Report No. NCEER-92-0032*, National Center for Earthquake Engineering Research, Buffalo, NY.

Constantinou, M.C. and Symans, M.D. (1993). Seismic response of structures with supplemental damping, *Journal of Structural Design of Tall Buildings,* 2: 77-92.

Constantinou, M.C., Symans, M.D., Tsopelas, P., and Taylor, D.P. (1993). Fluid viscous dampers in applications of seismic energy dissipation and seismic isolation, *Proceedings of ATC-17-1 Seminar on Seismic Isolation, Passive Energy Dissipation and Active Control*, San Francisco, CA, Mar. 11-12, 1993.

Constantinou, M.C., Tsopelas, P., Hammel, W., and Sigaher, A.N. (2001) Toggle-Brace-Damper Seismic Energy Dissipation System, *ASCE Journal of Structural Engineering*, Vol 127, No. 2.

Constantinou, M.C. and Tadjbakhsh, G.I (1983). Optimum design of a first story damping system, *Computers and Structures*, 17(2), pp: 305-310.

Cruz, C. and Miranda, E. (2016). Evaluation of damping ratios for the seismic analysis of tall buildings, *ASCE Journal of Structural Engineering*, 04016144.

Dargush, G.F. and Sant, R.S. (2005) Evolutionary aseismic design and retrofit of structures with passive energy dissipation, *Earthquake Engineering & Structural Dynamics,* 34: 1601-1626.

De Silva, C.W. (1981) An algorithm for the optimal design of passive vibration controllers for flexible systems, *Journal of Sound and Vibration.* 75, 495-502.

Doflot P. and Taylor D. (2008). Experience and practical considerations in the design of viscous dampers, *Proceedings of 3rd international conference on footbridge*, Porto, Portugal.

Dong, B., Sause, R., and Ricles, M.J. (2015), Equivalent linearized model of damper response for seismic design of steel structures with nonlinear viscous dampers, *Proceedings of 8th International Conference on Behavior of Steel Structures in Seismic Areas*, Shanghai, China.

Diotallevi, P.P., Landi, L. and Lucchi, S. (2014). A direct method for the design of viscous dampers to be inserted in existing buildings, *Proceedings of 10th National Conference on Earthquake Engineering*, Anchorage, Alaska.

Duerr, K. & Tesfamariam, S. (2012). Comparison of optimization methods for retrofit placement in a non-code conforming reinforce-concrete structure, *Proceedings of 15th World Conference on Earthquake Engineering,* Lisbon, Portugal.

Dynamic Isolation Systems (DIS) Inc. (2011). Brochures of viscous wall dampers: superior earthquake protection for flexible buildings. Dynamic Isolation Systems, Inc., McCarran, NV. Accessed Mar. 3, 2016, from: *http://www.dis-inc.com/pdf_files/DIS_VWD.pdf*.

Earthquake Solutions Inc. (2015). QuakeManager (Version Beta 2d) [*computer software*], Oakland, CA.

EERI (2010b). Canterbury Earthquake Clearinghouse: Mw7.1 earthquake on September 3, 2010. Accessed March 25, 2015, from *http://eqclearinghouse.org/co/20100903-christchurch/*.

EERI (2010a). Chile Earthquake Clearinghouse: M8.8 earthquake on February 27, 2010. Accessed March 25, 2015, from *http://eqclearinghouse.org/co/20100227-chile/*.

EERI (2012). Reconnaissance Team: "Performance of engineered structures in the Mw 9.0 Tohoku, Japan, Earthquake of March 11, 2011", *EERI Special Earthquake Report*, Earthquake Engineering Research Institute, Oakland, CA.

Espinoza, A. and Mahin, S. (2012). Seismic performance of reinforced concrete bridges allowed to uplift during multi-directional excitations, *PEER Report No. 2012/02,* Pacific Earthquake Engineering Research Center, University of California, Berkeley, CA.

Federal Office for the Environment (FOEN) of Switzerland (2008). *Seismic retrofitting of structures: strategies and collection of examples in Switzerland*, Federal Office for the Environment FOEN, Bern. Accessed Dec. 12th, 2015, from *https://www.weadapt.org/sites/weadapt.org/files/seismic_retrofittingofstructures.pdf.*

FEMA (1997). *NEHRP Guidelines for the Seismic Rehabilitation of Buildings and NEHRP Commentary on the Guidelines for the Seismic Rehabilitation of Buildings*, Federal Emergency Management Agency, FEMA 273 and FEMA 274 report, Washington, D.C.

FEMA (2000a). *Recommended Seismic Design Criteria for New Steel Moment-Frame Buildings*, Federal Emergency Management Agency, FEMA 350 report, Washington, D.C.

FEMA (2000b). *Recommended Seismic Evaluation and Upgrade Criteria for Existing Welded Steel Moment-Frame Buildings*, Federal Emergency Management Agency, FEMA 351 report, Washington, D.C.

FEMA (2000c). *Prestandard and Commentary for the Seismic Rehabilitation of Buildings*, Federal Emergency Management Agency, FEMA 356 report, Washington, D.C.

FEMA (2006a). *Techniques for the Seismic Rehabilitation of Existing Buildings*, Federal Emergency Management Agency, FEMA 547 report, Washington, D.C.

FEMA (2006b). *Designing for Earthquakes: A Manual for Architects, Chapter 8: Existing Buildings-Evaluation and Retrofit*, Federal Emergency Management Agency, FEMA 454 report, Washington, D.C.

FEMA, (2006c). *NEHRP Recommended Provisions: Design Examples, FEMA* 451, Building Seismic Safety Council, Federal Emergency Management Agency.

FEMA (2012a). *Seismic Performance Assessment of Buildings, Volume 1 – Methodology,* Federal Emergency Management Agency, FEMA P-58-1 report, Washington, D.C.

FEMA (2012b). *Seismic Performance Assessment of Buildings, Volume 2 – Implementation Guide*, Federal Emergency Management Agency, FEMA P-58-2 report, Washington, D.C.

FEMA (2012c). *Seismic Performance Assessment of Buildings, Volume 3 – Supporting Electronic Materials and Background Documentation,* Federal Emergency Management Agency, FEMA P-58-3 report, Washington, D.C.

Feng, D., Liu, W., Wang, S., Du, D., Xia, H., and Wang, Y. (2015). The applications of viscous wall dampers in steel structures, *Progress and market of steel structures*, No. 3, pp: 30-33. (in Chinese).

Filippou, F., Popov, E. and Bertero, V. Effects of bond deterioration on hysteretic behavior of reinforced concrete joints, *EERC Report No: 83-19*, Earthquake Engineering Research Center, University of California, Berkeley.

Flores, F.X. Jarrett, J.A. and Charney, F.A. (2012). The influence of gravity-only framing on the performance of steel moment frames, *Proceedings of 15th World Conference of Earthquake Engineering*, Lisbon, Portugal.

Freeman, S.A. Nicoletti, J. P. and Tyrell, J.V. (1975). Evaluation of existing buildings for seismic risk – A case study of Puget Sound Naval Shipyard, Bremerton, Washington, *Proceedings of the 1st U.S. National Conference on Earthquake Engineering*, Earthquake Engineering Research Institute, Oakland, California.

Fu, Y. M. (1996). Frame retrofit by using viscous and viscoelastic dampers, *Proceedings of 11th World Conference on Earthquake Engineering*, No. 428.

Fu, Y. and Kasai K. (1998). Comparative study of frames using viscous and viscoelastic dampers. *ASCE Journal of Structural Engineering.*, Architectural Institute of Japan (AIJ), 124: 513-522.

Fujimoto, M., Wada, A., Saeki, E., Takeuchi, T., and Watanabe, A. (1990). Development of unbonded brace, Tokyo Tech Research Repository, No.115, pp.91-96. Accessed Nov. 3, 2015, from: *http://t2r2.star.titech.ac.jp/rrws/file/CTT100672886/ATD100000413/.*

Furgo Inc. (2015). EZ-FRISK™ (Version 7.65) *[computer software]*, Houston, TX.

Furuya, O., Hamazaki, H. and Fujita, S. (1998). Study on proper distribution of storey-installation type damper for vibration control of slender structures using genetic algorithm, *Proceedings Of the 1998 ASME/JSME Joint Pressure Vessels and Piping Conference,* San Diego, CA, 297-304.

Gluck, N., Reinhorn, A.M., Gluck, J., and Levy, R. (1996). Design of supplemental dampers for control of structures, *ASCE Journal of Structural Engineering*, 122(12), 1394-1399.

Gross, J.L., Engelhardt, M.D., Uang, C.M., Kasai,K., and Iwankiw, N.R., (1999). Modification of existing welded steel moment frame connections for seismic resistance, *AISC Design Guide No.12*, American Institute of Steel Construction, Chicago, IL.

Gürgöze, M. and Müller, P.C. (1992). Optimal positioning of dampers in multi-body systems. *Journal of Sound and Vibration*, 158 (3), 517-530.

Gunel, H.M. and Ilgin, E.H. (2014). *Tall buildings: structural systems and aerodynamic form*. London and New York: Routledge.

Hahn, G.D., and Sathiavageeswaran, K.R. (1992). Effects of added-damper distribution on the seismic response of buildings, *Computers and Structures*, 43(5): 941-950.

Hayden, C., Bray, J.M and Abrahamson, N. (2014), Selection of Near-fault pulse motions. *ASCE Journal of Geotechnical and Geoenvironmental Engineering,* DOI:10.1061/(ASCE)GT.1943-5606.0001129.04014030.

Hejazi, F., Shoaei, M. D. and Jaafar, M. S. (2015). Analytical model for viscous wall dampers, *Computer-Aided Civil and Infrastructure Engineering*, (00):1-19.

Holland, J. (1975). *Adaptation in Natural and Artificial Systems*, University of Michigan Press, Ann Arbor, MI.

Holmes W., Kircher C., Petak W., Youssef, N. (2008). Seismic performance objectives for tall buildings, *PEER Report No. 2008/101*, Pacific Earthquake Engineering Research Center, University of California, Berkeley, CA.

Hwang J.-S. (2008). Seismic Design of structures with viscous dampers, *International Training Programs for Seismic Design of Building Structures*, pp. 123–138.

ICBO (1967) *Uniform Building Code*, International Conference of Building Officials, *1967 Edition*, Whittier, CA.

Inaudi, J.A. and Kelly, J.M. (1993). Optimum damping in linear isolation systems, *Earthquake Engineering & Structural Dynamics,* 22, 583-598.

Infanti, S., Kang, H.T. and Castellano, M.G. (2004). Retrofit of bridges in Korea using viscous damper technology, *Proceedings of 13th World Conference on Earthquake Engineering*, Vancouver, B.C., Canada, No. 2211.

Infanti, S., Tsiknias, T., Castellano, M.G., and Tomaselli, F. (2006). Viscous dampers: recent major applications in European bridges, *Proceedings of 6th World Congress on Joints, Bearings and Seismic Systems for Concrete Structures*, Halifax, Nova Scotia, Canada, No. 43.

Judd J., Charney, F. and Pryor, S. (2015). Retrofit of steel-frame buildings using enhanced gravity-frame connections, *Proceedings of 2nd Conference on Improving the Seismic Performance of Existing Buildings and Other Structures*, San Francisco, CA.

Kabeyasawa, T. (2005). Recent development of seismic retrofit methods in Japan, Japan Building Disaster Prevention Association, Japan. Accessed Jan. 6, 2015, from: *http://www.kenchiku-bosai.or.jp/files/2013/11/srm.pdf*.

Kasai, K., Fu, Y., and Watanabe, A. (1998). Passive control systems for seismic damage mitigation, *ASCE Journal of Structural Engineering*, 124(5).

Kasai, K., and Jodai, A. (2002). Dynamic property, behavior and their simplified estimation rules for a passive control system with stud-type viscoelastic damper, *Journal of Structural and Construction Engineering*, Architectural Institute of Japan (AIJ), 558:125-132. (in Japanese).

Kasai, K. Suzuki, A. and Onhara, K. (2003). Equivalent linearization of a passive control system having viscous dampers dependent on fractional power of velocity, *Journal of Structural and Construction Engineering,* Architectural Institute of Japan (AIJ), 574: 77-84. (in Japanese).

Kasai, K. and Iwasaki, K. (2006). Reduced expression for various passive control systems and conversion to shear spring model, *Journal of Structural and Construction Engineering*, Architectural Institute of Japan (AIJ), 605: 37-46. (in Japanese).

Kasai, K., Ogura, T., Suzuki, A. (2007). Passive control design method based on tuning of equivalent stiffness of nonlinear viscous dampers, *Journal of Structural and Construction Engineering,* Architectural Institute of Japan (AIJ), 678: 97-104. (in Japanese).

Kasai K., Lu. X., Pu W., Yamashita T., Arakawa Y., Zhou Y (2013). Effective retrofit using dampers for a steel tall building shaken by 2011 East Japan Earthquake—China-Japan Cooperation Program, *Proceedings of 20th International Conference on Urban Earthquake Engineering* (10CUEE), Tokyo, Japan.

Kelly, J.M. (1997). *Earthquake-Resistant design with rubber*, Springer-Verlag, London, Limited.

Kidder Mathews (2015). San Francisco office real estate market review 3rd quarter 2015. Retrieved March 2016, from *http://www.kiddermathews.com/downloads/research/office-market-research-san-francisco-2015-3q.pdf*.

Kilpatrick C. (2016, April 29). Megaprojects: $1.6 billion Oceanwide Center to transform SF's transbay district, *San Francisco Business Times*. Retrieved 2017, May 1, from *http://www.bizjournals.com/sanfrancisco/print-edition/2016/04/29/megaprojects-1-6-billion-oceanwide-center-to.html*

Kim, J., Choi, H., and Min, K-W. (2003). Performance-based design of added viscous dampers using capacity spectrum method, *Journal of Earthquake Engineering*, 7(1) :1-24.

Kimura, K., Yoshioka, K., Takeda, T. and Fukuya, Z. (1976). Tests on braces encased by mortar in-filled steel tubes, *Summaries of technical papers of annual meeting*. Architectural Institute of Japan, Structural Engineering Section, 1041-1042. (in Japanese).

Koduru, S.D. & Haukaas, T. (2010). Probabilistic seismic loss assessment of a Vancouver high-rise building, *ASCE Journal of Structural Engineering*, 136(3), 235-245.

Krishnan, S., Muto, M. (2011). Mechanism of collapse, sensitivity of ground motion features, and rapid estimation of response of tall steel moment frame buildings to earthquake excitation, *Technical Pre. EERL 2011-2, Earthquake Engineering Research Laboratory*, California Institute of Technology, Pasadena, CA.

Lai, J.-W., and Tsai, K.-C. (2004). Research and application of buckling restrained braces in Taiwan, *Proceedings of ANCER annual meeting*, Honolulu, Hawaii, USA.

Lai, J.-W., Wang, S. Schoettler, M. and Mahin, S. (2015). Seismic performance assessment of a tall building having Pre-Northridge moment-resisting connections, *PEER Report No. 2015/14,* Pacific Earthquake Engineering Research Center, University of California, Berkeley, CA.

LATBSDC (2017). *An Alternative Procedure for Seismic Analysis and Design of Tall Buildings Located in the Los Angeles Region*, Los Angeles Tall Buildings Structural Design Council, Los Angeles, CA.

Lavan, O. and Dargush, G. (2009). Multi-objective evolutionary seismic design with passive energy dissipation systems, *Journal of Earthquake Engineering*, 13, 758-790.

Lavan, O., Cimellaro, G.P. and Reinhorn A.M. (2008). Non-iterative optimization procedure for seismic weakening and damping of inelastic structures, *ASCE Journal of Structural Engineering*, 134(10), 1638-1648.

Lavan, O., Levy, R. (2004). Optimal design of supplemental viscous dampers for linear framed structures, *Proceedings of 13th World Conference on Earthquake Engineering*, Vancouver, B.C., Canada.

Lavan, O., Levy, R. (2005). Optimal design of supplemental viscous dampers for irregular shear-frames in the presence of yielding, *Earthquake Engineering & Structural Dynamics*, 34, 889-907.

Lee, S-H., Son, D-I, Kim, J. and Min, K-W. (2004). Optimal design of viscoelastic dampers using eigenvalue assignment, *Earthquake Engineering & Structural Dynamics*, 33,521-542.

Lee, D. and Taylor, D. P. (2001). Viscous damper development and future trends, *Journal of Structural Design of Tall Buildings*, 10, 311-320.

Levy, R. and Lavan, O. (2006). Fully stressed design of passive controllers in framed structures for seismic loading, *Structural and Multidisciplinary Optimization*, 32, 485-498.

Levy, R and Lavan, O. (2009). Quantitative comparison of optimization approaches for the design of supplemental damping in earthquake engineering practice, *ASCE Journal of Structural Engineering*, 135(3), 321-325.

Liang, X.-W., Dong, Z.-P., Wang, Y.-S., Deng, M.-K. (2009). Damage to tall buildings in areas with large epicentral distance during M8.0 Wenchuan earthquake, *Earthquake Engineering and Engineering Vibration,* 29(1): 24−31 (in Chinese).

Liu J. and Astaneh-A. A. (2000). Cyclic testing of simple connections including effects of slab, *ASCE Journal of Structural Engineering*, 2000, 126(1): 32-39.

Lin, W-H., and Chopra, A. K. (2002). Earthquake response of elastic SDF systems with nonlinear fluid viscous dampers, *Earthquake Engineering & Structural Dynamics,* 31: 1623-1642.

Liu, W., Tong, M., Wu, Y. and Lee, G. (2004). Optimized damping device configuration design of a steel frame structures based on building performance indices, *Earthquake Spectra.* 20(1), 67-89.

Londono, J.M., Wagg, D. J and Neild, S.A., (2014) "Supporting brace sizing in structures with added linear viscous fluid dampers: a filter design solution", *Earthquake Engineering & Structural Dynamics*, 43:1999-2013.

LoopNet (2014). San Francisco building properties for sale. *LoopNet.com.* Retrieved March 1st, 2014 from *http://www.loopnet.com/California/San-Francisco_Building-Properties-For-Sale/.*

Lopez-Garcia, D.L. (2001), A simple method for the design of optimal damper configurations in MDOF structures, *Earthquake Spectra*, 17(3):378-398.

Lopez-Garcia, D.L. and Soong, T.T. (2002), Efficiency of a simple approach to damper allocation in MDOF structures, *Journal of Structural Control,* 9:19-30.

Love, R.J., Yu, K., McNeill, S., and Zepeda, D. (2008). Retrofit of a critical care facility in Los Angeles with steel plate shear walls, *Structural Congress 2008*, Apr. 24-26, 2008, Vancouver, British Columbia, Canada. DOI*: https://doi.org/10.1061/41016(314)103.*

Lu, X.L., Zhou, Y. and Yan, F. (2008). Shaking table test and numerical analysis of RC frames with viscous wall dampers, *ASCE Journal of Structural Engineering,* 134(1): 64-76.

Magnusson Klemencic Associates, Inc. (MKA) (2016). [Preliminary design of Oceanwide tower], *Unpublished report.*

Makris, N. and Constantinou, M. C. (1990). Viscous dampers: testing, modeling and application in vibration and seismic isolation, *NCEER Report No. 90-0028*, National Center for Earthquake Engineering Research, Buffalo, NY.

Makris, N. and Constantinou, M. C. (1991). Fractional derivative Maxwell model for viscous dampers, *ASCE Journal of Structural Engineering*, Vol. 117, No.9. pp: 2708-2724.

Malley, I.J., Sinclair, M., Graf, T., Blaney, C., Fraynt, M., Uang, C., Newell, J. and Ahmed, T. (2009). Seismic upgrade of a 15-story steel moment frame building—satisfying performance criteria with application of experimental and analytical procedures, *Proceedings of ATC/SEI Conference on Improving the Seismic Performance of Existing Buildings and Other Structures*, Dec. 9-11, 2009, San Francisco, CA.

Martinez-Rodrigo M., Romero M.L. (2003). An optimum retrofit strategy for moment-resisting frames with nonlinear viscous dampers for seismic applications, *Engineering Structures,* 25: 913–925.

Masri, S.F., Bekey, G.A. and Caughey, T.K. (1981). Optimal pulse control of flexible structures, *Journal of Applied Mechanics*, ASME 48, 619-626.

Mathworks. (2016a). MATLAB and Optimization Toolbox Release, (Version R2016a). Natick, Massachusetts, United States.

Mathworks. (2016b). Constrained Optimization: User's Guide (r2016). Retrieved May 7th, 2017, from *https://www.mathworks.com/help/optim/ug/constrained-nonlinear-optimization-algorithms.html*.

McKenna F., Scott M., Fenves, G., (2010). Nonlinear finite-element analysis software architecture using object composition, *ASCE Journal of Computing in Civil Engineering*, 24(1): 95–107.

Menon, D., and Sengupta, A. K. (2007). *Handbook on Seismic Retrofit of Buildings*. Madras, India: Central Public Works Department and Indian Building Congress.

Milman M.H. & Chu, C.C. (1994). Optimization methods for passive damper placement and tuning, *Journal of Guidance, Control and Dynamics*, 17(4), 848-856.

Miranda, E., Medina, R., Mosqueda, G., Lignos, D., Fell, B., Eads, L., Hashemi, J., Zargar, S., and Negrete, M. (2014). Collapse assessment of multi-story buildings through hybrid testing, *Proceedings of 10th National Conference in Earthquake Engineering*, Anchorage, Alaska.

Miyamoto, H.K. (2010). *Probabilistic seismic risk identification of steel buildings with viscous dampers*, Doctoral dissertation, Tokyo Institute of Technology, 2010, NISEE e-Library.

Miyamoto K., Gilani A., Wada A., Ariyaratana C. (2010). Collapse risk of tall steel moment frame buildings with viscous dampers subjected to large earthquakes. Part I: damper limit states and failure modes of 10-story archetypes, *The Structural Design Tall and Special Buildings*, 19: 421–438.

Miyamoto, H.K., and Hanson, R.D. (2002). U.S. design of structures with damping systems, *Proceedings of Structural Engineering World Conference,* Yokohama, Japan.

Miyazaki, M. and Mitsusaka, Y. (1992). Design of a building with 20% or greater damping, *Proceedings of Tenth World Conference of Earthquake Engineering*, Balkema, Rotterdam.

Miyamoto, H.K., and Scholl, R. E. (1996). Case study: seismic rehabilitation of a non-ductile soft story concrete structure using viscous dampers, *Proceedings of 11th World Conference on Earthquake Engineering*, Acapulco, Mexico, No. 315.

Miyamoto, H.K., and Scholl, R.E. (1997). Design of steel pyramid using seismic dampers, *Proceedings of Structures Congress, XV*, ASCE, Portland, OR, pp. 1466-1470.

Moreschi, M.L. (2000). Seismic design of energy dissipation systems for optimal structural performance, *Doctoral dissertation*, Engineering Science & Mechanics, Virginia Tech, Blacksburgh, VA.

Moreschi, L.M. and Singh, M.P. (2003). Design of yielding metallic and friction dampers for optimal seismic performance, *Earthquake Engineering & Structural Dynamics*, 32(8), 1291-1311.

Natke, H.G. & Soong, T.T. (1993). Topological structural optimization under dynamic loads, *Computer aided optimum design of structures III*, pp: 67-78, Elsevier Science Publishers Ltd. Essex, UK, 1993.

NEHRP—National Earthquake Hazard Reduction Program (1994). *NEHRP Recommended Seismic Provisions for Seismic Regulations for New Buildings and Other Structures*, Federal Emergency Management Agency. Report No. FEMA 222A, Washington, D.C.

NEHRP—National Earthquake Hazard Reduction Program (2000). *NEHRP Recommended Seismic Provisions for Seismic Regulations for New Buildings and Other Structures, Appendix to Chapter 13, Structures with Damping Systems*, Federal Emergency Management Agency. Report No. FEMA 368 and 369, Washington, D.C.

NEHRP—National Earthquake Hazard Reduction Program (2015). *NEHRP Recommended Seismic Provisions for Seismic Regulations for New Buildings and Other Structures*, Federal Emergency Management Agency. Report No. FEMA P-1050-1/2015 Edition, Washington, D.C.

Newell, J., and Uang, C.M. (2006). Cyclic testing of steel moment connections for the Caltrans District 4 office building seismic upgrade, *Report No. SSRP-05/03*, Department of Structural Engineering, University of California, San Diego, La Jolla, CA.

Newell, J., Love J., Sinclair M., Chen Y-N., and Kasalanati A. (2011). Seismic design of a 15-story hospital using viscous wall dampers, *Proceedings of 42nd Structural Congress*, Las Vegas, Nevada, U.S.

NIST (2012). Soil-structure interaction for building structures, NEHRP Consultants Joint Venture, *NIST GCR 12-917-21* (ATC-83 report), Gaithersburg, MD.

Nocedal J. and Wright. S. (2006). *Numerical Optimization* (Second Edition), Springer Series in Operations Research, Springer Verlag, 2006.

Nudel, A., Marusich, S., Dana, M., and Roufegarinejad, A. (2015). Evaluation and remediation of pre-Northridge steel moment frame column splices, *Proceedings of 2nd Conference on Improving the Seismic Performance of Existing Buildings and Other Structures*, San Francisco, CA.

Occuhiuzzi A. (2009). Additional viscous dampers for civil structures: analysis of design methods based on effective evaluation of modal damping ratios, *Engineering Structures*, 1093-1101.

Park J. H., Kim, J. and Min K.W. (2004). Optimal design of added viscoelastic dampers and supporting braces, *Earthquake Engineering & Structural Dynamics*. 33(4): 465-484.

Park K.-S, Koh, H.-M., and Hahm D. (2004). Integrated optimum design of viscoelastically damped structural systems, *Engineering Structures,* 26, 581-591.

Panian, L., Korolyk, M., and Bucci, N. (2015). Seismic evaluation and retrofit of a 1970s high-rise welded moment frame structure—a performance-based approach, *Proceedings of 2nd Conference on Improving the Seismic Performance of Existing Buildings and Other Structures*, San Francisco, CA.

Pekcan, G., Mander, J. and Chen, S. (1999). Design and retrofit methodology for building structures with supplemental energy dissipating systems, *MCEER-99-0021*, Mid-American Center for Earthquake Engineering, Urbana, IL.

PEER (2010a). Guidelines for performance-based seismic design of tall buildings, *PEER Report No. 2010/05*, Pacific Earthquake Engineering Research Center, University of California, Berkeley, CA.

PEER (2010b). Modeling and acceptance criteria for seismic design and analysis of tall buildings, *PEER Report No. 2010/111,* Pacific Earthquake Engineering Research Center, University of California, Berkeley, CA.

PEER (2011). Case studies of the seismic performance of tall buildings designed by alternative means, *PEER Report No. 2011/05*, Pacific Earthquake Engineering Research Center, University of California, Berkeley, CA.

PEER (2017). Guidelines for performance-based seismic design of tall buildings, Version 2.0, *PEER Report No. 2017/06*, Pacific Earthquake Engineering Research Center, University of California, Berkeley, CA.

Puthanpurayil, A.M., Lavan, O., and Dhakal, R.P. (2015). Seismic loss optimization of frame buildings using viscous dampers, *Proceedings of Computational Methods in Structural Dynamics and Earthquake Engineering*, Crete Island, Greece, 2015.

Ramires, C. M. and Miranda, E. (2009). Building-specific loss estimation methods and tools for simplified performance-based earthquake engineering, *Blume Center technical report, Report No. 171*. The John A. Blume Earthquake Engineering Center, Stanford University.

Ramirez O.M., Constantinou M.C., Kircher C.A., Whittaker A.S., Johnson M.W., Gomez J.D., Chrysostomou C.Z. (2001). Development and evaluation of simplified procedures for analysis and design of buildings with passive energy dissipation systems, *MCEER-00-0010*, Mid-American Center for Earthquake Engineering, Urbana, IL.

Reinhorn A.M., Li C., Constantinou M.C. (1995). Experimental and analytical investigation of seismic retrofit of structures with supplemental damping, part I: fluid viscous damping devices, *NCEER-95-0001*, National Center for Earthquake Engineering Research, Buffalo, NY.

Reinhorn, A., and Li, C. (1995). Experimental and analytical investigation of seismic retrofit of structures with supplemental damping: part III-viscous damping walls, *NCEER-95-0013*, National Center for Earthquake Engineering Research, Buffalo, NY.

Rezaeian S., Bozorgnia Y., Idriss I.M., Campbell K.W., Abrahamson N.A., Silva W.J. (2012). Spectral damping scale factors for shallow crustal earthquakes in active tectonic regions, *PEER Report No. 2012/01,* Pacific Earthquake Engineering Research Center, University of California, Berkeley, CA.

Ribeiro F., Barbosa A., Scott M., Neves L. (2015). Deterioration modeling of steel moment-resisting frames using finite-length plastic hinge force-based beam-column elements, *ASCE Journal of Structural Engineering*, 141(2).

Rodriguez, G., Seim, C, Ingham T. (1994). Earthquake protective systems for the seismic upgrade of the Golden Gate Bridge, *Proceedings of the 3rd U.S.-Japan Workshop on Protective Systems for Bridges*, Berkeley, CA.

Sabelli, R. and Lopez, W. (2004). Design of buckling-restrained braced frames. *Modern Steel Construction*, March, 2004. Retrieved Jun. 30th, 2016, from *https://www.aisc.org/globalassets/modern-steel/archives/2004/03/2004v03_buckling.pdf.*

Sarno, L.D. and Elnashai, A.S. (2002). Seismic retrofitting of steel and composite building structures, *MAE report, Report No: 02/01*, Mid-America Earthquake Center, Civil and Environmental Engineering Department, University of Illinois at Urbana-Champaign.

Secure Shell. In Wikipedia (May 4th 2017). Retrieved May 7th 2017, from *https://en.wikipedia.org/wiki/Secure_Shell*.

Seleemah, A.A. and Constantinou, M.C. (1997). Investigation of seismic response of buildings with linear and nonlinear fluid viscous dampers, *NCEER Report No. 97-0004*, National Center for Earthquake Engineering Research, Buffalo, NY.

SFDBI (2014). *Requirements and Guidelines for the Seismic Design of New Tall Buildings using Non-Prescriptive Seismic-Design Procedures*, *Administrative Bulletin 83*, San Francisco Building Code, San Francisco Department of Building Inspection, San Francisco, CA.

Shahi, S., and Baker, J. W. (2011). An empirically calibrated framework for including the effects of near-fault directivity in probabilistic seismic hazard analysis, *Bulletin of the Seismological Society of America*, 101(2), 742-755.

Shen, Z. (2015). Major development of research and practices on seismic design of steel building structures in China, *Proceedings of 8th International Conference on Behavior of Steel Structures in Seismic Areas,* Shanghai, China.

Singh, M., Verma, N., and Moreschi, L.(2003), Seismic analysis and design with Maxwell dampers, *Journal of Engineering Mechanics*, 129(3):273-282.

Singh, P.M., and Moreschi, M.L. (2001). Optimal seismic response control with dampers, *Earthquake Engineering & Structural Dynamics,* 30,553-572.

Singh, P.M., and Moreschi, M.L. (2002). Optimal placement of dampers for passive response control, *Earthquake Engineering & Structural Dynamics,* 31, 955-976.

Singh, P.M., Verma, P.N. and Moreschi, M.L. (2003). Seismic analysis and design with Maxwell dampers, *Journal of Engineering Mechanics*, 129,273-282.

Smith, R. Merello, R. and Willford, M. (2010). Intrinsic and supplementary damping in tall buildings, *Structures and Buildings*, 163: 111-118.

Soltani, A. and Hu, J. (2014). Optimum parameter of a viscous damper for seismic and wind vibration, *International Journal of Civil, Architectural, Structural and Construction Engineering*, 8(2),192-196.

Soong, T.T. and Constantinou, M.C. (1994). *Passive and active structural vibration control in civil engineering*, Longman, New York.: Springer-Verlag Wien.

Soong T.T., Dargush G.F. (1997). *Passive Energy Dissipation Systems in Structural Engineering*, Chichester, U.K.: John Wiley and Sons.

Soong T.T., Reinhorn, A.M., Wang, Y.P., Lin, R.C. (1991). Full-scale implementation of active control I: design and simulation, *ASCE Journal of Structural Engineering*, 117(11):3516-36.

Soong, T.T., and Spencer, B.F. (2002). Supplemental energy dissipation: state-of-the-art and state-of-the-practice, *Engineering Structures*, 24:243-259.

Shukla, A.K. and Datta, T.K. (1999). Optimal use of viscoelastic dampers in building frames for seismic force, *ASCE Journal of Structural Engineering,* 125(4), 401-409.

Stewart J.P., Tileylioglu S. (2010). Input ground motions for tall buildings with subterranean levels, *TBI Task 8 Final Report*, Pacific Earthquake Engineering Research Center, University of California, Berkeley, CA.

STRUCTURE magzine (Dec. 2008). The addition at 185 Berry Street San Francisco, CA, by Simposon Gumpertz & Heger, Inc. *NCSEA 11th Annaul Awards Program*, special edition, p 41.

Stillmaker K., Kanvinde A., Galasso C. (2016). Fracture mechanics-based design of column splices with partial joint penetration welds, *ASCE Journal of Structural Engineering*, 142(2).

Symans, M.D., Constantinou, M.C. (1998). Passive fluid viscous damping systems for seismic energy dissipation, *ISET Journal of Earthquake Technology*, 35(4): 185–206.

Takewaki, I. (1997). Optimal damper placement for minimum transfer functions, *Earthquake Engineering & Structural Dynamics,* 26: 1113-1124.

Takewaki, I. (1999). Displacement-acceleration control via stiffness-damping collaboration, *Earthquake Engineering & Structural Dynamics,* 28, 1567-1585.

Takewaki, I. (2000a). An approach to stiffness-damping simultaneous optimization, *Computer Methods in Applied Mechanics and Engineering,* 189, 641-650.

Takewaki, I. (2000b). Optimal damper placement for planar building frames using transfer function, *Structural and Multidisciplinary Optimization,* 20(4), 280-287.

Takewaki, I. (2009). *Building Control with Passive Dampers—Optimal Performance-based Design for Earthquakes*, Chichester, U.K.: John Wiley and Sons.

Takewaki I., Moustafa A. Fujita K. (2013). *Earthquake Resilience of High-Rise Buildings -- Case Study of the 2011 Tohoku (Japan) Earthquake, Improving the Earthquake Resilience of Buildings*, Springer, DOI 10.1007/978-1-4471-4144-0_2.

Takewaki, I., Yoshitomi, S. (1998), Effects of support stiffness on optimal damper placement for a planar building frame, *Structural Design of Tall Buildings,* 7(4):323-336.

Takewaki, I., Yoshitomi, S., Uetani, K. and Tsuju, M. (1999). Non-monotonic optimal damper placement via steepest direction search, *Earthquake Engineering & Structural Dynamics,* 28: 655-670.

Taylor, D.P. (2000). Damper retrofit of the London Millennium footbridge—a case study in biodynamic design. North Tonawanda: Taylor Devices, Inc. Retrieved Dec. 3, 2015, from *http://taylordevices.com/Tech-Paper-archives/literature-pdf/66-DamperRetrofit-London.pdf*.

Taylor, D.P. (2010). History, design and applications of fluid dampers in structural engineering. North Tonawanda: Taylor Devices, Inc. Retrieved Dec. 3, 2015, from *http://www.taylordevices.com/Tech-Paper-archives/literature-pdf/68-HistoryDesign-Application.pdf*.

Taylor D.P., and Constantinou, M.C. (1995). Testing procedures for high-output fluid viscous dampers used in building and bridge structures to dissipate seismic energy, *Shock and Vibration*, 2(5):373-381.

Taylor D.P, and Constantinou, M. (1996). Fluid dampers for applications of seismic energy dissipation and seismic isolation, *Proceedings of 11th World Conference on Earthquake Engineering*, Acapulco, Mexico. No. 798.

Taylor, D.P., Constantinou, M.C. (1998). Development and Testing of an Improved Fluid Damper Configuration for Structures having High Rigidity, *Proceedings of the 69th Shock and Vibration Symposium*, St. Paul, MN.

Taylor D.P., Katz I. (2004). Seismic Protection with Fluid Viscous Dampers for the Torre Mayor, North Tonawanda: Taylor Devices, Inc. Retried from: *http://taylordevices.com/Tech-Paper-archives/literature-pdf/71-SeismicProtectionwithFVD.pdf*.

Taylor Device Inc. (2010). Fluid viscous dampers and lock-up devices. North Tonawanda: Taylor Devices, Inc. Retrieved Jan. 3, 2016, from *http://www.seismicdamper.com/src/technical-data/CLEVIS-CLEVIS.pdf*.

Taylor Device Inc. (2015). Structural applications of Taylor fluid viscous dampers. North Tonawanda: Taylor Devices, Inc. Retrieved Jan. 3, 2016, from *http://www.seismicdamper.com/src/technical-data/StructuralApplicationChart-2015.pdf*.

Taghavi S., and Miranda E. (2003). Response assessment of non-structural building elements, *PEER Report No. 2003/05*, Pacific Earthquake Engineering Research Center, University of California, Berkeley, CA.

Terzic V. (2011). Force-based element versus displacement-based element [*PowerPoint slides*]. Retrieved Jun. 3, 2016, from *http://opensees.berkeley.edu/wiki/images/c/c5/FBEvsDBE.pdf*.

Terzic V., Mahin A.S., and Comerio, C.M. (2015). Downtime modelling: challenges and prospects. *Manuscript submitted for publication*.

Texas Advanced Computing Center (TACC) (2017). Stampede User Guide (last updated: April 5, 2017). Retrieved May 7th, 2017, from *https://portal.tacc.utexas.edu/user-guides/stampede*.

TRC Inc. (2015). XTRACT (Version 3.0.9) [*computer software*], Lowell, LA.

Tsai, K.C., Hsian, P.C., Wang, K.J., Weng, Y.T., Lin, M.L., Lin, K.C., Chen, C.H., Lai, J.H. and Lin, S.L. (2008). Pseudo-dynamic tests of a full-scale CFT/BRB frame – Part I: specimen design, experiment and analysis, *Earthquake Engineering & Structural Dynamics,* Vol 37, pp: 1081-1098.

Tsuji, M. and Nakamura, T. (1996). Optimum viscous dampers for stiffness design of shear buildings, *The Structural Design of Tall Buildings*, 5,217-234.

Tsuneki, Y., Torii, S., Murakami, K. and Sueoka, T (2008). Middle-story isolated structural system of high-rise building, *Proceedings of 14th World Conference on Earthquake Engineering*, Beijing, China.

Uang, C-M., and Bertero, V.V. (1988). Use of energy as a design criterion in earthquake-resistant design, Report No. *UCB/EERC-88/18*, University of California, Berkeley, 1988.

Uriz, P. and Mahin, S. (2008). Toward earthquake-resistant design of concentrically braced steel-frame structures, *PEER Report No. 2008/08*, Pacific Earthquake Engineering Research Center, University of California, Berkeley, CA.

Uzarski, J., Arnold, C., eds. (2001). "Chi-Chi, Taiwan, earthquake of September 21, 1999, reconnaissance report, *Earthquake Spectra*, Supplement A to Vol. 17, Earthquake Engineering Research Institute, Oakland, CA.

Viola E. and Guidi F. (2008). Influence of the supporting braces on the dynamic control of buildings with added viscous dampers, *Structural Control and Health Monitoring*. DOI: 10.1002/stc.234.

Wakabayashi, M., Nakamura, T., Katagihara, A., Yogoyama, H., and Morisono, T. (1973). Experimental study on the elasto-plastic behavior of braces enclosed by precsast concrete panels under horizontal cyclic loading—part 1 and 2, *Summaries of technical papers of annual meeting*, vol. 10. Architectural Institute of Japan, Structural Engineering Section, 1041-1044 (in Japanese).

Wongprasert, N. and Symans, M.D. (2004). Application of a genetic algorithm for optimal damper distribution within the nonlinear seismic benchmark building, *ASCE Journal of Engineering Mechanics*, 130(4): 401-406.

Whittaker, A.S., Aiken, I., Bergman, D., Clark, P., Kelly, J. and Scholl, R. (1993). Code requirements for the design and implementation of passive energy dissipation systems. *Proceedings of ATC-17-1, Seminars on Seismic Isolation, Passive Energy Dissipation and Active Control*, Applied Technology Council, Redwood City, CA.

Whittle, J.K., Williams, M.S. Karavasllis, T.L. and Blakeborough, A. (2012). A comparison of viscous damper placement methods for improving seismic building design, *Journal of Earthquake Engineering,* 16,540-560.

Wu, B. Ou, J.P. and Soong, T.T. (1997). Optimal placement of energy dissipation devices for three-dimensional structures, *Engineering Structures,* 19(2),113-125.

Xie, Q. (2005). State of the art of buckling-restrained braces in Asia, *Journal of Constructional Steel Research,* 61:727-748.

Xu Y.L and Teng J. (2002) Optimum design of active/passive control devices for tall buildings under earthquake excitation, *Structural Design of Tall Buildings*, 11,109-127.

Yang, J.N., Lin, S., Kim, J-H and Agrawal, A.K. (2002). Optimal design of passive energy dissipation systems based on H∞ and H2 performances, *Earthquake Engineering & Structural Dynamics,* 31, 921-936.

Yang, T.Y. and Moehle, J., Stojadinovic, B. and Der Kiureghian, A. (2009). Seismic performance evaluation of facilities: methodology and implementation, *ASCE Journal of Structural Engineering*, October 2009, Vol. 135, No. 10, DOI: 10.1061/(ASCE)0733-9445(2009)135:10(1146)).

Yeung N., Pan D.E.A. (1998). The effectiveness of viscous-damping walls for controlling wind vibrations in multi-story buildings, *Journal of Wind Engineering & Industrial Aerodynamics,* 77&78: 337-348.

Yoshino, T., Karino, Y. (1971). Experimental study on shear wall with braces: part 2. *Summaries of technical papers of annual meeting*, vol. 11, Architectural Institute of Japan, Structural Engineering Section, 403-404. (in Japanese)

Youssef, N. and Hata, O. (2005). Seismic retrofit and instrumentation of Los Angeles City Hall, *SMIP05 Seminar on Unitization of Strong-Motion Data*, p. 115-130.

Zhang, R.H. and Soong, T.T. (1992). Seismic design of viscoelastic dampers for structural applications, *ASCE Journal of Structural Engineering*, 118, 1375-1392.